

Towards the development of a point-of-care detection system for  
acute respiratory infections



A thesis submitted in accordance with the conditions governing  
candidates for the degree of Doctor Philosophiae in Cardiff  
University

By Kyriaki Karagianni, MSc  
30th of September 2024  
Welsh School of Pharmacy and Pharmaceutical Sciences Cardiff  
University

## **Acknowledgments**

I would like to thank my supervisors for their supervision and support during this project, especially under the conditions caused by the COVID-19 pandemic. I would like to also thank the colleagues at floor 2 in Redwood and the Redwood team for their assistance and support throughout those four years. Special thanks go to the CMD team for their support during the first year of the project.

Additionally, I would like to thank my partner and my family for their love, support and encouragement.

I sincerely want to thank my friends – both old and new ones- for their company and support throughout the PhD. I will always be grateful for your assistance and the time spent together.

## Summary

Pneumonia, a severe lower respiratory tract infection, is one of the leading causes of child mortality, especially in lower-middle income countries. In England, 56,210 emergency admissions occurred between 2018-2019, with 3% of cases progressing to complicated pneumonia and secondary sepsis. As pneumonia is the most common cause of paediatric sepsis, early diagnosis and treatment of the underlying infection is crucial to prevent disease progression. The overarching aim of this project is to develop biosensors for the early and accurate diagnosis of pneumonia to ultimately provide guidance on patient treatment, and the risk of developing sepsis.

To realise this aim, three different biomarkers implicated in complicated pneumonia have been selected as targets for biosensor development, namely interleukin-6, endotoxin and beta-globin cell free DNA. Utilising electrochemical approaches coupled with recognition elements such as aptamers, antibodies, and molecularly imprinted polymers (MIP), biosensors capable of detecting these markers in citrated plasma have been developed.

Endotoxin is a notoriously difficult marker to detect in clinical samples, due to the presence of many interfering components that render the gold standard LAL assay unusable. The development of an aptamer-MIP hybrid sensor coupled with a thorough sample pre-treatment protocol enabled the successful detection of endotoxin from citrated plasma down to concentrations of 10 fg/mL. Utilising aptamer and a capture DNA sequence modified electrodes, detection of IL-6 and beta-globin DNA from citrated plasma has shown to be possible. The use of chemical sensitisers has increased both the sensitivity and dynamic range of these detection systems.

The positive results obtained throughout this project provide a platform for further development and integration of the biosensors into a miniaturised format suitable for deployment at point-of-care as a rapid, cost-effective diagnostic. Final testing of the system utilising clinical samples from paediatric pneumonia patients would provide validation of its utility in the clinical space.

## Table of contents

Acknowledgements	ii
Summary	iii
Table of contents	iv
List of figures	ix
List of tables.	xix
<b>Chapter 1 – General Introduction and literature review</b>	<b>1</b>
1.1 Executive summary	2
1.2 Pneumonia	3
1.2.1 Immunopathogenesis of pneumonia	
1.2.2 Adaptive immunity	7
1.2.3 Pneumonia diagnosis - current approaches	7
1.2.4 Point-of-care (POC) tests	9
1.2.5 History of POC tests	10
1.3 Review of biomarkers	12
1.3.1 The search for a suitable biomarker	12
1.3.2 Interleukin 6	12
1.3.3 Role in pneumonia	13
1.3.4 Interleukin 10	15
1.3.5 Role in pneumonia	15
1.3.6 C-reactive protein	17
1.3.7 Role in pneumonia	18
1.3.8 Procalcitonin	18
1.3.9 Role in pneumonia	19
1.3.10 Lipopolysaccharide	21
1.3.11 Role in pneumonia	22
1.3.12 Cell-free DNA	25
1.3.13 Beta-globin sequence in sepsis diagnosis	25
1.3.14 Biomarker review conclusions	26
1.4 Current and future focus on biosensors	
1.4.1 Electrochemical detection	29
1.4.2 Electrochemical immunoassays	30
1.4.3 Amperometric sensors	31
1.4.4 Voltametric sensors	34
1.4.5 Potentiometric sensors	36
1.4.6 Impedance biosensors	38
1.5 Biofouling and its prevention	39
1.5.1 Polymers for biofouling prevention	40
1.5.2 Hydrogels in biofouling prevention	41
1.5.3 Self-assembled monolayers (SAMs)	42

1.5.6 Electrochemical sensor limitations	44
1.6 Optical biosensors	44
1.6.1 Surface plasmon resonance (SPR) sensors	45
1.6.2 Localized surface plasmon resonance (LSPR)	47
1.6.3. Evanescent wave fluorescence biosensors	48
1.6.4 Bioluminescent optical fiber biosensors	48
1.6.5. Ellipsometric biosensors	49
1.6.6 Surface-enhanced Raman scattering (SERS) biosensors	49
1.7 Biosensor review conclusions	50
1.8 Scope of thesis	51
1.9 Bibliography	52
<b>Chapter 2 - Development of a sample preparation protocol for endotoxin detection using the LAL assay</b>	<b>84</b>
2.1 Introduction	85
2.1.1 Overview	85
2.1.2 Lipopolysaccharide	85
2.1.3 Endotoxin and disease	86
2.1.4 Endotoxin detection – LAL assay	87
2.1.5 Endotoxin detection – alternative assays	88
2.1.6 The CMD $\alpha$ BET <sup>®</sup> system	89
2.1.7. Endotoxin detection in clinical samples	91
2.1.8 Endotoxin masking – need for a sample preparation protocol	92
2.1.9 Aims and Objectives	94
2.2 Methods	96
2.2.1 Reagents and apparatus	96
2.2.2 Depyrogenation of equipment	96
2.2.3 Blood extraction, storage, and endotoxin spiking	96
2.2.4 Dilution, heating and addition of magnesium chloride	97
2.2.5 Sample pretreatment protocol 1: acid / base treatment	98
2.2.6 Sample pretreatment protocol 2: Optimized experimental protocol	98
2.2.7 Spike-hold study	98
2.3 Results and discussion	100
2.3.1 Requirement of a sample pretreatment protocol	100
2.3.2 $\alpha$ BET <sup>®</sup> instrument	100
2.3.3 Sample pretreatment: dilution	104
2.3.4 Sample pretreatment: acid / base treatment	106
2.3.5 Spike hold studies	108

2.3.6 Further optimization of sample pretreatment protocol – centrifugation	110
2.3.6.1 Calibration	110
2.3.6.2 Background endotoxin plasma levels	111
2.3.6.3 Determination of endotoxin recovery from spiked plasma samples	112
2.4 Conclusions and future direction	115
2.5 Bibliography	118
<b>Chapter 3 - Development of an electrochemical sensor for the detection of endotoxin using aptamers and molecularly imprinted polymer approaches</b>	122
<b>3.1 Introduction</b>	127
3.1.1 General overview	127
3.1.2 Aptamers	128
3.1.3 Aptamer – based biosensors	129
3.1.4. Electrochemistry overview	130
3.1.4.1 Cyclic voltammetry	131
3.1.4.2 Electrochemical Impedance Spectroscopy (EIS)	132
3.1.5 Molecularly imprinted polymers (MIPs)	136
3.1.5.1 General overview	136
3.1.5.2 Bulk imprinting	137
3.1.5.3 Surface imprinting	138
3.1.5.4 Hybrid imprinting	139
3.1.5.5 Monomer selection – APBA	139
3.1.6 Aims and Objectives	142
3.2 Materials and Methods	143
3.2.1 Reagents and apparatus	143
3.2.2. Methods	144
3.2.2.1 Aptamer handling	144
3.2.2.2 Cleaning of gold electrodes	144
3.2.2.3 Electrochemical activation of gold working electrodes	144
3.2.2.4 Development of self-assembled monolayers (SAMs)	145
3.2.2.5 Electropolymerization of 3-aminophenylboronic acid (APBA)	145
3.2.2.6 Surface imprinting and development of conventional MIPs	145
3.2.2.7 Surface imprinting and development of a hybrid MIP	146
3.2.2.8 Polymer washing / regeneration	146
3.2.3 Sensor characterization	146
3.2.3.1 Electrochemical impedance spectroscopy (EIS)	146

3.2.3.2 Evaluation of binding performance	147
3.3 Results and Discussion	148
3.3.1 Electrochemical activation of working electrodes	148
3.3.2 Development of an aptasensor for recognition of endotoxin	148
3.3.2.1 Screening of alkanethiols as spacer molecules	149
3.3.2.2 Evaluation of alkanethiol interaction with endotoxin	151
3.3.3 Endotoxin sensor characterization	154
3.3.3.1 Sensor stability, reproducibility and sensitivity	154
3.3.3.2 Performance in MES and TRIS buffers	158
3.3.5 Development and optimization of a hybrid molecularly imprinted polymer	160
3.3.5.1 APBA polymerization	160
3.3.5.2 Development of APBA non-imprinted polymer	162
3.3.5.3 Development of 'conventional' APBA molecularly imprinted polymer	162
3.3.5.4 Development of APBA Hybrid molecularly imprinted polymer	164
3.3.5.5 Comparison with gold-standard LAL assay	167
3.3.5.6 Comparison with literature	167
3.3.6 Biofouling studies	167
3.3.6.1 Human serum albumin (HSA) challenge	170
3.3.6.2 Challenge with HSA and endotoxin	171
3.3.6.3 Interleukin 6 challenge	172
3.3.6.4 AptamIP response to glucose and citrate	173
3.4 Conclusions and future work	174
3.5 Bibliography	175
<b>Chapter 4 - AptamIP sensor: Detection in blood plasma</b>	<b>184</b>
4.1 Introduction	185
4.1.1. General overview	185
4.1.2 Shortcomings of biosensors in clinical matrices	185
4.1.3 AptamIP – role in improving specificity and biofouling prevention	186
4.1.4 Recovery of endotoxin from plasma	187
4.1.5 Aims and objectives	188
4.2 Materials and Methods	189
4.2.1 Reagents and apparatus	189
4.2.2 Aptamer handling	189
4.2.3 Depyrogenation of equipment	189

4.2.4 Blood extraction, storage, and endotoxin spiking	189
4.2.5 Spike-hold study	190
4.2.6 Electrochemical characterization of sensors	190
4.2.7 Final sample preparation protocol	190
4.3 Results and Discussion	191
4.3.1 Requirement of a sample preparation protocol	191
4.3.1.1 Effect of simple plasma dilution	192
4.3.1.2 Effect of acid / base treatment and modifications (Chapter 2 protocol)	193
4.3.1.3 Physical separation (centrifugation and filtration)	196
4.3.1.4. Effect of sodium deoxycholate (NaDOC) on endotoxin recovery	198
4.3.1.5 Summary of various plasma treatments in unspiked plasma	201
4.3.1.6 Further refinement of the pre-treatment protocol	202
4.3.1 Spike-hold studies	205
4.3.1.1 Unspiked plasma stored at room temperature or in the refrigerator	205
4.3.1.2 Spiked plasma stored at room temperature or in the refrigerator	207
4.3.3. Regeneration of AptaMIP following use in plasma	212
4.3.4 Application of finalized sample preparation protocol to simple aptasensor	214
4.4 Conclusions and future work	215
4.5 Bibliography	216
<b>Chapter 5 - Development of electrochemical sensors for the detection of interleukin 6 and beta-globin using antibodies and aptamers</b>	<b>222</b>
5.1 Introduction	223
5.1.1 General overview	223
5.1.2 Interleukin 6 detection	223
5.1.3 DNA sensors and Beta-globin	225
5.1.4 Use of sensitizing molecules in electrochemical sensors	226
5.2 Aims and Objectives	228
5.3. Materials and methods	229
5.3.1 Materials overview	229
5.3.2 Methods	230
5.3.2.1 EDC/NHS coupling	230

5.3.2.2 Use of DNA sensitizers developed by collaborators in the School of Chemistry	230
5.4 Results and discussion	231
5.4.1 Use of EDC/NHS to develop an IL-6 immunosensor	231
5.4.2 Use of protein G to improve IL-6 immunosensor performance.	233
5.4.3 Evaluation of IL-6 aptamer functionality	235
5.4.3.1 Aptamer-only monolayer	235
5.4.3.2 DTBA IL6 aptasensor	237
5.4.4 Use of sensitizer on IL-6 aptasensor	238
5.4.4.1 Use of sensitized IL-6 aptasensor in water samples	240
5.4.4.2 Use of sensitized IL-6 aptasensor in plasma samples	242
5.4.4.3 Specificity tests on IL-6 aptasensor	244
5.4.5 Initial experiments to develop a beta globin sensor	246
5.4.6 Use of sensitizer in the beta-globin sensor	247
5.4.6.1 Use of sensitized beta globin sensor in plasma samples	250
5.4.6.2 Specificity tests on beta globin sensor	252
5.5 Conclusions	255
5.6 Bibliography	257
<b>Chapter 6 - General discussion, concluding remarks and future outlook</b>	<b>262</b>
6.1 General overview of thesis	263
6.2 Conclusion and future outlook	268
6.3 Bibliography	269

## List of figures

### Chapter 1

Figure 1.1 Epithelial immunity in the lung (Vareille et al. 2011)	4
Figure 1.2: TLR signalling, including the MyD88 signaling pathway (Zheng et al. 2019)	6
Figure 1.3: Toll-like receptor 4 structure (Krishnan et al. 2018)	
Figure.1.4: Chest x-ray of healthy patient (left) vs viral pneumonia (right). Adapted from (Ullah et al. 2023)	8
Figure 1.5: IL-6 structure (Protein Data Bank, 2021)	12
Figure 1.6: IL-10 structure (Protein Data Bank, 2024)	14
Figure 1.7: C-reactive protein, shown as a 5-mer (Protein data bank, 2024)	17
Figure 1.8: Procalcitonin structure (Protein data bank, 2024)	19
Figure 1.9: Endotoxin structure (Harm, 2021)	21
Figure 1.10: LPS attachment to soluble and membrane mediators (Martin 2000)	23
Figure 1.11: Haemoglobin subunit beta, which is encoded by the beta globin gene (Protein data bank, 2024)	26
Figure 1.12: Photo of electrochemical setup used in this study. Working electrode (black), reference electrode (glass) and counter electrode (white) are visible and immersed in ferro/ferricyanide solution in PBS.	30
Figure 1.13: One potential cycle in square wave voltammetry (Mirceski et al. 2013)	34
Figure 1.14: i) single generic linear voltage sweep ii) scan at 50 mV/s (Grieshaber et al. 2008)	35

Figure 1.15: Three types of thiolated monolayers: a) thioaromatic DNA monolayer b) ternary DNA monolayer and c) thiolated DNA tetrahedral nanostructures (Campuzano et al., 2019) 42

Figure 1.16: Photo of an exemplar SPR setup (Cropped from (Patel, 2017)) 46

## Chapter 2

Figure 2.1: Endotoxin structure, showing the Lipid A phospholipid at the bottom, the inner core above it, the outer core, and the O-antigen at the top 86

Figure 2.2: The LAL coagulation cascade leading to gel clot formation (Munford 2016) 88

Figures 2.3 A and B: Figure 2.3 A shows an example amplitude graph showing the clotting curves for endotoxin in water in concentrations of 1, 0.1 and 0.01 EU/mL. Figure 2.3 B shows the transformed Log values of time needed to reach 80% of starting amplitude on y axis and the transformed Log values of endotoxin concentration on x axis.  $R^2 = 0.9961$ ,  $R = 0.9980$ . 91

Figure 2.4: Spiking and testing schedule for the spike-hold studies. 99

Figure 2.5 Amplitude results obtained from spiked citrated plasma (N=4, profiles for individual repeats shown) following dilution 1 in 10 with endotoxin-free water. Black curve represents the amplitude results obtained from a 0.1 EU/mL standard. Test was run for 30 minutes. No significant reduction in amplitude is observed in the characteristic curve shape, which translates to no endotoxin recovery. 101

Figure 2.6: Amplitude results obtained from citrated plasma (N=4) following dilution 1 in 10 with endotoxin-free water and heating at 82.5°C for 10 minutes. Blue curve represents the amplitude results obtained from a 0.1 EU/mL standard. Test was run for 30 minutes. No significant reduction in amplitude is observed in the characteristic curve shape, which translates to no endotoxin recovery 102

Figure 2.7: Amplitude results obtained from citrated plasma (N=3) following dilution 1 in 10 with endotoxin-free water and magnesium chloride at three concentrations (1, 3 and 5 mM) followed by **heating** at 82.5°C for 10 minutes, showing detection of endotoxin. Positive control shows amplitude results for 0.1 EU/ml endotoxin in endotoxin-free water. Test was run for 30 minutes 103

Figure 2.8: Glass tubes containing treated sample with different  $MgCl_2$  concentrations. From left to right: Positive control, 1, 5 and 10mM. Note the precipitate at 10mM. 104

Figure 2.9: Amplitude results obtained from citrated plasma (N=3) following dilution 1 in 10 with endotoxin-free water and magnesium chloride at three concentrations (1, 5 and 10 mM) without heating. No significant reduction in amplitude is observed in the characteristic curve shape, which translates to no endotoxin recovery. Positive control shows amplitude results for 0.1 EU/ml endotoxin in endotoxin-free water. Test was run for 30 minutes.

104

Figure 2.10: Amplitude results obtained from citrated plasma (N=3) following dilution 1 in 10 with endotoxin-free water, 1M HCL, magnesium chloride at 5mM, heating at 82.5°C for 10 minutes and pH balancing, showing detection of endotoxin. Positive control shows amplitude results for 0.1 EU/ml endotoxin following the same treatment. Test was run for 30 minutes

105

Figure 2.11: From left to right: Positive control and plasma samples following treatment with acid/base in triplicate. Note the lack of precipitate.

106

Figure 2.12: Amplitude results obtained from citrated plasma spiked with 10 EU/mL to give a final concentration of 0.1 EU/ml when tested. Prior to analysis, spiked samples had been stored at **ambient** conditions and were subsequently subjected to the pre-treatment protocol described in Section 2.2.3. Black curve represents the amplitude results obtained from a 0.1 EU/mL standard. N=1 for each day as this was a screening experiment. Test was run for 30 minutes

107

Figure 2.13: Amplitude results obtained from citrated plasma spiked with 10 EU/mL to give a final concentration of 0.1 EU/mL and stored at 2 -8 °C. Prior to analysis, spiked samples had been stored at the **refrigerator** and were subsequently subjected to the pre-treatment protocol described in Section 2.2.3. Black curve represents the amplitude results obtained from a 0.1 EU/mL standard N=1 for each day as this was a screening experiment. Test was run for 30 minutes

107

Figure 2.14: Amplitude results obtained from citrated plasma spiked with 10 EU/mL to give a final concentration of 0.1 EU/ml when tested. Prior to analysis, spiked samples had been stored at **ambient** conditions and were subsequently subjected to the pre-treatment protocol described in Section 2.2.3 which includes centrifugation. Black curve represents the amplitude results obtained from a 0.1 EU/mL standard. N=1 for each day as this was a screening experiment. Test was run for 30 minutes

109

Figure 2.15: Amplitude results obtained from citrated plasma spiked with 10 EU/mL to give a final concentration of 0.1 EU/ml when tested. Prior to analysis, spiked samples had been **refrigerated** and were subsequently subjected to the pre-treatment protocol described in Section 2.2.3, which includes centrifugation. Black curve represents the amplitude results obtained from a 0.1 EU/mL standard. N=1 for each day as this was a screening experiment. Test was run for 30 minutes.

109

Figure 2.16. Endotoxin calibration curve, showing the transformed Log values of time needed to reach 80% of starting amplitude on y axis and the transformed Log values of endotoxin concentration on x axis.  $R^2 = 0.9925$ ,  $R = 0.9962$ .

111

Figure 2.17: Amplitude results obtained from unspiked citrated plasma following dilution 1 in 10 with endotoxin-free water and magnesium chloride at 5mM concentration, heating, pH adjustment and centrifugation. N=4.

111

Figure 2.18 A and Figure 2.18 B show the percentage of endotoxin recovery across seven days in samples stored at room temperature and fridge. Figure 2.18 A shows the percentage of endotoxin recovery following treatment with protocol 1. Figure 2.18 B shows the percentage of endotoxin recovery following treatment with protocol 2.

113

### Chapter 3

Figure 3.1: A typical electrochemical cell. CE: Counter electrode, RE: Reference electrode, WE: Working electrode (Lee et al. 2017)

131

Figure 3.2 Cyclic voltammogram of a bare gold electrode subjected to electropolishing between 0 V and 1.5 V in 0.5M  $H_2SO_4$ . (McCormick et al. 2021).

131

Figure 3.3: The relationship between a sinusoidally applied potential (blue line) and the resulting current measured (red line) as a function of frequency. The measured current is out of phase from the applied potential (Choi et al. 2020).

133

Figure 3.4: Lissajous plot generated by plotting the sinusoidal applied potential and the resulting sinusoidal current. The characteristic oval shape is representative of the phase

angle between the two signals, and its shape can change from a perfect circle to a straight line, depending on the phase shift. (Magar et al. 2021).

134

Figure 3.5: A typical Nyquist plot. Real impedance is on the x axis, while imaginary impedance is on the y axis. Impedance is represented as a vector of length (arrow). The phase angle is formed between the vector and the x axis. Impedance at low frequencies is shown on the x axis, on the left, whereas higher frequencies are found at the right of the x axis (Magar et al. 2021).

135

Figure 3.6: Randle's equivalent circuit consisting of solution resistance ( $R_s$ ), double layer capacitance ( $C_{dl}$ ), charge-transfer resistance ( $R_{ct}$ ) and Warburg's impedance ( $Z_w$ ).

135

Figure 3.7: EIS graphs obtained following assessment of a clean gold electrode (yellow), an electrode surface modified with 11-mercaptoundecanoic acid (blue) and a modified surface on to which a ligand has bound (red). Solution resistance  $R_s$  can be detected at the higher frequencies on the x axis (not visible in graph). Charge-transfer resistance can be seen in lower frequencies ( $R_{ct}$ ). During EIS measurements, a difference in charge-transfer resistance is noted between the modified electrode surface (MUA-modified electrode, blue) and following challenge with ligand (red). Warburg's impedance, a vertical line at the lower frequencies, can be seen, and is used to study diffusion processes.

136

Figure 3.8: The bulk imprinting process. Following the interaction of the template with the monomers in solution, polymerization is initiated which results in the formation of a molecularly imprinted cavity on removal of the template species (BelBruno 2019).

138

Figure 3.9. MIPs and their formation on gold electrodes. Polymer formation around an immobilized aptamer-endotoxin complex, following the removal of endotoxin, leaves behind an aptamer-lined imprinted site capable of recognizing endotoxin.

139

Figure 3.10 aminophenylboronic acid, the monomer of choice in this project.

140

Figure 3.11: Cyclic voltammogram showing the cleaning process of a gold electrode. The sharpness of the oxidation and reduction peaks improves between cycles 1 – 25. The process was repeated until no further changes in the voltammogram were observed.

148

Figure 3.12: Electrochemical impedance spectra of 6-mercaptohexanol (MCH), 4,4-dithiodibutyric acid (DTBA) and 11-mercaptopundecanoic acid (MUA) modified gold electrodes. N=3 for each alkanethiol. EIS curves are exemplar for each molecule.	150
Figure 3.13: SAMs were challenged with reduced (“activated”) aptamers. DTBA shows very little interaction, whereas an increase in impedance can be observed with MCH and MUA.	151
Figure 3.14. DTBA, MCH and MUA SAMs were challenged with endotoxin concentrations ranging from 0.1 to 1000 pg/mL in <b>PBS pH 7.4</b> . MCH and DTBA show little interaction with endotoxin whereas MUA shows significant interaction with endotoxin at higher concentrations (10, 100 and 1000 pg/mL)	152
Figure 3.15. DTBA, MCH and MUA SAMs were challenged with endotoxin concentrations ranging from 0.1 to 1000 pg/mL in <b>TE buffer pH 8</b> . MCH and DTBA show little interaction with endotoxin whereas MUA shows significant interaction with endotoxin at higher concentrations (1, 10, 100 and 1000 pg/mL)	152
Figure 3.16: DTBA, MCH and MUA SAMs were challenged with endotoxin concentrations ranging from 0.1 to 1000 pg/mL in <b>MES buffer pH 4.9</b> . MCH and DTBA show little interaction with endotoxin whereas MUA shows significant interaction with endotoxin at higher concentrations (1, 10, 100 and 1000 pg/mL)	153
Figure 3.17: Exemplar EIS graph showing the impedances of the aptasensor <b>in PBS</b> (N=3) following challenge with various concentrations of endotoxin (0.01 pg/mL up to 1000 pg/mL).	155
Figure 3.18.A and 3.18 B. Figure A shows the sensor’s differences in impedance following challenge with various concentrations of endotoxin (from 10 fg/mL up to 100 ng/mL). Figure B shows the dynamic range of the sensor, exhibiting good linearity between 0.5 pg/mL up to 1 ng/mL ( $r^2=0.9810$ ).	155
Figure 3.19: The aptasensor was challenged with a range of endotoxin concentrations, ranging from 0.002pM (0.01 pg/mL) up to 200 pM (1 ng/mL) to determine its binding performance. A one site-total model was used, showing a good fit with a $R^2$ of 0.9443.	158
Figure 3.20 A and B: Figure A shows the sensor’s differences in impedance in <b>MES buffer pH 4.9</b> following challenge with various concentrations of endotoxin (from 10 fg/mL up to 100 ng/mL). Figure B shows the dynamic range of the sensor, exhibiting linearity between 1 pg/mL and 500 pg/mL.	158
Figure 3.21 A and B: Figure A shows the sensor’s differences in impedance in <b>TRIS buffer pH 8</b> following challenge with various concentrations of endotoxin (from 10 fg/mL up to 100	

ng/mL). Figure B shows the dynamic range of the sensor, exhibiting linearity between 0.1 pg/mL and 100 pg/mL. 159

Figure 3.22: Voltammogram obtained following the polymerization of APBA (10 cycles). PAPBA is conducting in nature, as indicated by the increasing redox peaks, indicated by arrows. 160

Figures 3.23 A and B: EIS graphs showing the impedances obtained after each cycle (1-4) of APBA (50mM) polymerization. An increase in impedance is noted with each subsequent cycle. 161

Figure 3.24: EIS graphs showing the impedances obtained after cycles 5, 7 and 10 of APBA electropolymerization (25mM). An increase in impedance is noted with each subsequent cycle. 161

Figure 3.25 Dose response graph of the NIP when challenged with a variety of endotoxin concentrations, ranging from 1 fg/mL to 100 pg/mL. The NIP shows a moderate interaction with endotoxin at higher concentrations. 162

Figure 3.26: EIS graph showing the impedance of a MIP before washing (black curve) vs the impedance obtained following washing with 0.05% tween (red). A small decrease in impedance can be noted, indicative of endotoxin removal. 163

Figure 3.27: Exemplar EIS graph of an APBA molecularly imprinted polymer, showing a dynamic range of 1pg/mL up to 1 ng/mL 164

Figure 3.28: Following incubation with endotoxin, the MIP sensor showed a linear response between 1 pg/ml and 1 ng/ml ( $R^2 = 0.7587$ ). 164

Figure 3.29: CV graph showing the CV of a clean electrode (black), compared to the CV of a gold electrode modified by the attachment of endotoxin-aptamer complexes on its surface, prior to polymerization (green), which results in a decrease in peak current. The formation of a polymer layer results in a further decrease in peak current, indicated by the red CV curve. Following the washing step in 0.05% tween, a small increase in peak current can be noted (blue line). 165

Figure 3.30 A and B: EIS graph showing the impedances of the hybrid-MIP sensor. A dynamic range between 10 fg/mL and 1 ng/mL is demonstrated. Figure 3.30 B: Dose-response graphs of the apta-MIP and aptaNIP when challenged with a variety of LPS concentrations, ranging from 10 fg/ml to 1 ng/ml. The sensor shows a linear response between 10 fg/ml and 100 pg/ml ( $R^2 = 0.9321$ ), with a high increase in impedance (approx. 27% for 10 fg/mL) showing the best sensitivity so far in the study. N=3 for each data point. 166

Figure 3.31: Comparison of the two MIP systems developed in this study. A significant difference in the dynamic range and sensitivity between the two systems can be observed, with the hybrid system displaying superior performance. N=3 for all values.

166

Figure 3.32: Dose-response graph for the AptaMIP. GraphPad prism was used to calculate the binding kinetics and the Langmuir-Freundlich binding model (“one site-total”) was chosen. A  $R^2$  of 0.9246 was determined, and the system displays a  $K_d$  of 1.006 pM.

168

Figure 3.33 Comparison of the changes in  $\Delta R$  between the generated systems. The progression of the study, starting from the aptasensor and finishing with the apta-MIP, demonstrates a continuous improvement in performance. All systems used the model  $R_s((R_{ct}W)Q_{dl})$  to characterise the circuit.

169

Figure 3.34: Comparison of the changes in impedance following incubation of the aptaMIP and AptaMIP with various concentrations of HSA. Results indicate a concentration-dependent effect on biofouling.

170

Figure 3.35: Comparison of the changes in impedance following incubation of the AptaMIP with various concentrations **HSA + 10 pg/mL** of endotoxin. Results indicate that the combination of HSA with endotoxin leads to higher impedances compared with HSA alone, suggesting a synergistic effect.

171

Figure 3.36: Comparison of the changes in impedance following incubation of the MIP and AptaMIP with various concentrations of IL-6. Results indicate that out of all systems tested, the aptaMIP showed the lowest levels of interaction.

172

Figure 3.37: EIS graph showing the response of the aptaMIP (black) following incubation with trisodium citrate 3.2% (blue) and 3.5mM glucose (red). Very little change in impedance was noted across both samples. N=1 as this was a screening experiment.

173

## Chapter 4

Figure 4.1: EIS results showing the response of the aptaMIP following incubation with various dilutions of unspiked plasma (N=3). Incubation with tenfold diluted plasma caused a large increase in impedance (approximately 88%), and increased plasma concentrations resulted in further increases in impedance, suggesting high levels of biofouling that cannot be resolved by dilution alone.

191

Figure 4.2 A-C: EIS results showing the response of the aptaMIP following incubation of the Aptamip (black lines) with various dilutions of spiked citrated plasma (red lines). Figure 4.2 A shows the results following incubation with spiked undiluted plasma, B shows the results following incubation with spiked twofold diluted plasma, and C shows the results following incubation with spiked tenfold diluted plasma. 192

Figure 4.3: EIS results showing the response of the aptaMIP (black curve) following incubation with plasma treated according to the Chapter 2 protocol (red curve). A decrease in impedance (approximately -47%) was observed. 193

Figure 4.4 A and B: EIS results showing the response of the aptaMIP (black curve) following incubation with **unspiked** (A) and **spiked with 10 fg/mL** plasma (B) treated according to the Chapter 2 protocol, with a lower concentration of HCl and NaOH (0.1 M), as well as **5mM MgCl<sub>2</sub>** (red curve). An increase in impedance (approximately 80% for unspiked plasma and approximately 115% for spiked) was observed for both samples. 194

Figure 4.5 A: EIS results showing the response of the aptaMIP (black curve) following incubation with plasma treated according to the Chapter 2 protocol, with a lower concentration of HCl and NaOH (0.1 M each) **and without MgCl<sub>2</sub>** (red curve). An increase in impedance (approximately 55%) was observed. Figure 4.5 B shows the response of the aptaMIP (black line) following incubation with plasma **spiked with 10 fg/mL**, following the same preparation protocol 195

Figure 4.6 A: EIS results showing the response of the aptaMIP (black curve) following incubation with plasma filtered using a cellulose syringe filter (red curve). No changes in impedance were observed. Figure 4.6 B shows the response of the aptaMIP (black curve) following incubation with spiked plasma filtered using a cellulose syringe filter (red curve). A 4% change in impedance was observed. 197

Figure 4.7: EIS graph showing the aptaMIP (black line) response following incubation with a water sample spiked with 10 pg/mL endotoxin and then subjected to filtration through a cellulose syringe filter (red line) and the same solution without filtration (blue line). N=1 as this was a screening experiment. 197

Figure 4.8: EIS results showing the response of the aptaMIP (black curve) following incubation with plasma treated according to the Chapter 2 protocol, with a lower concentration of HCl and NaOH (0.1 M each) **without MgCl<sub>2</sub> and including centrifugation** (red curve). An increase in impedance (approximately 47%) was observed for the unspiked plasma, with an increase of 52% noted following addition of plasma spiked with 10 fg/mL endotoxin. 198

Figure 4.9: EIS results showing the response of the aptaMIP (black curve) following incubation with unspiked plasma treated according to the Chapter 2 protocol, with a lower concentration of HCl and NaOH (0.1 M each) **including NaDOC, without MgCl<sub>2</sub> and including centrifugation** (red curve). An increase in impedance (approximately 15%) was observed.

199

Figure 4.10: EIS graph showing the response of the aptaMIP following incubation with water and plasma samples spiked with 10 fg/mL endotoxin and subjected to treatment with the optimised sample treatment protocol, including dilution, acid-base treatment, NaDOC addition and centrifugation. N=1 as this was a screening experiment

200

Figure 4.11: Photo showing the formation of white precipitate at the bottom of a centrifuge tube, following the completion of the finalized sample preparation protocol.

200

Figure 4.12. Percentage change following incubation of the aptaMIP with unspiked plasma following various sample preparation treatments

201

Figure 4.13 Percentage change following incubation of the aptaMIP with plasma spiked with 10 fg/mL following various sample preparation treatments. The response obtained with 10 fg/mL endotoxin in water is added for comparison (light grey bar, rightmost side).

201

Figure 4.14. EIS graph showing the response of the aptaMIP to spiked plasma samples subjected to the optimised pre-treatment protocol described in 4.3.1.4. N=1 as this was a screening experiment.

202

Figure 4.15: EIS graph showing the dynamic range of the aptaMIP (dark blue line) following incubation with a range of treated plasma spiked with endotoxin (10 fg/mL – 100 pg/mL). An increase in impedance is noted with increasing concentrations.

203

Figure 4.16: Dose-response graph of the aptaMIP when challenged with a variety of endotoxin concentrations in both water and treated plasma, ranging from 10 fg/ml to 100 pg/ml. The sensor shows a good linear response in plasma between 10 fg/ml and 100 pg/ml ( $r^2 = 0.9321$   $r = 0.9654$ ).

204

Figure 4.17 A: EIS graph showing the impedances of unspiked plasma (N=3) following prolonged storage at **room temperature**, for up to 15 days. 4.17 B shows the % $\Delta R$  corresponding to figure 4.17 A.

205

Figure 4.18: EIS graph showing the impedances of unspiked plasma (N=3) following prolonged storage in the fridge, up to 15 days. 4.18 B shows the % $\Delta R$  corresponding to figure 4.18 A.

206

Figure 4.19 A: EIS graph showing the impedances of plasma spiked with 100 fg/mL endotoxin (N=3) following prolonged storage in the fridge, up to 15 days. 4.19 B shows the calculated spike recoveries for each day tested. 208

Figures 4.20 A and B show photos of plasma following prolonged storage. Figure 4.20 **A and B** show the treated spiked plasma samples, following incubation for 22, 17 9 and 2 days respectively, immediately after centrifugation. Figure 4.20 B shows sealed, untreated plasma samples, following incubation for t=0, 2 days and 7 days at room temperature 208

Figure 4.21 A: EIS graph showing the impedances of plasma spiked with 100 fg/mL endotoxin (N=3) following prolonged storage in the fridge, up to 15 days. 4.21 B shows the calculated spike recoveries for each day tested. 210

Figures 4.22 A and B show two sealed plasma samples incubated for 15 days, against two different backgrounds. Left sample was incubated in the fridge, right sample was incubated at room temperature. 211

Figure 4.23 EIS graph showing impedances following 1 hr incubation in 0.05% tween 20 (blue line) and subsequent incubation with 10 fg/mL (red line). No significant response was noted. 212

Figure 4.24 EIS showing impedances following 1 hr incubation in **5% acetic acid** and subsequent incubation with 10 fg/mL. No significant response was noted. 213

Figure 4.25: EIS graph showing the response of the aptasensor following the addition of spiked plasma subjected to the plasma preparation protocol used for the aptaMIP. 214

## Chapter 5

Figure 5.1: Schematic representation of the aptasensor fabrication process, as described in the Tertiş et al paper (Tertis et al. 2019). 224

Figure 5.2: The compound chosen to be taken forward for experiments with the IL-6 aptamer and beta globin. 230

Figure 5.3: EIS graph showing the impedance of MUA following EDC/NHS coupling (black line) and following 1hr incubation with anti-IL6 antibodies (red line). 231

Figure 5.4: EIS graph showing the dynamic range of a simple IL-6 immunosensor, following incubation with IL-6 (5 pg/m – 150 pg/mL). A decrease in impedance is noted following IL-6 binding. 232

Figure 5.5: EIS graph showing the dynamic range of a Protein G IL-6 immunosensor, following incubation with IL-6 (12.5 pg/m – 150 pg/mL). A decrease in impedance is noted following IL-6 binding. 233

Figure 5.6: Dose-response graph showing the absolute response of the Protein G sensor following incubation with IL-6 (12.5 pg/m – 150 pg/mL) in PBS. The sensor shows a limited linear response in PBS between 12.5 pg/ml and 75 pg/ml, with a  $r^2$  value of 0.9576. 234

Figure 5.7: Shows the  $\% \Delta R/R_0$  of alkanethiol SAMs following incubation with 25 pg/mL IL-6. 235

Figure 5.8: EIS graph showing the impedance of an IL6 aptamer monolayer (red) followed by MCH backfilling (blue). 236

Figure 5.9: EIS graph showing the impedance of an IL6 aptamer monolayer following MCH backfilling (red) followed by incubation with 5 pg/mL IL-6 (blue). A large reduction in impedance is noted. 236

Figure 5.10: EIS graph showing the impedance of an IL6 aptamer monolayer following MCH backfilling (black) followed by incubation with a range of IL-6 concentrations (0.1 – 10 pg/mL). 237

Figure 5.11: EIS graph showing the response of a DTBA-IL-6 aptasensor following incubation with IL-6 (100 fg/mL – 3 pg/mL). A decrease in impedance is noted following IL-6 binding. 238

Figure 5.12: EIS graph showing the impedances of the mixed DTBA-aptamer sensor (black) and the same sensor following incubation with the sensitizer (red). A sharp decrease in impedance is noted. 239

Figure 5.13: CVs of the aptasensor following incubation with sensitizer and further addition of IL-6 at 2 and 75 pg/mL. 240

Figure 5.14 EIS graph showing the detection range of the aptamer following incubation with sensitizer and various concentrations of IL-6 in water. 241

Figure 5.15: Shows the  $\% \Delta R/R_0$  of the sensor following following incubation with sensitizer and various concentrations of IL-6 in water.

241

Figure 5.16: EIS graph showing the detection range of the aptamer following incubation with sensitizer and various concentrations of IL-6 in citrated blood plasma.

243

Figure 5.17: Shows the  $\% \Delta R/R_0$  of the sensor following following incubation with sensitizer and various concentrations of IL-6 in citrated blood plasma. A linear range is noted between 10 fg/mL and 25 pg/mL

243

Figure 5.18: A shows the sensor's (black) response following incubation with citrated plasma following tenfold dilution. 5.18 B shows the  $\% \Delta R/R_0$  of the sensor following incubation with various HSA concentrations and tenfold diluted plasma. 5.18 C and D show the  $\% \Delta R/R_0$  of the sensor following following incubation with various concentrations of IL-10 and endotoxin.

244

Figure 5.19: EIS graph showing the response of a capture-DNA strand without any spacers. A reduction in impedance was observed on addition of the complementary strand.

246

Figure 5.20: EIS graph showing the MCH-backfilled DNA sensor following incubation with various concentrations of target DNA.

247

Figure 5.21: EIS graph showing the impedances of the MCH backfilled ss-DNA sensor (black) and the same sensor following incubation with the sensitizer (red). A sharp decrease in impedance is noted.

248

Figure 5.22: CVs of the MCH backfilled ss-DNA sensor following incubation with the sensitiser and further addition of beta-globin DNA at 0.01  $\mu$ M.

249

Figure 5.23 EIS graph showing the detection range of the MCH DNA sensor following incubation with sensitizer and various concentrations of beta globin in water.

249

Figure 5.24: Shows the  $\% \Delta R/R_0$  of the sensor following following incubation with sensitizer and various concentrations of beta globin in water. A linear range is noted between 0.01 and 2  $\mu$ M.

250

Figure 5.25: EIS graph showing the detection range of the aptamer following incubation with sensitizer and various concentrations of beta globin in citrated blood plasma.

251

Figure 5.26: Shows the  $\% \Delta R/R_0$  of the sensor following following incubation with sensitizer and various concentrations of beta globin in citrated blood plasma. A linear range is noted between 0.01 and 10  $\mu\text{M}$

251

Figure 5.27 A shows the  $\% \Delta R/R_0$  of the sensor following following incubation with various HSA concentrations and tenfold diluted plasma. 5.27 B and C show the  $\% \Delta R/R_0$  of the sensor following following incubation with various concentrations of IL-10 and endotoxin respectively.

253

## Chapter 6

Figure 6.1: EIS graph showing the detection range of the endotoxin aptasensor following incubation with sensitizer and various concentrations (0.001 fg/mL – 1 pg/mL) of endotoxin in water.

267

Figure 6.2: Shows the  $\% \Delta R/R_0$  of the sensor following following incubation with sensitizer and various concentrations of endotoxin in water. A linear range is noted between 0.001 fg/mL and 100 fg/mL

267

## List of tables

Table 1.1: Biosensor transducer types (Xu and Lee, 2020). 27

*Table 2.1: Sample preparation approaches presented in this chapter with experimental details* 94

# Chapter 1

## General Introduction and literature review

---

## 1.1 Overview

Pneumonia, a severe lower respiratory tract infection affecting the alveoli is one of the leading causes of death in children under 5, especially in developing countries (Rudan et al. 2008). In addition, despite vaccination coverage in the developed world it continues to be prevalent and a leading cause of child morbidity. In the UK, it is estimated that 473 for every 100,000 children between the ages of 0-5 will fall ill each year with pneumonia (British lung foundation, 2012). Pneumonia is caused by a number of bacteria, viruses and fungi. Bacteria commonly causing pneumonia include *Mycoplasma Pneumoniae*, *Streptococcus pneumoniae*, *Haemophilus influenzae*, *Legionella pneumophila*, *Chlamydothyla pneumoniae* (Stralin et al. 2005). Viruses include influenza viruses A, B (Flu A, Flu B); respiratory syncytial virus (RSV) subgroup A and B; parainfluenza virus (PIV1, PIV2, PIV3); adenovirus (AdV); rhinovirus (RV); enterovirus (EV); and coronavirus (CoV) Human metapneumovirus (hMPV) and human bocavirus (HBoV)(Stellrecht 2017). Fungi include *Pneumocystis jirovecii*, *Aspergillus spp.*, *Candida spp.* and *Chrysosporium spp.*, and are more prevalent in immunocompromised children, including malnourished and HIV+ children (Armstrong-James et al. 2014).

In addition, pneumonia can lead to the development of systemic conditions such as sepsis (Garcia-Vidal et al. 2010). Sepsis can be described as the body's rapidly evolving systemic immunological response to an infectious process that can lead to end-stage organ dysfunction and death and is the leading cause of death in children worldwide. As pneumonia is the most common cause of paediatric sepsis, early diagnosis and treatment is crucial to prevent disease progression to sepsis (Garcia-Vidal et al. 2010).

The overuse of antibiotics is one of the main drivers of antimicrobial resistance in the UK, with half of patients consulting their GPs for cold, cough or viral sore throat being prescribed antibiotics (McNulty et al. 2013). This may be due to the fact that limited diagnostic tests are available at point of care to help decision making and guide patient treatment, which is why such technology is really needed, hence this project. It would therefore be of great importance to not only develop a rapid pneumonia detection system, but also a platform capable of differentiating between viral or bacterial infection, which would therefore lead to the appropriate treatment and reduce misuse of antibiotics and become a player in the fight against antibiotic overuse (Lingervelder et al. 2019).

The overarching aim of this PhD project is to develop a point-of-care biosensor for the early, rapid and accurate diagnosis of bacterial pneumonia, though collaboration with other members of the interdisciplinary training hub of Cardiff University. Such a sensor would allow for the fast diagnosis of pneumonia, provide guidance on patient treatment, and assess the risk of developing sepsis secondary to pneumonia.

## 1.2 Pneumonia

Pneumonia is commonly described as an acute infection of the lung tissue, affecting mainly the lower airways (bronchi and alveoli), with its main symptoms being fever, cough, chest pain and shortness of breath (Katz and Williams 2018; Sattar and Sharma 2021). Pneumonia is a significant cause of morbidity and mortality, as well as economic burden to health systems worldwide, as lower respiratory tract infections are responsible for more deaths than any other infection in the US (Mizgerd 2008). However, pneumonia is a cause of concern especially in children, as it is the largest single cause of childhood morbidity and mortality worldwide in children between the ages of 28 days and 5 years (Collaborators 2018). In addition, pneumonia can also develop into complicated pneumonia, which happens in approximately 3% of pediatric cases, which can lead to parapneumonic effusion, empyema, necrotizing pneumonia, and lung abscess (de Benedictis et al. 2020). Moreover, pneumonia can also cause systemic complications, the most severe of which is sepsis and septic shock, metastasis of infection, multi organ failure, acute respiratory distress syndrome (ARDS) and death (de Benedictis et al. 2020). Pneumonia is additionally a major cause of economic burden for health systems, as across Europe, hospital care for the disease costs approximately €5.7 billion (Chalmers et al. 2017). In addition, in the UK, it is responsible for more hospital admissions and bed days in comparison to any other lung disease (Chalmers et al. 2017). Unfortunately, hospitalized patients due to pneumonia have a mortality rate of 5% to 15%, increasing to more than 30% for those admitted to intensive care, and eventually 29,000 deaths in the UK will be attributed to the disease (Lim et al. 2009; Chalmers et al. 2011; Chalmers et al. 2017). Approximately 2.56 million people die from pneumonia globally, and in 2017, 808,694 children under the age of five died of pneumonia, which made up a fifth of all deaths of children that year (Bakare et al. 2020; Lin et al. 2020).

Sepsis is defined as the body's excessive systemic immune response which can lead to homeostatic dysregulation, hypotension, organ failure and death (Gyawali et al. 2019). The prevention of pneumonia developing into sepsis is of great importance, as the mortality rate in Europe is estimated to be at around 40% (Levy et al. 2012). In addition, sepsis claims around 31,000 lives and costs the NHS in England about £2 billion (UK government, 2015). Therefore, it would make sense to focus on the prevention of sepsis secondary to pneumonia and its rapid and accurate diagnosis.

According to the American Thoracic Society, three classifications of pneumonia have been defined, based on the etiology and clinical setting where the disease was acquired. These are Community Acquired Pneumonia (CAP), which is acquired in a community setting outside of a hospital, Hospital Acquired Pneumonia (HAP), which is acquired 48hrs after hospital admission excluding ventilation, and Ventilator Associated Pneumonia (Abbina et al.), which is acquired 48hrs after endotracheal intubation (Jain et al. 2021). The most common bacterial pathogens responsible for CAP are *Pneumococcus*, *Haemophilus influenzae*, *Moraxella*

*catarrhalis*, Group A *Streptococcus*, among others, as well as less common bacteria such as *Legionella*, *Mycoplasma* and *Chlamydia* (Jain et al. 2021). Viruses commonly causing CAP include the influenza virus, followed by respiratory syncytial virus (RSV), parainfluenza virus, and adenoviruses (Jain et al. 2015). In addition, although not as common as the previous two causes, fungi responsible for pneumonia mainly in immunocompromised patients include *Histoplasma*, *Blastomyces*, and *Coccidioides* (Hage et al. 2012). In HAP and VAP, although many causative pathogens are shared with those found in CAP, some interesting pathogens are encountered, such as *Escherichia coli*, *Pseudomonas Aeruginosa*, *Acinetobacter* and *Enterobacter*, as well as Methicillin-resistant *Staphylococcus aureus* (Weiner et al. 2016). However, despite the plethora of bacteria responsible for CAP, the main causative pathogen is *S. pneumoniae*, followed by *Klebsiella pneumoniae* and *Haemophilus influenzae* (Brown 2012; Sattar and Sharma 2021).

### 1.2.1 Immunopathogenesis of pneumonia

The pathogenesis of pneumonia is a complex process, which involves the activation of both the innate and adaptive immune responses, signaling pathways and the production of various pro- and anti-inflammatory mediators, some of which will be described in more detail in the following section (review of biomarkers). As the host-pathogen interactions, the amount of inoculum and the immune responses from adaptive and innate immunity can determine the severity of pneumonia, it is important that they are understood in detail (Alcon et al. 2005).

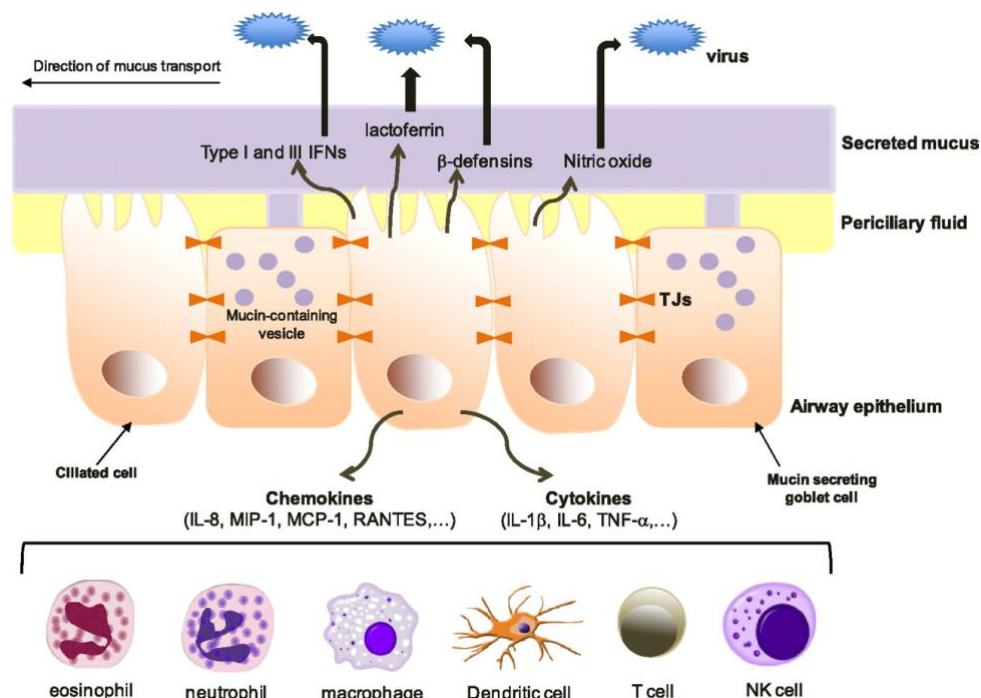


Figure 3.1 Epithelial immunity in the lung (Vareille et al. 2011)

**Innate immunity** is defined as the primordial system that plays a key role in the antimicrobial defense of the lung, through recognition and response to pathogens and microbial products in the lungs, as well as other tissues (Martin and Frevert 2005). Innate immunity involves the

anatomical barriers that inhibit the infiltration of pathogens into the lung environment, such as the layers of mucus, the tight adhesions between epithelial cells and the underlying structures, and the of fluid and antimicrobial molecules that assist mucociliary clearance. Figure 1.2 provides an outline of the epithelial immunity in the lung. The diverse cell populations found in the lung, such as ciliated cells and secretory cells including serous, club, neuroendocrine and goblet cells, contribute to the production of a number of diverse antimicrobial peptides and fluids that contribute to lung defense (Figure 1.2) (Whitsett and Alenghat 2015). The movement of ciliated cells is key to mucociliary clearance, as patients with primary ciliary dyskinesia show impaired bacterial clearance and severe lung disease (Knowles et al. 2013). Besides bacterial clearance, lung cells and especially lung goblet and club cells are responsible for the production of airway mucins which are fundamental in the defense against bacteria (Quinton et al. 2018). This is evident from studies where silencing the *Muc5b* gene in mice led to increased susceptibility to bacterial pneumonia, especially when caused by *S. pneumoniae*, and chronic inflammation (Roy et al. 2014). Additionally, the importance of mucus in host defense is evident from studies assessing the lower mucin content in cystic fibrosis patients' sputum and its association with susceptibility to lung infections (Henderson et al. 2014). Finally, the lung epithelial cells produce a plethora of host-defense molecules, such as human  $\beta$ -defensins, lysozyme, lactoferrin, cathelicidin LL37 and surfactant proteins A and D, all of which contribute to lung defense (Whitsett and Alenghat 2015).

Besides the passive protection provided by epithelial cells, they also play an important role in modulating the immune response following pathogen recognition. Epithelial cells undergo transcriptional responses upon recognition of pathogen-associated molecular patterns (PAMPs), damage-associated molecular patterns (DAMPs), cytokines and others (Quinton et al. 2018). Toll-like receptors, a class of pattern-recognition receptors, are expressed in a number of innate immune cells such as dendritic cells and macrophages, in addition to non-immune cells, such as fibroblast cells and epithelial cells. Although TLR signaling is not unique to lung cells, in lung epithelial cells it is critical for driving mucosal immune responses (Whitsett and Alenghat 2015). With regards to bacterial pneumonia, TLR4, which is expressed in the outer membrane of the cells, is the major recognition receptor of lipopolysaccharide (Armstrong et al. 2004). Figure 1.3 shows its structure. The downstream molecular signaling initiated by LPS binding to TLR4 is well established and has been described extensively (Takeuchi and Akira 2010; Kawasaki and Kawai 2014). TLR4 exhibits the unique property of activating two signaling pathways, the MyD88- and TRIF-dependent signalling pathways , which can be seen in figure 1.2 below (Takeuchi and Akira 2010). TLR4 can also be visualized in figure 1.3 below.

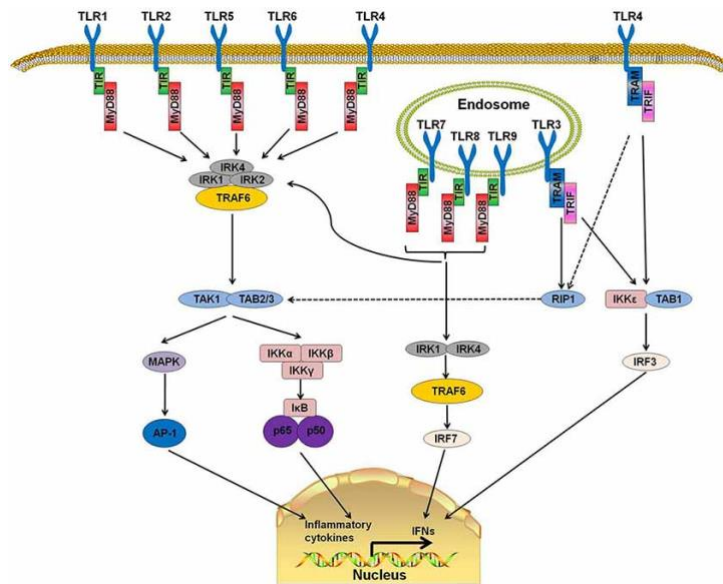


Figure 1.2: TLR signalling, including the MyD88 signaling pathway (Zheng et al. 2019)

The MyD88-dependent pathway (Figure 8) is required for early activation of NFκB while the TRIF-dependent pathway is crucial for the late phase activation of NFκB in response to LPS binding (Covert et al. 2005). In general, TLR4 activation eventually leads to the production of pro-inflammatory cytokines, such as TNF, IL-1β, IL-6, IL-18, anti-inflammatory cytokines, such as IL-10, transforming growth factor-beta (TGF-β), etc. as well as angiogenic mediators (vascular endothelial growth factor (VEGF), epidermal growth factor (EGF), TGF-β, etc. (Korneev et al. 2017). Finally, the last component of the innate lung immunity are the alveolar macrophages, located on the lower respiratory tract, which under normal conditions exhibit anti-inflammatory effects and are required for the clearance of clear environmental debris, excess lung surfactant and apoptotic cells (Hussell and Bell 2014). However, upon recognition of infection through their pathogen recognition receptors, they transform into promoters of inflammation (Taylor et al. 2005). Alveolar macrophages directly contribute to the fight against the infection by phagocytosing bacteria, plus the composition of reactive oxygen and nitrogen intermediates, which further assists with bactericidal activity. Finally, they also coordinate the inflammatory response through the utilization of RelA from the NF-κB transcription factor family, which enables them to release cytokines such as (TNF)-α, IL-6 and granulocyte colony stimulating factor (G-CSF) (Quinton et al. 2018).

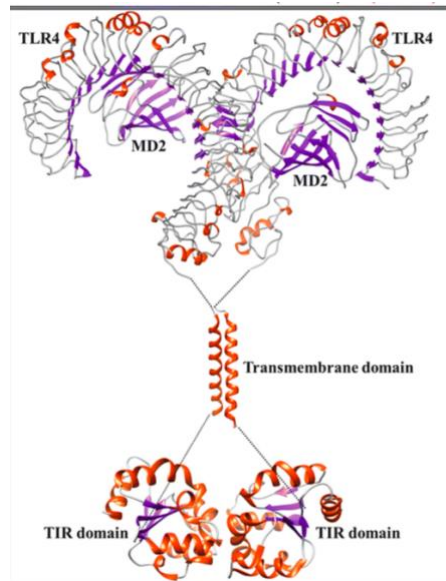


Figure 1.3: Toll-like receptor 4 structure (Krishnan et al. 2018)

### 1.2.2 Adaptive immunity

Adaptive immunity, also known as acquired immunity, is defined as the antigen dependent defense system, based primarily on the antigen-specific receptors expressed on the surfaces of T- and B-lymphocytes (Chaplin 2010). CD4+ T cells created by prior respiratory infections provide a high level of protection in comparison to primary effectors, as they produce a great variety of cytokines plus they better distribute T follicular helper (T<sub>FH</sub>) cells at the infection site. Of great importance in bacterial pneumonia are CD4+ Th17 cells, which are characterized by their capacity to produce interleukin 17, a pro-inflammatory cytokine which affects many cells in the body, including lung epithelial cells, and stimulates host defence against extracellular bacteria and fungi in the lungs (Tesmer et al. 2008; Chen and Kolls 2013). In adult humans, it has been demonstrated that in *S. pneumoniae* lung infection, CD4+ T cells produce IL-17 upon recognition of either pneumococcus or pneumococcal proteins, independent of serotype (Lundgren et al. 2012). This is also supported by a study where mice were challenged with one pneumococcal serotype before infection with another one, and it was demonstrated that both IL-17 and CD4+ T cells are needed for protection against heterotypic pneumococcal pneumonia (Wang et al. 2017b). IL-17 is also important in *Klebsiella pneumoniae* pneumonia, as it has been demonstrated, in a mouse model study involving mice infected with this pathogen, that TLR4 activation leads to IL-23 production by dendritic cells, which subsequently stimulates IL-17 production from CD4+ and CD8+ cells (Happel et al. 2003).

### 1.2.3 Pneumonia diagnosis - current approaches

According to diagnostic guidelines, a chest x-ray is considered the gold standard in the diagnosis of pediatric pneumonia, following initial clinical screening criteria, as it shows if there is any damage to the lungs (pulmonary infiltrate) and which areas are affected, but it cannot easily differentiate between bacterial pneumonia and pneumonia caused by other pathogens, neither can it identify the causative pathogen or co-infection, plus it is not always

available, especially in low-resource settings (Pahal et al. 2021). Exemplar x-rays of a healthy patient vs a pneumonia patient can be seen in figure 1.4 below. In addition, even after improvements, consolidation may not be visible or present in the early stages of the disease, which delays the diagnosis (Goodman et al. 2019). Lung ultrasound is an attractive point-of-care alternative to a chest x-ray, as it is faster, has high sensitivity and specificity, has no complications, can be used easily in resource-limited settings and does not include radiation exposure (Mackenzie 2016). However it suffers from the same drawbacks as a chest x-ray in terms of not identifying the infective cause (Mackenzie 2016).

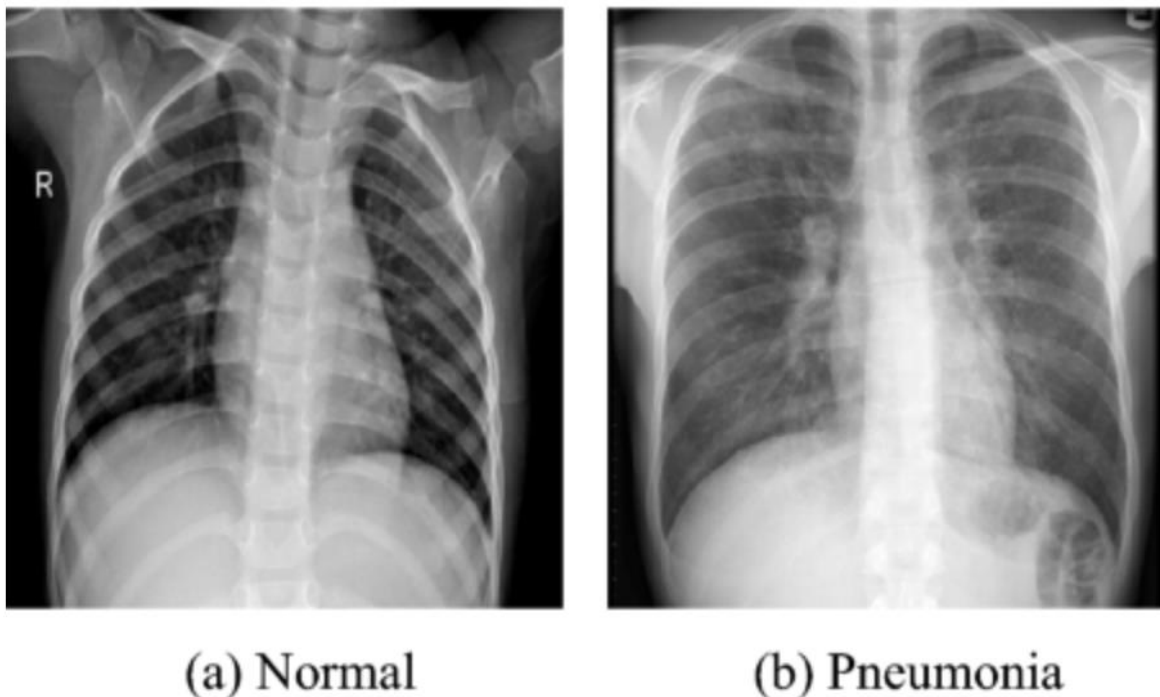


Figure.1.4: Chest x-ray of healthy patient (left) vs viral pneumonia (right). Adapted from (Ullah et al. 2023)

Older microbiology methods for pneumonia detection include blood cultures and the study of sputum or bronchoalveolar lavage fluid under a microscope, where identification of a pathogen provides good evidence of a pathogen causing pneumonia, however these methods require long incubation periods and have limited sensitivity, as well as a low yield (Murdoch et al. 2017; Kitsios et al. 2018). Culture-based microbiological tests have often been found to be negative in cases with a diagnosis of pneumonia, which may complicate treatment and delay antibiotic management (Jain et al. 2015). In the case of *S. pneumoniae* infections, blood cultures also have low sensitivity (van der Eerden et al. 2005). In addition, these methods have a long turnaround time of approximately 3 days, which can further delay treatment (Vincent et al. 2015). Furthermore, these sputum samples may also carry bacteria present as asymptomatic colonizers which may cause the detection of false positives or complicate the identification process (Murdoch et al. 2017). One benefit of blood tests is the indication of

whether the pathogen has spread into the blood, which can assist with the rapid treatment of sepsis (Shah et al. 2011). Viral cultures, which are considered the gold standard for the final diagnosis of viral infections also have drawbacks, mainly the long turnaround time of 10-15 days, which can significantly delay treatment, as well as the difficulty in culturing some viruses, the viability of the viruses in the specimen and the invasive sampling in the case of pneumonia (Freeman and Leigh 2021).

Nowadays, **Polymerase Chain Reaction (PCR)** has replaced in many cases the culture methods, as it has now become widely available, is rapid, accurate and specific, and is capable of detecting pathogens at miniscule amounts without the need for live organisms (Lorente et al. 2000). It is widely used for the detection of respiratory pathogens in a variety of body fluids (Lorente et al. 2000). In the case of PCR-based detection of *S. pneumoniae*, it depends on the amplification of *pneumococcus*-specific genes, such as the pneumolysin gene, pneumococcal surface adhesin A and pneumococcal autolysin A genes (Torres et al. 2016). A benefit of quantitative PCR is the ability to predict disease presentation and severity, which can correlate with levels of pneumococci DNA in clinical PCR samples (Torres et al. 2016). Another benefit is the ability to perform pneumococcal serotyping, which can be valuable in cases of bacteremia and severe pneumonia, and can also assess the effect of the pneumococcal vaccine to the patient, in addition to identifying genes associated with antibiotic resistance (Torres et al. 2016). Moreover, in comparison with culture methods, it allows the identification of noncultivable pathogens (Avni et al. 2010). However, one of the most well-known setbacks of PCR is the frequent contamination rate, usually caused by exogenous material or previously used extracts and primers, which can reduce specificity (Avni et al. 2010). Furthermore, another well-known PCR issue is the high rate of false-positive results, usually caused by human DNA and inhibitors present in blood, which can interfere with the hybridization process (Radstrom et al. 2004). Finally, issues arise with regards to the non-specific binding of the primers to repeat sequences in the DNA, problems with the binding of the primer to the template as well as incomplete primer binding all reduce the sensitivity and specificity of PCR (Radstrom et al. 2004).

#### **1.2.4 Point-of-care (POC) tests**

Given the drawbacks associated with many of the traditional diagnostic methods, the increase in demand for rapid, accurate and easy to use point-of-care (POC) diagnostic tests makes sense. In the last decades, POC tests have transformed the diagnostic process, by removing the need for sample analysis in a remote laboratory and by providing results in a short amount of time (usually around 15 minutes, in case of respiratory viruses <3 hours), thus leading to possible changes in patient care and facilitating antibiotic stewardship (Kozel and Burnham-Marusich 2017; Dave et al. 2019; Vos et al. 2019). They may range from handheld to benchtop size. As a result of their convenience, quick results turnaround and portability, POC tests have gained popularity in hospitals, care homes, ambulances and research centers in low resource settings (Dave et al. 2019). Currently, a number of POC tests have been employed for the

detection of hemoglobin concentrations, complete blood count (CBC), pregnancy testing, blood glucose concentration, cardiac biomarkers, coagulation testing, platelet function, group A streptococcus, HIV testing, malaria screening and others, and may replace laboratory testing for some tests (Larsson et al. 2015). An international survey of primary care clinicians found that the most commonly used POC tests were for blood glucose, urine pregnancy and urine leucocytes/nitrite (Howick et al. 2014). A main driving factor in the development of the POC market is the development of technology which includes the discovery of novel biomarkers, nanoparticle approaches and new imaging and connectivity methods, such as wireless or smartphone connectivity (Luppa et al. 2011). Despite the advances in technology, some characteristics are common in all settings, and some of the most important requirements in a POC test include (Unold and Nichols 2010):

- Being simple to use
- Reagents and consumables remaining stable in storage and usage.
- Results should be consistent with an established laboratory method.
- The device, alongside with the required reagents and consumables must be safe to use.

### **1.2.5 History of POC tests**

Possibly the first documented example of an immunoassay used for the detection of an infectious disease took place in 1917, where Dochez and Avery discovered that polysaccharide originating from *S. pneumoniae* could be detected by performing antigen detection from the serum and urine from patients with lobar pneumococcal pneumonia, and the authors commented on the importance of rapid antigen detection in the rapid diagnosis of a disease (Dochez and Avery 1917). Research in the efficient and rapid detection of antigens or antibodies continued throughout the decades, which resulted in the development of the radioimmunoassay and enzyme-linked immunoassay (Goodman et al.) in the 60s and 70s, respectively, with ELISA remaining today as the most widely used immunoassay platform technology in laboratory settings (Kozel and Burnham-Marusich 2017). Despite automation making ELISA a high-throughput procedure, it is still held back by the time-consuming, complex, multi-step nature of the assay, the need for training and the reliance on laboratory equipment (Kozel and Burnham-Marusich 2017). Still, the development of the beforementioned immunoassays led to interest in antigen detection and consequently to the development of early point-of-care tests. One such example which utilized capillary migration, was the development of porous strips of cellulose acetate with covalently attached antibodies coupled with enzyme-labeled antibodies to detect C-reactive protein in the 80s (Glad and Grubb 1981). At around the same time, coupling of antibodies to either colloidal gold or latex particles and their use as a label for immunoassays was discovered, and they were used for the detection of human placental lactogen (HPL) and human chorionic gonadotrophin (HCG) (Leuvering et al. 1980). This led the way towards the development of lateral flow immunoassay (LFIA) platforms which are widely employed today, such as the

home pregnancy tests and the rapid test for the diagnosis of streptococcal pharyngitis, in the case of infectious diseases (Kozel and Burnham-Marusich 2017). In particular, in the field of infectious diseases, most POC tests employ immunoassays, such as namely agglutination, immunochromatographic and immunofiltration tests (Clerc and Greub 2010). However, research is now looking into the development of new technologies, biomarkers and detection methods which could revolutionize the diagnosis and treatment of many conditions.

Despite the increasing popularity of lateral flow tests, many practices show hesitation in their implementation, mainly due to concerns over accuracy and reliability (Lingervelder et al. 2019). This was also observed during the COVID-19 pandemic, where concern was raised over the performance and reliability of rapid COVID tests (Wise 2020). The concern in effectiveness was observed in a study 15 years ago and unfortunately a similar level of concern remains to date (Howick et al. 2014). A reason why this issue remains may be due to the fact that few studies have focused on patient outcomes rather than test accuracy (Hislop et al. 2010). In that aspect, technological advancements and research have played an important role in the development of more accurate assays (Larsson et al. 2015). In addition, POC tests, because of their distributed nature tend to be more expensive compared to tests performed in a central laboratory, although not always, as is the case for some tests designed for use in low-resource settings (Asha et al. 2014). Despite the concerns, the speed and mobility offered by POC tests compared to traditional laboratory testing has been noted, as well as their role in improving patient care, workflow efficiency, and even provide financial benefits in health systems (Larsson et al. 2015). Over the past decades, the market for POC devices has increased as well as their use, with growth rates expected to average >15% in the US in the coming years (Larsson et al. 2015). Additionally, one of the ways to improve POC implementation, use and development is through communication and collaboration with medical professionals and physicians (Howick et al. 2014).

To date, no POC tests are available for pneumonia and/or sepsis secondary to pneumonia, nor are there any tests for monitoring disease progression or severity. Diagnosis of sepsis is mostly made based on chest x-rays, fulfillment of clinical criteria, and/or blood tests, which involve PCR, the drawbacks of which were discussed beforehand. Therefore, the need for the development of such a test is evident and will guide the aims of this project.

## 1.3 Review of biomarkers

### 1.3.1 The search for a suitable biomarker

By definition, a biomarker is “A defined characteristic that is measured as an indicator of normal biological processes, pathogenic processes or responses to an exposure or intervention” (Califf 2018). Ideally, a biomarker should be detectable early in disease, accessible, analytically stable throughout sample transport and treatment and easily quantifiable (Maksymowych 2014). Therefore, a literature review was undertaken at the first stages of the project, using the NCBI database and Ovid as search tools. Biomarkers were selected on their relevance to pneumonia or sepsis secondary to pneumonia, following an extensive literature search.

### 1.3.2 Interleukin 6

Interleukin-6 is a pleiotropic soluble mediator produced in response to tissue damage and infections and has been shown to have an effect in inflammatory processes, immune response and hematopoiesis (Tanaka et al. 2014). IL-6 (26 kDa in size) is a four-helical cytokine made up of 184 amino acids and is encoded by the IL6 gene (Figure 10) (Yasukawa et al. 1987). IL-6 is visualized in figure 1.5 below.



*Figure 1.5: IL-6 structure (Protein Data Bank, 2021)*

Its production has been observed by a number of cell types, including mast cells, macrophages, dendritic cells, T and B cells, and importantly, epithelial cells including lung epithelial cells (Mauer et al. 2015). Additionally, IL-6 has been shown to play a major role in host defense against viral, bacterial, fungal and parasitic infections (Gou et al. 2019). IL-6 is well known for its major role in the acute phase response, which is caused at the initial stages of infection and is characterized by the increased circulating levels of inflammatory markers produced by the liver (Quinton et al. 2009). In fact, IL-6 is responsible for the synthesis of the whole spectrum of acute phase proteins and mediators (Castell et al. 1989). Moreover, increased IL-6 levels are associated with several inflammatory and immune disorders, such as Crohn’s disease and rheumatoid arthritis (Hashizume 2020). Interestingly, a human genotype

linked to the -174 promoter region of IL-6, causing over induction of the cytokine, has been linked to protection against extrapulmonary pneumococcus infection (Schaaf et al. 2005). Finally, IL-6 has been shown to be important in the defense against pneumococcus. Therefore, IL-6 is not only a clinically important biomarker to study, but it is also one of the earliest biomarkers produced and its measurement can play a crucial role in the early detection of pneumonia.

### **1.3.3 Role in pneumonia**

At the first stages of pneumonia, alveolar macrophages produce proinflammatory cytokines, including IL-6 and tumor-necrosis factor  $\alpha$  (TNF- $\alpha$ ) which are capable of synchronizing and amplifying the immune response (Lee et al. 2010b). This attracts leukocytes to the site of infection, which further amplifies the immune response (Khattab et al. 2018). The role of IL-6 in community acquired pneumonia has been widely assessed in a number of studies. In a study, serum IL-6 levels appeared to be significantly higher in comparison with other cytokines or chemokines at admission (Endeman et al. 2011). Interestingly, it was also observed that IL-6 levels on admission were higher in patients with pneumonia caused by *S. pneumoniae* in comparison with nonpneumococcal pneumonia, which could possibly be explained by the fact that pneumococcal pneumonia is caused by an extracellular pathogen, possibly causing invasive disease and an enhanced immune response (Mufson 1999). Similar results were found by Ortqvist et al, where high IL-6 levels were not only associated with bacteremic pneumococcal pneumonia but also higher mortality (Ortqvist et al. 1995). Furthermore, IL-6 levels can be used as a measure of stress severity and disease severity (Puren et al. 1995). In addition, IL-6 levels in severe pneumonia have been also linked to confusion (Martinez et al. 2011).

Importantly, IL-6 also appears to be of relevance in pediatric pneumonia, which is evidenced by a number of studies. Khattab et al. found significantly elevated levels of serum IL-6 in correlation with pneumonia severity in children. Moreover, a positive correlation was found between IL-6 levels and length of hospital stay as well as disease severity, with high IL-6 levels linked to severe disease symptoms (Khattab et al. 2018). This comes in agreement with the results of two previous similar studies on pediatric pneumonia, where plasma IL-6 was also significantly elevated in pneumonia and was proportional to disease severity (Haugen et al. 2015; Saghafian-Hedengren et al. 2017). Furthermore, the link between IL-6 and indicators of disease severity was also highlighted in another study involving 15 cytokines and chemokines (Michelow et al. 2007). In children under 5 years of age, a study found that increased serum IL-6 levels were associated with pneumococcal pneumonia at concentrations above 12.5 pg/ml (Vasconcellos et al. 2018).

IL-6 has a narrow diagnostic window, as its serum levels are at the highest levels at day 1 of infection and begin to decline after day 3 in children and suggests that measuring cytokines 24-48hrs after the infection in order to characterize cytokine kinetics (Fuchs et al. 2018).

Following the same trend as previous studies, the same study also found an increased risk of hospitalization linked to high IL-6 levels in addition to antibiotic treatment. Another study found that IL-6 levels in the serum of children with severe pneumonia was higher at admission, further supporting the role of IL-6 in early diagnosis (de Brito et al. 2016).

IL-6 also has potential as a mortality prediction measure. Khattab et al noted the highest levels of IL-6 production from all patients were noted in the two patients who died. Combining the cytokine may provide an accurate measure of mortality, such as a study where IL-6 in combination with C-reactive protein showed a predictive value for predicting 30-day mortality in adults (Menendez et al. 2009). In addition, a study in children who required mechanical ventilation, significantly high IL-6 levels were observed in patients younger than 5 years old who died, further supporting the use of IL-6 as a mortality predictor (Nguyen Thi Dieu et al. 2017). Furthermore, IL-6 has been associated with not only worse pneumonia symptoms, but also with severe pneumonia and disease progression (de Brito et al. 2016).

#### 1.3.4 Interleukin 10

Interleukin 10 is well known for its role as an anti-inflammatory cytokine and its importance in maintaining homeostasis (Couper et al. 2008). It has a molecular weight of approximately 18.7 kDa and is transcribed by the IL10 gene (Iyer and Cheng 2012). Figure 1.6 shows its structure. It is a key immunoregulator during infection with viruses, fungi, bacteria, protozoans and parasites (Couper et al. 2008). In addition, it is the lead cytokine of the IL-10 family, which includes IL-10, IL-20, subfamily members IL-19, IL-20, IL-22, IL-24, and IL-26, and the distantly related cytokines IL-28A, IL-28B, and IL-29 (Ouyang and O'Garra 2019). IL-10 binds to IL-10R, a dimeric receptor predominantly expressed on leukocytes which exclusively detects IL-10, and an ubiquitously expressed IL-10R2 chain involved in the recognition of other cytokines from the IL-10 family (Rojas et al. 2017). IL-10 can be visualized in figure 1.6 below.

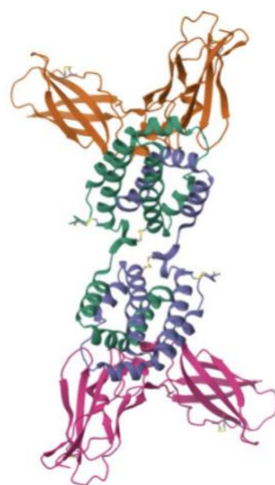


Figure 1.6: IL-10 structure (Protein Data Bank, 2024)

Initially thought of as an activity of activated CD4+ cells, its immunosuppressive effects were highlighted later, following cloning experiments (Fiorentino et al. 1991; Moore et al. 1993). It is produced by almost all cells of the immune system, including dendritic cells (DCs), macrophages, monocytes, T cells, natural killer (NK) cells, and B cells (Gabrysova et al. 2014). In macrophages and dendritic cells, its production is triggered after downstream signaling following pattern recognition receptors, such as Toll-like receptors (Gabrysova et al. 2014). Additionally, T cells are another major source of IL-10, and Th cell subsets are known to produce the cytokine in response to cytokines produced by other cells in response to infection, such as IL-12, IL-4, IL-17 and IL-27, as well as TGF- $\beta$  (Ouyang and O'Garra 2019). The immunosuppressive effect of IL-10 plays a major role in protecting the host from collateral damage caused by excessive cytokine production (Ouyang and O'Garra 2019). IL-10 has a unique suppressive effect in the immune response as it has been shown to inhibit the formation of pro-inflammatory cytokines such as IFN $\gamma$ , tumor necrosis factor  $\alpha$  (TNF $\alpha$ ), IL-1 $\beta$ , and IL-6, in myeloid cells and antigen-presenting cells (Walter 2014). In particular, it plays an important role in acute bacterial infections, including pneumonia (Duell et al. 2012). In addition, IL-10 has been shown to have a direct effect on the survival and memory of Th2 and Th17 cells (Coomes et al. 2017). Overall, it has been observed that IL-10 is an important modulator of the immune response, and of interest in the host response in pneumonia.

### **1.3.5 Role in pneumonia**

As IL-10 has been shown to play an important role in modulating the immune response in bacterial infections, it is of interest to examine its effects in bacterial and viral pneumonia and disease progression. In one study which included pneumonia patients from all age groups, elevated IL-10 levels were associated with systemic inflammatory response syndrome, and IL-10 levels correlated with disease severity (Glynn et al. 1999). In another study, significantly high IL-6 and IL-10 levels were noted in severe pneumonia in adult patients, with increased cytokine levels associated with disease severity (Zobel et al. 2012). In a mouse model, it was shown that *S. pneumoniae* infection caused a significant increase in lung IL-10 production and hinted that the cytokine has an important protective role against organ failure (Penaloza et al. 2015). The same study also confirmed that lack of IL-10 in the early stages of pneumococcal pneumonia leads to increased susceptibility and risk of death, caused by excessive neutrophil recruitment into the lung and overproduction of pro-inflammatory cytokines (Penaloza et al. 2015). With regards to severe pneumonia symptoms, high IL-10 has been linked to arterial hypotension (Martinez et al. 2011).

IL-10 is also important in pediatric pneumonia. In children with bacterial pneumonia that required mechanical ventilation, IL-10 levels were found to be higher in patients younger than 6 years old in comparison with older patients (Nguyen Thi Dieu et al. 2017). In particular, the balance between serum IL-6 and IL-10 can be helpful in determining the severity of

pneumonia. In a study involving 25 children with pneumonia, serum IL-10 levels were low at admission, however they were also associated with lymphocytosis, which may suggest that the cytokine may have an effect on the immune response (de Brito et al. 2016). This comes in contrast with a study by Antunes, where elevated IL-10 levels were found at admission, and in a study by Endeman et al., where serum IL-10 was found elevated on admission and fell rapidly after 2 days in hospital (Antunes et al. 2002; Endeman et al. 2011).

Interestingly, in children with severe *Mycoplasma* pneumonia or with *Mycoplasma* pneumonia and asthma, IL-10 levels were significantly lower in comparison with those with mild symptoms, which may suggest that asthmatic children may show inhibited IL-10 responses (Ding et al. 2016). This comes in contrast with a newer study, which found increased serum levels of IL-10 in children with *Mycoplasma* pneumonia in combination with wheezing (Medjo et al. 2017).

A link between elevated IL-10 levels and RSV infection has been observed, as it has been demonstrated that virus-specific T-cells, as well as multiple CD4+T cell in the lung are responsible for the production of large amount of IL-10, and that lack of IL-10 production is directly associated with disease severity (Weiss et al. 2011). Elevated IL-10 levels have been observed in patients with RSV pneumonia (Ye et al. 2015). The protective role of IL-10 in RSV infections has been well-examined, with studies finding that IL-10 blockade leads to increased disease severity, pulmonary inflammation and lethal injury (Sun et al. 2009; Loebbermann et al. 2012).

With regards to using IL-10 as a mortality predictor, a few studies have found interesting results. One study assessed the serum cytokine levels of septic patients and found a connection between elevated IL-10 levels on day 3 and mortality (Lekkou et al. 2004). In addition, persistently high serum IL-10 levels have been associated with increased mortality in septic shock following community acquired infections, which may suggest that overproduction of the cytokine may inhibit the immune response and lead to disease progression (Sfeir et al. 2001). Another study, which comes in agreement, also found elevated serum levels of IL-10 in 81% of septic patients (van der Poll et al. 1997). Furthermore, a strong link between high serum IL-10 and mortality in patients with severe fever (van Dissel et al. 1998). This was also noted in pneumonia patients that required mechanical ventilation, where increased IL-10 was an accurate predictor of mortality (Wu et al. 2006). Additionally, it has been demonstrated that polymorphisms associated with higher IL-10 production are linked to higher risk of death from sepsis following pneumonia (Gallagher et al. 2003). A study by Kellum et al. found that various levels of IL-10 in combination with IL-6 was linked to higher mortality, with the combination of high IL-10 and IL-6 levels linked to the highest mortality overall (Kellum et al. 2007). This also comes in agreement with Martinez et al., who also found that high IL-10 and IL-6 levels were also linked to higher 30-day mortality in adults (Martinez

et al. 2011). Additionally, high IL-6 and low IL-10 levels have also been linked to increased lung injury in SIRS (Chien et al. 2006).

In general, there is some conflict over the role of the cytokine in pneumonia and sepsis, with some studies showing that increased IL-10 has a protective effect, while other point that high IL-10 levels are associated with increased mortality.

### 1.3.6 C-reactive protein

C-reactive protein (CRP) is an acute phase serum protein which plays a major role in host defense and inflammation (Mold et al. 1999). It has a molecular weight of 120,000 Daltons and is made up of five identical sub-units that contain each 206 amino acids (Moutachakir et al. 2017). Its structure is shown in figure 1.7 below. It is a highly conserved protein, found in a variety of species, from arthropods to humans (Pathak and Agrawal 2019). In severe inflammation, its concentration has been found to increase by more than 10000-fold (Kushner 1982). The human CRP structure consists of a pentameric protein, made up of five identical non-covalently bound subunits of 206 amino acid residues with a molecular weight of ~23 kDa (Shrive et al. 1996). CRP composition mostly takes place in the liver by hepatocytes but also by smooth muscle cells, macrophages, endothelial cells, lymphocytes, and adipocytes, under transcriptional control by the cytokine IL-6 and TNF $\alpha$  (Sproston and Ashworth 2018; Fernandes et al. 2019).

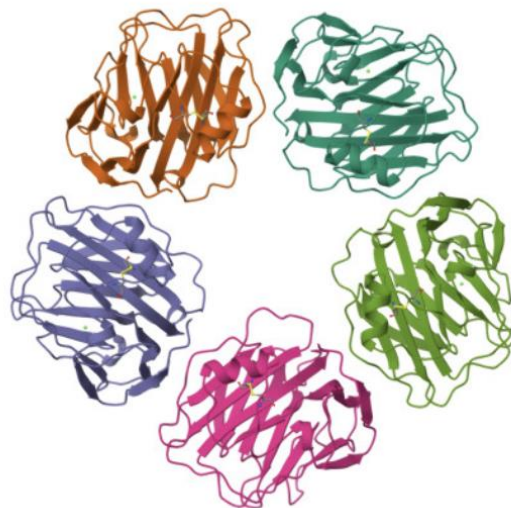


Figure 1.7: C-reactive protein, shown as a 5-mer (Protein data bank, 2024)

In the case of a bacterial infection, CRP, in the presence of calcium, binds to polysaccharides, such as phosphocholine (Larsson et al.) on pneumococcal C-polysaccharide and triggers the activation of the complement system through the classical pathway, by being recognized by C1q (Mold et al. 1999). Following C1q binding, C3 is engaged, as well as the terminal membrane attack complex (C5-C9) (Pepys and Hirschfield 2003). CRP binding can also allow

factor H binding and therefore activation of the alternative complement system pathway (Pepys and Hirschfield 2003).

### **1.3.7 Role in pneumonia**

Because of its role in defense against bacteria, is one of the most widely used clinical biomarkers for the diagnosis and monitoring of bacterial infections, including sepsis (Faix 2013). However, the use of CRP has been criticized for its lack of specificity, despite its wide use as an early biomarker of sepsis (Faix 2013). A series of studies have looked at using CRP as a biomarker of bacterial pneumonia, either by itself or in combination with other biomarkers. For example, Alcoba et al. used elevated CRP as a general predictor of pediatric pneumococcal pneumonia as well as of complications (Alcoba et al. 2017). In another study, serum CRP values above 200 mg/L were likely associated with pneumonia (Ruiz-Gonzalez et al. 2016). Moreover, CRP has also been used as a qualitative biomarker of pneumonia in pleural fluid (Requejo and Coccoza 2003). A multivariate model incorporating CRP concluded that high levels of the biomarkers are associated with disease severity, and can predict the risk of complications (Barak-Corren et al. 2020). Similarly, another study found a correlation between elevated CRP levels and increased length of hospital stay in children with pneumonia (Williams et al. 2016). Moreover, a study by Agnello et al. observed a relationship between high CRP levels and pneumonia severity and complications, such as pleural effusion and lobar consolidation (Agnello et al. 2016).

CRP has also shown some potential in differentiating bacterial from viral pneumonia, as a study in Africa has looked at CRP values in various secretions and found that CRP values were positively associated with bacterial pneumonia and negatively associated with RSV pneumonia (Higdon et al. 2017).

Of course, there are some drawbacks to the use of CRP. Florin et al. in a recent systematic review on biomarkers for pediatric pneumonia, concluded that CRP is “generally not useful to discriminate non-severe from severe disease” (Florin et al. 2020). In addition, the low specificity of CRP can confuse diagnosis, as CRP can also be used as a biomarker of malaria (Paul et al. 2012). In addition, malnourished children have shown differences in the production of inflammatory mediators (Ekanem et al. 1997). Finally, HIV infection can also reduce the specificity of CRP, making it less useful in countries affected by large numbers of HIV positive cases (Mendelson et al. 2018).

### **1.3.8 Procalcitonin**

Procalcitonin (PCT) is a 116-amino acid polypeptide measurable in serum, and is produced by the medullary C-glands of the thyroid (Creamer et al. 2019). The mRNA product from the thyroid is named preprocalcitonin, and is further modified into 116 amino acid procalcitonin (Vijayan et al. 2017). Following modification, it is further cleaved into 3 different molecules: active calcitonin (32 amino acid), katalcalcitonin (21 amino acid) and N-terminal procalcitonin

(57 amino acid) (Vijayan et al. 2017). Its structure is shown in figure 1.8 below. In a healthy subject, almost all procalcitonin is converted to calcitonin, with very little amounts detected in serum. However, in the inflammatory state following bacterial infection, its levels increase rapidly. Bacterial LPS, microbial toxins and inflammatory mediators such as IL-6 and TNF- $\alpha$  trigger PCT release into the bloodstream (Vijayan et al. 2017). Reports have found a rapid increase in concentration, with some studies detecting an increase in PCT levels 4hrs following bacterial infection (Gilbert 2010; Vijayan et al. 2017).

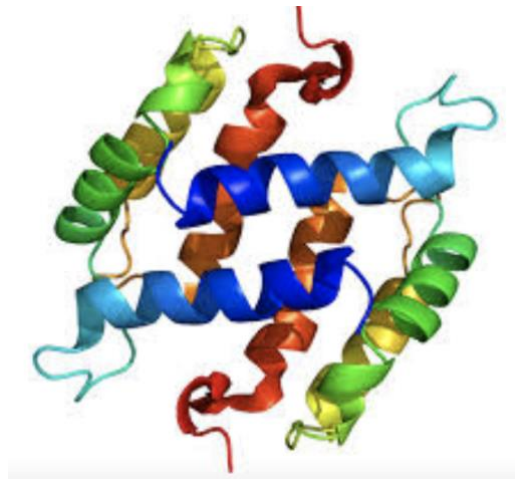


Figure 1.8: Procalcitonin structure (Protein data bank, 2024)

The rapid increase of procalcitonin following infection makes it a widely used biomarker in the early detection of sepsis, despite criticisms on the lack of specificity (Lapillonne et al. 1998). Some studies have suggested that procalcitonin may be more sensitive and specific compared to CRP (Simon et al. 2004; Nargis et al. 2014). In a well-known study in 1993, procalcitonin was found significantly elevated in sepsis but close to the normal range in bacterial or viral infections, making it an important sepsis biomarker (Assicot et al. 1993). In addition, there have been many attempts to use procalcitonin as a means to differentiate bacterial from viral pneumonia, with various levels of success. For example, a study by Muller et al. in critically ill patients with community acquired pneumonia found that serum procalcitonin could distinguish between viral and bacterial pneumonia and was related to symptom severity (Muller et al. 2007). A previous trial by Toikka et al. found that procalcitonin levels  $>2$  ng/mL could suggest bacterial pneumonia (Toikka et al. 2000). Moreover, another study in adult patients found that although procalcitonin was not useful in the discrimination between viral and bacterial pneumonia, high levels were related to increased possibility of infection by bacterial pathogens (Self et al. 2017).

### 1.3.9 Role in pneumonia

Procalcitonin has been involved in a number of trials as a bacterial pneumonia biomarker, and a number of trials in children have generated interesting results. For example, a recent trial by Wang et al. in hospital-acquired pneumonia in children found that procalcitonin may be a

reliable biomarker (Wang et al. 2021b). A study by Mahajan et al. in febrile children younger than three years old showed that procalcitonin was superior to traditional screening tests for a number of bacterial infections, including bacterial pneumonia (Mahajan et al. 2014). Another trial in children with community-acquired pneumonia suggested that procalcitonin threshold of 1 mg / L may be more sensitive and specific than CRP or IL-6 in the diagnosis of bacterial pneumonia and differentiation from viral pneumonia (Moulin et al. 2001). Another trial by Hatzistilianou et al. found that serum PCT concentration on admission has a higher sensitivity, specificity and positive predictive value for bacterial pneumonia than either CRP (Hatzistilianou et al. 2002). However, a number of studies have also contrasted these findings. For example, a large study on community-acquired pneumonia found that procalcitonin has limited risk predictive ability in comparison with other risk assessment systems (Huang et al. 2008). In another large, more recent study, procalcitonin was also found to have lower diagnostic accuracy in comparison with IL-6 and CRP, which comes in contrast with the findings of previous studies (Wussler et al. 2019). Another trial found that procalcitonin had limited diagnostic ability and also was not useful in discriminating patients with bacterial from viral pneumonia (Kamat et al. 2020).

In addition, studies have also looked at using procalcitonin as a mortality predictor (Schuetz et al. 2009). A study by Jensen et al. in the intensive care unit found that elevated procalcitonin level at admission, as well as an increase of procalcitonin on the first day after admission were linked with a higher risk of mortality (Jensen et al. 2006). This also comes in agreement with a similar study which focused on pneumonia, which also found that elevated procalcitonin levels from the first until the third day following admission were a good predictor of mortality (Boussekey et al. 2006). However, in less critically ill patients, procalcitonin did not show consistent results as a prognostic biomarker (Kruger et al. 2008).

Furthermore, procalcitonin appears to have a use in discriminating pediatric pneumonia patients with low risk of bacterial pathogens and possibly reduce prescription of antibiotics (Stockmann et al. 2018). Christ-Crain et al. conducted a randomized trial in adult patients with community-acquired pneumonia and procalcitonin-guided treatment led to shortened antibiotic treatment (Christ-Crain et al. 2006). Another similar study in pediatrics, although it used a smaller sample size, found that procalcitonin guidance reduced antibiotic prescriptions by 14% (Esposito et al. 2011). Similarly, a previous large-scale trial in the intensive care setting also showed promising results in the use of procalcitonin in suspected bacterial infections (Bouadma et al. 2010). Furthermore, a trial by Briel et al. in adult patients showed that procalcitonin-guided therapy also led to 72% lower antibiotic prescriptions and shorter treatment times (Briel et al. 2008). However, in contrast with these two studies, procalcitonin guidance has also been shown to not be useful in reducing antibiotic prescriptions in children, although antibiotic treatment duration was reduced (Baer et al. 2013). This was also the conclusion in a large-scale study by Huang et al., which showed no significant difference in

the number of antibiotic prescriptions between the procalcitonin-guided group and the usual-care group (Huang et al. 2018).

### 1.3.10 Lipopolysaccharide

Lipopolysaccharide (LPS), also known as endotoxin, is one of the most well studied bacterial surface molecules and one of the most potent microbial mediators of Gram-negative bacteria. It is ubiquitously associated with the development of sepsis and septic shock (Opal 2010). LPS is the most prominent 'alarm molecule' sensed by the host's system of innate immunity, warning the host of invasion by Gram-negative bacteria (Opal 2010). Lipopolysaccharide (LPS) is made up of three different regions: the hydrophobic lipid A region, Core Regions and O-specific antigen (Rietschel et al. 1987). Its structure is shown in figure 1.9 below. The lipid A region, which exhibits diversity among bacterial species, is found in the lipid bilayer of the membrane and is responsible for most of the immunologic activity of LPS and is made up of a phosphorylated diglucosamine backbone with four to seven acyl chains attached to it (Park and Lee 2013). Lipid A is considered the endotoxin center of the LPS, as studies have shown that synthetic Lipid A triggers the same immune response as unmodified Lipid A (Rietschel et al. 1987). The core region and O-specific antigen extend from the core out to the environment (Lerouge and Vanderleyden 2002). The core region, which is made up of carbohydrates, is conserved among bacterial species, while the O-specific antigen, which is made up of repeating carbohydrate units, only plays a small role in the activation of the innate immune response (Park and Lee 2013). LPS affects the permeability of the outer membrane, by protecting against small, hydrophobic molecules that would otherwise damage the phospholipid layer, such as antimicrobial agents (Nikaido 2003).

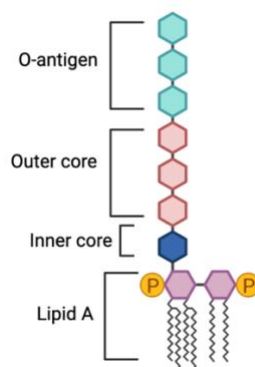


Figure 1.9: Endotoxin structure (Harm, 2021)

LPS is recognized as the most important microbial mediator in the pathogenesis of sepsis (Opal 2010). Sepsis is one of the most severe diseases caused by abnormal TLR4 activation, which can result from elevated LPS levels in blood, overexpression of pro-inflammatory cytokines, activation of blood coagulation system and accumulation of fibrinogen degradation (Keynan et al. 2011). As *S. pneumoniae* is one of the most common pathogens in pneumonia and one of the pathogens complicating pneumonia into sepsis, its detection through using

LPS as a biomarker appears promising (Shah et al. 2016). Initial LPS detection studies in the 1940s involved the rabbit pyrogen test (RPT), however due to drawbacks associated with this method it has been replaced (Hartung 2015). It has been substituted by the Limulus amoebocyte lysate (LAL) assay, developed by Levin and Bang, in the 1960's (Levin and Bang 1968). However, there are some drawbacks associated with this method, mainly the poor recovery of endotoxin from biological samples (Hausmann et al. 2000). Therefore, two new detection methods were developed, the monocyte activation test (MAT) and the recombinant factor C (rFC) (Perdomo-Morales et al. 2011; Bolden and Smith 2017). The MAT test is based on the measurement of cytokine IL-1 beta after exposure of the sample to human blood, while the rFC test uses protease zymogen activated by endotoxin binding, which then produces p-nitroaniline which can be electrochemically detected (Inoue et al. 2010). In addition, LPS can be detected by silver staining and visualized by gel electrophoresis (Qiang et al. 2015). However, these methods are not routinely used for LPS detection, and there is still need for an inexpensive, easy to use and reliable LPS biomarker.

### **1.3.11 Role in pneumonia**

As LPS is constantly present in the nasopharyngeal flora and the environment, the lung is continuously exposed to inflammatory signals (Guillot et al. 2004). As endotoxin is the main bacterial signal responsible for the activation of innate immunity, it plays a major role at the initiation of inflammatory cascades and processes in the lung. The first cells in the lung environment to interact with LPS are alveolar macrophages, along with pulmonary epithelial cells, both of which play an important role in the innate defense of the lung (Guillot et al. 2004). It has been speculated that the lipid A compartment, which is responsible for the biological activity of endotoxin, may be directly recognized by leukocytes (Martin 2000). Through recognition of endotoxin by TLR4, downstream signaling cascades leading to the production of pro-inflammatory cytokines are initiated (Guillot et al. 2004). The signaling cascades initiated by TLR4 activation can be found at page 32. Figure 1.10 also illustrates how endotoxin attachment to mediators induces inflammation.

The lower respiratory tract also includes alveolar fluid, which normally contains lipoprotein binding protein, which is synthesized in the liver, and soluble CD14 (sCD14), a pattern-recognition receptor (Pugin et al. 1993). LPS attachment to both factors further enhances the inflammatory response in the lung environment, which can however result in enhanced lung injury and susceptibility to infection (Guillot et al. 2004).

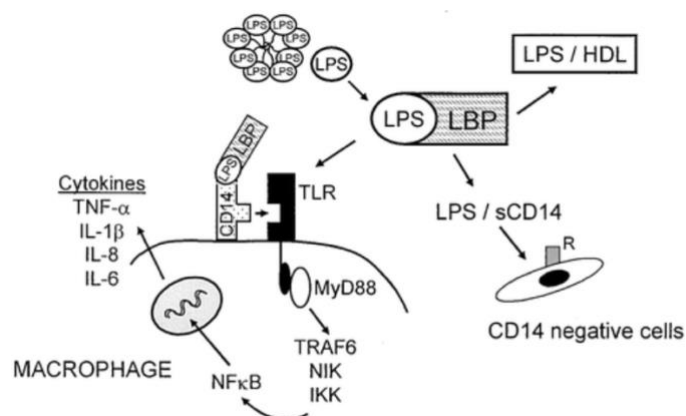


Figure 1.10: LPS attachment to soluble and membrane mediators (Martin 2000)

In the last years, molecular recognition elements have gained plenty of interest as alternatives to antibodies (Trunzo and Hong 2020). A class of them, aptamers, which are synthetic single-stranded DNAs or RNAs capable of binding to targets with high affinity and selectivity have been employed in the detection of LPS (Zhuo et al. 2017). In addition, when compared to antibodies, they exhibit better shelf-life, resistance to denaturation and degradation as well as overall better integration into biosensor systems (Cai et al. 2006). They are selected from a randomized pool of oligonucleotides by a method called Systematic Evolution of Ligands by Exponential enrichment (SELEX) (Kandimalla and Ju 2004). Aptamers fold into well-ordered 3-D structures where the ligand becomes an intrinsic part of the nucleic acid structure (Xie et al. 2016). Aptamer-based detection of LPS has been performed in a number of studies and various detection methods have been developed.

In a study by Xie et al., an assay based on hybridization chain reaction was developed, which used a pair of complementary hairpin oligomers to generate a chain reaction of hybridization events, followed by streptavidin horseradish peroxidase treatment and capture by the immobilized capture probe (Xie et al. 2016). This double-aptamer method generated low detection limits (1.73 ng/mL) and fast detection of LPS. Another assay developed by Ye et al. used ssDNA aptamer containing 27 nucleotides (LA27), able to bind to LPS from three different sources: *Salmonella enterica*, *Pseudomonas aeruginosa* 10 and *Escherichia coli* O55: B5, following a graphene oxide-based fluorescence polarization assay (Ye et al. 2019).

Aptamers have also gained interest when used in electrochemical biosensors. The construction of a detection system utilizing aptamers immobilized on thin film gold electrodes, combined with measurement of the electrochemical signal using electrochemical impedance spectroscopy (EIS) provides sensitive quantification of the biomarker (Cai et al. 2006). A number of aptamer sequences have been used to bind LPS, and according to a study by Kim et al. the one with the best affinity had the sequence (Kim et al. 2012):

5'- CTT CTG CCC GCC TCC TTC CTA GCC GGA TCG CGC TGG CCA GAT GAT ATA AAG GGT CAG  
CCC CCC AGG AGA CGA GAT AGG CGG ACA CT - 3'

**Peptide-based LPS detection** involves the use of peptides such as polymyxin B, which is a polypeptide antibiotic with activity against most Gram-negative bacteria (Poirel et al. 2017). Polymyxin binds to the negatively charged LPS, and through an interaction with between the  $\alpha,\gamma$ -diaminobutyric acid (Dab) residue of the positively charged polymyxin and phosphate groups of the negatively charged lipid A membrane, the displacement of divalent cation such as  $\text{Ca}^{2+}$  and  $\text{Mg}^{2+}$  from the negatively charged phosphate groups of membrane lipids is observed (Dixon and Chopra 1986). This results in LPS destabilization and subsequently a decrease in membrane stability, leading to cytoplasm leakage and cell death (Falagas and Kasiakou 2005). Additionally, polymyxins are capable of binding and neutralizing LPS released from lysed cells, as well as inhibit vital enzymes, such as type II NADH-quinone oxidoreductases (NDH-2) in the bacterial inner membrane (Li et al. 2005; Deris et al. 2014). Polymyxin B has been used in a number of biosensors in literature; one example is provided by Zandieh et al., who developed a label-free, LSPR-based sensor for the detection of endotoxin. A SAM made up of 3-Mercaptopropionic acid and EDC-NHS (1-ethyl-3-(3-dimethylaminopropyl)carbodiimide and N-hydroxysuccinimide) was synthesized on the surface, on which silver nanoparticles were deposited on, following by immobilization of Polymyxin B on the surface of nanoparticles. The sensor had a detection limit of  $340 \text{ pg mL}^{-1}$  for *E. coli* (Zandieh et al. 2018). Ding et al. developed an EIS-based sensor, using conjugated Polymyxin B on gold electrodes modified with 4,4'-dithiodibutyric acid, using carbodiimide and sulfo-NHS chemistry. The sensor exhibited sensitive detection of LPS over the 0.2–0.8 ng/mL concentrations from the shift of the charge transfer resistance (Ding et al. 2007). Wang et al. developed a polymyxin-cloth enzyme immunoassay, where a polyester polymyxin coated cloth captured the endotoxin, followed by immunodetection using antibodies (Wang et al. 1996). A rapid flow-through assay developed by Kalita et al used drops of LPS-containing serum on absorbent pads, followed by addition gold nanoparticles conjugated to polymyxin B, which resulted in visible color change, observable to the naked eye. The platform detected LPS in the range of 10 pg/mL to 10 ng/mL (Kalita et al. 2017) Finally, a more recent example by Reta et al. involves the use of porous silicon nanochannel sensors, including microchannels modified with Polymyxin B. LPS detection was performed through the measurement of changes in the diffusion through the nanochannels of an electroactive species added to the solution, caused by the nanochannel blockage upon LPS binding to polymyxin B. The sensor showed a limit of detection of 1.8 ng/ml and was successful in the detection of *Pseudomonas aeruginosa* and *E. coli* in wastewater treatment samples (Reta et al. 2019).

Aside from polymyxin, an artificial labelled peptide named KC-13 was used in a graphene oxide sensor developed by Lim et al. Upon LPS binding, the LPS-KC-13 complex was detached from graphene oxide and caused a spike in fluorescence, which resulted in ultrasensitive and low level LPS detection (130 pM), one of the lowest noted in literature (Lim et al. 2015).

Moreover, magnetic aptasensors have shown promise in LPS detection, with one such example provided by Zuo et al., who developed a flow-cytometry based magnetic aptasensor. The system used an aptamer-based sandwich with magnetic beads and two LPS binding aptamers. The fluorescence generated by LPS binding would be quantified through flow cytometry and detect endotoxin from *E. coli* in the range of  $10^{-8}$  to  $10^0$  mg mL<sup>-1</sup>, even in the presence of interferents (Zuo et al. 2014). Moreover, sensors based on antibody-antibody binding have been developed in the past; one example of a magnetoelastic resonance sensor is provided by Guntupalli et al., who used polyclonal antibodies on the surface of a magnetostrictive platform made up of ferromagnetic alloys, with endotoxin detection limits of up to  $5 \times 10^3$  CFU/ml (Guntupalli et al. 2007). Additionally, surface-coated gold nanorods with different polymers capable of binding LPS showed different interaction with the endotoxin. The nanorods were immobilized onto glass slides and were coated with various polymers including sodium polyacrylate, poly(allylamine) hydrochloride, heparin, polydiallyldimethyl ammonium chloride, and methoxyl polyethylene glycol thiol. The highest affinity was observed for *E. coli* LPS to the poly (allylamine hydrochloride) coated nanorods (Abadeer et al. 2015).

#### **1.3.12 Cell-free DNA**

DNA sequences are often chosen as biomarkers; however, this section will be focused on extracellular, or cell-free DNA (cfDNA). cfDNA is defined as DNA fragments (approximately 160 base pairs) released from cells during apoptosis, and can be detected in cerebrospinal fluid, pleural fluid, urine, saliva and blood (Yan et al. 2021). cfDNA found in blood can be used for tumour diagnosis and monitoring, pre-natal monitoring, organ transplant monitoring and organ dysfunction (Pietrzak et al. 2023). cfDNA responds to blood cell viability changes caused by either trauma or disease, and various cfDNA have demonstrated diagnostic potential for sepsis diagnosis, especially when used in conjunction with other biomarkers (Urosevic et al. 2022). During the first 24hrs of sepsis, where cell apoptosis is paramount in sepsis pathogenesis, cfDNA levels have been found in increased levels in blood in many studies (Garnacho-Montero et al. 2014; Duplessis et al. 2018; Beltran-Garcia et al. 2021). Systematic reviews have demonstrated that in septic patients within 24hrs of admission, cfDNA levels were significantly higher compared to non-septic patients (Charoensappakit et al. 2023). Additionally, elevated cfDNA levels have been associated with disease severity and mortality in both pneumonia and COVID-19, showing promise as a prognostic biomarker (Andargie et al. 2021)

#### **1.3.13 Beta-globin sequence in sepsis diagnosis**

One of the aims of the project was the development of detection systems for a multitude of markers, including nucleic acid targets. Therefore, the identification of a suitable DNA marker was desired. Following a literature search, it was discovered that cfDNA has potential for the diagnosis for sepsis, and one of the genes frequently detected in septic patients is the sequence of nuclear  $\beta$  globin (Saukkonen et al. 2008; Urosevic et al. 2022). The beta globin

gene encodes the  $\beta$ -Globin protein (HBB), one of the haemoglobin subunits, and its release in the bloodstream is indicative of cell death, often observed in sepsis (Aldakeel et al. 2020). The structure of haemoglobin subunit beta is shown in figure 1.11 below.

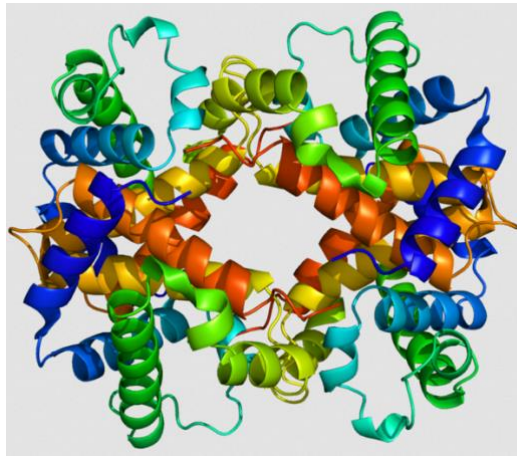


*Figure 1.11: Haemoglobin subunit beta, which is encoded by the beta globin gene (Protein data bank, 2024)*

In a study by Saukkonen et al., beta globin cfDNA was quantified at admission and 72hrs later, using RT-PCR. The study showed that high cfDNA concentrations at both admission and 72 hrs later were higher among non-survivors and showed a moderate association between elevated cfDNA and ICU mortality (Saukkonen et al. 2008). Beta globin has also been in other studies as a sepsis biomarker, where its diagnostic and prognostic value has been demonstrated. Kalantar et al. used beta globin as part of a RNA and DNA panel in a metagenomic study, which combined host and microbial markers to develop a model that predicted sepsis in 74% of suspected and 89% of intermediate sepsis cases (Kalantar et al. 2022).

#### **1.3.14 Biomarker review conclusions**

In order to ensure the project is completed in a timely manner and to ensure the most efficient and accurate biomarkers for the sensor, three biomarkers had to be chosen. After performing a comprehensive literature review, it was concluded that IL-6 is an ideal early-phase biomarker, which will enable the fastest detection of pneumonia. Combined with LPS detection, a distinction between bacterial and viral pneumonia can be made and guidance can be provided on patient treatment and antibiotic prescription. Finally, the addition of a DNA sequence biomarker will enable collaboration with other members of the interdisciplinary training hub of the university working on nucleic acid detection and amplification platforms, in addition to providing a novel biomarker to predict the risk of sepsis secondary to pneumonia and the risk of developing severe disease.

#### **1.4 Current and future focus on biosensors**

A biosensor is defined as device capable of measuring biological or chemical reactions, through the generation of signals proportional to the concentration of an analyte (Bhalla et al. 2016). They are widely used nowadays in disease monitoring, drug discovery, detection of pollutants, disease-causing pathogens and markers that are indicators of a disease, in various bodily fluids such as saliva, sputum, whole blood etc. (Bhalla et al. 2016). Biosensors are capable of detecting biomarkers from various sources by utilizing the interaction between a biological component with a physicochemical detector, which means that every biosensor contains two essential components; a biorecognition component and a transducing component (Xu and Lee 2020). The biorecognition component offers high selectivity between the chosen analyte and the recognition unit. Depending on the concentration of the chosen analyte, a measurable signal such as change in mass, film thickness, charge, dielectric constant, or fluorescence can be generated and detected (Xu and Lee 2020). Depending on the type of signal detection mechanism, a biosensor can be categorized into types based on the transduction mechanism as shown in Table 1.

**Table 1.1:** Biosensor transducer types (Xu and Lee, 2020).

<b>Transducer type</b>	<b>Subtypes</b>	<b>Signal measured</b>
Electrochemical	Amperometric, Conductometric, Impedimetric, Potentiometric, Voltametric	Electrical current changes, electrical conductivity changes, changes in impedance, Changes in zero-current potential, changes after varying potential applied to electrode
Optical	Surface plasmon resonance, Optical waveguides, Optical resonators, Photonic crystals, Optical fibers	Changes in light absorption, reflectance, fluorescence, Raman scattering, or refractive index.
Field-effect transistor (Valentini et al.) based		Current changes between source and drain electrode
Organic electrochemical transistor (OECT) based		Current change because of ion injections from the electrolyte of interest into a semiconductor
Piezoelectric		Resonance frequency changes due to mass change in a crystal
Thermometric		Temperature change caused by biological reactions
Magnetic		Magnetic field changes

Besides the transduction mechanism, biosensors are also characterized based on metrics such as sensitivity, limit of detection, selectivity, and accuracy (Xu and Lee, 2020). In particular, **selectivity** and **sensitivity** may be the most important features of a biosensor, and is defined as the capability of a biosensor to detect a specific analyte in a sample containing other biomarkers or components and contaminants, while sensitivity is defined as the minimum amount of analyte that can be detected by a biosensor, expressed by limit of detection (LOD) (Bhalla et al. 2016). The limit of detection (LOD) is the minimal change in concentration that the sensor can confidently distinguish from the absence of the analyte (Xu and Lee, 2020).

One example of high selectivity is the interaction of an antibody with an antigen, as antibodies can selectively bind to the antigen even when it's mixed with other biological component, which makes antibodies one of the most commonly used bioreceptors in biosensing platforms (Bhalla et al. 2016). There are various ways of achieving high selectivity, such as using highly specific bioreceptors (aptamers or antibodies), permselective membranes and use of nanomaterials (Xu and Lee, 2020). In particular, thanks to advancements in nanotechnology and nanoscience signal amplifications are possible. Such examples include functional nanomaterials, such as metal nanoparticles, quantum dots, carbon-based nanomaterials, magnetic nanoparticles and polymers to design advanced single-stranded DNA biosensors (Zhu et al. 2015). These nanomaterials also possess a range of benefits, such as biological compatibility, high surface area, chemical stability, nontoxicity, excellent catalytic activity and conductivity (Zhu et al. 2015). Therefore, they can be of great assistance in detection signal amplification, platform stabilization and development of a highly selective platform. Indeed, a number of projects have developed biosensing platforms with remarkable selectivity. For example, a one-step graphene/poly(xanthurenic acid) nanocomposite used to immobilise capture probe DNA showed significant sensitivity and selectivity in the impedimetric detection of DNA (Yang et al. 2013a). The same group also developed a novel electrode material composed of sulfonated polyaniline (Rocchitta et al.) enhanced by graphene oxide (GNO), which also provided highly sensitive and selective electrochemical DNA detection (Yang et al. 2013b). Similarly, a highly conductive, label-free electrochemical DNA biosensor based on azophloxine-functionalized graphene nanosheets was developed, which also exhibited high sensitivity and selectivity, plus extraordinary capability for single nucleotide polymorphisms (SNPs) detection (Guo et al. 2013). In addition, an aptasensor utilizing carbon nanospheres allowed the immobilization of target MUC-1 aptamer, which amplified the electrochemical signals and further increased sensitivity and selectivity (Cao et al. 2014). More applications of nanomaterials and aptasensors and the benefits they offer to sensors will be discussed later in the review, but so far the role of nanomaterials in signal amplification is evident.

In addition to sensitivity and selectivity, further factors of importance are **reproducibility and accuracy**, as biosensors can provide important guidance regarding a patient's clinical outcome and treatment options (Xu and Lee, 2020). Reproducibility is defined as the ability

of the biosensor to generate identical responses for a duplicated experimental set-up and is largely dependent on the transducer and the electronics of the sensor (Bhalla et al. 2016).

Similar to the previous paragraph, the incorporation of nanotechnology and nanomaterials has made significant contributions to biosensor accuracy. For example, a colorimetric sensor utilizing gold nanoparticles for the detection of histamine, using UV–vis and fluorescence methods offered greater accuracy and sensitivity in comparison with previous projects (El-Nour et al. 2017).

#### **1.4.1 Electrochemical detection**

With regards to detection methods employed in multiplex biosensors, electrochemical (EC) methods provide a number of benefits compared to other processes as they offer an easy to perform and low-cost approach as well as good detection limits, plus biomarkers can be detected in a short time without the need for powerful instruments (Hammond et al. 2016; Campuzano et al. 2017). Additionally, they are low-cost, low power devices with great potential for miniaturization, which makes them of great interest for applications in point-of-care devices (Daniels and Pourmand 2007). They have been already successful and widely employed for the detection of glucose in whole blood for many years, and there has been a lot of progress in the incorporation of nanomaterials in such devices (Saei et al. 2013; Gooding 2019). Electrochemical biosensors have been employed successfully for individual or multiplexed determination of biomarkers at different molecular levels (Campuzano et al. 2019). An electrochemical biosensor operates by detecting the biomarker of interest and producing an electrical signal proportional to the concentration of the biomarker and is made up of three electrodes: a sensing electrode which detects the biomarker, a reference electrode and a counter electrode used to complete the circuit for current flow, all separated by an electrolyte (Hammond et al. 2016). A typical photo of the setup is shown in figure 1.12 below. As the demand for electrochemical biosensors has grown significantly over the past years, a wide variety of novel nanomaterials have led to the development of electrochemical affinity biosensors capable of detecting pathogens in body fluids (Campuzano et al. 2017). In addition, nanomaterials such as carbon nanotubes (CNTs) and gold nanoparticles (AuNPs) have been used as electrode modifiers and advanced labels (Campuzano et al. 2017). Electric spectroscopic methods, such as impedance and impedance-derived methods have demonstrated impressive efficiency and sensitivity in label-free biosensors, such as aptasensors (Garrote et al. 2019).

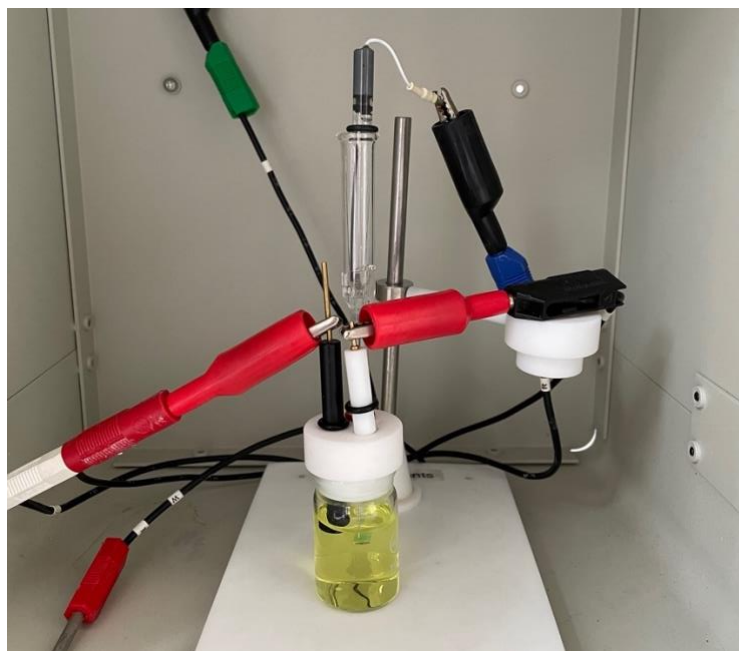


Figure 1.12: Photo of electrochemical setup used in this study. Working electrode (black), reference electrode (glass) and counter electrode (white) are visible and immersed in ferro/ferricyanide solution in PBS.

#### 1.4.2 Electrochemical immunoassays

Electrochemical biosensors can be categorized on based on their detection mechanism. One subtype of an electrochemical sensor is the **direct electrochemical immunoassay** (dECIA), which employs a design similar to direct enzyme linked immunoassay (Goodman et al.). These sensors involve the use of immobilized antibodies against the desired biomarker on a functionalized electrode and provide label-free, real-time detection, which makes them a popular choice for newer sensors (Mollarasouli et al. 2019; Khan and Mujahid 2020). One application of this method is presented by Ma et al., who developed an electrochemiluminescent label-free sensor for the detection of prostate specific antigen. Graphite-like carbon nitride, which exhibits good photocatalytic performance, was combined with gold nanoparticles and luminol to provide an accurate sensor with a detection limit of  $0.927 \text{ pg mL}^{-1}$  (Ma et al. 2018a). However, label-free sensors suffer from non-specific protein adsorption, which significantly impairs their sensitivity. Therefore, the use of a blocking agent, such as bovine serum albumin, casein, thionic compounds or polyethylene glycol is necessary (Mollarasouli et al. 2019). Another example of electrochemical sensor is the **indirect competitive electrochemical immunoassay** (icECIA), which prevents the binding of the biomarker with the biosensor, and the signal generated is amplified through an auxiliary interaction of the nanolabeled competitor and receptor. An example of a competitive biosensor is offered by Amor-Gutiérrez et al, who used screen-printed carbon electrodes nanostructured with gold nanoparticles and an antibody that only reacts with an epitope present in the unfolded p53 protein, providing a highly sensitive and accurate biomarker for Alzheimer's disease in plasma (Amor-Gutiérrez et al. 2020). Another competitive immunosensor for the quantification of microcystin-LR was developed by Zhang et al., who

used glassy carbon electrodes modified by electrodeposition of graphene oxide, with anti-MC-LR antibodies immobilized on the electrode surface. The catalytic effect on the oxidation of ascorbic acid was exploited to detect MC-LR (Zhang et al. 2019). **Sandwich Nanoparticles Labeled Electrochemical Immunoassays (sECIA-NP)** employ a labelled secondary antibody, which can improve the limit of detection in many cases. However, the addition of a label may cause issues, such as a drastic change in the binding properties of the receptor, which is not significant for DNA sensors but may cause issues with protein targets (Daniels and Pourmand 2007). One application of this mechanism is demonstrated by Peng et al., who used Titanium Phosphate (Shah et al.) hollow spheres of 40 nm shell with efficient loading of gold nanoparticles. The secondary antibody was immobilized on TiP/AgNPs nanospheres and used to bind IL-6, followed by the formation of a complex on the electrode, which enabled the sensitive detection of IL-6 (Peng et al. 2011). Deng et al. also developed an IL-6 sensor on the same detection principle, using gold nanoparticles stabilized with cetyltrimethylammonium bromide, which acted as a nanolabel for the secondary antibody (Deng et al. 2011). **Sandwich Enzyme Linked Electrochemical Immunoassays (sELECIA)**, enzymes such as horseradish peroxidase (HRP) are used for the labelling of the secondary antibody and the amount of catalyzed substrate is used for the detection of the concentration the biomarker in the sample (Khan and Mujahid 2020). An example of such a sensor is provided by Wang et al., who used graphene sheets and silica nanoparticles loaded with HRP in order to quantitatively detect  $\alpha$ -fetoprotein, with a detection limit of 4 pg ml<sup>-1</sup> (Wang et al. 2014a). Another recent example is provided by Medetalibeyoglu et al., who developed a sandwich immunoassay using glassy carbon electrodes in combination with gold nanoparticles as carriers of the primary antibody, in combination with secondary antibody bioconjugates as an amplification tag and H<sub>2</sub>O<sub>2</sub> as non-enzymatic substrate. The platform allowed the sensitive detection of procalcitonin, with a detection limit of 2.0 fg mL<sup>-1</sup> (Medetalibeyoglu et al. 2020).

Moreover, electrochemical biosensors can be categorized based on the electrical measurement technique employed into three categories: Amperometric, potentiometric, voltametric, conductometric and impedance (Daniels and Pourmand 2007; Grieshaber et al. 2008).

#### 1.4.3 Amperometric sensors

**Amperometric** biosensors, commonly used as amperometric enzyme electrodes, operate through consumption of their target substrate. The first precursor of today's biosensors, developed by Clark and Lyons for the continuous measurement of blood glucose, was an amperometric bioelectrode (Clark Jr and Lyons 1962). They are dynamic, catalytic devices based on enzymes that upon reaction with the substrate of interest either consume oxygen (oxidases), produce hydrogen peroxide or produce (indirectly) the reduced form of nicotinamide adenine dinucleotide (phosphate), NAD(P)H, e.g., dehydrogenase (Prodromidis and Karayannis 2002). There are three generations of amperometric biosensors: The first-generation biosensors, also known as mediatorless amperometric biosensors, measure the

concentration of analytes and/or products of enzymatic reactions. Sensors exploiting oxidases and dehydrogenases belong to this generation. First generation sensors have shown notable sensitivity and quick turnaround times of about one second, however they suffer from the need for electrode pretreatment and regular corrections with regards to interference, plus they are particularly sensitive to biofouling (Rocchitta et al. 2016).

Typically, *chronoamperometry* is the electrochemical technique of choice, in which the current is measured as a function of time, after the electrode is driven at an appropriate constant potential. The measured current change is proportional to the amount of electro-oxidized or reduced species, which in turn can be directly or inversely proportional to biomarker concentration. However, additional detection methods based on electrochemical oxidation/reduction of species directly or indirectly, such as potentiometric stripping analysis, stripping voltamperometry, differential pulse voltamperometry, coulometry, etc. (Belluzo et al. 2008).

**Second generation** enzymatic amperometric biosensors, also known as mediator amperometric biosensors, use mediators as oxidizing agents, which enables the sensor to function at low potentials without the need for oxygen dependence and interference by other molecules (Scheller et al. 1991). Mediators may be added to the sample or immobilized on the electrode surface (Rocchitta et al. 2016). The most widely-used mediators include ferricyanide and ferrocene, although, methylene blue, phenazines, methyl violet, alizarin yellow, Prussian blue, thionin, azure A and C, toluidine blue and inorganic redox ions are also commonly used (Chaubey and Malhotra 2002). Unfortunately, the addition of mediators makes this generation of biosensors unstable, which is why they are rarely used nowadays (Rocchitta et al. 2016). **Third generation** enzymatic amperometric biosensors are based on bioelectrocatalysis and involve direct electron transfer between enzyme and electrode. They are made up of three components: the enzyme as bio-recognition element, the redox polymer (or the nano-scale wiring element) to ensure the signal distribution and the electrode as the entrapping surface. As they are still in development, they are not widely used for analysis, however they show promising results with short response times (Rocchitta et al. 2016). However, enzymatic amperometric biosensors often suffer from interference caused by chemicals present in the sample matrix, such as small molecule metabolites, proteins, macromolecules and cells, plus substances formed during biological processes, such as blood clotting. Additionally, conditions such as inflammation can alter the sample environmental parameters, by causing changes in the chemical composition of the markers or the pH, which can affect enzyme performance and therefore sensor accuracy (Rocchitta et al. 2016).

In addition to enzymes, antibodies, antigens and aptamers can also be implemented in amperometric biosensing platforms. Amperometric immunosensors exploit the specific binding of antibodies to substrates, and if enzyme-linked antibodies are used, then a competitive assay similar to an ELISA can be developed (Rocchitta et al. 2016). An example of

a label-free amperometric immunosensor for the detection of prostate-specific antigen is provided by Okuno *et al.*, through the utilization of single-walled carbon nanotube array-modified microelectrodes, with a detection limit of 0.25 ng/mL (Okuno et al. 2007). A more recent example, designed for the detection of C-reactive protein in serum is offered by Thangamuthu *et al.*, who developed an immunosensor strip made up of a screen printed carbon electrode functionalized with anti-CRP functionalized gold nanoparticles with a detection limit of 17 ng/mL. (Thangamuthu et al. 2018). A technique often employed in amperometric immunosensors involves the entrapment of the antibody onto a polymeric membrane surface, such as Nafion, and an example of such an application is offered by Zhuo et al. who developed a three-electrode system for the detection of  $\alpha$ -1-fetoprotein, through the immobilization of thionine into a Nafion interface and the assembly of a gold nanoparticle layer on top of it, which contained antibodies against  $\alpha$ -1-fetoprotein (Zhuo et al. 2005). However, despite the high specificity of immunosensors, cross-reactions are often observed, usually manifesting as false-positive results caused by non-specific antibodies (Belluzo et al. 2008).

**Amperometric aptasensors** are a relatively new subtype and provide benefits over antibody amperometric sensors, such as improved stability and specificity (Belluzo et al. 2008). The implantation of amperometry in aptasensors provides simple signal outputs that that can be used to determine kinetic parameters of target-binding events at millisecond or even sub-millisecond frequencies, which makes them ideal for monitoring fast, transient and dynamic processes (Lee et al. 2006; Kim et al. 2011). There are a number of amperometric aptasensor applications; For example, in 2004, when the first electrochemical aptasensor was introduced, it employed amperometric sandwich-based biosensor based on glucose dehydrogenase-labeled signaling aptamers(Ikebukuro et al. 2004). In another example, Baker et al. developed a rapid label-free amperometric aptasensor for the detection of cocaine in biological fluids (Baker et al. 2006). Furthermore, a reagentless amperometric aptasensor for the detection of thrombin was developed (Radi et al. 2006). A more recent aptamer-based microfluidic biosensor was developed by He et al. for the detection of vasopressin; amperometry was employed for sensitive, continuous measurement of the biomarker (He et al. 2013). Finally, a sensitive amperometric aptasensor designed for the detection of cell-surface N-glycan expression, using porous core-shell palladium gold nanoparticles (Liu et al. 2018).

Finally, a plethora of **amperometric DNA or RNA** based biosensors have been developed. In these sensors, a single-stranded nucleic acid sequence is attached to an electrode to capture its complementary DNA or RNA strand. Following that, the binding is detected using different approaches, usually through the use of an electrochemical reporter of the hybridization (Belluzo et al. 2008). There are a number of DNA amperometric sensor examples published, such as platforms developed for the rapid detection of uropathogenic bacteria through bacterial 16S rRNA recognition or genosensors on gold films capable of detecting the viral

DNA sequence of the SARS virus (Abad-Valle et al. 2005; Liao et al. 2006). More recently, an amperometric DNA chip sensor has found use in the detection of infectious pathogens such as *Streptococcus pyogenes*, through the use of gold nanoparticles embedded with a carbon electrode modified with DNA probes (Singh et al. 2017)

#### 1.4.4 Voltametric sensors

**Voltametric sensors** provide information on the concentration of chemically available analytes (Bakker and Pretsch 2005). Voltametric sensors work by applying potential to the working electrode versus the reference electrode together with a potentiostat and measuring the current by means of electrochemical oxidation or reduction of analyte. In the case of analyte detection, the current forms a peak which is proportional to the concentration of analyte (Labib et al. 2016; Dhanjai et al. 2018). The essential operational function of voltametric devices can be described as the transfer of electrons to or from the analyte (Stradiotto et al. 2003). There are a number of voltametric techniques used in biosensing, such as linear sweep voltammetry, alternating current voltammetry, cyclic voltammetry, differential pulse voltammetry, square wave voltammetry, anodic stripping voltammetry, cathodic stripping voltammetry and adsorptive stripping voltammetry (Labib et al. 2016). From the beforementioned techniques, the most widely used one are cyclic voltammetry, differential pulse voltammetry and square wave voltammetry (Rahman et al. 2015).

Square wave voltammetry (SWV) combines the advantages of other voltametric techniques, such as the sensitivity of pulse techniques, the insight into the electrode mechanism provided by cyclic voltammetry and the kinetic information provided by impedance techniques. The potential generated in square wave voltammetry shows stair-shaped potential pulses, and at each step of the staircase ramp, two equal in height and oppositely directed potential pulses are imposed (Figure 1.13). The last two potential pulses complete a signal potential cycle (Mirceski et al. 2013).

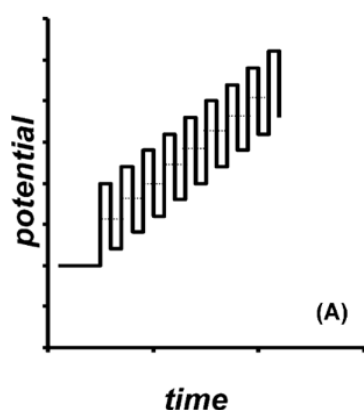


Figure 1.13: One potential cycle in square wave voltammetry (Mirceski et al. 2013)

A number of voltametric sensors based on SWV have been developed; one example by Goyal et al. used single-walled carbon nanotubes and SWV in combination with cyclic voltammetry to determine the oxidation of paracetamol at the electrode surface. This sensor was used for

the detection of paracetamol in urine, with a detection limit of  $2.9 \times 10^{-9}$  M (Goyal et al. 2010). Another example is provided by Gupta et al., who used carbon paste electrodes to determine the concentration of hydroxylamine in wastewater, and its testing in real sample confirmed the sensitivity and accuracy of the sensor (Gupta et al. 2015). Moreover, there are plenty of examples of aptasensors used for the detection of inflammatory markers, such as the label “signal-off” aptasensor developed by Liu et al. for the detection of interferon gamma. The sensor used a thiolated aptamer immobilized on a gold electrode, and upon binding of the analyte, the conformational change induced on the aptamer caused a decrease in the electron transfer and therefore of the current, which was assessed using SWV, resulting in accurate and sensitive detection of the biomarker (Liu et al. 2010).

**Cyclic voltammetry (Kitsios et al.)** has also been extensively used in biosensors, as it provides the opportunity to obtain information about the redox potential and electrochemical reaction rates; one example is information about the chemical rate constant in the analyte solution. When CV is performed, the voltage is swept between two values at a fixed rate, however, when the voltage reaches  $V_2$  the scan is reversed, and the voltage is swept back to  $V_1$  (Figure 1.14). As the duration of the scan determines which part of the chemical reaction is observed, sufficient time must be allowed for the reaction to complete, otherwise varying results may be observed (Grieshaber et al. 2008).

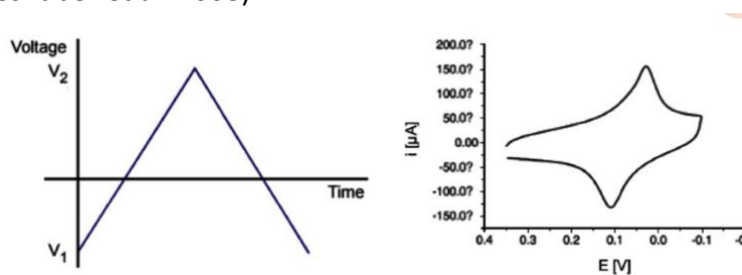


Figure 1.14: i) single generic linear voltage sweep ii) scan at 50 mV/s (Grieshaber et al. 2008)

In cyclic voltammetry, voltage is measured between the reference electrode and the working electrode, while the current is measured between the working electrode and the counter electrode. The observed results are then plotted as current vs voltage (voltammogram). Due to the increase in voltage toward the electrochemical reduction potential of the analyte, an increase in current is also observed. As the voltage is increased toward  $V_2$  past this reduction potential, the current decreases, resulting in the formation of a peak due to the decrease in analyte concentration close to the electrode surface. The voltage reversal needed to complete the scan toward  $V_1$  causes the reoxidation of the product from the initial reaction, which causes the formation of a second peak (Figure 3.ii). This also provides information on the reversibility of a reaction (Grieshaber et al. 2008).

There is a wide range of sensors using cyclic voltammetry reported in the literature. For example, antibodies immobilized on a gold surface were used to measure human IgG, coupled with an amplification strategy using on a cross-linking network based on streptavidin and

biotin labeled protein, and cyclic voltammetry was used as the electrochemical sensing method. The platform, combined with the amplification strategy, exhibited good sensitivity and was capable of detecting IgG in the range of 2–10  $\mu\text{g/ml}$  (Pei et al. 2001). Additionally, there is a plethora of aptasensors using cyclic voltammetry. Wang et al. developed a sandwich structure in combination with gold nanoparticles for the detection of platelet-derived growth factor, based on the knowledge that the growth factor has two aptamer binding sites. Thanks to the sandwich design, the platform exhibited significant signal amplification and increased sensitivity, and was able to detect the biomarker in question in undiluted blood serum with good accuracy and high specificity (Wang et al. 2009). Deng et al. developed an aptamer-based sensor for the detection of the same molecule, based on the direct electrochemistry of glucose oxidase. In this sensor, graphene-gold nanoparticles were deposited on the surface of a gold electrode, following by deposition of the glucose oxidase layer. Following that, gold nanoclusters were deposited on top of the glucose oxidase layer, to capture the aptamer. The sensor exhibited very good sensitivity and a detection limit of 1.7 pM, although it wasn't tested in serum or biological samples (Deng et al. 2013). Moreover, RNA aptasensors have also been described, with an example of a label-free aptasensor for the detection of human osteopontin presented by Meirinho et al. The RNA aptamer was deposited on streptavidin-modified gold surface, and after the binding of osteopontin, cyclic voltammetry was employed, which confirmed the sensor's selectivity, sensitivity and low limit of detection, with and without the presence of interfering proteins (Meirinho et al. 2015). Finally, a more recent cyclic voltammetry application in aptasensors is described by Aydin et al., who developed a poly(pyrrole N-hydroxy succinimide) polymer covered disposable indium tin oxide electrode sheet for the detection of IL-6. The label-free, disposable sensor showed good specificity and sensitivity with a limit of detection of 10.2  $\text{fg mL}^{-1}$  (Aydin et al. 2020).

#### 1.4.5 Potentiometric sensors

**Potentiometric sensors** measure, in an electrochemical shell, the accumulation of a charge potential at the working electrode in comparison to the reference electrode, when zero or very little current flows between them (Grieshaber et al. 2008). As they measure the ion activity in the sample, they consist a unique class of chemical sensors that can be very useful in bioavailability studies (Bakker and Pretsch 2005).

Initially, reference electrodes made up of Ag/AgCl or Hg/Hg<sub>2</sub>Cl<sub>2</sub> were used because of stable and reliable potential response during measurement. However, their need for bulky electrode solutions developed the need for alternative solutions (Zdrachek and Bakker 2019b). The implementation of ion-selective electrodes (ISE) has helped potentiometric sensors achieve impressively low detection limits, and this technology is routinely applied for the analysis of key blood electrolytes, such as potassium, sodium, calcium, chloride and pH (Young 1997). ISEs are made of 2 electrodes; the indicator electrode, which includes a membrane, usually polymeric, at the end that is able to up-take the desired ion species and the reference

electrode (Allen 2003; Bakker and Pretsch 2007). Thanks to ISEs, potentiometric sensors offer the benefit of true trace-level analysis at sub-nanomolar concentrations (Bakker and Pretsch 2005). Additionally, they offer the benefits of small size, rapid response, ease of use, low cost and resistance to color and turbid interferences (Ding and Qin 2020). Ever since the impressive improvement in the limit of detection and ISE sensitivity by Pretsch et al. in 1997, thanks to technological improvements, the LOD has been lowered by factors of  $10^6$  and  $10^{10}$  (Sokalski et al. 1997; Bakker and Pretsch 2007). Not surprisingly, the development of new ISE materials, such as solid-contact ISE materials, has been one of the most active research areas in the field of potentiometric sensors. Such materials include polymers such as poly(3,4-ethylenedioxythiophene) (PEDOT), polypyrrole, and poly(3-octylthiophene) (POT), but also newer materials, such as carbon nanotubes, reduced graphene oxide and gold clusters (Zdrachek and Bakker 2019b). Recently, there have been many implementations of ISEs in point-of-care diagnostics; one example is an electrochemical paper-based analytical device equipped with a small ion-selective paper electrode, for the detection of chloride ions in aqueous solutions (Lan et al. 2014). Another example is a sensing array platform for the continuous detection of the carbon cycle in freshwater ecosystems (Pankratova et al. 2015). Potentiometric biosensors have also found applications in wearable electronics, and even tattoo-based potentiometric biosensors have been designed (Parrilla et al. 2016; Parrilla et al. 2019). Moreover, a number of recent innovations in the field of potentiometric sensors have provided suggestions which can further improve detection times and accuracy, such as a carbonate-selective membrane electrode containing a highly selective tweezer-type ionophore in combination with a pH electrode, designed for  $\text{PCO}_2$  detection, which provided a vastly improved response time in freshwater ecosystems (Zdrachek and Bakker 2019a).

As there is a growing demand for accurate and rapid DNA detection systems, potentiometric sensors in combination with nanoparticles can provide DNA and RNA analysis using very small amounts of sample volumes, even microliters (Ding and Qin 2020). Examples of ISE electrodes in combination with nanoparticles include a poly(vinyl chloride)membrane sensor for Cr(III) ions in combination with  $\text{TiO}_2$  nanoparticles, which exhibited improved performance in comparison to existing electrodes (Fekri et al. 2011). Other examples involve the use of PbS or  $\text{Ag}_2\text{S}$  nanoparticles; both examples resulted in improved response times and accurate detection of analytes (Shukla et al. 2002; Song et al. 2008). Finally, carbon paste electrodes (CPE) show a number of advantages over membrane electrodes, including renewability, stable response and high selectivity (Kakhki 2013). With regards to DNA detection, there are plenty of potentiometric sensors. A potentiometric microsensor platform developed by Numnuam et al. used a sandwich DNA hybridization method for capturing a secondary oligonucleotide attached to CdS-nanocrystal tags, and through the quantification of released  $\text{Cd}^{2+}$  through a polymer selective microelectrode, highly-sensitive DNA quantification is possible, with a detection limit of 28 fmol (Numnuam et al. 2008). Another approach included using liposome nanocarriers loaded with calcium signaling ions, which provided the benefit of avoiding the use of potentially toxic CdS tags, as well as sub-fmol DNA detection. The

platform was assessed for *Escherichia coli* rRNA detection, where it exhibited excellent sensitivity (Chumbimuni-Torres et al. 2010). Additionally, enzyme tags may be used for the quantification of DNA hybridization. One such application is described by Wu et al., who used a low-volume solid-contact silver ion-selective electrode to quantify the released silver ions produced by the biometallization reaction of the alkaline-phosphatase enzyme tag. The platform enabled the detection of 16S rRNA of *E.coli* with good sensitivity (10 CFU in 4ml sample) (Wu et al. 2009). A recent example by Qin et al. describes the use of two enzymatic tags, horseradish peroxidase (HRP) and alkaline phosphatase in a platform based on a magnetic beads-enzyme sandwich assay, where it was demonstrated that the intermediates of both the HRP-H<sub>2</sub>O<sub>2</sub> oxidation reaction and the ALP-catalyzed hydrolysis can be simultaneously detected by a single ISE (Ding et al. 2018). The same group has also developed a label-free DNA assay, exploiting the G-quadruplex/hemin DNAzyme-catalyzed oxidative coupling of monomeric phenols, which resulted in a sensitive DNA sensor with a detection limit of 0.02 ng/ml (Wang et al. 2014b). Finally, potentiometric sensors have also been developed for microRNA detection. Goda et al. developed a microelectrode array for use following a reverse transcription polymerase chain reaction (Goda et al. 2012). A more recent platform used a nanopore-based platform based on potentiometry to accurately measure microRNA production (Makra et al. 2017).

However, there are some drawbacks associated with potentiometric sensors. For example, in cases where nanoparticles are used, redox sensitivity is often a problem in potentiometric sensors. In cases where conducting materials are used in the membrane phase, nanoparticles embedded in the membrane can participate in redox reactions, which can affect sensor sensitivity. Because of this, the amount of oxygen dissolved in the sample solution is of great importance to these electrodes and should be carefully monitored (Kakhki 2013).

#### 1.4.6 Impedance biosensors

**Impedance biosensors** Electrochemical impedance spectroscopy (EIS) can be used to determine the resistive and capacitive properties of materials upon stimulation of the system by a small amplitude excitation signal (~2–10 mV). The frequency is altered over a wide range to generate an impedance spectrum (Labib et al. 2016). As EIS measured both electrical resistance and reactance, it allows for the analysis of both real and imaginary components of impedance, as shown in Figure 5 (Grieshaber et al. 2008). More detail around EIS will be provided in Chapter 3, however a brief description is provided here.

$$Z(j\omega) = \frac{U(j\omega)}{I(j\omega)} = Z_r(\omega) + jZ_i(\omega); \quad \omega = 2\pi f$$

*Equation 1.1: EIS equation (Grieshaber et al. 2008)*

One big advantage of EIS is that it enables the label-free and real-time detection of biomolecules through the measurement of small changes in the electrode-electrolyte interface impedance, which enables the detection and quantification of probe-analyte

interactions (Manickam et al. 2012). Thanks to EIS, the study of conductivity/resistivity or capacitance of electrochemical systems and the processes that may affect them, such as the degradation of insulating polymers. If, following coating with an insulating polymer and exposure to enzymes, free ions are able to penetrate into the polymer, the impedance characteristics of the transducing element would be modified (Fernández-Sánchez et al. 2005). For example, a recent study used EIS to assess the fabrication process of a hydrogen peroxide (HRP) biosensor (Tong et al. 2007). Additionally, EIS has also been used in the fabrication step of a label-free screen-printed gold electrode for EIS detection of bacteria through the selective detection of lectin (Gamella et al. 2009). Another, more recent example of the technology being used in the fabrication stage is provided by Han et al., who used EIS to control the fabrication and the recognition of analytes on the electrode surface and develop a label-free EIS cytosensor for cancer cells (Han et al. 2016).

With regards to electrochemical sensing, there is a plethora of EIS biosensors in literature. For example, Tung et al. developed an electrochemical biosensor for the detection of a weak interaction between dengue virus and its receptor (C-type lectin domain family 5, member A), by using anodic aluminum oxide modified with gold nanoparticles, and used EIS to detect the hybridization event (Tung et al. 2014). Yang et al. developed an ultrasensitive sensor using gold nanoparticles deposited on carbon nanotubes for the detection of IL-6 in serum with a low detection limit of  $0.01 \text{ fg mL}^{-1}$  (Yang et al. 2013c). Additionally, there are plenty of EIS-based aptasensors. For example, Reich et al. developed a sensor using an aptamer for the detection of staphylococcal protein A, co-immobilized with 6-mercaptohexanol onto gold electrodes. The sensor provided accurate detection of *Staphylococcus aureus* at a limit of  $10 \text{ CFU}\cdot\text{mL}^{-1}$  in 10 minutes (Reich et al. 2017). Sypabekova et al. developed an aptamer for the detection of *Mycobacterium tuberculosis* secreted protein MPT64 co-immobilized with 6-mercaptohexanol, which exhibited good sensitivity and selectivity with a detection limit of  $4.1 \text{ fM}$  (Sypabekova et al. 2019). Another interesting example is described by Songjaroen et al., who developed a microwire based, electrochemical DNA immunoassay sensor for the detection of C-reactive protein (CRP) in serum samples, using a ss-DNA aptamer plus anti-CRP antibodies, with a detection range between  $3.125\text{--}25 \text{ mg/L}$  (Songjaroen et al. 2016).

### 1.5 Biofouling and its prevention

EC detection is significantly held back by the susceptibility of the electrochemical platform to biological fouling (**biofouling**), which is defined as the non-specific adsorption of biological materials, such as proteins, cells and oligonucleotides on electrode surfaces which leads to electrode fouling (Gooding 2019). These biological contaminants attach to the platform after a series of interactions, such as hydrophobic, electrostatic and intermolecular, and result in the formation of a dense contaminant layer coating the electrode, which significantly inhibits signal recognition and transduction. This biofoulant layer causes issues with sensing not only through physically inhibiting attachment of the biomarker to the electrode but by also interfering with electron transfer through electrochemical responses (Lin and Li 2020).

Biofouling is not exclusive to sensors, but also medical implants, textiles, food packaging and storage and water purification systems, however its prevention is of great importance to electrochemical biosensors, as deterioration of sensor performance can be detrimental for biosensing platforms (Banerjee et al. 2011; Gooding 2019). As biosensors are the most active field in analytical chemistry and the need for reliable sensors keep increasing, a series of antifouling methods have been developed (Lin and Li 2020). An ideal antifouling agent should be biocompatible, naturally inert and able to withstand the conditions a complex environment, such as various bodily fluids (e.g. whole blood) (Lin and Li 2020). Most antifouling strategies focus on the construction of antifouling electrochemical platforms through the use of materials such as polymers, hydrogels, peptides, and thiolated self-assembled monolayers (SAMs), which will be described below (Campuzano et al. 2019). A past example of biofouling prevention with regards to glucose biosensing in whole blood sensors, was the application of a semi-permeable **membrane** which allowed the passage of the small molecule of glucose but prevented the passage of proteins (Barfidokht and Gooding 2014). Such membranes continue to find use in today's biosensors, and they include Nafion, hyaluronic acid, humic acids, phosphorylcholine, 2-methacryloyloxyethyl phosphorylcholine, polyurethanes with phospholipid polar groups and poly vinyl alcohol hydrogels (Vaddiraju et al. 2010).

### 1.5.1 Polymers for biofouling prevention

The use of hydrophilic, conducting, zwitterionic, and pH-responsive methacrylate **polymers** as a non-specific protein adsorption reducing agents is quite widespread, with hydrophilic polymers forming a hydration layer which prevents biofouling (Campuzano et al. 2019). As the electrode surface, usually made of gold or carbon-based structures, tends to have hydrophobic surfaces which attracts hydrophobic contaminants, a hydrophilic layer made up of a polymer can tightly bind water molecules and form a hydration layer which prevents biofouling (Lin and Li 2020) Poly (ethylene glycol) (Bonini et al.)-containing polymers are being considered the gold-standard in hydrophilic antifouling polymers, thanks to their ease in synthesis, globular nature, versatile functionalization, and superior biocompatibility profiles (Abbina et al. 2017; Campuzano et al. 2019). In addition to hydrophilic effects, PEG also exhibits antifouling properties thanks to steric hindrance effects (Francolini et al. 2017). There are two ways of treating an electrode surface with PEG; firstly, by applying a pre-synthesized PEG onto the surface and secondly by growing *in situ* the polymer via a surface adsorbed initiation group (Gölander et al. 1992). Moreover, size and packing density have been found to play an important role in PEG antifouling properties, with longer polymer lengths associated with reduced non-specific protein adsorption, possibly because of increased surface coverage (Bertesteanu et al. 2014; Francolini et al. 2017). In that respect, spontaneous formation of PEG chains on the electrode surface has been found to be particularly effective (Prime and Whitesides 1991). Additionally, innovative PEG polymers can provide enhanced antifouling properties to gold surfaces (Su et al. 2019). However, despite its widespread use and promising properties, PEG is held back by some limitations, such as low surface densities

and susceptibility to oxidative damage (Damodaran and Murthy 2016). PEG is oxidized rapidly in the presence of oxygen, metal ions and enzymes able to oxidize PEG hydroxyl groups, which may affect long-term effectiveness, especially in samples such as saliva (Damodaran and Murthy 2016). Finally, the formation of long chain PEG polymers can reduce the electrode sensitivity (Campuzano et al. 2019).

There are other polymers with antifouling properties. One example is conducting polymers conjugated to antifouling materials, before grafting to the electrode surface (Lin and Li 2020). One such polymer was utilized by Yang et al. by using poly(3,4-ethylenedioxythiophene)-poly(styrene sulfonate) (PEDOT: PSS), which functions as an anti-fouling modification on a glassy carbon electrode, with promising results (Yang et al. 2013d). Zwitterionic polymers, which carry a 1:1 positively and negatively charged residue and have an overall neutral charge, aim to overcome electrostatic attraction as all proteins contain both charged residues. Examples of such zwitterionic substances are phosphocholine, sulfobetaine and carboxybetaine. To create an antifouling layer, zwitterionic polymer brushes form a denser and thicker hydration layer than PEG on the electrode surface. However the activity of zwitterionic substances can be compromised, especially in cases of very low ionic solution, exceptionally large molecular weight, extreme high or low packing density, or significantly low temperature (Chen et al. 2010). Finally, pH-responsive methacrylate polymers, a relatively new antifouling strategy, has shown promising results.

### 1.5.2 Hydrogels in biofouling prevention

Other than polymers, **hydrogels** have also found numerous applications as antifouling agents in sensors. The simplest definition of hydrogel is a water-swollen, cross-linked polymeric network produced by the reaction of one or more monomers (Ahmed 2015). As they show outstanding biocompatibility and excellent water absorption properties, they are important candidates in electrode modification with regards to antifouling (Campuzano et al. 2019) In addition, there are more benefits to their use, such as their interaction with biological components at molecular level, their regulating viscoelastic properties, being reactive to external stimuli, providing important antifouling properties, and their easy synthesis methods and easy incorporation of bioreceptors on their surfaces. The most commonly used polymers for hydrogel synthesis are polypyrrole, polyaniline, and poly(ethylenedioxy thiophene) (Tavakoli and Tang 2017). An example of hydrogels as antifouling agents is shown by Rong et al., where a nanocomposite network composed of polypyrrole hydrogel (PPy hydrogel) with gold nanoparticles attached showed promising results and a very good detection range for label-free determination of carcinoembryonic antigen (Rong et al. 2015). **Peptides** have also shown promising results against non-specific protein adsorption. Polypeptides (or N-substituted glycines) have emerged as a class of sequence-specific materials, and thanks to their easy synthesis and control over their sequence and structure they can be designed into polymers having both hydrophilic and hydrophobic parts, by controlling the peptoid unit (Leng et al. 2015). An example of a successful aptasensor is presented by Cui et al., who

designed a sensitive and low-fouling aptasensor for the detection of alpha-fetoprotein, by using self-assembled aptamers and short-chained zwitterionic peptides, attached to a gold electrode by gold-sulfur bonding (Cui et al. 2017).

### 1.5.3 Self-assembled monolayers (SAMs)

Finally, **self-assembled monolayers (SAMs)** made up of thiol-tethered DNA probes on gold electrodes are commonly used in biosensors. They form an interface between the sensor surface and organic and biological materials, including fouling agents (Vericat et al. 2010). SAMs provide an easy way to functionalize electrode surfaces by organic molecules (both aliphatic and aromatic) containing free anchor groups such as thiols, disulphides, amines, silanes, or acids (Chaki and Vijayamohan 2002). SAMs provide the benefit of immense flexibility based on their terminal functionality (hydrophobic or hydrophilic) and chain length. For example, highly-packed, membrane-like structures can be generated by using long chain alkane thiols (Chaki and Vijayamohan 2002). In order to further control the monolayer structure and improve binding with the target, a second alcohol-terminated diluent thiol component is often introduced. Mercaptohexanol (MCH), 2-mercaptoethanol, 4-mercaptobutan-1-ol, 2-mercaptoundecanoic acid, and 11-mercaptoundecanol are commonly used for such purposes. The molecules are attached on the surface of the gold electrode and their arrangement, formed in either solution or vapor phase, is influenced by intermolecular forces (Vericat et al. 2010). To combat non-specific protein adsorption and provide control over the spacing between the probes, a range of methods to alter surface chemistry have been developed, such as thioaromatic DNA monolayers, ternary monolayers and tetrahedral DNA nanostructures (Campuzano et al. 2019). An additional benefit of SAM use include their ability to form on a variety of surface shapes, sizes and topographies, and an example is provided in Figure 1.15 below (Vericat et al. 2010).

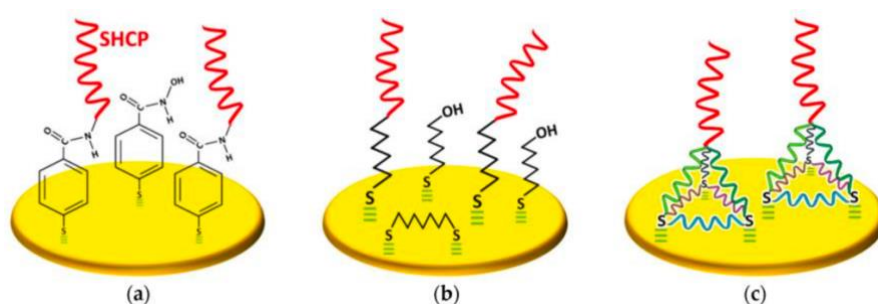


Figure 1.15: Three types of thiolated monolayers: a) thioaromatic DNA monolayer b) ternary DNA monolayer and c) thiolated DNA tetrahedral nanostructures (Campuzano et al., 2019)

The use of S-headgroup compounds, such as **thiols**, **dithiols**, disulfides and sulfides provide several benefits when used on oxide-free metals and on semi-conductors. A thiol molecule is made up of the sulfur headgroup, which binds strongly to the substrate, the hydrocarbon chain which stabilizes the monolayer through van der Waals interactions, and the terminal group, which can have various functionalities and can be modified to provide the SAM with various properties, such as hydrophobicity. Dithiols, which are -SH terminated thiols, are

commonly used to bind nanoparticles and metallic ions to the monolayer. They can be easily prepared from gas phase or in liquid environments, the strength of the S–Au bond and by van der Waals interactions provide stability and are relatively stable in ambient conditions. In this SAM subtype, the most commonly used molecules are alkanethiols and, less commonly, those of arenethiols, alkanedithiols and arenedithiols. Commonly used sulfides and disulfides include dialkyldisulfides and dialkylsulfides (Vericat et al. 2010). The advantages of thioaromatic DNA monolayers include improved antifouling performance, packing efficiency and high electrical conductivity (Miranda-Castro et al. 2018).

**Ternary SAMs** involve the self-assembling of two thiolated compounds as spacers coupled with an appropriate thiolated capture probe on gold electrodes, with the final charged component being a molecule such as 3-mercaptopropionic acid (MPA), or a cyclic or linear dithiol (Campuzano et al. 2019). They provide the benefit of improved signal-to-noise characteristics of many biosensors in comparison to common SAMs. A number of studies have found they provide better non-specific protein adsorption compared to thiol SAMs, such as the simple, highly compact monolayer developed by Wu et al. which combined a SHCP, mercaptohexanol and dithiothreitol in an electrochemical biosensor for the detection of DNA in bodily fluids (Wu et al. 2010). Ternary SAMs have also been successfully implemented in aptasensors, with an example by Ding et al. constructing a label-free EIS aptasensor, using RNA aptamer capture probe modified with 1,6-hexanedithiol (HDT) and 6-mercapto-1-hexanolphosphate (MCH) on a gold interdigitated electrode array (Ding et al. 2017).

**PEG-based SAMs** and its derivatives are commonly used as substrate modifications on both Au and Si, to prevent non-specific protein adsorption, as well as to increase hydrophilicity. PEG molecules are attached to gold substrates after functionalization with a thiol group, while various techniques have been utilized for silicon, such as modification with oxysilane groups (Cerruti et al. 2008). However, as the sulfur-thiol bond in PEG monolayers has been found to weaken after a few hours in ambient conditions, a series of strategies have been adopted to improve stability, such as PEG-thiol SAMs prepared using an alkylic chain as a spacer between the thiol end-group and the EG units (Huertas et al. 2018). PEG architecture is also important for antifouling efficacy, with a comparison of three PEG attachment methods by Henry et al. for DNA biosensors found that the combination of the capture probe with bipodal aromatic PEG alkanethiol on an electrode chip provided improved antifouling performance and increased sensor sensitivity when compared with the other two methods (Henry et al. 2010). Additionally, spacer length has also been proven to be crucial, with a study on PEG spacer length by Fernández et al. indicating that among all spacers tested (PEG-4, PEG-6, PEG-8 and PEG-12), PEG-6 offered the best antifouling properties (González-Fernández et al. 2018).

Finally, **tetrahedral DNA** nanostructures have also found applications as antifouling scaffolds. Tetrahedral DNA structures form when four appropriately designed ss-oligonucleotides (three of them thiolated) are annealed together in solution, forming a highly rigid tetrahedron

with a linear sequence protruding at the top, which allows for attaching recognition elements with an upright rotation and away from the electrode surface (Campuzano et al. 2019). Thanks to the easy synthesis, rigidity and adaptability of the nanostructure, plus the well-defined probe-to-probe spacing make it an attractive antifouling option (Goodman et al. 2004; Pei et al. 2010). A platform developed by Dong et al. found that tetrahedral nanostructure probes had a 5000-fold higher affinity for the biomarker and less non-specific protein adsorption compared to single point-tethered oligonucleotides (Dong et al. 2015). Tetrahedral DNA structures have been widely used for DNA probe immobilization, with a platform developed by Ge et al. using a protruding DNA hairpin “helper” structure to effectively detect microRNA with a detection limit of 10 aM (Ge et al. 2014). Additionally, antibodies have also been immobilized on the nanostructures, and in the case of Wang et al., an antibody against pneumococcal surface protein A was used, which resulted in a sensor with a low limit of detection (LOD) of 0.218 ng/mL, capable of detecting *S. pneumoniae* in a range of uncultured body fluids (Wang et al. 2017a). Moreover, tetrahedral structures have been used for the display of aptamers as biosensing molecules, which significantly improves detection in comparison with conventional probe creation methods (Pei et al. 2010). An example is the ultrasensitive serum cocaine sensor developed by Wen et al, which used a tetrahedral structure with a protruding anti-cocaine aptamer. The tetrahedral structure not only prevented interprobe entanglement, but also ensured high selectivity and sensitivity (Wen et al. 2011).

#### **1.5.6 Electrochemical sensor limitations**

EIS assays often require laborious optimization and control stages for interface development, especially in the case of complex biological samples or multiple biomarkers which may significantly hold back the development of the sensor (Garrote et al. 2019). However, biofouling prevention methods can significantly help with this issue. Another challenge in label-free EIS assays is the quality control of the self-assembled monolayer, which can greatly affect the performance of the biosensor. As the SAM is susceptible to defects from a variety of factors, such as thiol purity, surface roughness etc., extra attention needs to be paid to this stage (Garrote et al. 2019). Additionally, the control of the quality of SAM is of great importance and a frequent cause of problems in research, as the ideal SAM is far from achievable thanks to a number of defects, especially in the case of hard-to control dithiol SAMs (Vericat et al. 2010).

#### **1.6 Optical biosensors**

Optical biosensors are another common type of sensors which provide a range of benefits such as direct, real-time and label-free detection of many biological and chemical markers, plus they have a record of good performance as biosensors (Damborsky et al. 2016). Some further advantages offered by optical biosensors include the provision of critical information during the binding process of the biomarker or chemical compound, such as binding interactions, binding kinetics, association-dissociation rates and mathematical affinity

(Altintas 2018). Optical sensors measure the change in the optical properties in the presence of the biomarker, such as absorption, reflectance, emission, or interferometric pattern, which are then recorded by a photodetector (Peltomaa et al. 2018). In addition, optical biosensors provide high specificity, sensitivity, small size and cost-effectiveness (Damborsky et al. 2016). Besides healthcare and diagnostics, optical biosensors have also found applications in environmental monitoring, drug discovery and the food industry (Chen and Wang 2020).

Optical biosensors can be generally be classified in two categories: label-free and label-based. Label based sensors use, as suggested, labels, such as fluorescent or luminescent dyes, enzymes or nanoparticles (Damborsky et al. 2016). They are widely used for measurement in spectroscopy via fluorescence, phosphorescence, absorption, refraction, Raman surface-enhanced Raman scattering and dispersion spectrometry. The most widely used detection for optical sensors includes Surface Plasmon Resonance (SPR), Wavelength based SPR, Ellipsometry etc. (Khansili et al. 2018). In the case of fluorescence of luminescence methods which are widely used today, they attach with high sensitivity and specificity to targets, with detection limits down to one molecule, and the intensity of the fluorescence is related to the presence of the biomarker and the interaction strength between the biomarker and sensing molecule (Fan et al. 2008). However they also have a number of drawbacks, such as the requirement of costly fluorescent or luminescent agents, such as tags or dyes (Li et al. 2020). In addition, label-based methods are held back by laborious labeling processes that can cause interference with the function of a biomolecule. Additionally, quantitative analysis is difficult due to the fluorescence signal bias, as the number of fluorophores on each molecule cannot be accurately estimated (Fan et al. 2008).

Label-free optical biosensors offer a more attractive optical sensor, as they provide high sensitivity, direct and real-time measurement in addition to multiplexing capabilities (Peltomaa et al. 2018). Label-free sensors detect molecules in their natural forms, without the need for labelling or alteration. Furthermore, label-free sensing reduces costs and effort needed to develop assays, simply by removing elements such as shelf-life and background fluorescence (Khansili et al. 2018). Moreover, label-free sensors measure changes associated by sample concentration or surface density instead of total sample mass, such as refractive index, which makes them ideal for the detection of markers found in ultrasmall amounts (Fan et al. 2008).

### **1.6.1 Surface plasmon resonance (SPR) sensors**

SPR sensors are based on the SPR phenomenon which takes place on the surface of metal (or other conducting materials) at the interface of two media such as glass and liquid when it is illuminated by polarized light at a specific angle. This generates surface plasmons, which then leads to a reduction of the intensity of reflected light at a specific angle, which is also known as the resonance angle. This effect is proportionate to the mass on the surface. A sensorgram can be generated through the measurement of the shift of reflectivity, angle or wavelengths

versus time. In all configurations, the SPR phenomenon enables direct, label-free and real-time changes of refractive index at the sensor surface, which is proportionate to the biomolecule concentration (Khansili et al. 2018). A typical SPR sensor uses a combination of an optical detector part, usually measuring intensity shift, a sensor chip with a gold surface, and a layer for ligand immobilization, which is integrated with a fluidics system, enabling a flow-through operation. Additionally, the chip contains a functional layer enabling the attachment of sensing molecules, usually through formation of a SAM covered with a carboxymethylated dextran, allowing the effective immobilization of protein using N-hydroxysuccinimide (NHS) chemistry (Damborsky et al. 2016). An exemplar photo of a SPR setup is shown in photo 1.16 below.



*Figure 1.16: Photo of an exemplar SPR setup (Cropped from (Patel, 2017))*

Three types of SPR analyses are used: kinetic analysis, equilibrium analysis and concentration analysis. For the characterization of molecular interactions, such as ligand–analyte binding, antibody–antigen interaction, receptor characterization etc., kinetic and equilibrium analyses are preferred, while concentration analysis has applications in other fields, such as in clinical diagnostics, environmental analysis, food industry etc. (Damborsky et al. 2016). There is an abundance of sensors utilizing SPR, such as the SPR biosensor system with dispersionless microfluidics for the direct and label-free detection of a soluble vascular endothelial growth factor receptor, with a detection limit of 25 ng/mL (Pimkova et al. 2012). SPR sensors have also been developed for a number of inflammatory biomarkers such as IL-6 production after LPS induction (Chou et al. 2010), C-reactive protein (Meyer et al. 2006), IL-10 (Yoon et al. 2010) and procalcitonin (Sener et al. 2013). Additionally, SPR was used in a study by MacKenzie et al. in order to study in depth the kinetics of the LPS OAg of Salmonella serogroup B bacteria binding wild type Fab and scFv monomers (MacKenzie et al. 1996). Moreover, Roche et al. applied SPR to gain information about the specificity and avidity of protective antibodies against Francisella tularensis LPS (Roche et al. 2011). Finally, SPR can be combined with other techniques; one such example was the process employed by Broecker et al., who

combined SPR with STD-NMR (Saturation Transfer Difference-Nuclear Magnetic Resonance) and studies the *Yersinia pestis* LPS (Broecker et al. 2014). However, SPR also presents some limitations, such as difficulty discriminating between specific and non-specific interactions with the sensor surface and difficulties in detecting the binding of low molecular weight compounds (Ahmed et al. 2010). In addition, an issue with SPR is the limited sensor area, causing a diminished capacity; increasing the sensor surface, or performing several runs, might diminish this limitation (Catimel et al. 2001). Finally, **SPR imaging** (SPRi) takes the SPR analysis a step further by combining the sensitivity of SPR and spatial imaging in a microarray format, which enables the simultaneous study of numerous different interactions (Damborsky et al. 2016). A successful application of SPRi is described by Li et al., who used SPRi to study the kinetics behind the binding of immunosuppressive drug (FK506) and its target protein (FK506-binding protein 12 (FKBP12), with very good sensitivity (Li et al. 2015).

### **1.6.2 Localized surface plasmon resonance (LSPR)**

**LSPR** exploits the unique optical properties of metallic nanoparticles (gold, silver, copper aluminum etc.), which are not observed in larger metal structures. LSPR is an optical phenomenon induced as collective oscillation of conduction band electrons produced by the interaction of light with these nanoparticles (Khansili et al. 2018). Therefore, the difference between SPR and LSPR is that induced plasmons oscillate locally on the nanostructure rather than along the metal/dielectric interface (Damborsky et al. 2016). An interesting feature of LSPR is the possibility of tuning the SPR intensity by modifying the size, shape, composition, and environment of the nanostructures, such as metal nanoparticles, carbon nanotubes or nanowires (Abbas et al. 2011). A classic application of LSPR is the red color of aqueous dispersions of colloidal gold particles (Damborsky et al. 2016). Therefore, LSPR is a popular nanoscale phenomenon with considerable recent interest, as it allows for better optimization, adaptation and miniaturization in comparison with SPR, and can even deliver the same performance as SPR but with significantly lower surface densities of interacting molecules (Piliarik et al. 2012; Damborsky et al. 2016). An example of a successful LSPR-based microarray nanochip for the immunoglobulins, C-reactive protein and fibrinogen was developed by Endo et al., utilizing antibodies immobilized on nanospots, with a detection system of detection limits of  $100 \text{ ng} \cdot \text{l}^{-1}$  (Endo et al. 2006). Another example is the platform developed by Yuan et al., which utilized antibodies immobilized on a nanochip made up of silver nanoparticles, provided sensitive detection of human epididymis secretory protein 4 (HE4) biomarker, with a detection limit of 4 pM (Yuan et al. 2012). Importantly, LSPR can also be enhanced by fluorescence, which improves on one of LSPRs weaknesses: limited spectral sensitivity and impaired detection of low molecular weight molecules. One such application was designed by Mei and Tang, who developed an ordered gold nanorod (GNR) assembly in a vertical standing array on a glass substrate, which resulted in enhanced LSPR effect between the adjacent nanoparticles. The addition of fluorescence offered a highly functional and ultrasensitive DNA biosensor, with a detection limit of 10 pM (Mei and Tang 2017). An interesting paper-based biosensing platform was developed by Andreea Campu et al., utilizing

LSPP, Surface Enhanced Raman Spectroscopy (SERS), and Metal Enhanced Fluorescence (MEF). They exploited unique optical properties of gold nanobipyramids onto cellulose fiber through the plasmonic calligraphy approach using a commercial pen and developed a point-of-care sensor combining three technologies (Campu et al. 2019).

### **1.6.3. Evanescent wave fluorescence biosensors**

In **evanescent wave fluorescence biosensors**, the biological recognition and the consequent binding event occur within the confines of an evanescent wave, that is, the wave that arises from the manner in which light behaves when confined in an optical waveguide or fibers (Damborsky et al. 2016). In the evanescent field, analytes are recognized by the partner receptors immobilized onto the surface of a waveguide and therefore change the guiding properties of the waveguide; in particular, the waveguide is shifted into the effective mode index. The changes in the effective mode index can be examined by the optical properties of the waveguide, i.e., phase, amplitude, resonant momentum, variations corresponding to the object concentration, and biomolecular conformation. As the evanescent wave phenomenon takes place near the surface, it can be used to generate fluorescent signals upon excitation of molecules close to the surface. This can help minimize background noise and enhance signal of bound analytes (Estevez et al. 2012). A benefit of evanescent wave biosensors is the fact that signal does not become weaker with reduced sample volume, instead it is proportional to the concentration of analyte that come into contact with the surface, making them an ideal choice for use in samples with limited volumes (Huertas et al. 2019). An example of such a biosensor was developed by Lochhead et al., which used microarrays of recombinant antigens and antibodies in a fluidic channel, providing multiple parallel fluorescence immunoassay results for a single sample, resulting in effective HIV, syphilis and hepatitis C diagnosis with excellent sensitivity (Lochhead et al. 2011).

### **1.6.4 Bioluminescent optical fiber biosensors**

Bioluminescent optical fiber biosensors use bioluminescent cells, and the bioluminescent signal is transferred from the analyte to optical fiber (Damborsky et al. 2016). In contrast to fluorescence, bioluminescence does not require indirect radiation and offers excellent sensitivity, however it is held back by its low-brightness nature and difficult engineering of novel bioluminescent molecules. In order to prepare bioluminescent reporters for biosensor use, luciferins, which are light-emitting bioluminescent compounds, modified into labile, inactive structures (i.e., caged luciferins) that become uncaged in the presence of the analyte. C-6 position modifications are the most common alteration for d-luciferin. (Yeh and Ai 2019). An example of a bioluminescence sensor using modified *E coli* cells, capable of producing a luminescent signal in the presence of toxic agents. Following cell immobilization to an optic fiber, the sensor reported effective detection of atrazine, a herbicide in drinking water, with a detection limit of 10 pg/L (Jia et al. 2012). Another bioluminescence sensor exploited the properties of modified d-luciferin, by introduction of a methanol moiety to the molecule,

which resulted in sensitive detection of human carboxylesterase 1 in cells (Wang et al. 2016). Finally, a microfluidic thread-based analytical device developed by Tomimuro et al., for antibody detection of hepatitis, HIV and dengue fever in whole blood by means of bioluminescence resonance energy-transfer (Brett) switching sensor proteins (Tomimuro et al. 2020).

#### **1.6.5. Ellipsometric biosensors**

Ellipsometric biosensors measure changes in the polarization of light when it is reflected from a surface (Damborsky et al. 2016). It is known as the best technique for the study of surfaces and various applications of it, such as image ellipsometry and spectroscopic ellipsometry are commonly employed in biosensing (Li et al., 2017). Imaging ellipsometry offers a number of benefits, such as high-throughput multiplexed analysis and quantitative real-time testing which does not involve any labelling or expensive components or maintenance (Elwing 1998; Sun et al. 2015). Additionally, ellipsometry provides the advantage of determination of the total amount of protein in an adsorbed layer without the need for destruction of the protein. As the surfaces used for ellipsometry must be flat and reflecting, metallic (in particular gold), spin-coated polymer surfaces and silicon surfaces are ideal. Ellipsometry has found many applications in the study of protein adsorption and conformational changes induced upon them, as well as antibody adsorption and competitive protein adsorption (Elwing 1998). There are a number of biosensor applications using ellipsometry, such as the microarray biosensor based on total internal reflection imaging ellipsometry (TIRIE), which used antibodies immobilized on a PEGylated phospholipid membrane, with a detection limit of 18.2 U/ml (Zhang et al. 2011). Another example using a label-free microarray-based ellipsometric sensor is provided by Fei et al., who immobilized biotinylated receptors on a streptavidin-functionalized solid surface and by measuring the binding curves of influenza A strains, their analysis was possible (Fei et al. 2015). Qi et al. developed a platform using anti-avian influenza antibodies immobilized on silicon wafers, which allowed for rapid and sensitive detection of H5N1 and H9N2 strains in less than 10 minutes (Qi et al. 2010). Another similar example is a method developed by Sun et al. based on high spatial resolution imaging ellipsometry, using anti-cytomegalovirus antibodies immobilized on silicon wafers, provided sensitive detection with sensitivity of 0.01 IU/mL (Sun et al. 2015). Furthermore, a rapid solution-immersed silicon biosensor using a direct antigen-antibody affinity assay resulted in sensitive detection of hepatitis B virus (Diware et al. 2017). Finally, ellipsometry can be combined and enhanced with surface plasmon enhancing, by the incorporation of a thin metal film between the biolayer and the prism, which resulted in acceptable detection of biomarkers (Yuan et al. 2009).

#### **1.6.6 Surface-enhanced Raman scattering (SERS) biosensors**

SERS sensors are based on electromagnetic field enhancement in the proximity of shaped nanostructures, such as textured metallic surfaces or gold/silver nanoparticles. An example of such a sensor was developed by Srivastava et al., by immobilizing antibodies against

vitellogenin on nanosculpted thin films made of silver on silicon substrates, which resulted in a sensitive sensor a limit of detection of 5 ng · l<sup>-1</sup> (Srivastava et al. 2014). The combination of SERS with epidermal growth factor receptors (EGFRs) attached to a hollow-core photonic crystal fiber, followed by an anti-EGFR antibody conjugated SERS nanotag, resulted in sensitive detection of proteins in very small sample volumes (U et al. 2012). Finally, SERS has been used for miRNA detection; Kim et al. used a complementary DNA probe platform and gold nanopillars to develop a highly sensitive, selective, label-free miRNA sensing (Kim et al. 2019).

However, optical biosensors also come with some **limitations**. Due to the high cost of some instruments required for their use, their applications are limited and mostly confined to academic and pharmaceutical environments (Dey and Goswami 2011; Damborsky et al. 2016).

As it has been understood that early and accurate diagnosis of a disease is critical for effective treatment and improved patient outcomes, the belief that a singular biomarker is adequate for accurate diagnosis of a disease, according to research, has been challenged (Dincer et al. 2017). Moreover, there is a lot of interest in the development of systems capable of detecting multiple pathogens simultaneously, and developing a rapid, low-cost, and reliable quantification (Dincer et al. 2017). In that light, **multiplexing** (simultaneous detection of multiple analytes) has become a popular topic in POC research in the last decade (Spindel and Sapsford 2014). As it has been understood that disease and therapeutic response often involve the inter-play between many biological processes, it would make sense to focus on the multiple detection of biomarkers rather than a single entity (Donzella and Crea 2011). The measurement of multiple biomarkers is important as one biomarker may be indicative of more than one disease and related diseases can manifest with similar physical symptoms (Spindel and Sapsford 2014). As an example, the detection of sepsis, a frequent complication of pneumonia, requires the measurement of multiple biomarkers (Zupančič et al., 2020). Unfortunately, as no single sepsis biomarker shows appropriate specificity and sensitivity for disease diagnosis, multiplex detection of multiple biomarkers is considered the preferred POC diagnostic method (Reinhart et al. 2012).

### **1.7 Biosensor review conclusions**

Following a thorough literature search and assessment of the pros and cons of each sensor type, it was decided to proceed using electrochemical sensors in this project. The main criteria that led to this decision is their ease of fabrication, rapid set up, the non-requirement of expensive or complicated equipment or reagents, and the potential for miniaturization and transfer into POC devices (Campuzano et al. 2017).

## 1.8 Scope of thesis

The overarching aim of this project was to develop sensing platforms for three different types of biomarkers: A protein marker, namely IL-6, a nucleic acid, namely the DNA sequence for beta-globin, and endotoxin, a lipid-sugar conjugate. To achieve this, electrochemistry was used in order to develop sensors that can be ideally transferred to POC platforms, or alternative sensing instruments such as SPR platforms.

Regarding endotoxin detection, in Chapter 2 initial experiments focused on developing sample preparation approaches for use with the gold standard LAL assay. Spike-and-dilution studies, where plasma samples are spiked and stored over a period of time and under defined conditions before testing have been undertaken to allow the study of interactions with plasma components over time.

Chapter 3 builds on existing research from within the group and is focused on the development of aptamer-based sensors, including the development of a conventional aptasensor and a hybrid-imprinted molecularly imprinted polymer (aptaMIP). aptaMIPs have been developed by previous lab members in the past for the successful detection of PSA and endotoxin (Jolly, 2016, Demertzis, 2019).

Chapter 4 combines the insights of Chapter 2 and 3. A complete sample preparation protocol for the detection of endotoxin in blood plasma has been developed and described in this Chapter. Deployment of the aforementioned protocol to spike-and-dilution samples allowed for performance comparisons to be made between the newly developed sensing systems and the existing LAL assay.

Chapter 5 focuses on the combined efforts of the Cardiff Interdisciplinary Training Hub (IDTH), which led to the use of sensitizers developed by collaborators in the School of Chemistry for the detection of IL-6 and beta-globin DNA. IL-6 detection has been facilitated by aptamers, whereas a complementary ss-DNA strand will be used for beta-globin DNA detection.

Each sensor has been challenged with citrated blood plasma following suitable preparation, to demonstrate their efficiency in clinical settings and their potential applications in real-life diagnostics.

## 1.9 Bibliography

- Abad-Valle, P. et al. 2005. Genosensor on gold films with enzymatic electrochemical detection of a SARS virus sequence. *Biosens Bioelectron* 20(11), pp. 2251-2260. doi: 10.1016/j.bios.2004.10.019
- Abadeer, N. S. et al. 2015. Interactions of Bacterial Lipopolysaccharides with Gold Nanorod Surfaces Investigated by Refractometric Sensing. *ACS Appl Mater Interfaces* 7(44), pp. 24915-24925. doi: 10.1021/acsami.5b08440
- Abbas, A. et al. 2011. New trends in instrumental design for surface plasmon resonance-based biosensors. *Biosens Bioelectron* 26(5), pp. 1815-1824. doi: 10.1016/j.bios.2010.09.030
- Abbina, S. et al. 2017. Hyperbranched polyglycerols: recent advances in synthesis, biocompatibility and biomedical applications. *J Mater Chem B* 5(47), pp. 9249-9277. doi: 10.1039/c7tb02515g
- Agnello, L. et al. 2016. Utility of serum procalcitonin and C-reactive protein in severity assessment of community-acquired pneumonia in children. *Clin Biochem* 49(1-2), pp. 47-50. doi: 10.1016/j.clinbiochem.2015.09.008
- Ahmed, E. M. 2015. Hydrogel: Preparation, characterization, and applications: A review. *J Adv Res* 6(2), pp. 105-121. doi: 10.1016/j.jare.2013.07.006
- Ahmed, F. E. et al. 2010. Surface Plasmon Resonance (SPR) Spectrometry as a Tool to Analyze Nucleic Acid-Protein Interactions in Crude Cellular Extracts. *Cancer Genomics - Proteomics* 7(6), p. 303.
- Alcoba, G. et al. 2017. A three-step diagnosis of pediatric pneumonia at the emergency department using clinical predictors, C-reactive protein, and pneumococcal PCR. *Eur J Pediatr* 176(6), pp. 815-824. doi: 10.1007/s00431-017-2913-0
- Alcon, A. et al. 2005. Pathophysiology of pneumonia. *Clin Chest Med* 26(1), pp. 39-46. doi: 10.1016/j.ccm.2004.10.013
- Aldakeel, S. A. et al. 2020. Identification of seven novel variants in the beta-globin gene in transfusion-dependent and normal patients. *Arch Med Sci* 16(2), pp. 453-459. doi: 10.5114/aoms.2019.84825
- Allen, J. R. 2003. pH Electrodes, Ion-Selective Electrodes, and Oxygen Sensors: Electrochemical Sensors Used in the Medical Field. *Laboratory Medicine* 34(7), pp. 544-547. doi: 10.1309/XLUGKHJ85FKBTAFF
- Altintas, Z. 2018. Optical Biosensors and Applications to Drug Discovery for Cancer Cases. *Biosensors and Nanotechnology*. pp. 327-348.

- Amor-Gutiérrez, O. et al. 2020. Competitive electrochemical immunosensor for the detection of unfolded p53 protein in blood as biomarker for Alzheimer's disease. *Analytica Chimica Acta* 1093, pp. 28-34. doi: <https://doi.org/10.1016/j.aca.2019.09.042>
- Andargie, T. E. et al. 2021. Cell-free DNA maps COVID-19 tissue injury and risk of death and can cause tissue injury. *JCI Insight* 6(7), doi: 10.1172/jci.insight.147610
- Antunes, G. et al. 2002. Systemic cytokine levels in community-acquired pneumonia and their association with disease severity. *Eur Respir J* 20(4), pp. 990-995. doi: 10.1183/09031936.02.00295102
- Armstrong, L. et al. 2004. Expression of functional toll-like receptor-2 and -4 on alveolar epithelial cells. *Am J Respir Cell Mol Biol* 31(2), pp. 241-245. doi: 10.1165/rcmb.2004-0078OC
- Armstrong-James, D. et al. 2014. A neglected epidemic: fungal infections in HIV/AIDS. *Trends Microbiol* 22(3), pp. 120-127. doi: 10.1016/j.tim.2014.01.001
- Asha, S. E. et al. 2014. Impact from point-of-care devices on emergency department patient processing times compared with central laboratory testing of blood samples: a randomised controlled trial and cost-effectiveness analysis. *Emerg Med J* 31(9), pp. 714-719. doi: 10.1136/emered-2013-202632
- Assicot, M. et al. 1993. High serum procalcitonin concentrations in patients with sepsis and infection. *Lancet* 341(8844), pp. 515-518. doi: 10.1016/0140-6736(93)90277-n
- Avni, T. et al. 2010. PCR using blood for diagnosis of invasive pneumococcal disease: systematic review and meta-analysis. *J Clin Microbiol* 48(2), pp. 489-496. doi: 10.1128/JCM.01636-09
- Aydın, E. B. et al. 2020. The development of an ultra-sensitive electrochemical immunosensor using a PPy-NHS functionalized disposable ITO sheet for the detection of interleukin 6 in real human serums. *New Journal of Chemistry* 44(33), pp. 14228-14238. doi: 10.1039/D0NJ03183F
- Baer, G. et al. 2013. Procalcitonin guidance to reduce antibiotic treatment of lower respiratory tract infection in children and adolescents (ProPAED): a randomized controlled trial. *PLoS ONE* 8(8), p. e68419. doi: 10.1371/journal.pone.0068419
- Bakare, O. O. et al. 2020. Diagnostic approaches of pneumonia for commercial-scale biomedical applications: an overview. *All Life* 13(1), pp. 532-547. doi: 10.1080/26895293.2020.1826363
- Baker, B. R. et al. 2006. An electronic, aptamer-based small-molecule sensor for the rapid, label-free detection of cocaine in adulterated samples and biological fluids. *J Am Chem Soc* 128(10), pp. 3138-3139. doi: 10.1021/ja056957p

- Bakker, E. and Pretsch, E. 2005. Potentiometric sensors for trace-level analysis. *Trends Analyt Chem* 24(3), pp. 199-207. doi: 10.1016/j.trac.2005.01.003
- Bakker, E. and Pretsch, E. 2007. Modern potentiometry. *Angew Chem Int Ed Engl* 46(30), pp. 5660-5668. doi: 10.1002/anie.200605068
- Banerjee, I. et al. 2011. Antifouling coatings: recent developments in the design of surfaces that prevent fouling by proteins, bacteria, and marine organisms. *Adv Mater* 23(6), pp. 690-718. doi: 10.1002/adma.201001215
- Barak-Corren, Y. et al. 2020. The prognostic value of C-reactive protein for children with pneumonia. *Acta Paediatr*, doi: 10.1111/apa.15580
- Barfidokht, A. and Gooding, J. J. 2014. Approaches Toward Allowing Electroanalytical Devices to be Used in Biological Fluids. *Electroanalysis* 26(6), pp. 1182-1196. doi: <https://doi.org/10.1002/elan.201400097>
- Belluzo, M. S. et al. 2008. Assembling Amperometric Biosensors for Clinical Diagnostics. *Sensors (Basel)* 8(3), pp. 1366-1399. doi: 10.3390/s8031366
- Beltran-Garcia, J. et al. 2021. Comparative Analysis of Chromatin-Delivered Biomarkers in the Monitoring of Sepsis and Septic Shock: A Pilot Study. *Int J Mol Sci* 22(18), doi: 10.3390/ijms22189935
- Bertesteanu, S. et al. 2014. Biomedical applications of synthetic, biodegradable polymers for the development of anti-infective strategies. *Curr Med Chem* 21(29), pp. 3383-3390. doi: 10.2174/0929867321666140304104328
- Bhalla, N. et al. 2016. Introduction to biosensors. *Essays Biochem* 60(1), pp. 1-8. doi: 10.1042/EBC20150001
- Bolden, J. and Smith, K. 2017. Application of Recombinant Factor C Reagent for the Detection of Bacterial Endotoxins in Pharmaceutical Products. *PDA J Pharm Sci Technol* 71(5), pp. 405-412. doi: 10.5731/pdajpst.2017.007849
- Bonini, F. et al. 2007. Surface imprinted beads for the recognition of human serum albumin. *Biosensors and Bioelectronics* 22(9), pp. 2322-2328. doi: <https://doi.org/10.1016/j.bios.2006.12.034>
- Bouadma, L. et al. 2010. Use of procalcitonin to reduce patients' exposure to antibiotics in intensive care units (PRORATA trial): a multicentre randomised controlled trial. *Lancet* 375(9713), pp. 463-474. doi: 10.1016/S0140-6736(09)61879-1
- Boussekey, N. et al. 2006. Procalcitonin kinetics in the prognosis of severe community-acquired pneumonia. *Intensive Care Med* 32(3), pp. 469-472. doi: 10.1007/s00134-005-0047-8

- Brett, C. M. A. 2022. Electrochemical Impedance Spectroscopy in the Characterisation and Application of Modified Electrodes for Electrochemical Sensors and Biosensors. *Molecules* 27(5), doi: 10.3390/molecules27051497
- Briel, M. et al. 2008. Procalcitonin-guided antibiotic use vs a standard approach for acute respiratory tract infections in primary care. *Arch Intern Med* 168(18), pp. 2000-2007; discussion 2007-2008. doi: 10.1001/archinte.168.18.2000
- Broecker, F. et al. 2014. Epitope recognition of antibodies against a *Yersinia pestis* lipopolysaccharide trisaccharide component. *ACS Chem Biol* 9(4), pp. 867-873. doi: 10.1021/cb400925k
- Brown, J. S. 2012. Community-acquired pneumonia. *Clin Med (Lond)* 12(6), pp. 538-543. doi: 10.7861/clinmedicine.12-6-538
- Cai, H. et al. 2006. Label-free protein recognition using an aptamer-based impedance measurement assay. *Sensors and Actuators B: Chemical* 114(1), pp. 433-437. doi: <https://doi.org/10.1016/j.snb.2005.06.017>
- Califf, R. M. 2018. Biomarker definitions and their applications. *Exp Biol Med (Maywood)* 243(3), pp. 213-221. doi: 10.1177/1535370217750088
- Campu, A. et al. 2019. Multimodal Biosensing on Paper-Based Platform Fabricated by Plasmonic Calligraphy Using Gold Nanopyramids Ink. *Front Chem* 7, p. 55. doi: 10.3389/fchem.2019.00055
- Campuzano, S. et al. 2019. Antifouling (Bio)materials for Electrochemical (Bio)sensing. *Int J Mol Sci* 20(2), doi: 10.3390/ijms20020423
- Campuzano, S. et al. 2017. Molecular Biosensors for Electrochemical Detection of Infectious Pathogens in Liquid Biopsies: Current Trends and Challenges. *Sensors (Basel)* 17(11), doi: 10.3390/s17112533
- Cao, H. et al. 2014. A novel aptasensor based on MUC-1 conjugated CNSs for ultrasensitive detection of tumor cells. *Analyst* 139(19), pp. 4917-4923. doi: 10.1039/c4an00844h
- Castell, J. V. et al. 1989. Interleukin-6 is the major regulator of acute phase protein synthesis in adult human hepatocytes. *FEBS Lett* 242(2), pp. 237-239. doi: 10.1016/0014-5793(89)80476-4
- Catimel, B. et al. 2001. The use of biosensors for microaffinity purification: an integrated approach to proteomics. *Journal of Biochemical and Biophysical Methods* 49(1), pp. 289-312. doi: [https://doi.org/10.1016/S0165-022X\(01\)00205-6](https://doi.org/10.1016/S0165-022X(01)00205-6)
- Cerruti, M. et al. 2008. Poly(ethylene glycol) monolayer formation and stability on gold and silicon nitride substrates. *Langmuir* 24(19), pp. 10646-10653. doi: 10.1021/la801357v

Chaki, N. K. and Vijayamohan, K. 2002. Self-assembled monolayers as a tunable platform for biosensor applications. *Biosensors and Bioelectronics* 17(1), pp. 1-12. doi: [https://doi.org/10.1016/S0956-5663\(01\)00277-9](https://doi.org/10.1016/S0956-5663(01)00277-9)

Chalmers, J. et al. 2017. Community-acquired pneumonia in the United Kingdom: a call to action. *Pneumonia (Nathan)* 9, p. 15. doi: 10.1186/s41479-017-0039-9

Chalmers, J. D. et al. 2011. Severity assessment tools to guide ICU admission in community-acquired pneumonia: systematic review and meta-analysis. *Intensive Care Med* 37(9), pp. 1409-1420. doi: 10.1007/s00134-011-2261-x

Chaplin, D. D. 2010. Overview of the immune response. *J Allergy Clin Immunol* 125(2 Suppl 2), pp. S3-23. doi: 10.1016/j.jaci.2009.12.980

Charoensappakit, A. et al. 2023. Cell-free DNA as diagnostic and prognostic biomarkers for adult sepsis: a systematic review and meta-analysis. *Sci Rep* 13(1), p. 19624. doi: 10.1038/s41598-023-46663-2

Chaubey, A. and Malhotra, B. D. 2002. Mediated biosensors. *Biosensors and Bioelectronics* 17(6), pp. 441-456. doi: [https://doi.org/10.1016/S0956-5663\(01\)00313-X](https://doi.org/10.1016/S0956-5663(01)00313-X)

Chen, C. and Wang, J. 2020. Optical biosensors: an exhaustive and comprehensive review. *Analyst* 145(5), pp. 1605-1628. doi: 10.1039/c9an01998g

Chen, K. and Kolls, J. K. 2013. T cell-mediated host immune defenses in the lung. *Annu Rev Immunol* 31, pp. 605-633. doi: 10.1146/annurev-immunol-032712-100019

Chen, S. et al. 2010. Surface hydration: Principles and applications toward low-fouling/nonfouling biomaterials. *Polymer* 51(23), pp. 5283-5293. doi: <https://doi.org/10.1016/j.polymer.2010.08.022>

Chien, J. Y. et al. 2006. Temporal changes in cytokine/chemokine profiles and pulmonary involvement in severe acute respiratory syndrome. *Respirology* 11(6), pp. 715-722. doi: 10.1111/j.1440-1843.2006.00942.x

Chou, T. H. et al. 2010. Quantification of Interleukin-6 in cell culture medium using surface plasmon resonance biosensors. *Cytokine* 51(1), pp. 107-111. doi: 10.1016/j.cyto.2010.04.004

Christ-Crain, M. et al. 2006. Procalcitonin guidance of antibiotic therapy in community-acquired pneumonia: a randomized trial. *Am J Respir Crit Care Med* 174(1), pp. 84-93. doi: 10.1164/rccm.200512-1922OC

Chumbimuni-Torres, K. Y. et al. 2010. Amplified potentiometric transduction of DNA hybridization using ion-loaded liposomes. *Analyst* 135(7), pp. 1618-1623. doi: 10.1039/c0an00198h

Clark Jr, L. C. and Lyons, C. 1962. ELECTRODE SYSTEMS FOR CONTINUOUS MONITORING IN CARDIOVASCULAR SURGERY. *Annals of the New York Academy of Sciences* 102(1), pp. 29-45. doi: <https://doi.org/10.1111/j.1749-6632.1962.tb13623.x>

Clerc, O. and Greub, G. 2010. Routine use of point-of-care tests: usefulness and application in clinical microbiology. *Clin Microbiol Infect* 16(8), pp. 1054-1061. doi: 10.1111/j.1469-0691.2010.03281.x

Collaborators, G. B. D. L. R. I. 2018. Estimates of the global, regional, and national morbidity, mortality, and aetiologies of lower respiratory infections in 195 countries, 1990-2016: a systematic analysis for the Global Burden of Disease Study 2016. *Lancet Infect Dis* 18(11), pp. 1191-1210. doi: 10.1016/S1473-3099(18)30310-4

Coomes, S. M. et al. 2017. CD4(+) Th2 cells are directly regulated by IL-10 during allergic airway inflammation. *Mucosal Immunol* 10(1), pp. 150-161. doi: 10.1038/mi.2016.47

Correa, W. et al. 2017. Biophysical Analysis of Lipopolysaccharide Formulations for an Understanding of the Low Endotoxin Recovery (LER) Phenomenon. *Int J Mol Sci* 18(12), doi: 10.3390/ijms18122737

Couper, K. N. et al. 2008. IL-10: the master regulator of immunity to infection. *J Immunol* 180(9), pp. 5771-5777. doi: 10.4049/jimmunol.180.9.5771

Covert, M. W. et al. 2005. Achieving stability of lipopolysaccharide-induced NF-kappaB activation. *Science* 309(5742), pp. 1854-1857. doi: 10.1126/science.1112304

Creamer, A. W. et al. 2019. Procalcitonin in respiratory disease: Use as a biomarker for diagnosis and guiding antibiotic therapy. *Breathe* 15(4), pp. 296-304. doi: 10.1183/20734735.0258-2019

Cui, M. et al. 2017. Mixed Self-Assembled Aptamer and Newly Designed Zwitterionic Peptide as Antifouling Biosensing Interface for Electrochemical Detection of alpha-Fetoprotein. *ACS Sens* 2(4), pp. 490-494. doi: 10.1021/acssensors.7b00103

Damborsky, P. et al. 2016. Optical biosensors. *Essays Biochem* 60(1), pp. 91-100. doi: 10.1042/EBC20150010

Damodaran, V. B. and Murthy, N. S. 2016. Bio-inspired strategies for designing antifouling biomaterials. *Biomater Res* 20, p. 18. doi: 10.1186/s40824-016-0064-4

Daniels, J. S. and Pourmand, N. 2007. Label-Free Impedance Biosensors: Opportunities and Challenges. *Electroanalysis* 19(12), pp. 1239-1257. doi: 10.1002/elan.200603855

Dave, V. P. et al. 2019. MicroRNA amplification and detection technologies: opportunities and challenges for point of care diagnostics. *Lab Invest* 99(4), pp. 452-469. doi: 10.1038/s41374-018-0143-3

de Benedictis, F. M. et al. 2020. Complicated pneumonia in children. *Lancet* 396(10253), pp. 786-798. doi: 10.1016/S0140-6736(20)31550-6

de Brito, R. d. C. C. M. et al. 2016. The balance between the serum levels of IL-6 and IL-10 cytokines discriminates mild and severe acute pneumonia. *BMC pulmonary medicine* 16(1), pp. 170-170. doi: 10.1186/s12890-016-0324-z

Deng, C. et al. 2011. Sensitive electrochemical immunosensor based on enlarged and surface charged gold nanoparticles mediated electron transfer. *Sensors and Actuators B: Chemical* 160(1), pp. 471-474. doi: <https://doi.org/10.1016/j.snb.2011.08.010>

Deng, K. et al. 2013. An aptamer-based biosensing platform for highly sensitive detection of platelet-derived growth factor via enzyme-mediated direct electrochemistry. *Anal Chim Acta* 759, pp. 61-65. doi: 10.1016/j.aca.2012.11.018

Deris, Z. Z. et al. 2014. A secondary mode of action of polymyxins against Gram-negative bacteria involves the inhibition of NADH-quinone oxidoreductase activity. *J Antibiot (Tokyo)* 67(2), pp. 147-151. doi: 10.1038/ja.2013.111

Dey, D. and Goswami, T. 2011. Optical biosensors: a revolution towards quantum nanoscale electronics device fabrication. *J Biomed Biotechnol* 2011, p. 348218. doi: 10.1155/2011/348218

Dhanjai et al. 2018. Voltammetric sensing of biomolecules at carbon based electrode interfaces: A review. *TrAC Trends in Analytical Chemistry* 98, pp. 174-189. doi: <https://doi.org/10.1016/j.trac.2017.11.010>

Dincer, C. et al. 2017. Multiplexed Point-of-Care Testing - xPOCT. *Trends Biotechnol* 35(8), pp. 728-742. doi: 10.1016/j.tibtech.2017.03.013

Ding, J. and Qin, W. 2020. Recent advances in potentiometric biosensors. *TrAC Trends in Analytical Chemistry* 124, p. 115803. doi: <https://doi.org/10.1016/j.trac.2019.115803>

Ding, J. et al. 2018. Sequential and Selective Detection of Two Molecules with a Single Solid-Contact Chronopotentiometric Ion-Selective Electrode. *Anal Chem* 90(3), pp. 1734-1739. doi: 10.1021/acs.analchem.7b03522

Ding, S. et al. 2017. Rapid and Label-Free Detection of Interferon Gamma via an Electrochemical Aptasensor Comprising a Ternary Surface Monolayer on a Gold Interdigitated Electrode Array. *ACS Sens* 2(2), pp. 210-217. doi: 10.1021/acssensors.6b00581

Ding, S. et al. 2016. Decreased Interleukin-10 Responses in Children with Severe *Mycoplasma pneumoniae* Pneumonia. *PLoS ONE* 11(1), p. e0146397. doi: 10.1371/journal.pone.0146397

Ding, S.-J. et al. 2007. A new method for detection of endotoxin on polymyxin B-immobilized gold electrodes. *Electrochemistry Communications* 9(5), pp. 1206-1211. doi: <https://doi.org/10.1016/j.elecom.2006.12.029>

Diware, M. S. et al. 2017. Label-free detection of hepatitis B virus using solution immersed silicon sensors. *Biointerphases* 12(1), p. 01A402. doi: 10.1116/1.4977075

Dixon, R. A. and Chopra, I. 1986. Leakage of periplasmic proteins from *Escherichia coli* mediated by polymyxin B nonapeptide. *Antimicrob Agents Chemother* 29(5), pp. 781-788. doi: 10.1128/aac.29.5.781

Dochez, A. R. and Avery, O. T. 1917. The Elaboration of Specific Soluble Substance by *Pneumococcus* during Growth. *J Exp Med* 26(4), pp. 477-493. doi: 10.1084/jem.26.4.477

Dong, S. et al. 2015. Electrochemical DNA Biosensor Based on a Tetrahedral Nanostructure Probe for the Detection of Avian Influenza A (H7N9) Virus. *ACS Appl Mater Interfaces* 7(16), pp. 8834-8842. doi: 10.1021/acsami.5b01438

Donzella, V. and Crea, F. 2011. Optical biosensors to analyze novel biomarkers in oncology. *J Biophotonics* 4(6), pp. 442-452. doi: 10.1002/jbio.201000123

Duell, B. L. et al. 2012. Recent insights into microbial triggers of interleukin-10 production in the host and the impact on infectious disease pathogenesis. *FEMS Immunol Med Microbiol* 64(3), pp. 295-313. doi: 10.1111/j.1574-695X.2012.00931.x

Duplessis, C. et al. 2018. Evaluating the discriminating capacity of cell death (apoptotic) biomarkers in sepsis. *J Intensive Care* 6, p. 72. doi: 10.1186/s40560-018-0341-5

Ekanem, E. E. et al. 1997. Serum C-reactive protein and C3 complement protein levels in severely malnourished Nigerian children with and without bacterial infections. *Acta Paediatr* 86(12), pp. 1317-1320. doi: 10.1111/j.1651-2227.1997.tb14905.x

El-Nour, K. M. A. et al. 2017. Gold Nanoparticles as a Direct and Rapid Sensor for Sensitive Analytical Detection of Biogenic Amines. *Nanoscale Res Lett* 12(1), p. 231. doi: 10.1186/s11671-017-2014-z

Elwing, H. 1998. Protein absorption and ellipsometry in biomaterial research. *Biomaterials* 19(4), pp. 397-406. doi: [https://doi.org/10.1016/S0142-9612\(97\)00112-9](https://doi.org/10.1016/S0142-9612(97)00112-9)

Endeman, H. et al. 2011. Systemic cytokine response in patients with community-acquired pneumonia. *Eur Respir J* 37(6), pp. 1431-1438. doi: 10.1183/09031936.00074410

Endo, T. et al. 2006. Multiple label-free detection of antigen-antibody reaction using localized surface plasmon resonance-based core-shell structured nanoparticle layer nanochip. *Anal Chem* 78(18), pp. 6465-6475. doi: 10.1021/ac0608321

Esposito, S. et al. 2011. Procalcitonin measurements for guiding antibiotic treatment in pediatric pneumonia. *Respir Med* 105(12), pp. 1939-1945. doi: 10.1016/j.rmed.2011.09.003

Estevez, M. C. et al. 2012. Integrated optical devices for lab-on-a-chip biosensing applications. *Laser & Photonics Reviews* 6(4), pp. 463-487. doi: <https://doi.org/10.1002/lpor.201100025>

Faix, J. D. 2013. Biomarkers of sepsis. *Crit Rev Clin Lab Sci* 50(1), pp. 23-36. doi: 10.3109/10408363.2013.764490

Falagas, M. E. and Kasiakou, S. K. 2005. Colistin: the revival of polymyxins for the management of multidrug-resistant gram-negative bacterial infections. *Clin Infect Dis* 40(9), pp. 1333-1341. doi: 10.1086/429323

Fan, X. et al. 2008. Sensitive optical biosensors for unlabeled targets: a review. *Anal Chim Acta* 620(1-2), pp. 8-26. doi: 10.1016/j.aca.2008.05.022

Farhana, A. and Khan, Y. S. 2021. Biochemistry, Lipopolysaccharide. *StatPearls*. Treasure Island (FL).

Fei, Y. et al. 2015. Characterization of Receptor Binding Profiles of Influenza A Viruses Using An Ellipsometry-Based Label-Free Glycan Microarray Assay Platform. *Biomolecules* 5(3), pp. 1480-1498. doi: 10.3390/biom5031480

Fekri, m. h. et al. 2011. An electrochemical Cr(III)-Selective Sensor-Based on a Newly Synthesized Ligand and Optimization of Electrode With a Nano Particle. *International Journal of Electrochemical Science* 6,

Fernandes, C. D. et al. 2019. Host Inflammatory Biomarkers of Disease Severity in Pediatric Community-Acquired Pneumonia: A Systematic Review and Meta-analysis. *Open Forum Infectious Diseases* 6(12), doi: 10.1093/ofid/ofz520

Fernández-Sánchez, C. et al. 2005. Electrochemical impedance spectroscopy studies of polymer degradation: application to biosensor development. *TrAC Trends in Analytical Chemistry* 24(1), pp. 37-48. doi: <https://doi.org/10.1016/j.trac.2004.08.010>

Fiorentino, D. F. et al. 1991. IL-10 inhibits cytokine production by activated macrophages. *J Immunol* 147(11), pp. 3815-3822.

Florin, T. A. et al. 2020. Biomarkers and Disease Severity in Children With Community-Acquired Pneumonia. *Pediatrics* 145(6), doi: 10.1542/peds.2019-3728

Francolini, I. et al. 2017. Antifouling and antimicrobial biomaterials: an overview. *APMIS* 125(4), pp. 392-417. doi: 10.1111/apm.12675

Freeman, A. M. and Leigh, J. T. R. 2021. Viral Pneumonia. *StatPearls*. Treasure Island (FL).

- Fuchs, A. et al. 2018. Cytokine kinetic profiles in children with acute lower respiratory tract infection: a post hoc descriptive analysis from a randomized control trial. *Clin Microbiol Infect* 24(12), pp. 1341 e1341-1341 e1347. doi: 10.1016/j.cmi.2018.03.016
- Gabrysova, L. et al. 2014. The regulation of IL-10 expression. *Curr Top Microbiol Immunol* 380, pp. 157-190. doi: 10.1007/978-3-662-43492-5\_8
- Gallagher, P. M. et al. 2003. Association of IL-10 polymorphism with severity of illness in community acquired pneumonia. *Thorax* 58(2), pp. 154-156. doi: 10.1136/thorax.58.2.154
- Gamella, M. et al. 2009. Microorganisms recognition and quantification by lectin adsorptive affinity impedance. *Talanta* 78(4-5), pp. 1303-1309. doi: 10.1016/j.talanta.2009.01.059
- Garcia-Vidal, C. et al. 2010. Pneumococcal pneumonia presenting with septic shock: host- and pathogen-related factors and outcomes. *Thorax* 65(1), p. 77. doi: 10.1136/thx.2009.123612
- Garnacho-Montero, J. et al. 2014. Prognostic and diagnostic value of eosinopenia, C-reactive protein, procalcitonin, and circulating cell-free DNA in critically ill patients admitted with suspicion of sepsis. *Crit Care* 18(3), p. R116. doi: 10.1186/cc13908
- Garrote, B. L. et al. 2019. Perspectives on and Precautions for the Uses of Electric Spectroscopic Methods in Label-free Biosensing Applications. *ACS Sens* 4(9), pp. 2216-2227. doi: 10.1021/acssensors.9b01177
- Ge, Z. et al. 2014. Hybridization chain reaction amplification of microRNA detection with a tetrahedral DNA nanostructure-based electrochemical biosensor. *Anal Chem* 86(4), pp. 2124-2130. doi: 10.1021/ac4037262
- Gilbert, D. N. 2010. Use of plasma procalcitonin levels as an adjunct to clinical microbiology. *J Clin Microbiol* 48(7), pp. 2325-2329. doi: 10.1128/JCM.00655-10
- Glad, C. and Grubb, A. O. 1981. Immunocapillary migration with enzyme-labeled antibodies: rapid quantification of C-reactive protein in human plasma. *Anal Biochem* 116(2), pp. 335-340. doi: 10.1016/0003-2697(81)90367-5
- Glynn, P. et al. 1999. Circulating interleukin 6 and interleukin 10 in community acquired pneumonia. *Thorax* 54(1), pp. 51-55. doi: 10.1136/thx.54.1.51
- Goda, T. et al. 2012. A label-free electrical detection of exosomal microRNAs using microelectrode array. *Chem Commun (Camb)* 48(98), pp. 11942-11944. doi: 10.1039/c2cc36111f
- Gölander, C. G. et al. 1992. Properties of Immobilized PEG Films and the Interaction with Proteins. In: Harris, J.M. ed. *Poly(Ethylene Glycol) Chemistry: Biotechnical and Biomedical Applications*. Boston, MA: Springer US, pp. 221-245.

González-Fernández, E. et al. 2018. Effect of spacer length on the performance of peptide-based electrochemical biosensors for protease detection. *Sensors and Actuators B: Chemical* 255, pp. 3040-3046. doi: <https://doi.org/10.1016/j.snb.2017.09.128>

Gooding, J. J. 2019. Finally, a simple solution to biofouling. *Nat Nanotechnol* 14(12), pp. 1089-1090. doi: 10.1038/s41565-019-0573-0

Goodman, D. et al. 2019. Challenges in the diagnosis of paediatric pneumonia in intervention field trials: recommendations from a pneumonia field trial working group. *The Lancet Respiratory Medicine* 7(12), pp. 1068-1083. doi: 10.1016/S2213-2600(19)30249-8

Goodman, R. P. et al. 2004. The single-step synthesis of a DNA tetrahedron. *Chem Commun (Camb)* (12), pp. 1372-1373. doi: 10.1039/b402293a

Gou, X. et al. 2019. IL-6 During Influenza-Streptococcus pneumoniae Co-Infected Pneumonia-A Protector. *Front Immunol* 10, p. 3102. doi: 10.3389/fimmu.2019.03102

Goyal, R. N. et al. 2010. Voltammetric biosensors for the determination of paracetamol at carbon nanotube modified pyrolytic graphite electrode. *Sensors and Actuators B: Chemical* 149(1), pp. 252-258. doi: <https://doi.org/10.1016/j.snb.2010.05.019>

Grieshaber, D. et al. 2008. Electrochemical Biosensors - Sensor Principles and Architectures. *Sensors (Basel)* 8(3), pp. 1400-1458. doi: 10.3390/s80314000

Guillot, L. et al. 2004. Response of human pulmonary epithelial cells to lipopolysaccharide involves Toll-like receptor 4 (TLR4)-dependent signaling pathways: evidence for an intracellular compartmentalization of TLR4. *J Biol Chem* 279(4), pp. 2712-2718. doi: 10.1074/jbc.M305790200

Guntupalli, R. et al. 2007. A magnetoelastic resonance biosensor immobilized with polyclonal antibody for the detection of Salmonella typhimurium. *Biosens Bioelectron* 22(7), pp. 1474-1479. doi: 10.1016/j.bios.2006.06.037

Guo, Y. et al. 2013. Ultrasensitive and label-free electrochemical DNA biosensor based on water-soluble electroactive dye azophloxine-functionalized graphene nanosheets. *Electrochimica Acta* 113, pp. 69-76. doi: <https://doi.org/10.1016/j.electacta.2013.09.039>

Gupta, V. et al. eds. 2015. *Simultaneous Determination of Hydroxylamine, Phenol and Sulfite in Water and Waste Water Samples Using A Voltammetric Nanosensor*.

Gyawali, B. et al. 2019. Sepsis: The evolution in definition, pathophysiology, and management. *SAGE Open Med* 7, p. 2050312119835043. doi: 10.1177/2050312119835043

Hage, C. A. et al. 2012. Endemic mycoses: overlooked causes of community acquired pneumonia. *Respir Med* 106(6), pp. 769-776. doi: 10.1016/j.rmed.2012.02.004

Hammond, J. L. et al. 2016. Electrochemical biosensors and nanobiosensors. *Essays Biochem* 60(1), pp. 69-80. doi: 10.1042/EBC20150008

Han, L. et al. 2016. A Label-Free Electrochemical Impedance Cytosensor Based on Specific Peptide-Fused Phage Selected from Landscape Phage Library. *Sci Rep* 6, p. 22199. doi: 10.1038/srep22199

Happel, K. I. et al. 2003. Cutting edge: roles of Toll-like receptor 4 and IL-23 in IL-17 expression in response to *Klebsiella pneumoniae* infection. *J Immunol* 170(9), pp. 4432-4436. doi: 10.4049/jimmunol.170.9.4432

Harm, S. et al. 2021. An in vitro study on factors affecting endotoxin neutralization in human plasma using the Limulus amoebocyte lysate test. *Sci Rep* 11(1), p. 4192. doi: 10.1038/s41598-021-83487-4

Hartung, T. 2015. The human whole blood pyrogen test - lessons learned in twenty years. *ALTEX* 32(2), pp. 79-100. doi: 10.14573/altex.1503241

Hashizume, M. 2020. Outlook of IL-6 signaling blockade for COVID-19 pneumonia. *Inflamm Regen* 40, p. 24. doi: 10.1186/s41232-020-00134-7

Hatzistilianou, M. et al. 2002. Serum procalcitonin, adenosine deaminase and its isoenzymes in the aetiological diagnosis of pneumonia in children. *Int J Immunopathol Pharmacol* 15(2), pp. 119-127. doi: 10.1177/039463200201500207

Haugen, J. et al. 2015. Cytokine Concentrations in Plasma from Children with Severe and Non-Severe Community Acquired Pneumonia. *PLoS ONE* 10(9), p. e0138978. doi: 10.1371/journal.pone.0138978

Hausmann, M. J. et al. 2000. Gel clot LAL assay in the initial management of peritoneal dialysis patients with peritonitis: a retrospective study. *Nephrol Dial Transplant* 15(5), pp. 680-683. doi: 10.1093/ndt/15.5.680

He, P. et al. 2013. Label-free electrochemical monitoring of vasopressin in aptamer-based microfluidic biosensors. *Anal Chim Acta* 759, pp. 74-80. doi: 10.1016/j.aca.2012.10.038

Henderson, A. G. et al. 2014. Cystic fibrosis airway secretions exhibit mucin hyperconcentration and increased osmotic pressure. *J Clin Invest* 124(7), pp. 3047-3060. doi: 10.1172/JCI73469

Henry, O. Y. et al. 2010. Bipodal PEGylated alkanethiol for the enhanced electrochemical detection of genetic markers involved in breast cancer. *Biosens Bioelectron* 26(4), pp. 1500-1506. doi: 10.1016/j.bios.2010.07.095

Higdon, M. M. et al. 2017. Association of C-Reactive Protein With Bacterial and Respiratory Syncytial Virus-Associated Pneumonia Among Children Aged <5 Years in the PERCH Study. *Clin Infect Dis* 64(suppl\_3), pp. S378-S386. doi: 10.1093/cid/cix150

Hislop, J. et al. 2010. Systematic review of the clinical effectiveness and cost-effectiveness of rapid point-of-care tests for the detection of genital chlamydia infection in women and men. *Health Technol Assess* 14(29), pp. 1-97, iii-iv. doi: 10.3310/hta14290

Howick, J. et al. 2014. Current and future use of point-of-care tests in primary care: an international survey in Australia, Belgium, The Netherlands, the UK and the USA. *BMJ Open* 4(8), p. e005611. doi: 10.1136/bmjopen-2014-005611

Huang, D. T. et al. 2008. Risk prediction with procalcitonin and clinical rules in community-acquired pneumonia. *Ann Emerg Med* 52(1), pp. 48-58 e42. doi: 10.1016/j.annemergmed.2008.01.003

Huang, D. T. et al. 2018. Procalcitonin-Guided Use of Antibiotics for Lower Respiratory Tract Infection. *N Engl J Med* 379(3), pp. 236-249. doi: 10.1056/NEJMoa1802670

Huertas, C. S. et al. 2018. Label-free DNA-methylation detection by direct ds-DNA fragment screening using poly-purine hairpins. *Biosens Bioelectron* 120, pp. 47-54. doi: 10.1016/j.bios.2018.08.027

Huertas, C. S. et al. 2019. Advanced Evanescent-Wave Optical Biosensors for the Detection of Nucleic Acids: An Analytic Perspective. *Front Chem* 7, p. 724. doi: 10.3389/fchem.2019.00724

Hussell, T. and Bell, T. J. 2014. Alveolar macrophages: plasticity in a tissue-specific context. *Nat Rev Immunol* 14(2), pp. 81-93. doi: 10.1038/nri3600

Ikebukuro, K. et al. 2004. Electrochemical Detection of Protein Using a Double Aptamer Sandwich. *Analytical Letters* 37(14), pp. 2901-2909. doi: 10.1081/AL-200035778

Inoue, K. Y. et al. 2010. Electrochemical detection of endotoxin using recombinant factor C zymogen. *Electrochemistry Communications* 12(8), pp. 1066-1069. doi: <https://doi.org/10.1016/j.elecom.2010.05.028>

Iyer, S. S. and Cheng, G. 2012. Role of interleukin 10 transcriptional regulation in inflammation and autoimmune disease. *Crit Rev Immunol* 32(1), pp. 23-63. doi: 10.1615/critrevimmunol.v32.i1.30

Jain, S. et al. 2015. Community-Acquired Pneumonia Requiring Hospitalization among U.S. Adults. *N Engl J Med* 373(5), pp. 415-427. doi: 10.1056/NEJMoa1500245

Jain, V. et al. 2021. Pneumonia Pathology. *StatPearls*. Treasure Island (FL).

Jensen, J. U. et al. 2006. Procalcitonin increase in early identification of critically ill patients at high risk of mortality. *Crit Care Med* 34(10), pp. 2596-2602. doi: 10.1097/01.CCM.0000239116.01855.61

Jia, K. et al. 2012. A lower limit of detection for atrazine was obtained using bioluminescent reporter bacteria via a lower incubation temperature. *Ecotoxicol Environ Saf* 84, pp. 221-226. doi: 10.1016/j.ecoenv.2012.07.009

Kakhki, R. M. 2013. Application of nanoparticles in the potentiometric ion selective electrodes. *Russian Journal of Electrochemistry* 49(5), pp. 458-465. doi: 10.1134/S1023193513050078

Kalantar, K. L. et al. 2022. Integrated host-microbe plasma metagenomics for sepsis diagnosis in a prospective cohort of critically ill adults. *Nat Microbiol* 7(11), pp. 1805-1816. doi: 10.1038/s41564-022-01237-2

Kalita, P. et al. 2017. In vitro flow-through assay for rapid detection of endotoxin in human sera: A proof-of-concept. *Nanomedicine: Nanotechnology, Biology and Medicine* 13(4), pp. 1483-1490. doi: <https://doi.org/10.1016/j.nano.2017.01.012>

Kamat, I. S. et al. 2020. Procalcitonin to distinguish viral from bacterial pneumonia: A systematic review and meta-analysis. *Clinical Infectious Diseases* 70(3), pp. 538-542. doi: 10.1093/cid/ciz545

Kandimalla, V. B. and Ju, H. 2004. New Horizons with A Multi Dimensional Tool for Applications in Analytical Chemistry—Aptamer. *Analytical Letters* 37(11), pp. 2215-2233. doi: 10.1081/AL-200028005

Katz, S. E. and Williams, D. J. 2018. Pediatric Community-Acquired Pneumonia in the United States: Changing Epidemiology, Diagnostic and Therapeutic Challenges, and Areas for Future Research. *Infect Dis Clin North Am* 32(1), pp. 47-63. doi: 10.1016/j.idc.2017.11.002

Kawasaki, T. and Kawai, T. 2014. Toll-like receptor signaling pathways. *Front Immunol* 5, p. 461. doi: 10.3389/fimmu.2014.00461

Kellum, J. A. et al. 2007. Understanding the inflammatory cytokine response in pneumonia and sepsis: results of the Genetic and Inflammatory Markers of Sepsis (GenIMS) Study. *Arch Intern Med* 167(15), pp. 1655-1663. doi: 10.1001/archinte.167.15.1655

Keynan, Y. et al. 2011. Toll-Like Receptors Dysregulation after Influenza Virus Infection: Insights into Pathogenesis of Subsequent Bacterial Pneumonia. *ISRN Pulmonology* 2011, p. 142518. doi: 10.5402/2011/142518

Khan, M. A. and Mujahid, M. 2020. Recent Advances in Electrochemical and Optical Biosensors Designed for Detection of Interleukin 6. *Sensors (Basel)* 20(3), doi: 10.3390/s20030646

Khansili, N. et al. 2018. Label-free optical biosensors for food and biological sensor applications. *Sensors and Actuators B: Chemical* 265, pp. 35-49. doi: <https://doi.org/10.1016/j.snb.2018.03.004>

- Khattab, A. A. et al. 2018. Clinical study of serum interleukin-6 in children with community-acquired pneumonia. *Egyptian Pediatric Association Gazette* 66(2), pp. 43-48. doi: <https://doi.org/10.1016/j.epag.2018.03.003>
- Kim, D. et al. 2011. Electroanalytical eavesdropping on single cell communication. *Anal Chem* 83(19), pp. 7242-7249. doi: 10.1021/ac200666c
- Kim, S. E. et al. 2012. Harnessing aptamers for electrochemical detection of endotoxin. *Anal Biochem* 424(1), pp. 12-20. doi: 10.1016/j.ab.2012.02.016
- Kim, W. H. et al. 2019. A label-free, ultra-highly sensitive and multiplexed SERS nanoplasmonic biosensor for miRNA detection using a head-flocked gold nanopillar. *Analyst* 144(5), pp. 1768-1776. doi: 10.1039/c8an01745j
- Kitsios, G. D. et al. 2018. Respiratory Microbiome Profiling for Etiologic Diagnosis of Pneumonia in Mechanically Ventilated Patients. *Front Microbiol* 9, p. 1413. doi: 10.3389/fmicb.2018.01413
- Knowles, M. R. et al. 2013. Primary ciliary dyskinesia. Recent advances in diagnostics, genetics, and characterization of clinical disease. *Am J Respir Crit Care Med* 188(8), pp. 913-922. doi: 10.1164/rccm.201301-0059CI
- Korneev, K. V. et al. 2017. TLR-signaling and proinflammatory cytokines as drivers of tumorigenesis. *Cytokine* 89, pp. 127-135. doi: 10.1016/j.cyto.2016.01.021
- Kozel, T. R. and Burnham-Marusich, A. R. 2017. Point-of-Care Testing for Infectious Diseases: Past, Present, and Future. *J Clin Microbiol* 55(8), pp. 2313-2320. doi: 10.1128/JCM.00476-17
- Krishnan, J. et al. 2018. TLR4 (Toll-Like Receptor 4). In: Choi, S. ed. *Encyclopedia of Signaling Molecules*. Cham: Springer International Publishing, pp. 5472-5483.
- Kruger, S. et al. 2008. Procalcitonin predicts patients at low risk of death from community-acquired pneumonia across all CRB-65 classes. *Eur Respir J* 31(2), pp. 349-355. doi: 10.1183/09031936.00054507
- Kushner, I. 1982. The phenomenon of the acute phase response. *Ann N Y Acad Sci* 389, pp. 39-48. doi: 10.1111/j.1749-6632.1982.tb22124.x
- Labib, M. et al. 2016. Electrochemical Methods for the Analysis of Clinically Relevant Biomolecules. *Chem Rev* 116(16), pp. 9001-9090. doi: 10.1021/acs.chemrev.6b00220
- Lan, W. J. et al. 2014. Paper-based potentiometric ion sensing. *Anal Chem* 86(19), pp. 9548-9553. doi: 10.1021/ac5018088
- Lapillonne, A. et al. 1998. Lack of specificity of procalcitonin for sepsis diagnosis in premature infants. *Lancet* 351(9110), pp. 1211-1212. doi: 10.1016/S0140-6736(05)79165-0

Larsson, A. et al. 2015. The state of point-of-care testing: a European perspective. *Ups J Med Sci* 120(1), pp. 1-10. doi: 10.3109/03009734.2015.1006347

Lee, K. H. et al. 2006. Dopamine efflux in the rat striatum evoked by electrical stimulation of the subthalamic nucleus: potential mechanism of action in Parkinson's disease. *Eur J Neurosci* 23(4), pp. 1005-1014. doi: 10.1111/j.1460-9568.2006.04638.x

Lee, Y. L. et al. 2010. Systemic and bronchoalveolar cytokines as predictors of in-hospital mortality in severe community-acquired pneumonia. *J Crit Care* 25(1), pp. 176 e177-113. doi: 10.1016/j.jcrc.2009.05.002

Lekkou, A. et al. 2004. Cytokine production and monocyte HLA-DR expression as predictors of outcome for patients with community-acquired severe infections. *Clin Diagn Lab Immunol* 11(1), pp. 161-167. doi: 10.1128/cdli.11.1.161-167.2004

Leng, C. et al. 2015. Surface Structure and Hydration of Sequence-Specific Amphiphilic Polypeptoids for Antifouling/Fouling Release Applications. *Langmuir* 31(34), pp. 9306-9311. doi: 10.1021/acs.langmuir.5b01440

Lerouge, I. and Vanderleyden, J. 2002. O-antigen structural variation: mechanisms and possible roles in animal/plant-microbe interactions. *FEMS Microbiol Rev* 26(1), pp. 17-47. doi: 10.1111/j.1574-6976.2002.tb00597.x

Leuvering, J. H. et al. 1980. Sol particle immunoassay (SPIA). *J Immunoassay* 1(1), pp. 77-91. doi: 10.1080/01971528008055777

Levin, J. and Bang, F. B. 1968. Clottable protein in Limulus; its localization and kinetics of its coagulation by endotoxin. *Thromb Diath Haemorrh* 19(1), pp. 186-197.

Levy, M. M. et al. 2012. Outcomes of the Surviving Sepsis Campaign in intensive care units in the USA and Europe: a prospective cohort study. *Lancet Infect Dis* 12(12), pp. 919-924. doi: 10.1016/S1473-3099(12)70239-6

Li, J. et al. 2005. Evaluation of colistin as an agent against multi-resistant Gram-negative bacteria. *Int J Antimicrob Agents* 25(1), pp. 11-25. doi: 10.1016/j.ijantimicag.2004.10.001

Li, S. et al. 2015. Dextran hydrogel coated surface plasmon resonance imaging (SPRi) sensor for sensitive and label-free detection of small molecule drugs. *Applied Surface Science* 355, pp. 570-576. doi: <https://doi.org/10.1016/j.apsusc.2015.05.020>

Li, X. et al. 2020. Vertical nanowire array-based biosensors: device design strategies and biomedical applications. *J Mater Chem B* 8(34), pp. 7609-7632. doi: 10.1039/d0tb00990c

Liao, J. C. et al. 2006. Use of electrochemical DNA biosensors for rapid molecular identification of uropathogens in clinical urine specimens. *J Clin Microbiol* 44(2), pp. 561-570. doi: 10.1128/JCM.44.2.561-570.2006

Lim, S. K. et al. 2015. Peptide-assembled graphene oxide as a fluorescent turn-on sensor for lipopolysaccharide (endotoxin) detection. *Anal Chem* 87(18), pp. 9408-9412. doi: 10.1021/acs.analchem.5b02270

Lim, W. S. et al. 2009. BTS guidelines for the management of community acquired pneumonia in adults: update 2009. *Thorax* 64 Suppl 3, pp. iii1-55. doi: 10.1136/thx.2009.121434

Lin, C. J. et al. 2020. Factors associated with hospitalization for community-acquired pneumonia in home health care patients in Taiwan. *Aging Clin Exp Res* 32(1), pp. 149-155. doi: 10.1007/s40520-019-01169-8

Lin, P. H. and Li, B. R. 2020. Antifouling strategies in advanced electrochemical sensors and biosensors. *Analyst* 145(4), pp. 1110-1120. doi: 10.1039/c9an02017a

Lingervelder, D. et al. 2019. Point-of-care testing in primary care: A systematic review on implementation aspects addressed in test evaluations. *Int J Clin Pract* 73(10), p. e13392. doi: 10.1111/ijcp.13392

Liu, J. X. et al. 2018. Nonenzymatic Amperometric Aptamer Cytosensor for Ultrasensitive Detection of Circulating Tumor Cells and Dynamic Evaluation of Cell Surface N-Glycan Expression. *ACS Omega* 3(8), pp. 8595-8604. doi: 10.1021/acsomega.8b01072

Liu, Y. et al. 2010. Aptamer-based electrochemical biosensor for interferon gamma detection. *Anal Chem* 82(19), pp. 8131-8136. doi: 10.1021/ac101409t

Lochhead, M. J. et al. 2011. Rapid multiplexed immunoassay for simultaneous serodiagnosis of HIV-1 and coinfections. *J Clin Microbiol* 49(10), pp. 3584-3590. doi: 10.1128/JCM.00970-11

Loebbermann, J. et al. 2012. IL-10 regulates viral lung immunopathology during acute respiratory syncytial virus infection in mice. *PLoS ONE* 7(2), p. e32371. doi: 10.1371/journal.pone.0032371

Lorente, M. L. et al. 2000. Diagnosis of pneumococcal pneumonia by polymerase chain reaction (PCR) in whole blood: a prospective clinical study. *Thorax* 55(2), pp. 133-137. doi: 10.1136/thorax.55.2.133

Lundgren, A. et al. 2012. Characterization of Th17 responses to *Streptococcus pneumoniae* in humans: comparisons between adults and children in a developed and a developing country. *Vaccine* 30(26), pp. 3897-3907. doi: 10.1016/j.vaccine.2012.03.082

Luppa, P. B. et al. 2011. Point-of-care testing (POCT): Current techniques and future perspectives. *Trends Analyt Chem* 30(6), pp. 887-898. doi: 10.1016/j.trac.2011.01.019

- Ma, H. et al. 2018. Label-free electrochemiluminescent immunosensor for detection of prostate specific antigen based on mesoporous graphite-like carbon nitride. *Talanta* 188, pp. 729-735. doi: <https://doi.org/10.1016/j.talanta.2018.06.029>
- MacKenzie, C. R. et al. 1996. Analysis by surface plasmon resonance of the influence of valence on the ligand binding affinity and kinetics of an anti-carbohydrate antibody. *J Biol Chem* 271(3), pp. 1527-1533. doi: 10.1074/jbc.271.3.1527
- Mackenzie, G. 2016. The definition and classification of pneumonia. *Pneumonia (Nathan)* 8, p. 14. doi: 10.1186/s41479-016-0012-z
- Mahajan, P. et al. 2014. Procalcitonin as a marker of serious bacterial infections in febrile children younger than 3 years old. *Acad Emerg Med* 21(2), pp. 171-179. doi: 10.1111/acem.12316
- Makra, I. et al. 2017. Potentiometric sensing of nucleic acids using chemically modified nanopores. *Nanoscale* 9(2), pp. 739-747. doi: 10.1039/c6nr05886h
- Manickam, A. et al. 2012. Interface design for CMOS-integrated Electrochemical Impedance Spectroscopy (EIS) biosensors. *Sensors (Basel)* 12(11), pp. 14467-14488. doi: 10.3390/s121114467
- Martin, T. R. 2000. Recognition of bacterial endotoxin in the lungs. *Am J Respir Cell Mol Biol* 23(2), pp. 128-132. doi: 10.1165/ajrcmb.23.2.f189
- Martin, T. R. and Frevert, C. W. 2005. Innate immunity in the lungs. *Proc Am Thorac Soc* 2(5), pp. 403-411. doi: 10.1513/pats.200508-090JS
- Martinez, R. et al. 2011. Factors associated with inflammatory cytokine patterns in community-acquired pneumonia. *Eur Respir J* 37(2), pp. 393-399. doi: 10.1183/09031936.00040710
- Mauer, J. et al. 2015. Versatile functions for IL-6 in metabolism and cancer. *Trends Immunol* 36(2), pp. 92-101. doi: 10.1016/j.it.2014.12.008
- McNulty, C. A. et al. 2013. Expectations for consultations and antibiotics for respiratory tract infection in primary care: the RTI clinical iceberg. *Br J Gen Pract* 63(612), pp. e429-436. doi: 10.3399/bjgp13X669149
- Medetalibeyoglu, H. et al. 2020. Validated electrochemical immunosensor for ultra-sensitive procalcitonin detection: Carbon electrode modified with gold nanoparticles functionalized sulfur doped MXene as sensor platform and carboxylated graphitic carbon nitride as signal amplification. *Sensors and Actuators B: Chemical* 319, p. 128195. doi: <https://doi.org/10.1016/j.snb.2020.128195>

Medjo, B. et al. 2017. Increased Serum Interleukin-10 but not Interleukin-4 Level in Children with *Mycoplasma pneumoniae* Pneumonia. *J Trop Pediatr* 63(4), pp. 294-300. doi: 10.1093/tropej/fmw091

Mei, Z. and Tang, L. 2017. Surface-Plasmon-Coupled Fluorescence Enhancement Based on Ordered Gold Nanorod Array Biochip for Ultrasensitive DNA Analysis. *Anal Chem* 89(1), pp. 633-639. doi: 10.1021/acs.analchem.6b02797

Meirinho, S. G. et al. 2015. Development of an electrochemical RNA-aptasensor to detect human osteopontin. *Biosens Bioelectron* 71, pp. 332-341. doi: 10.1016/j.bios.2015.04.050

Mendelson, F. et al. 2018. C-reactive protein and procalcitonin to discriminate between tuberculosis, *Pneumocystis jirovecii* pneumonia, and bacterial pneumonia in HIV-infected inpatients meeting WHO criteria for seriously ill: a prospective cohort study. *BMC Infect Dis* 18(1), p. 399. doi: 10.1186/s12879-018-3303-6

Menendez, R. et al. 2009. Biomarkers improve mortality prediction by prognostic scales in community-acquired pneumonia. *Thorax* 64(7), pp. 587-591. doi: 10.1136/thx.2008.105312

Meyer, M. H. et al. 2006. SPR-based immunosensor for the CRP detection--a new method to detect a well known protein. *Biosens Bioelectron* 21(10), pp. 1987-1990. doi: 10.1016/j.bios.2005.09.010

Michelow, I. C. et al. 2007. Systemic cytokine profile in children with community-acquired pneumonia. *Pediatr Pulmonol* 42(7), pp. 640-645. doi: 10.1002/ppul.20633

Miranda-Castro, R. et al. 2018. Understanding the Factors Affecting the Analytical Performance of Sandwich-hybridization Genosensors on Gold Electrodes. *Electroanalysis* 30(7), pp. 1229-1240. doi: <https://doi.org/10.1002/elan.201800049>

Mirceski, V. et al. 2013. Square-Wave Voltammetry: A Review on the Recent Progress. *Electroanalysis* 25(11), pp. 2411-2422. doi: <https://doi.org/10.1002/elan.201300369>

Mizgerd, J. P. 2008. Acute lower respiratory tract infection. *N Engl J Med* 358(7), pp. 716-727. doi: 10.1056/NEJMra074111

Moerer, O. et al. 2007. A German national prevalence study on the cost of intensive care: an evaluation from 51 intensive care units. *Crit Care* 11(3), p. R69. doi: 10.1186/cc5952

Mold, C. et al. 1999. Regulation of complement activation by C-reactive protein. *Immunopharmacology* 42(1), pp. 23-30. doi: [https://doi.org/10.1016/S0162-3109\(99\)00007-7](https://doi.org/10.1016/S0162-3109(99)00007-7)

Mollarasouli, F. et al. 2019. The Role of Electrochemical Immunosensors in Clinical Analysis. *Biosensors (Basel)* 9(3), doi: 10.3390/bios9030086

- Moore, K. W. et al. 1993. Interleukin-10. *Annu Rev Immunol* 11, pp. 165-190. doi: 10.1146/annurev.iy.11.040193.001121
- Moulin, F. et al. 2001. Procalcitonin in children admitted to hospital with community acquired pneumonia. *Arch Dis Child* 84(4), pp. 332-336. doi: 10.1136/adc.84.4.332
- Moutachakir, M. et al. 2017. Immunoanalytical characteristics of C-reactive protein and high sensitivity C-reactive protein. *Ann Biol Clin (Paris)* 75(2), pp. 225-229. doi: 10.1684/abc.2017.1232
- Mufson, M. A. 1999. Pneumococcal Pneumonia. *Curr Infect Dis Rep* 1(1), pp. 57-64. doi: 10.1007/s11908-999-0011-9
- Muller, B. et al. 2007. Diagnostic and prognostic accuracy of clinical and laboratory parameters in community-acquired pneumonia. *BMC Infect Dis* 7, p. 10. doi: 10.1186/1471-2334-7-10
- Murdoch, D. R. et al. 2017. The Diagnostic Utility of Induced Sputum Microscopy and Culture in Childhood Pneumonia. *Clin Infect Dis* 64(suppl\_3), pp. S280-S288. doi: 10.1093/cid/cix090
- Nargis, W. et al. 2014. Procalcitonin versus C-reactive protein: Usefulness as biomarker of sepsis in ICU patient. *Int J Crit Illn Inj Sci* 4(3), pp. 195-199. doi: 10.4103/2229-5151.141356
- Nguyen Thi Dieu, T. et al. 2017. Clinical characteristics and cytokine changes in children with pneumonia requiring mechanical ventilation. *J Int Med Res* 45(6), pp. 1805-1817. doi: 10.1177/0300060516672766
- Nikaido, H. 2003. Molecular basis of bacterial outer membrane permeability revisited. *Microbiol Mol Biol Rev* 67(4), pp. 593-656. doi: 10.1128/membr.67.4.593-656.2003
- Numnuam, A. et al. 2008. Potentiometric detection of DNA hybridization. *J Am Chem Soc* 130(2), pp. 410-411. doi: 10.1021/ja0775467
- Okuno, J. et al. 2007. Label-free immunosensor for prostate-specific antigen based on single-walled carbon nanotube array-modified microelectrodes. *Biosens Bioelectron* 22(9-10), pp. 2377-2381. doi: 10.1016/j.bios.2006.09.038
- Opal, S. M. 2010. Endotoxins and other sepsis triggers. *Contrib Nephrol* 167, pp. 14-24. doi: 10.1159/000315915
- Ortqvist, A. et al. 1995. Diagnostic and prognostic value of interleukin-6 and C-reactive protein in community-acquired pneumonia. *Scand J Infect Dis* 27(5), pp. 457-462. doi: 10.3109/00365549509047046
- Ouyang, W. and O'Garra, A. 2019. IL-10 Family Cytokines IL-10 and IL-22: from Basic Science to Clinical Translation. *Immunity* 50(4), pp. 871-891. doi: 10.1016/j.immuni.2019.03.020

- Pahal, P. et al. 2021. Typical Bacterial Pneumonia. *StatPearls*. Treasure Island (FL).
- Pankratova, N. et al. 2015. Potentiometric sensing array for monitoring aquatic systems. *Environ Sci Process Impacts* 17(5), pp. 906-914. doi: 10.1039/c5em00038f
- Park, B. S. and Lee, J. O. 2013. Recognition of lipopolysaccharide pattern by TLR4 complexes. *Exp Mol Med* 45, p. e66. doi: 10.1038/emm.2013.97
- Parrilla, M. et al. 2016. A Textile-Based Stretchable Multi-Ion Potentiometric Sensor. *Adv Healthc Mater* 5(9), pp. 996-1001. doi: 10.1002/adhm.201600092
- Parrilla, M. et al. 2019. Wearable potentiometric ion sensors. *TrAC Trends in Analytical Chemistry* 110, pp. 303-320. doi: <https://doi.org/10.1016/j.trac.2018.11.024>
- Patel, K. et al. 2017. A Novel Surface Plasmon Resonance Biosensor for the Rapid Detection of Botulinum Neurotoxins. *Biosensors (Basel)* 7(3), doi: 10.3390/bios7030032
- Pathak, A. and Agrawal, A. 2019. Evolution of C-Reactive Protein. *Front Immunol* 10, p. 943. doi: 10.3389/fimmu.2019.00943
- Paul, R. et al. 2012. Study of C reactive protein as a prognostic marker in malaria from Eastern India. *Adv Biomed Res* 1, p. 41. doi: 10.4103/2277-9175.100140
- Pei, H. et al. 2010. A DNA nanostructure-based biomolecular probe carrier platform for electrochemical biosensing. *Adv Mater* 22(42), pp. 4754-4758. doi: 10.1002/adma.201002767
- Pei, R. et al. 2001. Amplification of antigen–antibody interactions based on biotin labeled protein–streptavidin network complex using impedance spectroscopy. *Biosensors and Bioelectronics* 16(6), pp. 355-361. doi: [https://doi.org/10.1016/S0956-5663\(01\)00150-6](https://doi.org/10.1016/S0956-5663(01)00150-6)
- Peltomaa, R. et al. 2018. Optical Biosensors for Label-Free Detection of Small Molecules. *Sensors (Basel)* 18(12), doi: 10.3390/s18124126
- Penaloza, H. F. et al. 2015. Interleukin-10 plays a key role in the modulation of neutrophils recruitment and lung inflammation during infection by *Streptococcus pneumoniae*. *Immunology* 146(1), pp. 100-112. doi: 10.1111/imm.12486
- Peng, J. et al. 2011. Synthesis of silver nanoparticle-hollow titanium phosphate sphere hybrid as a label for ultrasensitive electrochemical detection of human interleukin-6. *Small* 7(20), pp. 2921-2928. doi: 10.1002/smll.201101210
- Pepys, M. B. and Hirschfield, G. M. 2003. C-reactive protein: a critical update. *J Clin Invest* 111(12), pp. 1805-1812. doi: 10.1172/JCI18921

- Perdomo-Morales, R. et al. 2011. Monocyte activation test (MAT) reliably detects pyrogens in parenteral formulations of human serum albumin. *ALTEX* 28(3), pp. 227-235. doi: 10.14573/altex.2011.3.227
- Pietrzak, B. et al. 2023. Circulating Microbial Cell-Free DNA in Health and Disease. *Int J Mol Sci* 24(3), doi: 10.3390/ijms24033051
- Piliarik, M. et al. 2012. High-resolution biosensor based on localized surface plasmons. *Opt Express* 20(1), pp. 672-680. doi: 10.1364/OE.20.000672
- Pimkova, K. et al. 2012. Surface plasmon resonance biosensor for the detection of VEGFR-1-- a protein marker of myelodysplastic syndromes. *Anal Bioanal Chem* 402(1), pp. 381-387. doi: 10.1007/s00216-011-5395-3
- Poirel, L. et al. 2017. Polymyxins: Antibacterial Activity, Susceptibility Testing, and Resistance Mechanisms Encoded by Plasmids or Chromosomes. *Clin Microbiol Rev* 30(2), pp. 557-596. doi: 10.1128/CMR.00064-16
- Prime, K. L. and Whitesides, G. M. 1991. Self-assembled organic monolayers: model systems for studying adsorption of proteins at surfaces. *Science* 252(5009), pp. 1164-1167. doi: 10.1126/science.252.5009.1164
- Prodromidis, M. I. and Karayannis, M. I. 2002. Enzyme Based Amperometric Biosensors for Food Analysis. *Electroanalysis* 14(4), pp. 241-261. doi: [https://doi.org/10.1002/1521-4109\(200202\)14:4<241::AID-ELAN241>3.0.CO;2-P](https://doi.org/10.1002/1521-4109(200202)14:4<241::AID-ELAN241>3.0.CO;2-P)
- Pugin, J. et al. 1993. Lipopolysaccharide activation of human endothelial and epithelial cells is mediated by lipopolysaccharide-binding protein and soluble CD14. *Proc Natl Acad Sci U S A* 90(7), pp. 2744-2748. doi: 10.1073/pnas.90.7.2744
- Puren, A. J. et al. 1995. Patterns of cytokine expression in community-acquired pneumonia. *Chest* 107(5), pp. 1342-1349. doi: 10.1378/chest.107.5.1342
- Qi, C. et al. 2010. Detection of avian influenza virus subtype H5 using a biosensor based on imaging ellipsometry. *Biosensors and Bioelectronics* 25(6), pp. 1530-1534. doi: <https://doi.org/10.1016/j.bios.2009.10.030>
- Qiang, W. et al. 2015. A fluorescent biosensing platform based on the polydopamine nanospheres intergrating with Exonuclease III-assisted target recycling amplification. *Biosens Bioelectron* 71, pp. 143-149. doi: 10.1016/j.bios.2015.04.029
- Quinton, L. J. et al. 2009. Mechanisms of the hepatic acute-phase response during bacterial pneumonia. *Infect Immun* 77(6), pp. 2417-2426. doi: 10.1128/IAI.01300-08
- Quinton, L. J. et al. 2018. Integrative Physiology of Pneumonia. *Physiol Rev* 98(3), pp. 1417-1464. doi: 10.1152/physrev.00032.2017

- Radi, A. E. et al. 2006. Reagentless, reusable, ultrasensitive electrochemical molecular beacon aptasensor. *J Am Chem Soc* 128(1), pp. 117-124. doi: 10.1021/ja053121d
- Radstrom, P. et al. 2004. Pre-PCR processing: strategies to generate PCR-compatible samples. *Mol Biotechnol* 26(2), pp. 133-146. doi: 10.1385/MB:26:2:133
- Rahman, M. M. et al. 2015. Electrochemical DNA hybridization sensors based on conducting polymers. *Sensors (Basel)* 15(2), pp. 3801-3829. doi: 10.3390/s150203801
- Reich, J. et al. 2016. Masking of endotoxin in surfactant samples: Effects on Limulus-based detection systems. *Biologicals* 44(5), pp. 417-422. doi: 10.1016/j.biologicals.2016.04.012
- Reich, J. et al. 2018. Investigation of the kinetics and mechanism of low endotoxin recovery in a matrix for biopharmaceutical drug products. *Biologicals* 53, pp. 1-9. doi: 10.1016/j.biologicals.2018.04.001
- Reich, J. et al. 2019. Low Endotoxin Recovery-Masking of Naturally Occurring Endotoxin. *Int J Mol Sci* 20(4), doi: 10.3390/ijms20040838
- Reich, P. et al. 2017. Development of An Impedimetric Aptasensor for the Detection of Staphylococcus aureus. *Int J Mol Sci* 18(11), doi: 10.3390/ijms18112484
- Reinhart, K. et al. 2012. New approaches to sepsis: molecular diagnostics and biomarkers. *Clin Microbiol Rev* 25(4), pp. 609-634. doi: 10.1128/CMR.00016-12
- Requejo, H. I. and Coccoza, A. M. 2003. C-reactive protein in the diagnosis of community-acquired pneumonia. *Braz J Infect Dis* 7(4), pp. 241-244. doi: 10.1590/s1413-86702003000400003
- Reta, N. et al. 2019. Label-Free Bacterial Toxin Detection in Water Supplies Using Porous Silicon Nanochannel Sensors. *ACS Sens* 4(6), pp. 1515-1523. doi: 10.1021/acssensors.8b01670
- Rietschel, E. T. et al. 1987. Lipid A, the endotoxic center of bacterial lipopolysaccharides: relation of chemical structure to biological activity. *Prog Clin Biol Res* 231, pp. 25-53.
- Rocchitta, G. et al. 2016. Enzyme Biosensors for Biomedical Applications: Strategies for Safeguarding Analytical Performances in Biological Fluids. *Sensors (Basel)* 16(6), doi: 10.3390/s16060780
- Roche, M. I. et al. 2011. Characterization of monoclonal antibodies to terminal and internal O-antigen epitopes of Francisella tularensis lipopolysaccharide. *Hybridoma (Larchmt)* 30(1), pp. 19-28. doi: 10.1089/hyb.2010.0083
- Rojas, J. M. et al. 2017. IL-10: A Multifunctional Cytokine in Viral Infections. *J Immunol Res* 2017, p. 6104054. doi: 10.1155/2017/6104054

Rong, Q. et al. 2015. Network nanostructured polypyrrole hydrogel/Au composites as enhanced electrochemical biosensing platform. *Sci Rep* 5, p. 11440. doi: 10.1038/srep11440

Roy, M. G. et al. 2014. Muc5b is required for airway defence. *Nature* 505(7483), pp. 412-416. doi: 10.1038/nature12807

Rudan, I. et al. 2008. Epidemiology and etiology of childhood pneumonia. *Bull World Health Organ* 86(5), pp. 408-416. doi: 10.2471/blt.07.048769

Ruiz-Gonzalez, A. et al. 2016. The Diagnostic Value of Serum C-Reactive Protein for Identifying Pneumonia in Hospitalized Patients with Acute Respiratory Symptoms. *J Biomark* 2016, p. 2198745. doi: 10.1155/2016/2198745

Ruiz-Valdepenas Montiel, V. et al. 2018. Delayed Sensor Activation Based on Transient Coatings: Biofouling Protection in Complex Biofluids. *J Am Chem Soc* 140(43), pp. 14050-14053. doi: 10.1021/jacs.8b08894

Saei, A. A. et al. 2013. Electrochemical biosensors for glucose based on metal nanoparticles. *TrAC Trends in Analytical Chemistry* 42, pp. 216-227. doi: <https://doi.org/10.1016/j.trac.2012.09.011>

Saghafian-Hedengren, S. et al. 2017. Assessment of Cytokine and Chemokine Signatures as Potential Biomarkers of Childhood Community-acquired Pneumonia Severity: A Nested Cohort Study in India. *Pediatr Infect Dis J* 36(1), pp. 102-108. doi: 10.1097/INF.0000000000001364

Sattar, S. B. A. and Sharma, S. 2021. Bacterial Pneumonia. *StatPearls*. Treasure Island (FL).

Saukkonen, K. et al. 2008. Cell-free plasma DNA as a predictor of outcome in severe sepsis and septic shock. *Clin Chem* 54(6), pp. 1000-1007. doi: 10.1373/clinchem.2007.101030

Schaaf, B. et al. 2005. The interleukin-6 -174 promoter polymorphism is associated with extrapulmonary bacterial dissemination in *Streptococcus pneumoniae* infection. *Cytokine* 31(4), pp. 324-328. doi: 10.1016/j.cyto.2005.05.008

Schuetz, P. et al. 2009. Procalcitonin and other biomarkers to improve assessment and antibiotic stewardship in infections--hope for hype? *Swiss Med Wkly* 139(23-24), pp. 318-326. doi: smw-12584

Self, W. H. et al. 2017. Procalcitonin as a Marker of Etiology in Adults Hospitalized With Community-Acquired Pneumonia. *Clin Infect Dis* 65(2), pp. 183-190. doi: 10.1093/cid/cix317

Sener, G. et al. 2013. Rapid real-time detection of procalcitonin using a microcontact imprinted surface plasmon resonance biosensor. *Analyst* 138(21), pp. 6422-6428. doi: 10.1039/c3an00958k

- Sfeir, T. et al. 2001. Role of interleukin-10 in monocyte hyporesponsiveness associated with septic shock. *Crit Care Med* 29(1), pp. 129-133. doi: 10.1097/00003246-200101000-00026
- Shah, N. S. et al. 2016. Bacterial and viral co-infections complicating severe influenza: Incidence and impact among 507 U.S. patients, 2013-14. *J Clin Virol* 80, pp. 12-19. doi: 10.1016/j.jcv.2016.04.008
- Shah, S. S. et al. 2011. Blood cultures in the emergency department evaluation of childhood pneumonia. *Pediatr Infect Dis J* 30(6), pp. 475-479. doi: 10.1097/INF.0b013e31820a5adb
- Shrive, A. K. et al. 1996. Three dimensional structure of human C-reactive protein. *Nat Struct Biol* 3(4), pp. 346-354. doi: 10.1038/nsb0496-346
- Shukla, S. et al. 2002. Synthesis and Characterization of Silver Sulfide Nanoparticles Containing Sol-Gel Derived HPC-Silica Film for Ion-Selective Electrode Application. *Journal of Sol-Gel Science and Technology* 23(2), pp. 151-164. doi: 10.1023/A:1013707702960
- Simon, L. et al. 2004. Serum procalcitonin and C-reactive protein levels as markers of bacterial infection: a systematic review and meta-analysis. *Clin Infect Dis* 39(2), pp. 206-217. doi: 10.1086/421997
- Singh, S. et al. 2017. DNA chip based sensor for amperometric detection of infectious pathogens. *Int J Biol Macromol* 103, pp. 355-359. doi: 10.1016/j.ijbiomac.2017.05.041
- Sokalski, T. et al. 1997. Large Improvement of the Lower Detection Limit of Ion-Selective Polymer Membrane Electrodes. *Journal of the American Chemical Society* 119(46), pp. 11347-11348. doi: 10.1021/ja972932h
- Song, W. et al. 2008. Preparation of PbS Nanoparticles by Phase-Transfer Method and Application to Pb-Selective Electrode Based on PVC Membrane. *Anal Lett* 41(15), pp. 2844-2859. doi: 10.1080/00032710802421780
- Songjaroen, T. et al. 2016. Label-free detection of C-reactive protein using an electrochemical DNA immunoassay. *Sensing and Bio-Sensing Research* 8, pp. 14-19. doi: <https://doi.org/10.1016/j.sbsr.2016.03.003>
- Spindel, S. and Sapsford, K. E. 2014. Evaluation of optical detection platforms for multiplexed detection of proteins and the need for point-of-care biosensors for clinical use. *Sensors (Basel)* 14(12), pp. 22313-22341. doi: 10.3390/s141222313
- Sproston, N. R. and Ashworth, J. J. 2018. Role of C-Reactive Protein at Sites of Inflammation and Infection. *Front Immunol* 9, p. 754. doi: 10.3389/fimmu.2018.00754
- Srivastava, S. K. et al. 2014. SERS biosensor using metallic nano-sculptured thin films for the detection of endocrine disrupting compound biomarker vitellogenin. *Small* 10(17), pp. 3579-3587. doi: 10.1002/smll.201303218

- Stellrecht, K. A. 2017. Molecular Testing for Respiratory Viruses. *Diagnostic Molecular Pathology*, pp. 123-137. doi: 10.1016/B978-0-12-800886-7.00011-X
- Stockmann, C. et al. 2018. Procalcitonin Accurately Identifies Hospitalized Children With Low Risk of Bacterial Community-Acquired Pneumonia. *J Pediatric Infect Dis Soc* 7(1), pp. 46-53. doi: 10.1093/jpids/piw091
- Stradiotto, N. R. et al. 2003. Electrochemical sensors: a powerful tool in analytical chemistry. *Journal of the Brazilian Chemical Society* 14, pp. 159-173.
- Stralin, K. et al. 2005. Design of a multiplex PCR for *Streptococcus pneumoniae*, *Haemophilus influenzae*, *Mycoplasma pneumoniae* and *Chlamydia pneumoniae* to be used on sputum samples. *APMIS* 113(2), pp. 99-111. doi: 10.1111/j.1600-0463.2005.apm1130203.x
- Su, H. et al. 2019. Novel thiolated-PEG linker molecule for biosensor development on gold surfaces. *Biosens Bioelectron* 141, p. 111477. doi: 10.1016/j.bios.2019.111477
- Sun, H. et al. 2015. Detection of Cytomegalovirus Antibodies Using a Biosensor Based on Imaging Ellipsometry. *PLoS ONE* 10(8), p. e0136253. doi: 10.1371/journal.pone.0136253
- Sun, J. et al. 2009. Effector T cells control lung inflammation during acute influenza virus infection by producing IL-10. *Nat Med* 15(3), pp. 277-284. doi: 10.1038/nm.1929
- Sypabekova, M. et al. 2019. An aptasensor for the detection of *Mycobacterium tuberculosis* secreted immunogenic protein MPT64 in clinical samples towards tuberculosis detection. *Sci Rep* 9(1), p. 16273. doi: 10.1038/s41598-019-52685-6
- Takeuchi, O. and Akira, S. 2010. Pattern recognition receptors and inflammation. *Cell* 140(6), pp. 805-820. doi: 10.1016/j.cell.2010.01.022
- Tanaka, T. et al. 2014. IL-6 in inflammation, immunity, and disease. *Cold Spring Harb Perspect Biol* 6(10), p. a016295. doi: 10.1101/cshperspect.a016295
- Tavakoli, J. and Tang, Y. 2017. Hydrogel Based Sensors for Biomedical Applications: An Updated Review. *Polymers (Basel)* 9(8), doi: 10.3390/polym9080364
- Taylor, P. R. et al. 2005. Macrophage receptors and immune recognition. *Annu Rev Immunol* 23, pp. 901-944. doi: 10.1146/annurev.immunol.23.021704.115816
- Tesmer, L. A. et al. 2008. Th17 cells in human disease. *Immunol Rev* 223, pp. 87-113. doi: 10.1111/j.1600-065X.2008.00628.x
- Thangamuthu, M. et al. 2018. Label-Free Electrochemical Immunoassay for C-Reactive Protein. *Biosensors (Basel)* 8(2), doi: 10.3390/bios8020034

- Toikka, P. et al. 2000. Serum procalcitonin, C-reactive protein and interleukin-6 for distinguishing bacterial and viral pneumonia in children. *Pediatr Infect Dis J* 19(7), pp. 598-602. doi: 10.1097/00006454-200007000-00003
- Tomimuro, K. et al. 2020. Thread-Based Bioluminescent Sensor for Detecting Multiple Antibodies in a Single Drop of Whole Blood. *ACS Sens* 5(6), pp. 1786-1794. doi: 10.1021/acssensors.0c00564
- Tong, Z. et al. 2007. A novel and simple biomolecules immobilization method: electro-deposition ZrO<sub>2</sub> doped with HRP for fabrication of hydrogen peroxide biosensor. *J Biotechnol* 128(3), pp. 567-575. doi: 10.1016/j.jbiotec.2006.12.008
- Torres, A. et al. 2016. Laboratory diagnosis of pneumonia in the molecular age. *European Respiratory Journal* 48(6), pp. 1764-1778. doi: 10.1183/13993003.01144-2016
- Trunzo, N. E. and Hong, K. L. 2020. Recent Progress in the Identification of Aptamers Against Bacterial Origins and Their Diagnostic Applications. *Int J Mol Sci* 21(14), doi: 10.3390/ijms21145074
- Tung, Y. T. et al. 2014. Nanostructured electrochemical biosensor for th0065 detection of the weak binding between the dengue virus and the CLEC5A receptor. *Nanomedicine* 10(6), pp. 1335-1341. doi: 10.1016/j.nano.2014.03.009
- U, S. D. et al. 2012. Highly sensitive SERS detection of cancer proteins in low sample volume using hollow core photonic crystal fiber. *Biosens Bioelectron* 33(1), pp. 293-298. doi: 10.1016/j.bios.2011.12.056
- Unold, D. and Nichols, J. H. 2010. Point-of-Care Testing: Needs, Opportunity, and Innovation, 3rd Edition, by Christopher P. Price, Andrew St John, and Larry J. Kricka, eds. *Clinical Chemistry* 56(12), pp. 1893-1894. doi: 10.1373/clinchem.2010.154872
- Urosevic, N. et al. 2022. Plasma cfDNA predictors of established bacteraemic infection. *Access Microbiol* 4(6), p. acmi000373. doi: 10.1099/acmi.0.000373
- Vaddiraju, S. et al. 2010. Emerging synergy between nanotechnology and implantable biosensors: a review. *Biosens Bioelectron* 25(7), pp. 1553-1565. doi: 10.1016/j.bios.2009.12.001
- Valentini, S. et al. 2019. Monocyte-activation test to reliably measure the pyrogenic content of a vaccine: An in vitro pyrogen test to overcome in vivo limitations. *Vaccine* 37(29), pp. 3754-3760. doi: 10.1016/j.vaccine.2018.10.082
- van der Eerden, M. M. et al. 2005. Value of intensive diagnostic microbiological investigation in low- and high-risk patients with community-acquired pneumonia. *Eur J Clin Microbiol Infect Dis* 24(4), pp. 241-249. doi: 10.1007/s10096-005-1316-8

- van der Poll, T. et al. 1997. Antiinflammatory cytokine responses during clinical sepsis and experimental endotoxemia: sequential measurements of plasma soluble interleukin (IL)-1 receptor type II, IL-10, and IL-13. *J Infect Dis* 175(1), pp. 118-122. doi: 10.1093/infdis/175.1.118
- van Dissel, J. T. et al. 1998. Anti-inflammatory cytokine profile and mortality in febrile patients. *Lancet* 351(9107), pp. 950-953. doi: 10.1016/S0140-6736(05)60606-X
- Vareille, M. et al. 2011. The airway epithelium: soldier in the fight against respiratory viruses. *Clin Microbiol Rev* 24(1), pp. 210-229. doi: 10.1128/CMR.00014-10
- Vasconcellos, A. G. et al. 2018. Systemic cytokines and chemokines on admission of children hospitalized with community-acquired pneumonia. *Cytokine* 107, pp. 1-8. doi: 10.1016/j.cyto.2017.11.005
- Vericat, C. et al. 2010. Self-assembled monolayers of thiols and dithiols on gold: new challenges for a well-known system. *Chem Soc Rev* 39(5), pp. 1805-1834. doi: 10.1039/b907301a
- Vijayan, A. L. et al. 2017. Procalcitonin: a promising diagnostic marker for sepsis and antibiotic therapy. *J Intensive Care* 5, p. 51. doi: 10.1186/s40560-017-0246-8
- Vincent, J. L. et al. 2015. Rapid Diagnosis of Infection in the Critically Ill, a Multicenter Study of Molecular Detection in Bloodstream Infections, Pneumonia, and Sterile Site Infections. *Crit Care Med* 43(11), pp. 2283-2291. doi: 10.1097/CCM.0000000000001249
- Vos, L. M. et al. 2019. Rapid Molecular Tests for Influenza, Respiratory Syncytial Virus, and Other Respiratory Viruses: A Systematic Review of Diagnostic Accuracy and Clinical Impact Studies. *Clin Infect Dis* 69(7), pp. 1243-1253. doi: 10.1093/cid/ciz056
- Walter, M. R. 2014. The molecular basis of IL-10 function: from receptor structure to the onset of signaling. *Curr Top Microbiol Immunol* 380, pp. 191-212. doi: 10.1007/978-3-662-43492-5\_9
- Wang, D. D. et al. 2016. A bioluminescent sensor for highly selective and sensitive detection of human carboxylesterase 1 in complex biological samples. *Chem Commun (Camb)* 52(15), pp. 3183-3186. doi: 10.1039/c5cc09874b
- Wang, H. et al. 1996. Salmonella detection by the polymyxin-cloth enzyme immunoassay using polyclonal and monoclonal detector antibodies. *International Journal of Food Microbiology* 29(1), pp. 31-40. doi: [https://doi.org/10.1016/0168-1605\(95\)00016-X](https://doi.org/10.1016/0168-1605(95)00016-X)
- Wang, H. et al. 2014a. Electrochemical immunosensor for alpha-fetoprotein detection using ferrocene and horseradish peroxidase as signal amplification labels. *Anal Biochem* 465, pp. 121-126. doi: 10.1016/j.ab.2014.08.016

Wang, J. et al. 2017a. Clinically Relevant Detection of Streptococcus pneumoniae with DNA-Antibody Nanostructures. *Anal Chem* 89(12), pp. 6900-6906. doi: 10.1021/acs.analchem.7b01508

Wang, J. et al. 2009. Combination of aptamer with gold nanoparticles for electrochemical signal amplification: application to sensitive detection of platelet-derived growth factor. *Biosens Bioelectron* 24(6), pp. 1598-1602. doi: 10.1016/j.bios.2008.08.030

Wang, W. et al. 2021. Utilization of serum procalcitonin as a biomarker in the diagnosis and treatment of children with bacterial hospital-acquired pneumonia. *Mol Cell Biochem* 476(1), pp. 261-267. doi: 10.1007/s11010-020-03902-8

Wang, X. et al. 2014b. A polymeric liquid membrane electrode responsive to 3,3',5,5'-tetramethylbenzidine oxidation for sensitive peroxidase/peroxidase mimetic-based potentiometric biosensing. *Anal Chem* 86(9), pp. 4416-4422. doi: 10.1021/ac500281r

Wang, Y. et al. 2017b. Cross-protective mucosal immunity mediated by memory Th17 cells against Streptococcus pneumoniae lung infection. *Mucosal Immunol* 10(1), pp. 250-259. doi: 10.1038/mi.2016.41

Weiner, L. M. et al. 2016. Antimicrobial-Resistant Pathogens Associated With Healthcare-Associated Infections: Summary of Data Reported to the National Healthcare Safety Network at the Centers for Disease Control and Prevention, 2011-2014. *Infect Control Hosp Epidemiol* 37(11), pp. 1288-1301. doi: 10.1017/ice.2016.174

Weiss, K. A. et al. 2011. Multiple CD4+ T cell subsets produce immunomodulatory IL-10 during respiratory syncytial virus infection. *J Immunol* 187(6), pp. 3145-3154. doi: 10.4049/jimmunol.1100764

Wen, Y. et al. 2011. DNA nanostructure-decorated surfaces for enhanced aptamer-target binding and electrochemical cocaine sensors. *Anal Chem* 83(19), pp. 7418-7423. doi: 10.1021/ac201491p

Whitsett, J. A. and Alenghat, T. 2015. Respiratory epithelial cells orchestrate pulmonary innate immunity. *Nat Immunol* 16(1), pp. 27-35. doi: 10.1038/ni.3045

Williams, D. J. et al. 2016. Predicting Severe Pneumonia Outcomes in Children. *Pediatrics* 138(4), doi: 10.1542/peds.2016-1019

Wise, J. 2020. Covid-19: Concerns persist about purpose, ethics, and effect of rapid testing in Liverpool. *BMJ* 371, p. m4690. doi: 10.1136/bmj.m4690

Wu, C. L. et al. 2006. Etiology and cytokine expression in patients requiring mechanical ventilation due to severe community-acquired pneumonia. *J Formos Med Assoc* 105(1), pp. 49-55. doi: 10.1016/s0929-6646(09)60108-x

- Wu, J. et al. 2010. Ternary surface monolayers for ultrasensitive (zeptomole) amperometric detection of nucleic acid hybridization without signal amplification. *Anal Chem* 82(21), pp. 8830-8837. doi: 10.1021/ac101474k
- Wu, J. et al. 2009. Potentiometric detection of DNA hybridization using enzyme-induced metallization and a silver ion selective electrode. *Anal Chem* 81(24), pp. 10007-10012. doi: 10.1021/ac9018507
- Wussler, D. et al. 2019. Clinical Utility of Procalcitonin in the Diagnosis of Pneumonia. *Clin Chem* 65(12), pp. 1532-1542. doi: 10.1373/clinchem.2019.306787
- Xie, P. et al. 2016. Highly sensitive detection of lipopolysaccharides using an aptasensor based on hybridization chain reaction. *Sci Rep* 6, p. 29524. doi: 10.1038/srep29524
- Xu, J. and Lee, H. 2020. Anti-Biofouling Strategies for Long-Term Continuous Use of Implantable Biosensors. *Chemosensors* 8(3), doi: 10.3390/chemosensors8030066
- Yan, Y. Y. et al. 2021. Cell-Free DNA: Hope and Potential Application in Cancer. *Front Cell Dev Biol* 9, p. 639233. doi: 10.3389/fcell.2021.639233
- Yang, T. et al. 2013a. Synchronous electrosynthesis of poly(xanthurenic acid)-reduced graphene oxide nanocomposite for highly sensitive impedimetric detection of DNA. *ACS Appl Mater Interfaces* 5(9), pp. 3495-3499. doi: 10.1021/am400370s
- Yang, T. et al. 2013b. Direct electrochemical DNA detection originated from the self-redox signal of sulfonated polyaniline enhanced by graphene oxide in neutral solution. *ACS Appl Mater Interfaces* 5(21), pp. 10889-10894. doi: 10.1021/am403090y
- Yang, T. et al. 2013c. An electrochemical impedance sensor for the label-free ultrasensitive detection of interleukin-6 antigen. *Sensors and Actuators B: Chemical* 178, pp. 310-315. doi: <https://doi.org/10.1016/j.snb.2012.12.107>
- Yang, X. et al. 2013d. Anti-fouling PEDOT:PSS modification on glassy carbon electrodes for continuous monitoring of tricresyl phosphate. *Sensors and Actuators B: Chemical* 177, pp. 659-667. doi: <https://doi.org/10.1016/j.snb.2012.11.057>
- Yasukawa, K. et al. 1987. Structure and expression of human B cell stimulatory factor-2 (BSF-2/IL-6) gene. *EMBO J* 6(10), pp. 2939-2945.
- Ye, H. et al. 2019. Fluorometric determination of lipopolysaccharides via changes of the graphene oxide-enhanced fluorescence polarization caused by truncated aptamers. *Mikrochim Acta* 186(3), p. 173. doi: 10.1007/s00604-019-3261-8
- Ye, Q. et al. 2015. Epidemiological characteristics and immune status of children with Respiratory Syncytial Virus. *J Med Virol* 87(2), pp. 323-329. doi: 10.1002/jmv.24047

- Yeh, H. W. and Ai, H. W. 2019. Development and Applications of Bioluminescent and Chemiluminescent Reporters and Biosensors. *Annu Rev Anal Chem (Palo Alto Calif)* 12(1), pp. 129-150. doi: 10.1146/annurev-anchem-061318-115027
- Yoon, S. I. et al. 2010. Structure and mechanism of receptor sharing by the IL-10R2 common chain. *Structure* 18(5), pp. 638-648. doi: 10.1016/j.str.2010.02.009
- Young, C. C. 1997. Evolution of Blood Chemistry Analyzers Based on Ion Selective Electrodes. *Journal of Chemical Education* 74(2), p. 177. doi: 10.1021/ed074p177
- Yuan, J. et al. 2012. Detection of serum human epididymis secretory protein 4 in patients with ovarian cancer using a label-free biosensor based on localized surface plasmon resonance. *Int J Nanomedicine* 7, pp. 2921-2928. doi: 10.2147/IJN.S32641
- Yuan, W. et al. 2009. Polarization-sensitive surface plasmon enhanced ellipsometry biosensor using the photoelastic modulation technique. *Sensors and Actuators A: Physical* 151(1), pp. 23-28. doi: <https://doi.org/10.1016/j.sna.2009.01.025>
- Zandieh, M. et al. 2018. Label-free and simple detection of endotoxins using a sensitive LSPR biosensor based on silver nanocolumns. *Anal Biochem* 548, pp. 96-101. doi: 10.1016/j.ab.2018.02.023
- Zdrachek, E. and Bakker, E. 2019a. From Molecular and Emulsified Ion Sensors to Membrane Electrodes: Molecular and Mechanistic Sensor Design. *Acc Chem Res* 52(5), pp. 1400-1408. doi: 10.1021/acs.accounts.9b00056
- Zdrachek, E. and Bakker, E. 2019b. Potentiometric Sensing. *Anal Chem* 91(1), pp. 2-26. doi: 10.1021/acs.analchem.8b04681
- Zhang, K. et al. 2019. A competitive microcystin-LR immunosensor based on Au NPs@metal-organic framework (MIL-101). *Chinese Chemical Letters* 30(3), pp. 664-667. doi: <https://doi.org/10.1016/j.ccllet.2018.10.021>
- Zhang, Y. et al. 2011. Serum tumor marker detection on PEGylated lipid membrane using biosensor based on total internal reflection imaging ellipsometry. *Sensors and Actuators B: Chemical* 159(1), pp. 121-125. doi: <https://doi.org/10.1016/j.snb.2011.06.059>
- Zheng, C. et al. 2019. Inflammatory Role of TLR-MyD88 Signaling in Multiple Sclerosis. *Front Mol Neurosci* 12, p. 314. doi: 10.3389/fnmol.2019.00314
- Zhu, C. et al. 2015. Electrochemical sensors and biosensors based on nanomaterials and nanostructures. *Anal Chem* 87(1), pp. 230-249. doi: 10.1021/ac5039863
- Zhuo, Y. et al. 2005. A reagentless amperometric immunosensor based on gold nanoparticles/thionine/Nafion-membrane-modified gold electrode for determination of  $\alpha$ -1-fetoprotein. *Electrochemistry Communications* 7(4), pp. 355-360. doi: <https://doi.org/10.1016/j.elecom.2005.02.001>

Zhuo, Z. et al. 2017. Recent Advances in SELEX Technology and Aptamer Applications in Biomedicine. *Int J Mol Sci* 18(10), doi: 10.3390/ijms18102142

Zobel, K. et al. 2012. Interleukin 6, lipopolysaccharide-binding protein and interleukin 10 in the prediction of risk and etiologic patterns in patients with community-acquired pneumonia: results from the German competence network CAPNETZ. *BMC pulmonary medicine* 12, p. 6. doi: 10.1186/1471-2466-12-6

Zuo, M. Y. et al. 2014. Detecting endotoxin with a flow cytometry-based magnetic aptasensor. *Anal Biochem* 466, pp. 38-43. doi: 10.1016/j.ab.2014.08.018

British Thoracic Society paediatric pneumonia audit. National audit period: 1 November 2016–31 January 2017

Zupančič, U., Jolly, P., Estrela, P., Moschou, D., and Ingber, D. (2020) Multiplexed Detection of Sepsis Markers in Whole Blood using Nanocomposite Coated Electrochemical Sensors.

## Chapter 2

# Development of a sample preparation protocol for endotoxin detection using the LAL assay

---

## 2.1 Introduction

### 2.1.1 Overview

This chapter focuses on the assessment of endotoxin activity in human plasma with evaluation of masking kinetics and development of a sample preparation protocol to allow for detection of endotoxin from clinical samples.

### 2.1.2 Lipopolysaccharide

Lipopolysaccharide (LPS), also known as endotoxin, is one of the most well studied bacterial surface molecules and is ubiquitously associated with the development of sepsis and septic shock, as well as the pathogenesis of a number of conditions, such as Alzheimer's and Parkinson's disease (Opal 2010; Vogt et al. 2017; Brown 2019). During sepsis, owing to inflammation which compromises the intestinal walls, translocation of endogenous endotoxin stores naturally found in the gut to the bloodstream is observed, which results in septic shock (Cangemi et al. 2016). In Gram-negative bacteria, 75% of the outer membrane is occupied by LPS (Lerouge and Vanderleyden 2002). The ability of endotoxin to stimulate the immune response is well documented (Opal 2010). LPS is large glycolipid made up of three structural domains: lipid A, the core oligosaccharide, and the O antigen (Figure 2.1).

Lipid A, a highly conserved, hydrophobic, glucosamine-based phospholipid, is responsible for the activation of the host's immune response (Bertani and Ruiz 2018). Lipid A consists of a central disaccharide of glucosamine (GlcN), phosphorylated at position 1 and 4', which carries four acyl chains linked via ester bonds at position 3 and 3', and via amide bonds at position 2 and 2' (Paracini et al. 2022). The core regions, which are found at the center of the endotoxin molecule, are linked to the glucosamines of Lipid A and consist of 3-deoxy-D-manno-oct-2-ulosonic acid (KDO) residues, heptoses, and various hexoses (Bertani and Ruiz 2018). The inner core sugars and KDO are subject to phosphorylation, which gives rise to an area of negative charge. The core regions, in contrast with Lipid A, vary from species to species and even between strains of specific species. Finally, the O-antigen, a diverse polysaccharide which often varies between strains of bacterial species, provides a unique target for recognition by host antibodies (Kintz et al. 2017). Typically, the O-antigen is composed of three to six repeating sugar residues, also known as O-units (Kalynych et al. 2014). Moreover, some bacteria, including mucosal pathogens, such as *Haemophilus influenzae*, do not synthesize the O-antigen at all (Choi et al. 2014). In these cases, the endotoxin molecule composed of only Lipid A and the core regions, is called lipooligosaccharide (LOS). Figure 2.1 shows the structure of endotoxin.

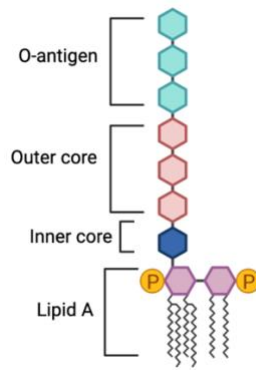


Figure 4.1: Endotoxin structure, showing the Lipid A phospholipid at the bottom, the inner core above it, the outer core, and the O-antigen at the top

The presence and repetition or absence of O-antigen also determines the form of endotoxin. For example, attachment of O-antigen to Lipid A leads to the formation of smooth LPS, also known as S-type LPS. Contrariwise, the absence of O-antigen results in the formation of rough LPS, also known as R-type LPS. Furthermore, the presence of just one repeating O-unit to Lipid A results in the composition of semi-rough LPS (SR-LPS) (Paracini et al. 2022). The terms smooth and rough refer to observations on bacterial colonies on solid culture media expressing the beforementioned LPS types (Hitchcock et al. 1986).

### 2.1.3 Endotoxin and disease

Endotoxin induces inflammation by binding to numerous endotoxin receptors in the human body, the most important of which is Toll-like receptor 4 (TLR4). TLR4 activation results in NF- $\kappa$ B transcriptional activation and production of pro-inflammatory cytokines such as IL-6 (Brown 2019). Other endotoxin receptors include RAGE, TREM2, macrophage scavenger receptors and the  $\beta$ 2 integrins (Paramo et al. 2015). Endotoxin can enter the bloodstream from both active infections and via passage through compromised mucosal membranes, especially the intestine, and is cleared by the liver (Brown 2019). In particular, endotoxin translocation is of particular importance to the pathogenesis of sepsis. The main drivers behind translocation are GI tract structural integrity alterations, caused by enterotoxins produced by gut bacteria, which target the tight junctions of the cells, as well as systemic inflammation (Brenchley and Douek 2012). In particular, overproduction of TNF and IL-1 are associated with increased microbial and endotoxin translocation levels (Brenchley and Douek 2012).

Elevated endotoxin levels are observed in several diseases and conditions. Increased endotoxin levels in the blood of diabetic patients (type 1 and type 2 diabetes) is a well-studied phenomenon (Gomes et al. 2017). This may be attributed to changes in the gut microbiota of diabetic patients, which can affect intestinal permeability. For example, in the gut of diabetic patients, lower levels of bifidobacteria, associated with reduced LPS translocation, are

recorded (Cani et al. 2008). Moreover, high levels of *Bacteroides* Gram-negative bacteria have been detected at increased levels in the gut of individuals with type 2 diabetes (Vogt et al. 2017). High endotoxin levels in diabetic patients have been associated with complications such as macroalbuminuria, dyslipidemia, insulin resistance, obesity, and chronic inflammation (Lassenius et al. 2011; Gomes et al. 2017). Endotoxin levels in the blood of fasting type 1 diabetes and type 2 diabetes patients has been recorded to be increased by ~235% and 66% compared with non-diabetic subjects, respectively (Gomes et al. 2017).

Additionally, endotoxin is implicated in numerous other conditions. As endotoxin is cleared by the liver, elevated circulating endotoxin levels (0.6-0.8 EU/ml) can be an indicator of advanced liver disease and cirrhosis (Brown 2019). Importantly, endotoxin is also implicated in neurodegeneration. There is a link between high endotoxin levels and Alzheimer's and Parkinson's disease (Brown 2019). Endotoxin has been associated with the formation of amyloid fibrils, and endotoxin has been detected in amyloid plaques in the brain (Vogt et al. 2017). Similarly to type 2 diabetes, in Alzheimer's and Parkinson's patients, increased levels of *Bacteroides* have been detected (Vogt et al. 2017). In addition, increased gut permeability, marked by elevated lipopolysaccharide-binding protein (LBP) levels has been observed in Parkinson's patients (Forsyth et al. 2011). A recent murine study showed that endotoxin injection (5 mg/Kg) induced memory deficits and loss of brain synapses and neurons, strengthening the link between endotoxin and neurodegeneration (Brown 2019). Finally, endotoxin has also been associated with ocular inflammation and age-related macular degeneration and atherosclerosis (Leung et al. 2009).

Most importantly, endotoxin is implicated in respiratory disease and disease progression. Endotoxin stores can naturally be found in the upper respiratory tract, such as in the mouth and nose (Munford 2016). There are numerous publications highlighting the role of endotoxin in respiratory disease. For example, inhaled endotoxin has been associated with asthma development (Liu 2002). Importantly, endotoxin is well-known for its pathogenic effects in the lung and especially endotoxin-mediated lung injury caused by immune system activation, free radicals produced by neutrophil and macrophage infiltration, and inflammatory-cell-derived proteinases (Brigham and Meyrick 1986).

Given the role of circulating endotoxin in numerous diseases, and its presence in the blood as a marker of early sepsis secondary to pneumonia, the importance of endotoxin detection in blood is highlighted.

#### *2.1.4 Endotoxin detection – LAL assay*

The limulus amoebocyte lysate (LAL) assay, which was developed around 1960 by Levin and Bang, works by measuring the formation of a gel-clot, turbidity or color change, depending on the assay, when an extract of horseshoe crab blood is exposed to endotoxin (Levin and

Bang 1968; Dullah and Ongkudon 2017). The LAL assay was approved by the Food and Drug Administration in the 1970s and is considered the gold standard and official method for endotoxin detection in drugs, medical devices and raw materials (Tamura et al. 2021). The assay is based on the activation of a clotting system which can be initiated by either Factor C activation by endotoxin, or by Factor G activation by (1–3)- $\beta$ -d-glucan, commonly found in the cell wall of fungi (Figure 2.2). Activation of either factor results in the cleavage of the pre-clotting enzyme which forms the clotting enzyme, which in turn results in the formation of a gel-clot or chromogenic substrate, depending on the assay (Munford 2016).

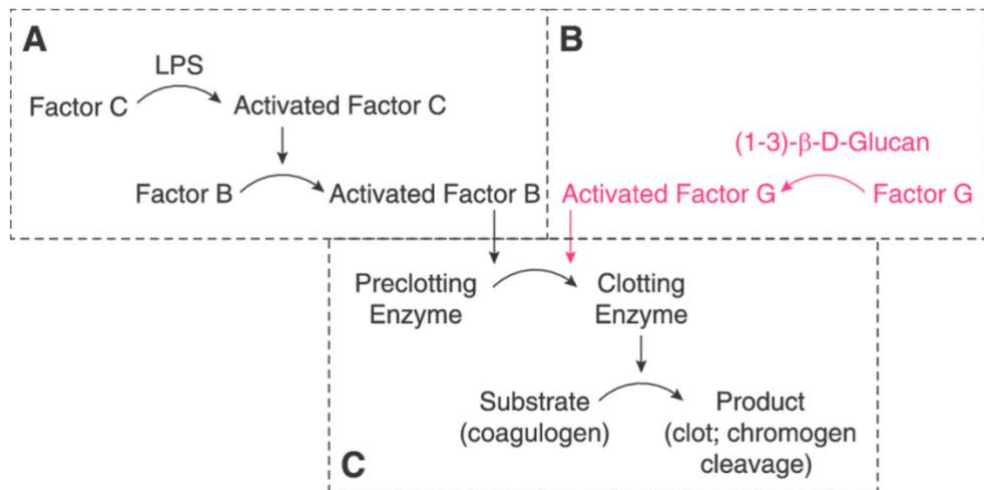


Figure 2.2: The LAL coagulation cascade leading to gel clot formation (Munford 2016)

Endotoxin activity levels are reported in EU/mL (endotoxin units). One EU is roughly equivalent to 0.1-0.2 ng endotoxin/mL of solution.

### 2.1.5 Endotoxin detection – alternative assays

There are number of other assays for the detection of endotoxin, such as the rabbit pyrogen test (RPT), the monocyte activation test (MAT) and the recombinant factor C (rFC) assay. Endotoxin detection studies in the 1940s involved the rabbit pyrogen test (RPT), however due to drawbacks associated with this method, such as the need for live animals, high cost and less than ideal limit of detection (0.5 EU) it has been largely replaced (Hartung 2015; Franco et al. 2018). An alternative to the LAL test, the monocyte activation test (MAT), was developed in 2010. The MAT test relies on the production of pro-inflammatory cytokines, such as IL-1 $\beta$  and IL-6, from human monocytes, and can detect down to 10 pg/ml of endotoxin (0.1 EU/mL) (Dullah and Ongkudon 2017; Vipond et al. 2019). However, due to natural variations in human blood, four different donors are required for sufficient testing, which restricts the accessibility to the assay. Additionally, the cells, samples and co-culture need to be incubated overnight, and the output is read using an ELISA, which results in long turnaround times and low throughput (Solati et al. 2015). Finally, the recombinant Factor C (rFC) test, developed in 2003

provides a promising alternative for endotoxin detection and eliminates interfering horseshoe crab blood component, as it isn't dependent on live animals for its production. However, its routine use is currently limited as there haven't been many long term studies proving its efficacy on pharmaceutical or biological samples. (Piehler et al. 2020). Additionally, the MAT assay relies on a fluorescence readout, so equipment tends to be expensive compared to standard tube / plate readers used in LAL (Molenaar-de Backer et al. 2023).

Research has found that the LAL assay is 3 to 300 times more sensitive than the RPT method, and the gel-clot assay has a detection limit down to 0.015 EU/ml, while the kinetic chromogenic and the turbidimetric LAL assay can have a detection limit down to 0.001 EU/mL (Piehler et al. 2020; Pasqua et al. 2021). The LAL assay is specific for the endotoxin of Gram-negative bacteria, however the presence of beta-glucans can activate LAL, leading to false positives (Piehler et al. 2020). In addition, as an enzymatic assay, the LAL assay is sensitive to sample conditions, such as pH and temperature, therefore particular attention needs to be paid to these factors to prevent assay inhibition (Aketagawa et al. 1993).

Two kinetic LAL assays are available: the kinetic turbidimetric assay (KTA) and the kinetic chromogenic assay (KCA). In KTA, the sample is mixed with the LAL reagent and the turbidity of the solution monitored over time. The rate of increase in turbidity is directly proportional to the concentration of endotoxin i.e., samples with higher levels of endotoxin contamination result in greater turbidity (Lonza, 2022). However, the KTA assay is sensitive to suspended or turbid materials and can result in a false positive if the sample is not prepared correctly (Joiner et al. 2002). In KCA, the LAL assay is combined with a peptide connected to p-nitroaniline, a yellow colorant. Upon activation of the enzymatic cascade, p-nitroaniline is released into the solution and the yellow colour is detected optically at 410nm (Lonza, 2002). Despite the higher sensitivity reported with the kinetic methods, the gel-clot assay remains the gold-standard in endotoxin testing especially in pharmaceuticals (Piehler et al. 2020).

#### *2.1.6 The CMD $\alpha$ BET<sup>®</sup> system*

The  $\alpha$ BET<sup>®</sup> system, developed by CMD, uses magneto-optical (MO) sensing technology and conventional gel-clot / turbidimetric LAL reagents to enable sensitive and rapid quantitation of endotoxin. The underpinning principle of the MO system is the monitoring of the rotational behaviour of inert magnetic nanorods introduced into the sample as 'reporters', the so-called reporters. The behaviour of the nanorods is monitored optically using polarized light.

Samples are prepared and added to a four-channel consumable cartridge along with the LAL reagent and CMD reporters. Once inserted into the  $\alpha$ BET<sup>®</sup> instrument, the sample is exposed to a rotating magnetic field whilst being interrogated optically. As the LAL assay proceeds, changes in the sample matrix occur (increase in viscosity and turbidity) which influence the behaviour of the nanorods. By monitoring the amplitude of the optical signal these changes

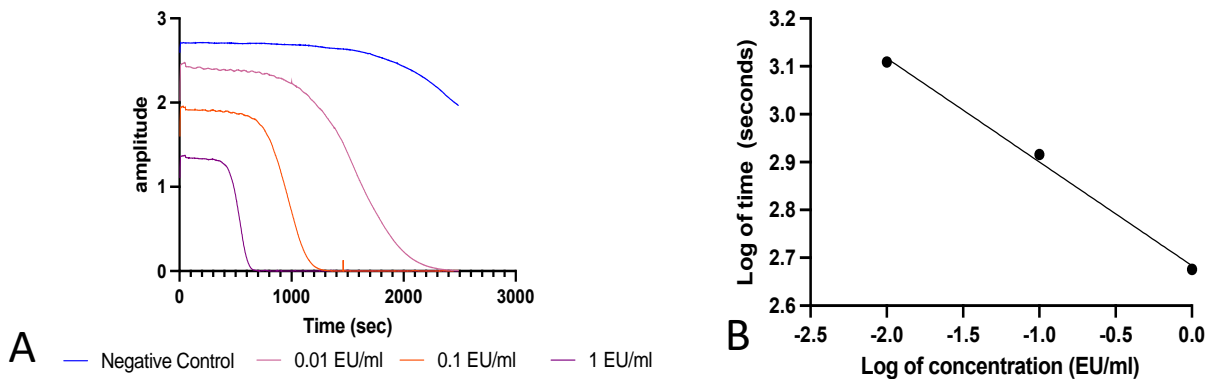
can be observed in real-time and correlated with endotoxin concentration; the quicker the change in the amplitude of the optical signal, the higher the endotoxin concentration.

The  $\alpha$ BET<sup>®</sup> system confers several advantages over traditional tube / plate reader systems, which are particularly useful when testing clinical samples. These include:

1. Time to result / sensitivity: The MO approach utilised in the  $\alpha$ BET<sup>®</sup> system is very sensitive to the small, early changes that occur when the LAL reagent reacts to the with endotoxin. This means that the maximum run time of an assay on the  $\alpha$ BET<sup>®</sup> system is 30 minutes, cf. 120 mins for a tube-reader based approach. This allows for more rapid screening of sample preparation approaches.
2. Reduced reagent / sample consumption: The  $\alpha$ BET<sup>®</sup> system requires just 7  $\mu$ L of LAL reagent and 14  $\mu$ L of sample per test. Traditional systems require 100 – 200  $\mu$ L of both.
3. Insensitivity to sample matrix colour / composition: The optical system of the  $\alpha$ BET<sup>®</sup> instrument utilises LEDs at a wavelength of 850 nm. Sample components do not absorb light at this wavelength, meaning that excellent signal recovery is achieved from samples that would typically be incompatible with the traditional optical systems used to monitor the LAL assay (Amit et al. 2016).

Whilst the underlying approach to interrogating the LAL assay differs in the  $\alpha$ BET<sup>®</sup> system, the data that is produced and its correlation with endotoxin concentration is the same as for the traditional tube / plate reader-based approaches. The amplitude of the MO signal is monitored as a function of time and the time at which the amplitude drops by 10% is recorded. A typical amplitude profile is provided in Figure 2.3A. Calibrations are generated by analysing standards of known endotoxin concentration and plotting the times at which a 10% drop in amplitude is recorded against endotoxin concentration in a log-log plot (Figure 2.3B). The calibration can then be used to calculate the endotoxin concentration in unknown samples.

As endotoxin testing is a regulatory requirement for injectable medicines and indwelling, blood-contacting, medical devices, the specifications for testing are outlined in the pharmacopoeias. For an endotoxin test to be considered valid, the correlation coefficient,  $r$ , of the calibration must be  $\geq 0.98$  and all spike recoveries must sit between 50% and 200% of expected (Eur. Pharm. Rev., 2017).



Figures 2.3 A and B: Figure 2.3 A shows an example amplitude graph showing the clotting curves for endotoxin in water in concentrations of 1, 0.1 and 0.01 EU/mL. Figure 2.3 B shows the transformed Log values of time needed to reach 80% of starting amplitude on y axis and the transformed Log values of endotoxin concentration on x axis.  $R^2 = 0.9961$ ,  $R = 0.9980$ .

Across  $\alpha$ BET<sup>®</sup> measurements, variations between recorded t=0 amplitude values can be observed. The system uses LEDs to optically interrogate the sample and small variations in power across the LEDs can lead to small differences in starting measurements. Additionally, the different cartridges used across experiments or imperfect sample mixing may also affect starting amplitude. In later sections, where plasma samples were used, lower starting amplitudes were recorded compared to aqueous samples. This may be attributed to the high protein content of the sample, which can adhere to nanorods, affecting their rotational behaviour, resulting in lower amplitudes and increased background “noise”. It is important to note, however, that those differences in starting amplitude do not influence the assay in any way, as relative change is measured, which is independent of starting amplitude.

#### 2.1.7. Endotoxin detection in clinical samples

It is important to note, that regardless of the benefits or drawbacks of each endotoxin testing method, none of them are routinely used to detect endotoxin in clinical samples. Despite the gold-standard status of the LAL assay, there haven't been any clinical applications of the assay in the detection of endotoxemia or bacteremia (Reich et al. 2019). The kinetic assays in particular are prone to interference when used for the assessment of plasma samples, due the yellow colour of plasma, which absorbs light at the same wavelength, potentially interfering with the results (Wong et al. 2016; Dheda et al. 2021). The endpoint gel-clot assay is less prone to interference by sample colour or interfering factors in plasma, which have been reported to interfere with the KCA assay (Wong et al. 2016).

The endotoxin activity assay (EEA), developed by Spectral Diagnostics, uses human neutrophils primed with endotoxin-antibody complexes and utilizes the oxidation of luminol

to semi-quantify endotoxin (low medium and high levels of endotoxin), and it's the only FDA approved test for endotoxin detection in blood (Yaguchi et al. 2012). With the exception of EEA, there is no standard test nor standard sample preparation protocol for the detection of endotoxin in clinical samples (Yaguchi et al. 2012; Reich et al. 2019).

Most importantly, detection in clinical matrices is often faced with interference from substances naturally present in the sample matrix, as well as the phenomenon of “Low endotoxin recovery” (LER), both of which will be described in more detail below (Reich et al. 2019). Interfering substances may interfere with either the assay itself, or with endotoxin alone. It is well known that blood components, such as lipoproteins and antimicrobial peptides can neutralize endotoxin, which makes its measurement in blood samples especially challenging (Pinto et al. 2014; Harm et al. 2021).

As there is no standard test or standard sample preparation protocol for the detection of endotoxin in clinical samples, several methods have been employed in literature (KTA, KCA, LAL). However, this produces varying results. Additionally, indirect measurement of endotoxin by quantification of lipopolysaccharide binding protein or using ELISAs utilizing antibodies against endotoxin have been performed, with moderate reliability for the detection of endotoxemia (Citronberg et al. 2016; Kim et al. 2016). Increased blood endotoxin levels have been detected in a number of studies in patients with community-acquired pneumonia (CAP), both viral and bacterial, utilizing a number of different detection methods (Cangemi et al. 2016; Sirivongrangson et al. 2020). In particular, a study utilizing ELISAs and antibodies against endotoxin has found that endotoxin blood levels of CAP patients at admission were significantly higher in comparison to healthy subjects (2 EU/ml vs 0.02 EU/ml respectively)(Cangemi et al. 2016). Similarly, using the endotoxin activity assay (EEA), endotoxin was detected in the blood of COVID-19 patients at admission, and increased endotoxin levels in blood were associated with complicated pneumonia and worse disease progression (Sirivongrangson et al. 2020). Both studies attributed endotoxin translocation to intestinal barrier failure, a well-reported phenomenon associated with early stages of sepsis secondary to pneumonia (Cangemi et al. 2016). However, it is important to note that across studies different methodologies were used (EAA, LAL, ELISAs), each measuring endotoxin in a different manner. For example, the LAL assay is a measure of endotoxin activity, or pyrogenicity, whereas the EAA assay is a semi-quantitative assay measuring the oxidative burst of primed neutrophils, and utilizes chemiluminescence (Yaguchi et al. 2012; Tamura et al. 2021). Due to a lack of standardized test for endotoxin in clinical samples, and the differences in measurements, it is difficult to compare studies and have confidence in the results presented, which signifies the need to develop a robust, standardized endotoxin detection platform for clinical samples.

#### *2.1.8 Endotoxin masking – need for a sample preparation protocol*

Despite the popularity of the LAL assay, its efficiency is under criticism due to the Low Endotoxin Recovery phenomenon (LER). LER was first described in 2013 by Chen and Vinther as the inability to recover the amount of spiked endotoxin in a test solution containing chelators and surfactants. In particular, LER cannot be resolved simply via dilution and/or magnesium addition, two well-known sample treatments which normally resolve recovery issues (Chen and Vinther, 2013). LER is defined as the inability to recover more than 50% activity over time when endotoxin is added to an undiluted product (Reich et al. 2019). This is of particular importance to endotoxin testing in blood, as anticoagulants such as citrate, which is commonly used, are chelators and can directly contribute to LER (Schwarz et al. 2017).

LPS is an amphiphilic molecule; in aqueous solutions, LPS is known to form aggregates (micelles) the size of which is dependent on various factors such as pH, temperature and the presence of divalent cations, such as calcium and magnesium cations (Harm et al. 2021). According to literature, LPS aggregates are the detectable form of endotoxin by Factor C and the human immune system (Mueller et al. 2004). Removal of the cations by chelators, such as anticoagulants, destabilizes the aggregates and results in endotoxin monomers, which are no longer detectable by in LAL assay (Harm et al. 2021). Additionally, magnesium cations are also important in the enzymatic clotting reaction of LAL, as studies have demonstrated that addition of magnesium improves LAL sensitivity, suggesting it is an important cofactor (Harm et al. 2021 Tsuji, 1983 #619).

Furthermore, there is a plethora of substances that interfere with the LAL assay and LPS in plasma, which include enzymes, proteins, lipids, antibodies, and nucleic acids (Reich et al. 2019). It is well known that endotoxin binds to blood components and is rarely found in circulation as a lone molecule. Endotoxin can bind to red blood cells, mononuclear cells, platelets, neutrophils, lipoproteins, and plasma proteins, with about 5% of plasma endotoxin found attached to platelets (Roth et al. 1993). In addition, circulating endotoxin can be found in a variety of structures and may remain in bacterial cell walls, found in outer membrane vesicles or bound to bacterial proteins (Munford 2016).

As the platelet thrombus and the fibrin clot, products of blood coagulation, trap endotoxin in blood and inhibit quantification through the LAL assay, serum is not used for endotoxin detection (Armstrong et al. 2013). Instead, plasma is considered an more suitable clinical sample matrix (Harm et al. 2021).

Chapters 3 and 4 describe how biosensor development for blood fractions is especially challenging. In summary, this is because of the complexity of the sample matrix and partly because of the non-specific adsorption of matrix components, such as cells, proteins and nucleic acids on sensor surfaces. (Campuzano et al. 2019). These fouling agents can adhere to the surface through hydrophobic, hydrophilic, and electrostatic interactions, and

consequently inhibit the interaction of the target molecule with recognition elements at the sensor surface (Campuzano et al. 2019). Development of a sample pretreatment protocol is therefore an essential part of developing a biosensor, especially for challenging matrices, and is considered a rate-limiting factor toward point-of-care diagnostics (Sin et al. 2014).

Previous attempts focused on the development of an electrochemical LPS aptasensor, showed that introduction of serum to the sensor, even after significant dilution (1 in 100,000) resulted in very high background “noise” levels, high levels of biofouling and low levels of endotoxin detection (Demertzis, 2019). Despite the development of a very sensitive LPS aptasensor for water-based samples, the excessive biofouling and assay inhibition observed in serum highlight the complexity of blood samples and the need for the development of an efficient sample preparation protocol.

### *2.1.9 Aims and Objectives*

Taking into consideration the lack of a rapid clinical detection system for endotoxin, the complexity of plasma as a sample matrix and the challenges in endotoxin detection, this chapter will present efforts to overcome the issues surrounding detection of this important molecule. The goal of this element of the project is the assessment of endotoxin activity in human plasma with evaluation of masking kinetics and the subsequent development of a sample preparation protocol to allow for detection of endotoxin from clinical samples. The efficiency of the protocol will be assessed through determining the recovery of spiked endotoxin introduced into samples, with the aim of achieving between 50 and 200% recovery, in line with regulatory guidance.

Therefore, the objectives of this chapter are:

- Reverse the anticoagulation and interferences caused by anticoagulants. Experiments will be focused on citrate, a commonly used anticoagulant in the intensive care unit in the UK (Trumper 2016).
- Reverse the endotoxin masking caused by the sample matrix components and combat low endotoxin recovery (LER).
- Clear the sample of further substances known to interfere with endotoxin detection to further combat LER and assay inhibition. Endotoxin is known for its adhesion to proteins, lipoproteins and nucleic acids (Harm et al. 2021).



## 2.2 Methods

### 2.2.1 Reagents and apparatus

All salts (magnesium chloride, sodium chloride, calcium chloride) were purchased from Sigma-Aldrich (UK) and were stored under ambient conditions. Sodium hydroxide was purchased from Fisher Scientific, while Hydrochloric acid was purchased from Sigma-Aldrich. Both were stored under ambient conditions. Lipopolysaccharide from *E. coli* (Control Standard Endotoxin, CSE) was purchased from Fujifilm Wako Chemicals USA Corporation and following reconstitution with endotoxin free water was stored at -20°C prior to use. Endotoxin-free water (Cytiva) was purchased from Fisher Scientific and was stored under ambient conditions. Pyrostar ES-F Limulus amoebocyte lysate (LAL) reagent, with a sensitivity of 0.015 EU/mL, was purchased from Fujifilm Wako Chemicals USA Corporation and stored at 2 - 8°C prior to reconstitution. Following reconstitution with endotoxin-free water, aliquots were stored at -20°C in capped depyrogenated HPLC vials prior to use. BD Vacutainer blood collection tubes were purchased from MediSupplies (UK). Depyrogenated borosilicate glass tubes and glassware were purchased from Fujifilm Wako Chemicals USA Corporation.

The system used for the quantification of endotoxin was the  $\alpha$ BET<sup>®</sup> system, developed by Cotton Mouton Diagnostics Ltd (CMD).

### 2.2.2 Depyrogenation of equipment

All glassware were depyrogenated using dry heat at 250°C for at least 30 minutes prior to use. Pyrogen-free pipette tips were used throughout the experiments (Fisher Scientific).  $\alpha$ BET<sup>®</sup> instrument cartridges were depyrogenated by pipetting 100 $\mu$ L of 1M sodium hydroxide into the wells, followed by 2hr incubation at room temperature and rinsing with endotoxin-free water. Endotoxin-free water was used for the preparation of all solutions and materials in this study. The solutions, where possible, were tested for the presence of endotoxin prior to experiments using the  $\alpha$ BET<sup>®</sup> instrument.

### 2.2.3 Blood extraction, storage, and endotoxin spiking

Venous blood was extracted (following informed consent) into a blue BD Vacutainer citrate tube containing 3.2% trisodium citrate. Immediately after extraction, the blood was centrifuged for 10 minutes at 3000 rpm (Lesche et al. 2016). The resultant plasma supernatant was aliquoted into depyrogenated HPLC vials, sealed with parafilm and stored in a freezer at -20°C until ready to use.

Plasma samples were then either thawed, aliquoted into glass tubes and spiked with 1 EU/mL of endotoxin to determine endotoxin recovery at t=0 or spiked with 15 $\mu$ L of 10 EU/mL stock,

for a final endotoxin concentration of 0.1 EU/mL in the prepared samples, sealed with parafilm and incubated at either ambient conditions or 2 - 8°C to study endotoxin masking kinetics.

For t=0 experiments, 40µL of plasma, 40µL of 1 EU/mL CSE and 320 µL of magnesium chloride (5mM), hydrochloric acid (1M) and sodium hydroxide (1 M) were aliquoted into depyrogenated glass tubes to give a final volume of 400 µL, and an endotoxin concentration of 0.1 EU/mL.

A number of sample preparation approaches were explored in a screening process in this chapter, which are presented below in table 2.1. Throughout the experiments, 40µL of spiked plasma were subjected to various treatments, all of which resulted in a final volume of 400µL. Through this screening process, two distinct sample preparation protocols emerged (herein referred to as Protocols 1 and 2). As those two protocols resulted in the best endotoxin recovery at t=0, they were used for the assessment of endotoxin masking over time.

*Table 2.1: Sample preparation approaches presented in this chapter with experimental details*

<b>Sample preparation protocol</b>	<b>Details</b>
Simple dilution (360µL endotoxin-free water)	Tenfold dilution with endotoxin-free water
Dilution (360µL endotoxin-free water) + Heating	Tenfold dilution with endotoxin-free water + heating at 82.5°C for 10 minutes
Dilution with MgCl <sub>2</sub>	Tenfold dilution MgCl <sub>2</sub> in endotoxin- free water (360 µL, 1, 3 and 5 mM)
Dilution with MgCl <sub>2</sub> heating	Tenfold dilution with MgCl <sub>2</sub> in endotoxin-free water (360 µL ,1, 3 and 5 mM) + heating at 82.5°C for 10 minutes
Dilution with MgCl <sub>2</sub> addition of endotoxin-free water, acid base treatment, heating ( <b>Protocol 1</b> ). Overall, tenfold dilution of plasma sample.	Dilution with MgCl <sub>2</sub> in endotoxin- free water (5mM, 200 µL), HCL addition (1M, 60 µL) heating at 82.5°C for 10 minutes, NaOH addition (1M, 60 µL)
Dilution with MgCl <sub>2</sub> , addition of endotoxin-free water acid base treatment, heating, centrifugation ( <b>Protocol 2</b> ). Overall, tenfold dilution of plasma sample.	Dilution with MgCl <sub>2</sub> in endotoxin- free water (5mM, 200 µL), HCL addition (1M, 60 µL) heating at 82.5°C for 10 minutes, NaOH addition (1M, 60 µL) + centrifugation

#### *2.2.4 Dilution, heating and addition of magnesium chloride*

Following addition of 40µL plasma and endotoxin or spiked plasma to depyrogenated glass tubes, magnesium chloride at the desired concentration (1 mM, 3 mM, 5 mM) was added to give a final volume of 400µL. The tubes were sealed with parafilm, heated at 82.5°C for 10

minutes before being cooled in ice-cold water for 3 minutes. In a depyrogenated vial, 30µL of CMD reagent was added to 50µL of LAL reagent, and 100µL of treated sample added. A 70µL aliquot of the nanorod/LAL/sample mixture was transferred into each channel of the αBET® cartridge. The cartridge was inserted into the αBET® instrument and the amplitude of the magneto-optical signal for each channel recorded over time.

#### *2.2.5 Sample pretreatment protocol 1: acid / base treatment*

Following addition of 40µL endotoxin free water, 40µL plasma or endotoxin/spiked plasma into depyrogenated glass tubes, 60µL of 1M hydrochloric acid was added, followed by 200µL of 5mM magnesium chloride. The tubes were sealed with parafilm, heated at 82.5°C for 10 minutes and cooled down in ice-cold water for 3 minutes. Sodium hydroxide (1M, 60µL) was added to give a total volume of 400µL. In a depyrogenated vial, 30µL of CMD reagent was added to 50µL of LAL reagent, and 100µL of treated sample added. A 70µL aliquot of the nanorod/LAL/sample mixture was transferred into each channel of the αBET® cartridge. The cartridge was inserted into the αBET® instrument and the amplitude of the magneto-optical signal for each channel recorded over time.

#### *2.2.6 Sample pretreatment protocol 2: Optimized experimental protocol*

Following addition of water, plasma or endotoxin/spiked plasma into depyrogenated glass tubes, 60µL of 1M hydrochloric acid was added, followed by 200µL of 5mM magnesium chloride. The tubes were sealed with parafilm, heated at 82.5°C for 10 minutes and cooled down in ice-cold water for 3 minutes. Sodium hydroxide (1M, 60µL) was added to give a total volume of 400µL. The samples were sealed with parafilm, packed into centrifuge tubes, and centrifuged at 3000rpm for 3 minutes. In a depyrogenated vial, 30µL of CMD reagent was added to 50µL of LAL reagent, and 100µL of the supernatant of the treated sample added. A 70µL aliquot of the nanorod/LAL/sample mixture was transferred into each channel of the αBET® cartridge. The cartridge was inserted into the αBET® instrument and the amplitude of the magneto-optical signal for each channel recorded over time.

#### *2.2.7 Spike-hold study*

According to regulators, the spike volume should be minimized to avoid changing the concentration of the undiluted sample (European Pharmaceutical Review, 2017). In spike-hold studies, 15µL of 10 EU/mL was added to 135µL of plasma to give an endotoxin concentration of 1 EU/mL. During sample preparation, 40µL of this plasma sample was diluted to a final volume of 400µL resulting in a final endotoxin concentration of 0.1 EU/mL.

Plasma samples were spiked as described, sealed with parafilm and incubated at either ambient conditions or 2 - 8°C to study endotoxin masking kinetics. Samples were assessed for

endotoxin recovery as per the schedule shown in figure 2.4 below. As this was a screening process, singular repeats were used (N=1).

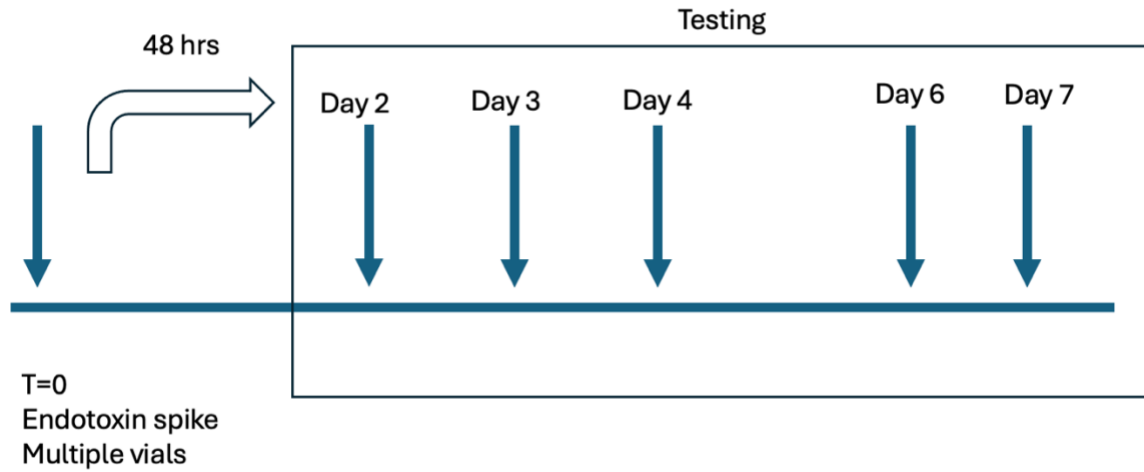


Figure 2.4: Spiking and testing schedule for the spike-hold studies.

## 2.3 Results and discussion

### 2.3.1 Requirement of a sample pretreatment protocol

Despite the advancements in biosensor technology, sample preparation remains a critical step in the translation of biosensors from laboratory to point-of-care. Sample matrix constituents, such as proteins and antibodies are capable of non-specifically binding to sensor surface, resulting in an overwhelming background signal that prevents the detection of analytes (Blaszykowski et al. 2012). Blood and its products are considered some of the most challenging sample matrices, as they are highly proteinaceous (60–80 g L<sup>-1</sup>) and are known for their biofouling properties. Therefore, adequate sample pre-treatment is required to remove the interfering substances (Blaszykowski et al. 2012).

As explained in the introduction, previous research focused on the development of a hybrid aptamer - molecularly imprinted polymer ('apta-MIP') based electrochemical biosensor for LPS demonstrated excellent sensitivity when LPS was introduced in simple sample matrices. On addition of dilute spiked serum samples however, significantly reduced performance was observed making endotoxin quantification almost impossible (Demertzis, 2019). As this was a novel sensor, it was impossible to pick apart the factors that resulted in low endotoxin recovery. Biofouling undoubtedly played a significant role, as evidenced by the significant responses observed with unspiked serum (negative control), however the interaction of LPS with sample components may also have rendered the endotoxin less detectable by limiting / inhibiting the interaction with the apta-MIP surface. In order to be able to build upon this work, it is important to know LPS is in a detectable form. Biofouling can often be overcome by modification of the sensor surface, but if LPS is being sequestered by one or more sample components then poor performance will always be observed.

For the purposes of this project, it is vital that a comprehensive plasma preparation protocol is developed, which will allow for sufficient endotoxin recovery with high replicability. Several sample preparations approaches have been attempted in pursuit of the final protocol, and the most substantial ones will be presented in this Chapter. As the most well-established endotoxin detection assay, the LAL assay has been used to evaluate the different strategies explored.

### 2.3.2 Sample pretreatment: dilution

One of the first steps taken when dealing with sub-optimal endotoxin recovery in pharmaceuticals or other sample matrices is dilution with endotoxin-free water, as most interferences tend to be concentration-dependent (Cooper 1990). Previous studies have shown that undiluted samples can interfere with the LAL assay and suggest dilution as an effective solution (Su and Ding 2015; Reich et al. 2016). Furthermore, LAL reagent

manufacturers often suggest dilution as a first-line solution against interference (Associates of Cape Cod, 2005; Lonza, 2012). Dilution aims to overcome interference caused by sample pH, high divalent ion concentrations, chelators such as anticoagulants, serine proteases and glucans (Lonza, 2019).

**Figure 2.5** shows amplitude profiles generated by the  $\alpha$ BET<sup>®</sup> system for spiked (1 EU/mL) plasma samples treated with 1 in 10 dilution with endotoxin-free water. A positive control (spiked water sample, subject to the same protocol) is indicated by the black line. No endotoxin can be detected by the LAL assay, showing that the interference cannot be resolved through dilution alone. This strengthens the hypothesis that endotoxin can be bound to plasma components and its recovery also affected by anticoagulants (Harm et al. 2021).

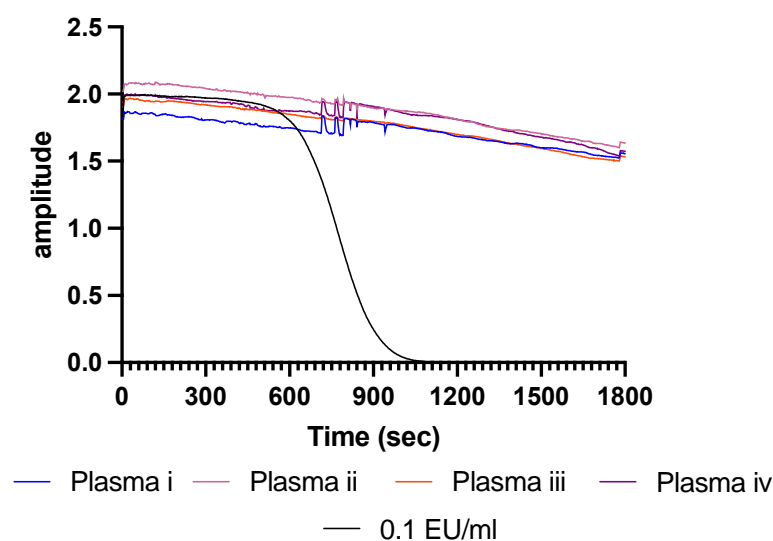


*Figure 2.5 Amplitude results obtained from spiked citrated plasma (N=4, profiles for individual repeats shown) following dilution 1 in 10 with endotoxin-free water. Black curve represents the amplitude results obtained from a 0.1 EU/mL standard. Test was run for 30 minutes. No significant reduction in amplitude is observed in the characteristic curve shape, which translates to no endotoxin recovery.*

**Heating** of blood fractions (plasma and serum) is often performed to denature proteins and enzymes which may bind to endotoxin or cause assay interference, allowing the heat-tolerant endotoxin to be detected (Wong et al. 2016). According to the literature, the temperature must not be below 60°C, with the average heating temperature being around 70°C-85°C and the recommended exposure time being 10 minutes (Hurley 1995; Wong et al. 2016). Dilution is needed alongside heating to prevent coagulation of plasma (Hurley 1995). Plasma samples were therefore diluted 1 in 10 with endotoxin-free water and heated at 82.5°C for 10 minutes. This temperature was chosen in order to ensure the denaturation of plasma proteins, such as HSA, which is the most abundant protein in blood and becomes denatures at around 68°C (Nnyigide and Hyun 2020). Additionally, in early experiments, it was discovered that temperatures higher than 82.5°C resulted in the formation of precipitate caused by the addition of MgCl<sub>2</sub>. To prevent heat denaturation of the proteins involved in the LAL cascade,

following heating, samples were cooled in ice-cold water for three minutes before being added to the LAL reagent.

**Figure 2.6** shows amplitude profiles generated by the  $\alpha$ BET<sup>®</sup> system for spiked (1 EU/mL) plasma samples treated with tenfold dilution with endotoxin free water and heating at 82.5°C. Although there was a hint of an improvement in endotoxin recovery, as shown by the slightly curved profiles of plasma i and iv samples, this was not seen for all samples and the threshold reduction in amplitude to allow for quantitation of endotoxin was not achieved. The time taken for the slight downward trend in amplitude is also extended – a water sample spiked with the same concentration of endotoxin and subjected to the same pre-treatment protocol is included in Figure 2.6 for reference.

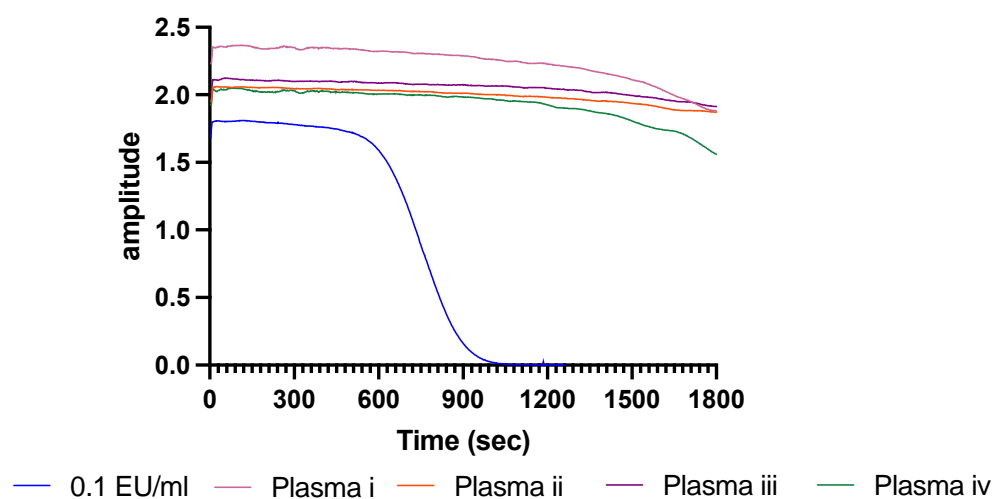


*Figure 2.6: Amplitude results obtained from citrated plasma (N=4) following dilution 1 in 10 with endotoxin-free water and heating at 82.5°C for 10 minutes. Blue curve represents the amplitude results obtained from a 0.1 EU/mL standard. Test was run for 30 minutes. No significant reduction in amplitude is observed in the characteristic curve shape, which translates to no endotoxin recovery*

Despite the heat induced denaturation of proteins and dilution of the sample, it is likely that the anticoagulant used (citrate) also affects the recovery of endotoxin. Sodium citrate is a well-known chelator which forms metal complexes with divalent cations, such as  $Mg^{2+}$  and  $Ca^{2+}$ , which is the basis of its anticoagulant properties (Reich et al. 2018). As mentioned in the introduction, in the presence of such divalent cations, LPS forms aggregates which are detectable by the LAL assay. Furthermore, it is likely that divalent cations play an important role in the stabilization of LPS structures and discourages the formation of complex structures which may not be detectable by the LAL assay, as well as being important in the coagulation reaction of LAL (Reich et al. 2018). Therefore, it was decided to add magnesium chloride into the sample in attempt to replenish the  $Mg^{2+}$  ion concentration depleted by the citrate. Magnesium chloride at concentrations of 1mM, 5mM and 10mM, were used as these have been frequently reported in literature as being appropriate for overcoming issues with low endotoxin recovery in pharmaceutical samples (Reich et al. 2018).

**Figure 2.7** shows the results of a complete sample preparation protocol, incorporating the three steps of dilution, addition of MgCl<sub>2</sub> at three concentrations (1, 3 and 5mM) and heating. A positive control (spiked water sample, subject to the same protocol) is indicated by the blue line. It is evident that endotoxin can be detected across all MgCl<sub>2</sub> treatments, further supporting the hypothesis that the addition of MgCl<sub>2</sub>, as well as dilution and heating, is necessary for the reversal of citrate interference and to allow endotoxin recovery (Reich et al. 2016). The best results are observed with the addition of 5mM MgCl<sub>2</sub>, followed by 3mM and 1mM.

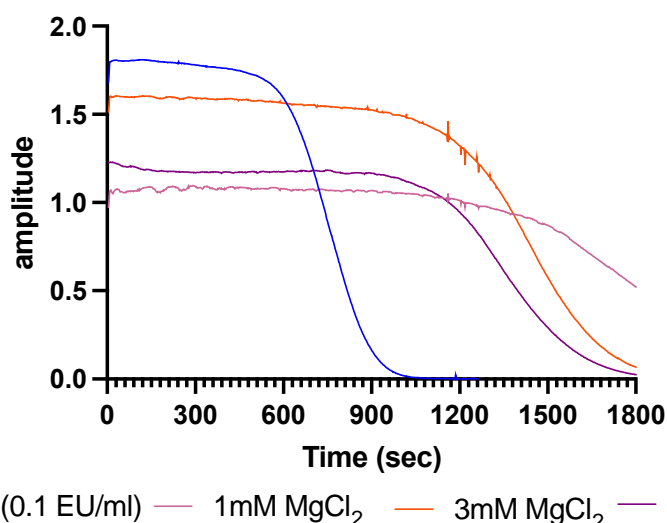


Figure 2.7: Amplitude results obtained from citrated plasma (N=3) following dilution 1 in 10 with endotoxin-free water and magnesium chloride at three concentrations (1, 3 and 5 mM) followed by heating at 82.5°C for 10 minutes, showing detection of endotoxin. Positive control shows amplitude results for 0.1 EU/ml endotoxin in endotoxin-free water. Test was run for 30 minutes

Experiments with higher MgCl<sub>2</sub> concentrations were also performed but due to excessive precipitation they were not continued (Figure 2.7). Moreover, MgCl<sub>2</sub> levels higher than 50mM have been shown to have inhibitory effects on the LAL cascade and can reduce endotoxin recovery (Tsuji and Steindler 1983).

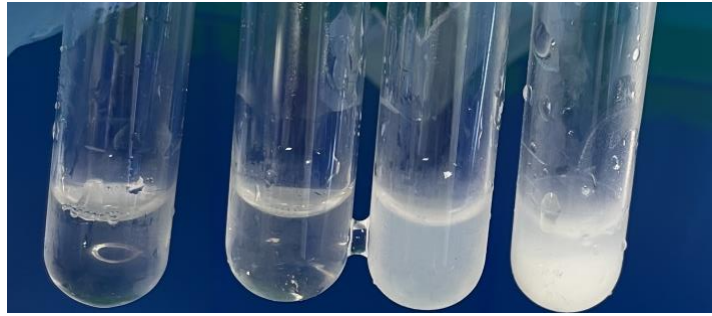


Figure 2.8: Glass tubes containing treated sample with different  $MgCl_2$  concentrations. From left to right: Positive control, 1, 5 and 10mM. Note the precipitate at 10mM.

All three elements of the sample protocol (dilution, heating and addition of  $Mg^{2+}$  ions) are needed to allow recovery of endotoxin. Removal of the heating step, whilst retaining the dilution and addition of magnesium chloride, showed no endotoxin recovery as per Figure 2.9.

**Figure 2.9** shows amplitude profiles for spiked (1 EU/mL) plasma samples treated with tenfold dilution with endotoxin free water and  $MgCl_2$  addition (1, 3 and 5 mM). A positive control (spiked water sample, subject to the same protocol) is indicated by the blue line. Compared to figure 2.7, it is evident that heating is a necessary step in the protocol, as its absence resulted in amplitude profiles similar to figure 2.6.

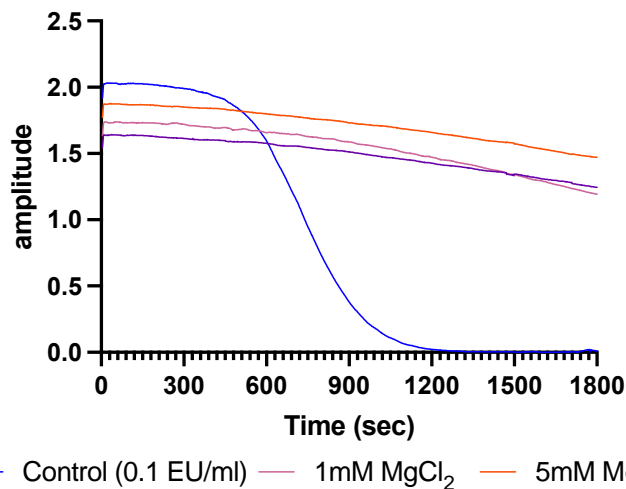


Figure 2.9: Amplitude results obtained from citrated plasma (N=3) following dilution 1 in 10 with endotoxin-free water and magnesium chloride at three concentrations (1, 5 and 10 mM) without heating. No significant reduction in amplitude is observed in the characteristic curve shape, which translates to no endotoxin recovery. Positive control shows amplitude results for 0.1 EU/ml endotoxin in endotoxin-free water. Test was run for 30 minutes.

### 2.3.3 Sample pretreatment: acid / base treatment

Despite the encouraging results obtained with the addition of MgCl<sub>2</sub>, there remained a large difference (600 seconds) in the response times between the positive control and the treated spiked samples. Moreover, one of the main issues encountered using that protocol was the protein precipitation caused by the combination of heating and addition of MgCl<sub>2</sub>, which often led to the development of “noise” and reproducibility issues. In a previous study, hydrochloric acid (HCl) was used to denature proteins before heating, with sodium hydroxide (NaOH) used to neutralize the treated sample (Demertzis, 2019). Since the LAL assay is an enzymatic assay, it is sensitive to pH fluctuations and special care must be taken to ensure sample pH is within the acceptable range of pH 6-8 (Aketagawa et al. 1993).

**Figure 2.10** shows the results of an improved sample preparation protocol, incorporating the four steps of dilution, addition of MgCl<sub>2</sub> at 5mM, pH treatment and heating. A positive control is indicated by the blue line. The detection of endotoxin in plasma is evident, and the plasma amplitudes show similar trends to the positive control. It is evident that acid denaturation is crucial for the complete denaturation of matrix interferences, and pH balancing using NaOH ensures the sample can be used with the LAL assay.

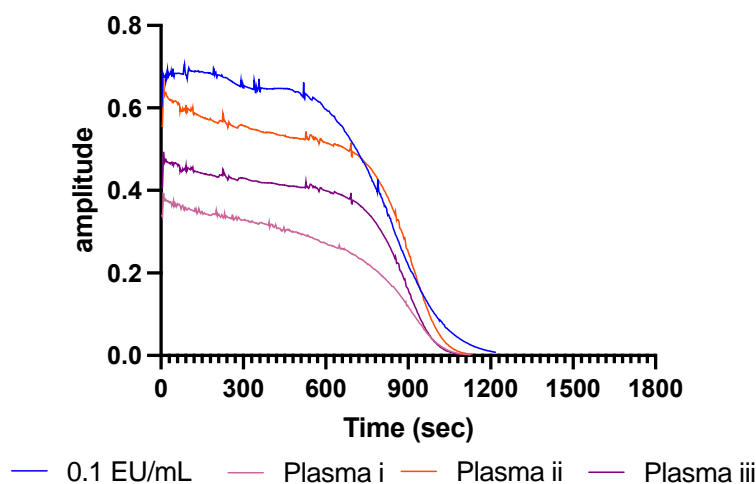


Figure 2.10: Amplitude results obtained from citrated plasma (N=3) following dilution 1 in 10 with endotoxin-free water, 1M HCL, magnesium chloride at 5mM, heating at 82.5°C for 10 minutes and pH balancing, showing detection of endotoxin. Positive control shows amplitude results for 0.1 EU/ml endotoxin following the same treatment. Test was run for 30 minutes

The use of hydrochloric acid to denature proteins and enzymes is well documented, and blood proteins, such as serum albumin, have been found to have a lower denaturation temperature at low pH (Fink et al. 1994; Baler et al. 2014). Additionally, lower pH has been found to prevent low endotoxin recovery (Tsuchiya 2017). This could possibly be explained because chelation of divalent ions is pH dependent, and high pH has been associated with increased endotoxin masking (Tsuchiya 2017). Moreover, the acid/base treatment results in clearer samples, with no/little precipitate, which ensures a clearer signal and more replicable results (Figure 2.11).

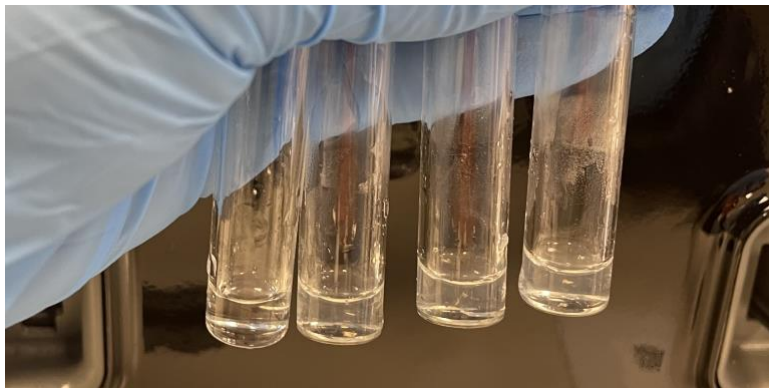


Figure 2.11: From left to right: Positive control and plasma samples following treatment with acid/base in triplicate. Note the lack of precipitate.

it is well recognised that endotoxin neutralization by citrate is challenging to overcome, and these experiments show encouraging results (Reich et al. 2018). To the researcher's knowledge, this method has not been used before in plasma and could potentially provide a new method for endotoxin recovery.

#### 2.3.4 Spike hold studies

Endotoxin masking is known to be a time-dependent phenomenon. As a result, regulatory authorities require that complex pharmaceutical samples e.g., biopharmaceuticals and those drug products known to contain materials likely to interfere with recovery of endotoxin, are tested in hold-time studies. In such studies, endotoxin is added (spiked) into the undiluted product and endotoxin recovery assessed as a function of time (Reich et al. 2019). This also applies to human plasma, where studies show that endotoxin activity in human plasma and serum decreases strongly over time, and that it is both a time and temperature dependent process (Harm et al. 2021).

As discussed earlier, endotoxin is rarely found isolated in blood, but is usually bound to enzymes, proteins, lipids, antibodies, platelets, and nucleic acids (Reich et al. 2019). In addition, patients usually present at the hospital at the later stages of infection, which suggests prolonged presence of elevated levels of endotoxin in the bloodstream (Paoli et al. 2018). In order to mimic the conditions under which the endotoxin may be found in the bloodstream and to study the masking kinetics, plasma samples were spiked and stored at ambient conditions. Additionally, as low temperature has been shown to prevent endotoxin masking by slowing down masking kinetics, plasma samples were also stored in the fridge (Tsuchiya 2017). Samples were assessed for endotoxin recovery as per testing schedule described in figure 2.3.

**Figure 2.12** shows the results of the analysis of spiked plasma samples stored under ambient conditions for a number of days and subjected to the sample preparation protocol described

in 2.3.2. **Figure 2.13** shows the results for the samples stored at 2 – 8°C. A clear reduction in endotoxin detection can be observed for both sample sets with each passing day. No endotoxin could be detected at day 7 within a 30-minute timeframe.

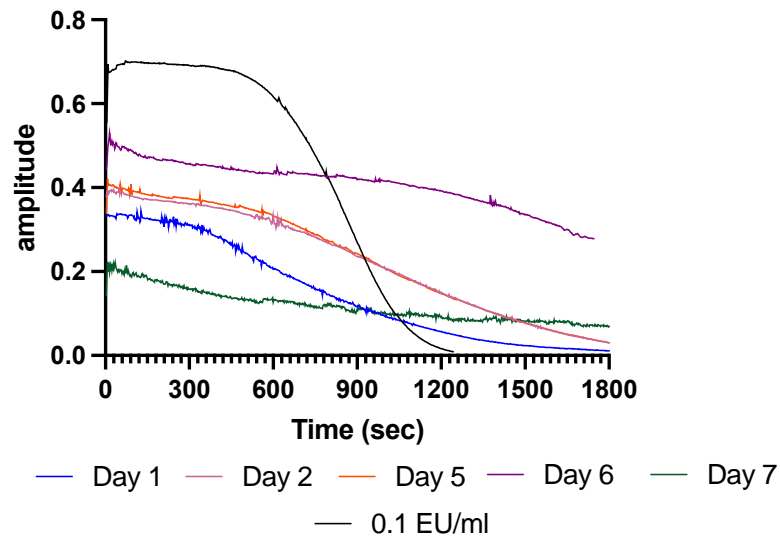


Figure 2.12: Amplitude results obtained from citrated plasma spiked with 10 EU/mL to give a final concentration of 0.1 EU/ml when tested. Prior to analysis, spiked samples had been stored at **ambient** conditions and were subsequently subjected to the pre-treatment protocol described in Section 2.2.3. Black curve represents the amplitude results obtained from a 0.1 EU/mL standard. N=1 for each day as this was a screening experiment. Test was run for 30 minutes

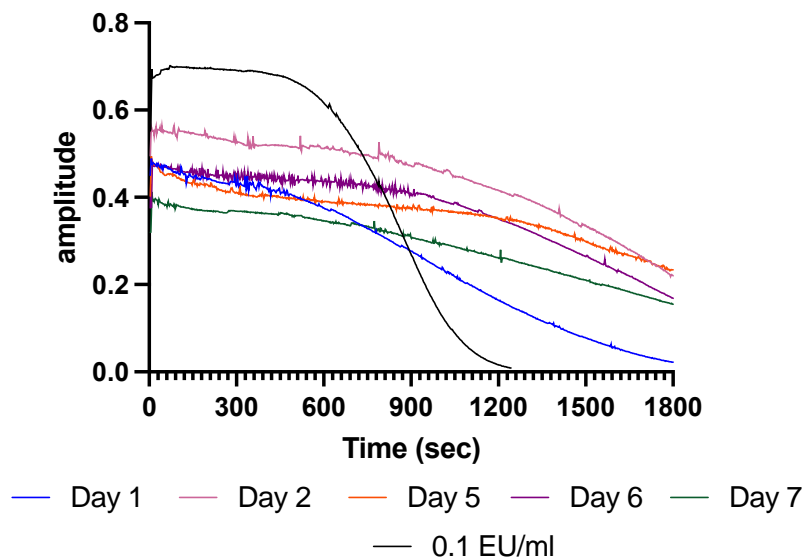


Figure 2.13: Amplitude results obtained from citrated plasma spiked with 10 EU/mL to give a final concentration of 0.1 EU/mL and stored at 2 -8 °C. Prior to analysis, spiked samples had been stored at the **refrigerator** and were subsequently subjected to the pre-treatment protocol described in Section 2.2.3. Black curve represents the amplitude results obtained from a 0.1 EU/mL standard N=1 for each day as this was a screening experiment. Test was run for 30 minutes.

Although in the early time points, some recovery of endotoxin was shown to be possible, it was not complete, and it diminished further as the days went on. This suggests that inhibition / interference remains or perhaps incomplete protein denaturation, and therefore a further modification to the sample pretreatment protocol was needed. Interestingly, improved endotoxin recovery was observed at samples stored at ambient temperatures, with the exception of day 7, where no endotoxin could be observed. This will be discussed in more detail in section 2.3.5.3.

One of the reasons why acid / base treatment may be beneficial is because of the endotoxin binding kinetics of human lipoproteins (Levine et al. 1993). Lipoproteins are known to bind to endotoxin with high affinity (Levine et al. 1993). Studies have shown that pH is important in the denaturation of lipoproteins, and that in acidic pH (< 6), the denaturation temperature of low-density lipoprotein (Calin et al.) decreases from 100°C to 75°C (Lu et al. 2012; Sneck et al. 2012). Moreover, it is well known that fibrinogen and plasma albumin are better denaturated with a combination of low pH and high temperature (> 37°C) (Fay and Hendrix 1931). Additionally, the acidification of the sample matrix, well below the isoelectric point of endotoxin (pI = 2.5) affects the strong negative charge of endotoxin, deactivating it and preventing re-binding to proteins (Ribeiro et al. 2010).

### *2.3.5 Further optimization of sample pretreatment protocol - centrifugation*

As described in section 2.3.3, despite the encouraging results, endotoxin recovery was not reproducibly achieved. A number of further experimental approaches were attempted, including prolonged heating times (15 and 20 minutes), different heating temperatures (62, 75, 95 and 100°C) and use of different salts and buffers (Tris buffer, NaCl<sub>2</sub> addition, Phosphate-buffered saline addition) all of which produced non-viable results due to precipitation (data not shown).

Therefore, it was decided to add centrifugation to the sample protocol. Centrifugation is commonly used in sample preparation, especially in serum and plasma, to deplete samples of lipoproteins and protein contaminants (Brennan et al. 2020). Following completion of the pre-treatment protocol described in Section 2.2.3 the sample vials were sealed with parafilm, packed into centrifuge tubes, and centrifuged at 3000rpm for 3 minutes.

**Figure 2.14** shows the results of applying this further optimised sample preparation protocol to plasma samples stored at ambient conditions. The results for the sample stored at 2 – 8°C are presented in **Figure 2.15**.

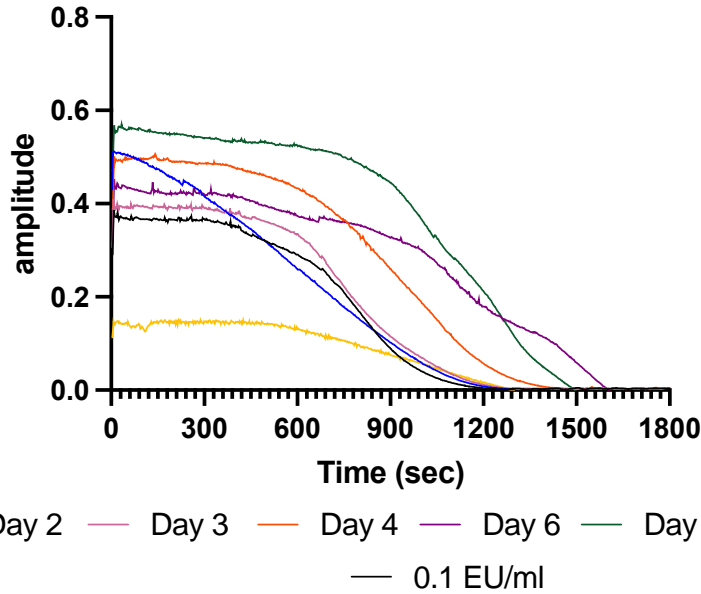


Figure 2.14: Amplitude results obtained from citrated plasma spiked with 10 EU/mL to give a final concentration of 0.1 EU/ml when tested. Prior to analysis, spiked samples had been stored at **ambient** conditions and were subsequently subjected to the pre-treatment protocol described in Section 2.2.3 which includes centrifugation. Black curve represents the amplitude results obtained from a 0.1 EU/mL standard. N=1 for each day as this was a screening experiment. Test was run for 30 minutes

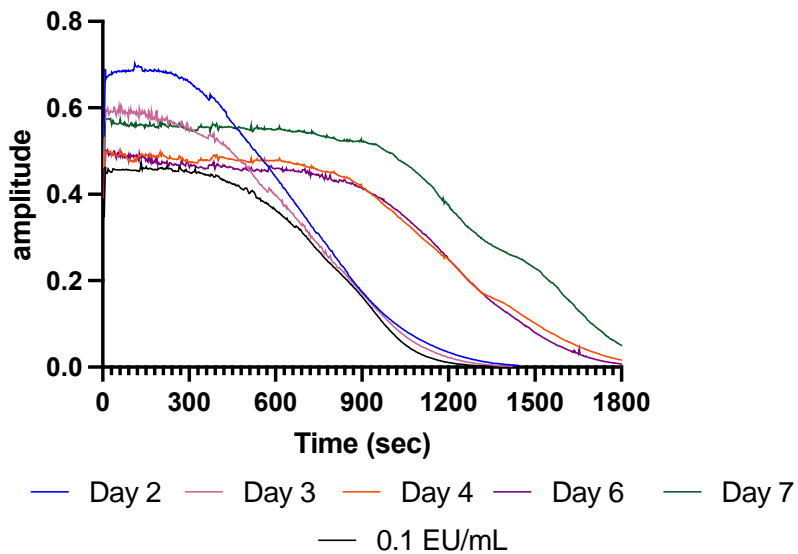


Figure 2.15: Amplitude results obtained from citrated plasma spiked with 10 EU/mL to give a final concentration of 0.1 EU/ml when tested. Prior to analysis, spiked samples had been **refrigerated** and were subsequently subjected to the pre-treatment protocol described in Section 2.2.3, which includes centrifugation. Black curve represents the amplitude results obtained from a 0.1 EU/mL standard. N=1 for each day as this was a screening experiment. Test was run for 30 minutes

Although reduction in endotoxin recovery is still observed with each passing day, the profiles are significantly improved when compared to Figures 2.12 and 2.13. Examining the amplitude profiles, it can be observed that higher endotoxin levels are recovered from samples stored at ambient temperature (figure 2.14) as compared to those stored in the fridge (figure 2.15),

with all tests terminating at around 1500 seconds. Interestingly, day 2 and day 3 clotting profiles were similar for samples stored at fridge (figure 2.15). The same effect was observed for day 4 and day 6 samples (figure 2.15). This similarity is not present in samples stored at ambient conditions (figure 2.14).

As this was a screening experiment, where sample approaches were tested on plasma incubated for numerous days until a suitable preparation protocol was developed, data for day 17 are only available for room temperature. Out of all the approaches, centrifugation provided the best results to date, reducing the response times significantly and providing clearer results with less “noise”. The addition of hydrochloric acid assists the denaturation of plasma proteins and lipoproteins, and through centrifugation, these components are removed from the sample matrix, which prevents them from re-attaching to endotoxin (Lu et al. 2012; Sneck et al. 2012).

It is understandable that the number of steps involved in this sample preparation protocol and preparation time (approximately 20 minutes) are less than ideal, especially as the aim of this project is the development of a “point-of-care” biosensor. However, this study has generated encouraging results regarding the recovery of endotoxin in citrated plasma, an especially challenging sample matrix, that can be taken forward and further optimized when coupled with electrochemical sensors (Chapters 3 and 4).

### *2.3.6 Determination of endotoxin recovery from spiked plasma samples*

#### 2.3.6.1 Calibration

A calibration curve (figure 2.16) was created using water-based endotoxin standards subjected to the optimized treatment protocol described in 3.3.4. The time needed to get to 80% of starting amplitude in four concentrations of endotoxin (1, 0.1, 0.01 and 0.001 EU/mL) was calculated. The data was then transformed into Log-Log plot of concentration vs. time. Standard linear regression was applied, giving rise to the equation  $Y = -0.1670 \cdot X + 2.786$  and coefficient of correlation,  $r$ , value of 0.9962, showing a strong linear relationship between the two values.  $N=3$  for each point.

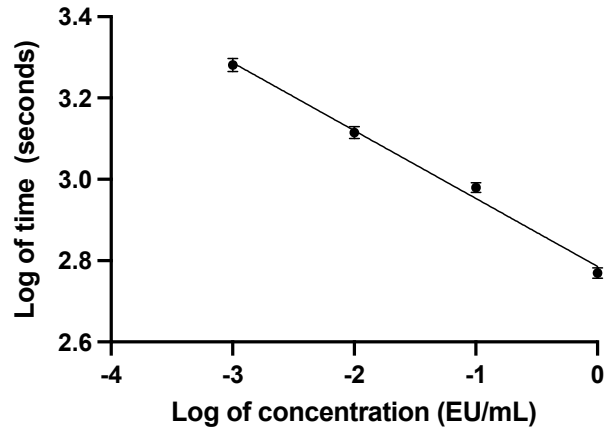


Figure 2.16. Endotoxin calibration curve, showing the transformed Log values of time needed to reach 80% of starting amplitude on y axis and the transformed Log values of endotoxin concentration on x axis.  $R^2 = 0.9925$ ,  $R = 0.9962$ .

### 2.3.6.2 Background endotoxin plasma levels

It is known that endotoxin is normally present in the blood plasma of healthy humans in small but detectable levels, thanks to translocation of endogenous sources from the upper respiratory tract and gastrointestinal tract. Endotoxin reaches the GI tract from oral secretions and food consumption and crosses the GI mucosa from the small intestine (Munford 2016). It was, therefore, important, to determine the “background” level of endotoxin in healthy humans. Unspiked plasma samples ( $n = 4$ ) were therefore subjected to the optimized sample preparation protocol and analysed. The amplitude profile is presented in Figure 2.17. The run time was extended beyond 1800 seconds to allow the complete profiles to be obtained, thus enabling calculation of the background level from extrapolation of the calibration curve parameters.

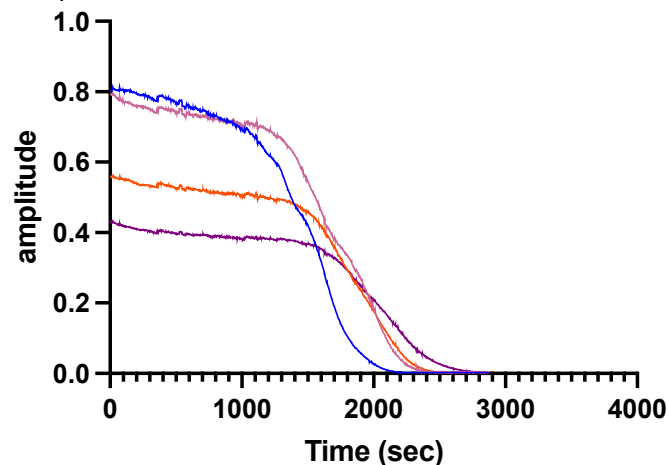


Figure 2.17: Amplitude results obtained from unspiked citrated plasma following dilution 1 in 10 with endotoxin-free water and magnesium chloride at 5mM concentration, heating, pH adjustment and centrifugation.  $N=4$ .

Using the calibration curve (figure 2.16), the mean amount of endotoxin present in plasma was found to be ~ 0.001 EU/mL (standard deviation: 0.0008 EU/mL). Nadhazi et al. found that, by using the kinetic chromogenic LAL assay, the endotoxin levels in the plasma of healthy donors ranged between 0.01-1.0 EU/ml, and in an older study, Pearson et al. found that, by using the LAL assay, the endotoxin concentration in healthy plasma ranged between 0.0002 and 0.001 EU/mL (Pearson et al. 1985; Nadhazi et al. 2002). Low level chronic endotoxemia is characterized by plasma levels > 50 pg/ml, or 0.5 EU/mL, and is associated with increased inflammation and a higher risk of atherosclerosis (Rice et al. 2003). In paediatrics, plasma endotoxin levels in healthy children have been reported as slightly higher, with Nier et al. reporting a detected range of 0.03-0.04 EU/mL in two studies (Nier et al. 2018; Nier et al. 2019). These findings, combined with the endotoxin background levels detected in this study show that endotoxin background levels are negligible and unlikely to influence endotoxin recovery results. However, due to the different patient groups in each study and the lack of a standardized endotoxin test for blood samples, there is a lack of confidence in the accuracy of those studies, which emphasizes the need for the development of a reliable, endotoxin testing platform.

### 2.3.6.3 Determination of endotoxin recovery from spiked plasma samples

In accordance with the European Pharmacopoeia, percentage spike recovery was calculated for each spiked plasma sample using the following formula (Eur. Pharm. Rev., 2019):

$$\% \text{ spike recovery} = \frac{\text{Endotoxin in spiked sample} - \text{Endotoxin in unspiked sample}}{\text{Amount of added endotoxin}} \times 100$$

According to guidelines, a spike recovery between 50 – 200% is considered acceptable, although 100% is ideal (Wong et al. 2016). The calibration curve presented in Figure 2.16 was used to determine the amount of endotoxin recovered from each sample in EU/mL.

**Figure 2.18 A** shows the endotoxin recovery percentages from samples stored under both ambient and fridge conditions, following treatment with sample preparation protocol 1, which included acid / base treatment. The data in this graph is linked to figures 2.12 and 2.13. The endotoxin recovery percentages for each day in room temperature are 26% for day 1, 5.46% for day 2, 5.12% for day 5, 0.66% for day 6. No endotoxin was recovered at day 7. The endotoxin recovery percentages for refrigerated samples are 6.18% for day 1, 0.75% for day 2, 0.36% for day 5, 0.66% for day 6 and 0.48 for day 7. N=1 for each day as this was a screening experiment.

**Figure 2.18 B** shows the endotoxin recovery percentages from samples stored under both ambient and fridge conditions, following treatment with sample preparation protocol 2, which included acid / base treatment and centrifugation. The data in this graph is linked to figures 2.14 and 2.15. The endotoxin recovery percentages for each day in room temperature

are 97% for day 2, 63% for day 3, 28% for day 4, 3.64% for day 6, 8% for day 7 and 10% for day 17. The endotoxin recovery percentages for refrigerated samples are 73% for day 1, 62% for day 2, 5% for day 4, 6% for day 6 and 2.49% for day 7. N=1 for each day as this was a screening experiment.

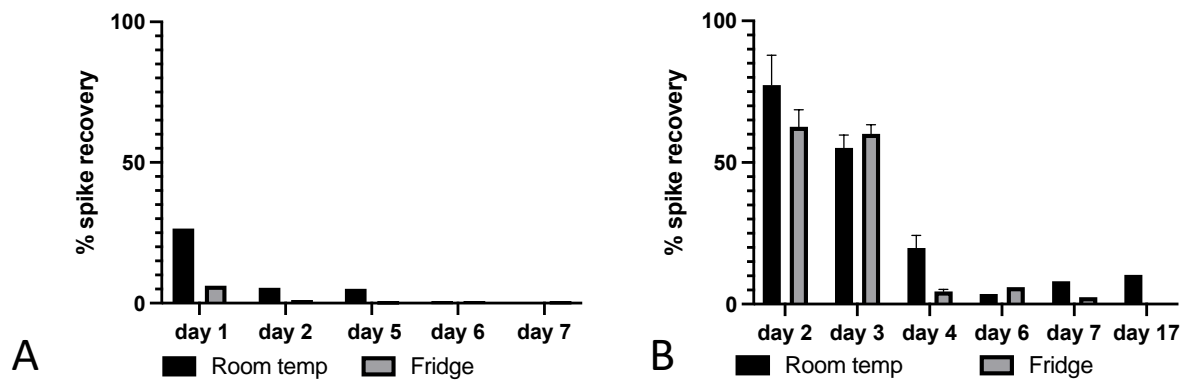


Figure 2.18 A and Figure 2.18 B show the percentage of endotoxin recovery across seven days in samples stored at room temperature and fridge. Figure 2.18 A shows the percentage of endotoxin recovery following treatment with protocol 1. Figure 2.18 B shows the percentage of endotoxin recovery following treatment with protocol 2.

Through graph comparison, it can be observed that higher endotoxin recovery is achieved by using the updated sample pretreatment protocol, which included centrifugation. It is possible that non-denatured proteins or other sample matrix constituents which were not broken down during the sample preparation steps were interfering with the assay. As the  $\alpha$ BET<sup>®</sup> instrument is sensitive to viscosity changes, it makes sense that centrifugation would improve recovery results, as proteins and macromolecules which may interfere with the nanorods or may reattach to endotoxin are removed. However, beyond day 3, results fall outside of the acceptable recovery range set by regulatory authorities, and this is something that will be investigated further into this project.

Interestingly, in both protocols, it can be noted that lower endotoxin recovery is observed in plasma samples stored at 2 - 8°C. This comes in contrast with previous findings, which stated that low temperature (4 - 8°C) plays an important role in the prevention of low endotoxin recovery, and that maximum endotoxin masking is observed at ambient temperature (Reich et al. 2016; Tsuchiya 2017). According to Reich et al., endotoxin masking kinetics can be decelerated at low temperatures. However, none of these studies used blood products in their experiments, instead a polysorbate 20/citrate matrix was used.

There could be a number of reasons why higher recovery is noted at ambient temperatures compared to 5°C. Overall, literature is poor regarding the stability of plasma and biochemical

markers in plasma at different conditions, however there are a few studies which may partially explain the results obtained.

An NMR-based study on plasma stability showed that plasma composition changes take place as early as 2.5 hours in storage at room temperature, with the most notable changes being observed in choline content and lipoproteins. Interestingly, a decrease in low density lipoprotein (Calin et al.) and very low-density lipoprotein (VLDL) was noted, as well as an increase in high-density lipoprotein (HDL). A possible mechanism for this is the discarding of phospholipids from LDL and VLDL to form HDL, without lipid oxidation being observed (Pinto et al. 2014). A similar decrease in LDL and increase in HDL was noted by Heins et al. (Heins et al. 1995). Combined with the knowledge that HDL is capable of binding and neutralizing endotoxin, unlike LDL and VLDL, this could partially explain the endotoxin masking phenomenon, as seen in figures 2.12-2.15. (Levine et al. 1993; Ma et al. 2004). As the NMR study examined samples stored at ambient conditions, this may explain masking in sample stored at ambient temperature (Pinto et al. 2014). The changes between plasma stored at room temperature and fridge are unknown.

A study on the storage of serum at room temperature has found increased uric acid levels throughout the experiment in samples stored at ambient temperature, something which is not observed in samples stored in the fridge (Pawluk-Sobecka et al. 2020). It is possible that uric acid may be one of the factors responsible for the increased endotoxin recovery noted at room temperature (figures 2.18 A and B), and this is something that could be investigated further. A few studies have associated plasma uric acid with low levels of plasma HDL (Chen et al. 2007; Norvik et al. 2016; Wang et al. 2018). Combined with the fact that HDL is known for binding to endotoxin, this could possibly explain the lower levels of endotoxin masking at ambient conditions (figure 2.18 A) This could be further investigated by performing cholesterol test on plasma samples stored at different conditions, or by measuring uric acid levels using standard colorimetric methods(Li et al. 2019a).

A few studies have provided evidence that plasma refrigeration affects the plasma proteome. In particular, it has been found that some plasma proteins are affected by degradation processes at lower temperatures. A study by Pasella et al, showed that vitamin D binding protein, alpha-1-antitrypsin, serotransferrin, apolipoprotein A-I, apolipoprotein E, haptoglobin and complement factor B, all decrease in concentration at 4°C, but are stable at ambient temperature. Additionally, the same study also found that serum albumin, fibrinogen gamma chain and haptoglobin remained stable at ambient temperature (Pasella et al. 2013). A study on plasma lipoproteins stored at 4°C found that after two days of storage, a significant increase in plasma HDL apolipoproteins was observed (Cohn et al. 2004). This increase in HDL, which is known for binding to endotoxin, could potentially partially explain the increase in endotoxin masking in samples stored at 2-5°C (Figures 2.18 A-B). The

difference in lipoprotein profiles between plasma stored at room temperature and fridge could be assessed in future experiments in more depth.

Moreover, some plasma enzymes, such as lactate dehydrogenase have shown cryo-instability at 4°C (Jacobs et al. 1986). Plasma stored at fridge temperatures often shows activation of proteolytic systems and activation of coagulation (Blomback et al. 1984). Cold-promoted activation of coagulation factor VII in plasma has been described in older studies (Morrissey et al. 1993). As Factor VII is proteolytically activated, this suggests that enzymatic processes are activated at low temperatures. In a study by Suontaka et al., activated Factor VIIa was detected at cold-stored plasma in amounts 40 times higher than fresh plasma, as well as increased levels of fibrinopeptide A, a sensitive indicator of coagulation (Suontaka et al. 2005). This activation of coagulation has been explained as the result of a depression of the functional C1 esterase inhibitor in low temperatures, resulting in activation of coagulation factor XII and prokallikrein, events that were confirmed in the study (Suontaka et al. 2005; Wu 2015). This activation of coagulation could potentially explain the decrease in endotoxin detection at lower temperatures (figures 2.13 and 2.15).

## **2.4 Conclusions and future direction**

Despite the LAL assay being the gold standard in endotoxin detection in pharmaceuticals and manufactured products, its use in blood has been held back by the presence of various inhibitors, proteins, lipids and interferents in the sample matrix (Harm et al. 2021). The optimized protocol developed in this study, which includes dilution, heating, acid / base treatment, magnesium addition and centrifugation, provides endotoxin recovery in levels acceptable by regulatory authorities (97% and 63% for days 2 and 3 in samples stored at room temperature and 73% and 62% for refrigerated samples for days 2 and 3). Despite the limited days after incubation where endotoxin can be recovered, there are potential clinical uses for the protocol developed. A study has found that endotoxin baseline levels at admission are significantly higher in comparison to healthy subjects (2 EU/mL vs 0.02 EU/mL respectively), which suggests that the sensor could be used to detect possible endotoxemia at admission (Cangemi et al. 2016). Importantly, the simulation of the endotoxemic environment and natural endotoxin masking process is extremely challenging and this study is an attempt to mimic it, however the real-life endotoxin masking conditions cannot be replicated in the lab.

It is understandable that the numerous steps involved may be a concern regarding “point-of-care” testing, however this study has provided evidence of successful endotoxin recovery in citrated plasma, one of the most complex sample matrices, for samples stored up to three days at ambient conditions and in low temperatures, with high sensitivity (0.1 EU/mL, or 10 pg/mL). Instead of “point-of-care”, it is possible that the development of a “near-patient” testing platform may be more feasible. Additionally, many of the steps involved in the sample preparation protocol can be automated, which can help reduce preparation time. For

example, the  $\alpha$ BET<sup>®</sup> system contains a heating block that can reach 82.5°C. Furthermore, a blood collection tube containing parts of the sample preparation protocol, such as hydrochloric acid, could potentially be developed in the future. It's also possible that centrifugation could be replaced by an in-line filtration / separation system.

To date, the exact mechanisms of endotoxin masking in blood are unclear, and data interpretation has been performed on limited studies on the storage of blood fractions following refrigeration and storage at room temperature. So far, the strongest hypothesis consists of endotoxin binding to high-density lipoprotein, the levels of which are elevated following storage at both room temperature and refrigeration (Heins et al. 1995; Pinto et al. 2014). In refrigerated plasma samples, the decrease in endotoxin recovery could be attributed to cold-activated coagulation, a phenomenon which has been observed before in literature, in combination with increased HDL levels (Cohn et al. 2004; Suontaka et al. 2005).

Citrate-mediated endotoxin masking has previously been found to be challenging to reverse (Reich et al. 2018). To date, successful endotoxin recovery has only been performed in heparinized plasma, with no success in citrated plasma (Harm et al. 2021). This study provides encouraging results in endotoxin detection in plasma derived from citrated blood, following up to 3 days incubation with endotoxin at both ambient temperatures and refrigeration.

Other analytical methods to quantify endotoxin are available, although few have been applied to clinical samples. For example, gas chromatography-mass spectrometry (GC-MS) can be used to quantify endotoxin in aqueous samples (Jackie et al. 2021). Additionally, HPLC has been used to separate endotoxin from plasma samples, followed by detection using tandem mass spectroscopy (MS/MS) (Pais de Barros et al. 2015). However, analytical assays are often held back by high run costs and prolonged turnaround times, in addition to needing specialized training for result interpretation, which limits their ability to provide clinically useful information in a relevant time frame.

This Chapter provides valuable insight on the recovery of endotoxin in one of the most challenging clinical matrices, citrated blood plasma. It was discovered that the implementation of an extensive sample preparation protocol consisting of dilution, pH treatment, heating and centrifugation allows for satisfactory endotoxin recovery, up to 3 days of incubation for plasma samples stored in either room temperature or fridge. One of the questions raised in this Chapter was whether the aptasensor and hybrid aptamer imprinted (aptaMIP) systems, developed by previous researchers in the researcher's lab, would allow for more sensitive detection of endotoxin. Moreover, as the LAL assay is sensitive to pH and temperature fluctuations as an enzymatic assay, it is hypothesized that the implementation of electrochemical platforms may allow the use of other sample preparation methods.



## 2.4 Bibliography

Aketagawa, J. et al. 1993. Activation of limulus coagulation factor G by several (1→3)-beta-D-glucans: comparison of the potency of glucans with identical degree of polymerization but different conformations. *J Biochem* 113(6), pp. 683-686. doi: 10.1093/oxfordjournals.jbchem.a124103

Armstrong, M. T. et al. 2013. Capture of lipopolysaccharide (endotoxin) by the blood clot: a comparative study. *PLoS ONE* 8(11), p. e80192. doi: 10.1371/journal.pone.0080192

Amit, K. et al. 2016. Assessment of malathion and its effects on leukocytes in human blood samples. *The Journal of Biomedical Research* 30(1), pp. 52-59. doi: 10.7555/JBR.30.20120073

Baler, K. et al. 2014. Electrostatic unfolding and interactions of albumin driven by pH changes: a molecular dynamics study. *J Phys Chem B* 118(4), pp. 921-930. doi: 10.1021/jp409936v

Bertani, B. and Ruiz, N. 2018. Function and Biogenesis of Lipopolysaccharides. *EcoSal Plus* 8(1), doi: 10.1128/ecosalplus.ESP-0001-2018

Blaszykowski, C. et al. 2012. Surface chemistry to minimize fouling from blood-based fluids. *Chem Soc Rev* 41(17), pp. 5599-5612. doi: 10.1039/c2cs35170f

Blomback, M. et al. 1984. Activation of blood coagulation, fibrinolytic and kallikrein systems during storage of plasma. *Vox Sang* 47(5), pp. 335-342. doi: 10.1111/j.1423-0410.1984.tb04136.x

Brenchley, J. M. and Douek, D. C. 2012. Microbial translocation across the GI tract. *Annu Rev Immunol* 30, pp. 149-173. doi: 10.1146/annurev-immunol-020711-075001

Brigham, K. L. and Meyrick, B. 1986. Endotoxin and lung injury. *Am Rev Respir Dis* 133(5), pp. 913-927.

Brown, G. C. 2019. The endotoxin hypothesis of neurodegeneration. *J Neuroinflammation* 16(1), p. 180. doi: 10.1186/s12974-019-1564-7

Calin, G. A. et al. 2002. Frequent deletions and down-regulation of micro- RNA genes miR15 and miR16 at 13q14 in chronic lymphocytic leukemia. *Proc Natl Acad Sci U S A* 99(24), pp. 15524-15529. doi: 10.1073/pnas.242606799

Campuzano, S. et al. 2019. Antifouling (Bio)materials for Electrochemical (Bio)sensing. *Int J Mol Sci* 20(2), doi: 10.3390/ijms20020423

Cangemi, R. et al. 2016. Low-grade endotoxemia and clotting activation in the early phase of pneumonia. *Respirology* 21(8), pp. 1465-1471. doi: 10.1111/resp.12854

Cani, P. D. et al. 2008. Changes in gut microbiota control metabolic endotoxemia-induced inflammation in high-fat diet-induced obesity and diabetes in mice. *Diabetes* 57(6), pp. 1470-1481. doi: 10.2337/db07-1403

Chen, L. Y. et al. 2007. Relationship between hyperuricemia and metabolic syndrome. *J Zhejiang Univ Sci B* 8(8), pp. 593-598. doi: 10.1631/jzus.2007.B0593

Choi, J. et al. 2014. Activation of innate immune responses by Haemophilus influenzae lipooligosaccharide. *Clin Vaccine Immunol* 21(5), pp. 769-776. doi: 10.1128/CVI.00063-14

Citronberg, J. S. et al. 2016. Reliability of plasma lipopolysaccharide-binding protein (LBP) from repeated measures in healthy adults. *Cancer Causes Control* 27(9), pp. 1163-1166. doi: 10.1007/s10552-016-0783-9

Cohn, J. S. et al. 2004. Storage of human plasma samples leads to alterations in the lipoprotein distribution of apoC-III and apoE. *J Lipid Res* 45(8), pp. 1572-1579. doi: 10.1194/jlr.D300041-JLR200

Cooper, J. F. 1990. Resolving LAL Test interferences. *J Parenter Sci Technol* 44(1), pp. 13-15.

Dheda, S. et al. 2021. Establishing a stable platform for the measurement of blood endotoxin levels in the dialysis population. *Diagnosis (Berl)* 8(2), pp. 249-256. doi: 10.1515/dx-2019-0088

Dullah, E. C. and Ongkudon, C. M. 2017. Current trends in endotoxin detection and analysis of endotoxin-protein interactions. *Crit Rev Biotechnol* 37(2), pp. 251-261. doi: 10.3109/07388551.2016.1141393

Fay, M. and Hendrix, B. M. 1931. THE EFFECT OF ACID DENATURATION UPON THE COMBINING POWER OF FIBRINOGEN. *Journal of Biological Chemistry* 93(2), pp. 667-675. doi: [https://doi.org/10.1016/S0021-9258\(18\)76468-5](https://doi.org/10.1016/S0021-9258(18)76468-5)

Fink, A. L. et al. 1994. Classification of acid denaturation of proteins: intermediates and unfolded states. *Biochemistry* 33(41), pp. 12504-12511. doi: 10.1021/bi00207a018

Forsyth, C. B. et al. 2011. Increased intestinal permeability correlates with sigmoid mucosa alpha-synuclein staining and endotoxin exposure markers in early Parkinson's disease. *PLoS ONE* 6(12), p. e28032. doi: 10.1371/journal.pone.0028032

Franco, E. et al. 2018. Endotoxins from a Pharmacopoeial Point of View. *Toxins (Basel)* 10(8), doi: 10.3390/toxins10080331

Gomes, J. M. G. et al. 2017. Metabolic endotoxemia and diabetes mellitus: A systematic review. *Metabolism* 68, pp. 133-144. doi: 10.1016/j.metabol.2016.12.009

Harm, S. et al. 2021. An in vitro study on factors affecting endotoxin neutralization in human plasma using the Limulus amoebocyte lysate test. *Sci Rep* 11(1), p. 4192. doi: 10.1038/s41598-021-83487-4

Hartung, T. 2015. The human whole blood pyrogen test - lessons learned in twenty years. *ALTEX* 32(2), pp. 79-100. doi: 10.14573/altex.1503241

Heins, M. et al. 1995. Storage of serum or whole blood samples? Effects of time and temperature on 22 serum analytes. *Eur J Clin Chem Clin Biochem* 33(4), pp. 231-238. doi: 10.1515/cclm.1995.33.4.231

Hitchcock, P. J. et al. 1986. Lipopolysaccharide nomenclature--past, present, and future. *J Bacteriol* 166(3), pp. 699-705. doi: 10.1128/jb.166.3.699-705.1986

Hurley, J. C. 1995. Endotoxemia: methods of detection and clinical correlates. *Clin Microbiol Rev* 8(2), pp. 268-292. doi: 10.1128/CMR.8.2.268

Jackie, J. et al. 2021. Rapid and Sensitive Direct Detection of Endotoxins by Pyrolysis-Gas Chromatography-Mass Spectrometry. *ACS Omega* 6(23), pp. 15192-15198. doi: 10.1021/acsomega.1c01446

Jacobs, E. et al. 1986. Stability of lactate dehydrogenase at different storage temperatures. *Clinical Biochemistry* 19(3), pp. 183-188. doi: [https://doi.org/10.1016/S0009-9120\(86\)80021-2](https://doi.org/10.1016/S0009-9120(86)80021-2)

Joiner, T. J. et al. 2002. Comparison of endotoxin testing methods for pharmaceutical products. *Int J Pharm Compd* 6(6), pp. 408-409.

Kalynych, S. et al. 2014. Progress in understanding the assembly process of bacterial O-antigen. *FEMS Microbiol Rev* 38(5), pp. 1048-1065. doi: 10.1111/1574-6976.12070

- Kim, K. E. et al. 2016. Lipopolysaccharide-binding protein plasma levels as a biomarker of obesity-related insulin resistance in adolescents. *Korean J Pediatr* 59(5), pp. 231-238. doi: 10.3345/kjp.2016.59.5.231
- Kintz, E. et al. 2017. Salmonella enterica Serovar Typhi Lipopolysaccharide O-Antigen Modification Impact on Serum Resistance and Antibody Recognition. *Infect Immun* 85(4), doi: 10.1128/IAI.01021-16
- Lassenius, M. I. et al. 2011. Bacterial endotoxin activity in human serum is associated with dyslipidemia, insulin resistance, obesity, and chronic inflammation. *Diabetes Care* 34(8), pp. 1809-1815. doi: 10.2337/dc10-2197
- Lerouge, I. and Vanderleyden, J. 2002. O-antigen structural variation: mechanisms and possible roles in animal/plant-microbe interactions. *FEMS Microbiol Rev* 26(1), pp. 17-47. doi: 10.1111/j.1574-6976.2002.tb00597.x
- Lesche, D. et al. 2016. Does centrifugation matter? Centrifugal force and spinning time alter the plasma metabolome. *Metabolomics* 12(10), p. 159. doi: 10.1007/s11306-016-1109-3
- Leung, K. W. et al. 2009. Bacterial endotoxin activates retinal pigment epithelial cells and induces their degeneration through IL-6 and IL-8 autocrine signaling. *Mol Immunol* 46(7), pp. 1374-1386. doi: 10.1016/j.molimm.2008.12.001
- Levin, J. and Bang, F. B. 1968. Clottable protein in Limulus; its localization and kinetics of its coagulation by endotoxin. *Thromb Diath Haemorrh* 19(1), pp. 186-197.
- Levine, D. M. et al. 1993. In vivo protection against endotoxin by plasma high density lipoprotein. *Proc Natl Acad Sci U S A* 90(24), pp. 12040-12044. doi: 10.1073/pnas.90.24.12040
- Li, L. et al. 2019. Colorimetric determination of uric acid based on the suppression of oxidative etching of silver nanoparticles by chloroauric acid. *Mikrochim Acta* 187(1), p. 18. doi: 10.1007/s00604-019-4004-6
- Liu, A. H. 2002. Endotoxin exposure in allergy and asthma: reconciling a paradox. *J Allergy Clin Immunol* 109(3), pp. 379-392. doi: 10.1067/mai.2002.122157
- Lu, M. et al. 2012. Kinetic analysis of thermal stability of human low density lipoproteins: a model for LDL fusion in atherogenesis. *J Lipid Res* 53(10), pp. 2175-2185. doi: 10.1194/jlr.M029629

Ma, J. et al. 2004. Role of apolipoprotein A-I in protecting against endotoxin toxicity. *Acta Biochim Biophys Sin (Shanghai)* 36(6), pp. 419-424. doi: 10.1093/abbs/36.6.419

Molenaar-de Backer, M. W. A. et al. 2023. In vitro alternative for reactogenicity assessment of outer membrane vesicle based vaccines. *Sci Rep* 13(1), p. 12675. doi: 10.1038/s41598-023-39908-7

Morrissey, J. H. et al. 1993. Quantitation of Activated Factor VII Levels in Plasma Using a Tissue Factor Mutant Selectively Deficient in Promoting Factor VII Activation. *Blood* 81(3), pp. 734-744. doi: <https://doi.org/10.1182/blood.V81.3.734.734>

Mueller, M. et al. 2004. Aggregates are the biologically active units of endotoxin. *J Biol Chem* 279(25), pp. 26307-26313. doi: 10.1074/jbc.M401231200

Munford, R. S. 2016. Endotoxemia-menace, marker, or mistake? *J Leukoc Biol* 100(4), pp. 687-698. doi: 10.1189/jlb.3RU0316-151R

Nadhazi, Z. et al. 2002. Plasma endotoxin level of healthy donors. *Acta Microbiol Immunol Hung* 49(1), pp. 151-157. doi: 10.1556/AMicr.49.2002.1.15

Nier, A. et al. 2019. Metabolic Abnormalities in Normal Weight Children Are Associated with Increased Visceral Fat Accumulation, Elevated Plasma Endotoxin Levels and a Higher Monosaccharide Intake. *Nutrients* 11(3), doi: 10.3390/nu11030652

Nier, A. et al. 2018. Non-Alcoholic Fatty Liver Disease in Overweight Children: Role of Fructose Intake and Dietary Pattern. *Nutrients* 10(9), doi: 10.3390/nu10091329

Nnyigide, O. S. and Hyun, K. 2020. The protection of bovine serum albumin against thermal denaturation and gelation by sodium dodecyl sulfate studied by rheology and molecular dynamics simulation. *Food Hydrocolloids* 103, p. 105656. doi: <https://doi.org/10.1016/j.foodhyd.2020.105656>

Norvik, J. V. et al. 2016. Overweight modifies the longitudinal association between uric acid and some components of the metabolic syndrome: The Tromso Study. *BMC Cardiovasc Disord* 16, p. 85. doi: 10.1186/s12872-016-0265-8

Opal, S. M. 2010. Endotoxins and other sepsis triggers. *Contrib Nephrol* 167, pp. 14-24. doi: 10.1159/000315915

- Pais de Barros, J. P. et al. 2015. Quantitative lipopolysaccharide analysis using HPLC/MS/MS and its combination with the limulus amoebocyte lysate assay. *J Lipid Res* 56(7), pp. 1363-1369. doi: 10.1194/jlr.D059725
- Paoli, C. J. et al. 2018. Epidemiology and Costs of Sepsis in the United States-An Analysis Based on Timing of Diagnosis and Severity Level. *Crit Care Med* 46(12), pp. 1889-1897. doi: 10.1097/CCM.0000000000003342
- Paracini, N. et al. 2022. Lipopolysaccharides at Solid and Liquid Interfaces: Models for Biophysical Studies of the Gram-negative Bacterial Outer Membrane. *Adv Colloid Interface Sci* 301, p. 102603. doi: 10.1016/j.cis.2022.102603
- Paramo, T. et al. 2015. Energetics of Endotoxin Recognition in the Toll-Like Receptor 4 Innate Immune Response. *Sci Rep* 5, p. 17997. doi: 10.1038/srep17997
- Pasella, S. et al. 2013. Pre-analytical stability of the plasma proteomes based on the storage temperature. *Proteome Sci* 11(1), p. 10. doi: 10.1186/1477-5956-11-10
- Pasqua, S. et al. 2021. Complete intra-laboratory validation of a LAL assay for bacterial endotoxin determination in EBV-specific cytotoxic T lymphocytes. *Mol Ther Methods Clin Dev* 22, pp. 320-329. doi: 10.1016/j.omtm.2021.05.002
- Pawlik-Sobecka, L. et al. 2020. The Influence of Serum Sample Storage Conditions on Selected Laboratory Parameters Related to Oxidative Stress: A Preliminary Study. *Diagnostics (Basel)* 10(1), doi: 10.3390/diagnostics10010051
- Pearson, F. C. et al. 1985. Detection of endotoxin in the plasma of patients with gram-negative bacterial sepsis by the Limulus amoebocyte lysate assay. *J Clin Microbiol* 21(6), pp. 865-868. doi: 10.1128/jcm.21.6.865-868.1985
- Piehler, M. et al. 2020. Comparison of LAL and rFC Assays-Participation in a Proficiency Test Program between 2014 and 2019. *Microorganisms* 8(3), doi: 10.3390/microorganisms8030418
- Pinto, J. et al. 2014. Human plasma stability during handling and storage: impact on NMR metabolomics. *Analyst* 139(5), pp. 1168-1177. doi: 10.1039/c3an02188b
- Reich, J. et al. 2016. Masking of endotoxin in surfactant samples: Effects on Limulus-based detection systems. *Biologicals* 44(5), pp. 417-422. doi: 10.1016/j.biologicals.2016.04.012

Reich, J. et al. 2018. Investigation of the kinetics and mechanism of low endotoxin recovery in a matrix for biopharmaceutical drug products. *Biologicals* 53, pp. 1-9. doi: 10.1016/j.biologicals.2018.04.001

Reich, J. et al. 2019. Low Endotoxin Recovery-Masking of Naturally Occurring Endotoxin. *Int J Mol Sci* 20(4), doi: 10.3390/ijms20040838

Ribeiro, M. M. et al. 2010. Endotoxin deactivation by transient acidification. *Cell Transplant* 19(8), pp. 1047-1054. doi: 10.3727/096368910X500643

Rice, J. B. et al. 2003. Low-level endotoxin induces potent inflammatory activation of human blood vessels: inhibition by statins. *Arterioscler Thromb Vasc Biol* 23(9), pp. 1576-1582. doi: 10.1161/01.ATV.0000081741.38087.F9

Roth, R. I. et al. 1993. Distribution of bacterial endotoxin in human and rabbit blood and effects of stroma-free hemoglobin. *Infect Immun* 61(8), pp. 3209-3215. doi: 10.1128/iai.61.8.3209-3215.1993

Schwarz, H. et al. 2017. Biological Activity of Masked Endotoxin. *Sci Rep* 7, p. 44750. doi: 10.1038/srep44750

Sin, M. L. et al. 2014. Advances and challenges in biosensor-based diagnosis of infectious diseases. *Expert Rev Mol Diagn* 14(2), pp. 225-244. doi: 10.1586/14737159.2014.888313

Sirivongrangson, P. et al. 2020. Endotoxemia and circulating bacteriome in severe COVID-19 patients. *Intensive Care Med Exp* 8(1), p. 72. doi: 10.1186/s40635-020-00362-8

Sneck, M. et al. 2012. Conformational changes of apoB-100 in SMase-modified LDL mediate formation of large aggregates at acidic pH. *J Lipid Res* 53(9), pp. 1832-1839. doi: 10.1194/jlr.M023218

Solati, S. et al. 2015. An improved monocyte activation test using cryopreserved pooled human mononuclear cells. *Innate Immun* 21(7), pp. 677-684. doi: 10.1177/1753425915583365

Su, W. and Ding, X. 2015. Methods of Endotoxin Detection. *J Lab Autom* 20(4), pp. 354-364. doi: 10.1177/2211068215572136

Suontaka, A. M. et al. 2005. Occurrence of cold activation of transfusion plasma during storage at +4 degrees C. *Vox Sang* 88(3), pp. 172-180. doi: 10.1111/j.1423-0410.2005.00617.x

Tamura, H. et al. 2021. Outstanding Contributions of LAL Technology to Pharmaceutical and Medical Science: Review of Methods, Progress, Challenges, and Future Perspectives in Early Detection and Management of Bacterial Infections and Invasive Fungal Diseases. *Biomedicines* 9(5), doi: 10.3390/biomedicines9050536

Trumper, C. 2016. Citrate anticoagulation in the ICU: the Leeds experience. *Br J Nurs* 25(16), pp. 902-906. doi: 10.12968/bjon.2016.25.16.902

Tsuchiya, M. 2017. Factors Affecting Reduction of Reference Endotoxin Standard Activity Caused by Chelating Agent/Detergent Matrices: Kinetic Analysis of Low Endotoxin Recovery. *PDA J Pharm Sci Technol* 71(6), pp. 478-487. doi: 10.5731/pdajpst.2017.008086

Tsuji, K. and Steindler, K. A. 1983. Use of magnesium to increase sensitivity of Limulus amoebocyte lysate for detection of endotoxin. *Appl Environ Microbiol* 45(4), pp. 1342-1350. doi: 10.1128/aem.45.4.1342-1350.1983

Vipond, C. et al. 2019. Development and validation of a monocyte activation test for the control/safety testing of an OMV-based meningococcal B vaccine. *Vaccine* 37(29), pp. 3747-3753. doi: 10.1016/j.vaccine.2018.06.038

Vogt, N. M. et al. 2017. Gut microbiome alterations in Alzheimer's disease. *Sci Rep* 7(1), p. 13537. doi: 10.1038/s41598-017-13601-y

Wang, H. et al. 2018. Roles of hyperuricemia in metabolic syndrome and cardiac-kidney-vascular system diseases. *Am J Transl Res* 10(9), pp. 2749-2763.

Wong, J. et al. 2016. A comparative study of blood endotoxin detection in haemodialysis patients. *J Inflamm (Lond)* 13, p. 24. doi: 10.1186/s12950-016-0132-5

Wu, Y. 2015. Contact pathway of coagulation and inflammation. *Thromb J* 13, p. 17. doi: 10.1186/s12959-015-0048-y

Yaguchi, A. et al. 2012. Combining intermediate levels of the Endotoxin Activity Assay (EAA) with other biomarkers in the assessment of patients with sepsis: results of an observational study. *Crit Care* 16(3), p. R88. doi: 10.1186/cc11350

## Chapter 3

# Development of an electrochemical sensor for the detection of endotoxin using aptamers and molecularly imprinted polymer approaches

---

## 3.1 Introduction

### 3.1.1 General overview

Aptamers are synthetic nucleic acid sequences (20 – 50 nucleotides long) capable of specifically interacting with the analyte of choice, which can range from ions to whole cells (Jiang et al. 2022). As they behave similarly to antibodies and exhibit a number of advantages such as stability, reusability, quick response time and high specificity, they have gained traction in the last twenty years in the field of diagnostics and therapeutics (Ilgu and Nilsen-Hamilton 2016). Aptamers interact with their target through van der Waals, hydrogen bonding, and electrostatic interactions with high affinity and specificity (Pendergrast et al. 2005). Given their advantages over traditional biorecognition molecules such as antibodies, they have gained popularity, with increasing numbers of published paper observed each year (Jiang et al. 2022).

Since the identification of an endotoxin-binding aptamer by Kim et al., an increasing number of aptamer-based sensors for the detection of endotoxin have been developed, the majority of which employ electrochemical or fluorescent detection methods (Kim et al. 2012; Su et al. 2012; Ma et al. 2018b; Jiang et al. 2022). Such sensors are capable of detecting endotoxin in miniscule amounts, down to picograms and femtograms. However, the majority of aptamer-based endotoxin sensors reported in the literature have demonstrated their performance in aqueous solution and not in clinical samples, which limits their real-life application.

As mentioned in the introduction of *Chapter 2*, the detection of endotoxin in clinical matrices is especially challenging. Components of the sample matrix, such as nucleic acids, lipids, protein etc., as well as additives, such as anticoagulants, can interfere with the detection assays (Harm et al. 2021). The gold-standard in endotoxin detection, the LAL assay, hasn't found any clinical applications to date, and there is no standardized method for the detection of endotoxin in clinical samples (Reich et al. 2019). As the detection of endotoxin is far from being standardized and literature on the detection of endotoxin in clinical samples is poor, this Chapter will focus on the development and optimisation of an aptasensor for the rapid detection of endotoxin in blood plasma.

Previous work in the researcher's group showed the development of an aptasensor, as well as a hybrid molecularly imprinted polymer. Both sensors exhibited impressive performance in aqueous solutions, however the introduction of blood serum spiked with endotoxin showed very high "noise" levels and excessive biofouling (Demertzis, 2019). One of the questions raised following the development of those sensors was whether the introduction of an extensive sample preparation protocol, such as the one presented in *Chapter 2*, could overcome this issue, and enable the detection of endotoxin in blood plasma.

Therefore, the aim of this chapter is to build upon previous research on the development of an electrochemical aptasensor and a hybrid molecularly imprinted polymer. Further attempts at optimization will be presented, as well as preparation of the sensor to be implemented into plasma samples.

### 3.1.2 Aptamers

Aptamers were first described in the 1990s (Ellington and Szostak 1990). Aptamers are nucleic acid sequences (DNA or RNA) and are produced *in vitro* by going through an extensive selection process known as *SELEX* (Systematic Evolution of Ligands by EXponential enrichment) (Ilgu and Nilsen-Hamilton 2016). Briefly, during *SELEX* a library consisting of random nucleotide sequences ( $10^{15}$ – $10^{18}$ ) is assessed for its interaction with the target molecule. Bioinformatics analysis of the sequencing data is used to isolate and identify high-affinity aptamers for the target molecules. Finally, sequences that demonstrate significant binding affinity throughout cycles of binding, selection and amplification are taken forward for selectivity studies (Aljohani et al. 2022).

Despite their small size (20 – 50 nucleotide long) and low molecular weight (5-30 kDa, about  $1/10^{\text{th}}$  of antibodies), their tertiary structures provide a large surface area for precise binding with target analytes (Morita et al. 2018). Aptamer targets exhibit dissociation constants ( $K_d$ ) in the range of micro- to picomolar, similar to antibodies, and they can even distinguish between two molecules that vary structurally in a single position (Ilgu and Nilsen-Hamilton 2016; Morita et al. 2018). Additionally, they can be chemically modified easily thanks to their oligonucleotide properties, which in turns makes them suitable for many sensing applications. One important modification includes the addition of unnatural nucleotides, which can be achieved by altering the sugar rings, as well using locked nucleic acids (where the 2'- and 4'-ribose positions are covalently bound). This prevents aptamer degradation by nucleases and prevents degradation in samples (Aljohani et al. 2022).

Aptamers also show promising potential as therapeutics. Compared to antibodies, which are highly immunogenic, aptamers produce minimal immune responses and can target a wider variety of molecules, plus they exhibit higher stability (Nimjee et al. 2017). Furthermore, aptamers can target highly toxic or non-immunogenic antigens, something not possible for antibodies produced by animals (Aljohani et al. 2022). Compared to the production of monoclonal antibodies, which is expensive and time-consuming, the screening process of aptamers is both quicker and more economical (Aljohani et al. 2022). Currently, there is one therapeutic aptamer approved by the the US Food and Drug Administration (FDA), for the treatment of macular degeneration (Li et al. 2021). A number of aptamers are however in pre-clinical studies or clinical trials for the treatment for a number of other conditions, including acute myeloid leukemia, Hodgkin's lymphoma, hemophilia and sickle cell disease

(Aljohani et al. 2022). In 2023, a new RNA aptamer, Avacincaptad pegol, a complement inhibitor, gained FDA approval for the treatment of geographic atrophy secondary to age-related macular degeneration (Mahmoudian et al. 2024). However, despite the advances in the potential application of aptamers, research is still needed to unlock their full potential in diagnostics and therapeutics.

### *3.1.3 Aptamer – based biosensors*

As mentioned previously, the ability of aptamers to detect a plethora of target molecules, such as metal ions, amino acids, viral proteins and even whole cells and bacteria, has made them an attractive choice for the development of biosensors (Feng et al. 2014). Moreover, their ease of immobilization on detection surfaces, thanks to their easily modifiable 5' and 3', has also contributed to their increase in popularity (Jiang et al. 2022).

Electrochemical aptasensors, which measure a change in potential, impedance or current, are popular in the development of point-of-care diagnostics. Some of their benefits include fast response times, miniaturization, low cost and ease of fabrication (Abd-Ellatief and Abd-Ellatief 2021). The first electrochemical aptasensor in literature was described in 2004 (Ikebukuro et al. 2004). Almost twenty years later, an increasing number of aptasensors have been developed; the most common aptasensor target in literature is thrombin (Yan et al. 2013).

One of the first steps in the fabrication of an electrochemical aptasensor is the attachment of the aptamer on the gold surface. The most common approach includes the use of thiolated aptamers, which directly bind to gold through Au-S bonds (Leff et al. 1996). Sulfur compounds are well-known for attaching to gold surfaces, but also to silver, platinum, palladium, mercury and semiconductors (Mandler and Kraus-Ophir 2011). The thiol is usually placed at the 5' end of the aptamer, to prevent misfolding (Ying et al. 2018). The use of thiolated aptamers is usually paired with the use of alkanethiols, which serve to remove any non-attached aptamers, ensure their upright orientation, and provide anti-biofouling effects (Abd-Ellatief and Abd-Ellatief). The alkanethiol may be introduced after aptamer attachment or co-immobilized. Some commonly used alkanethiols include 6- mercaptohexanol (MCH), mercaptoundecanoic acid (MUA) and 4,4 dithiodibutyric acid (DTBA) (Levicky et al. 1998; Jang and Keng 2008; Amiri and Golmohammadi 2020). Despite the anti-biofouling properties of the alkanethiols, the effect is limited and therefore if the sensors are to be used in clinical samples, additional steps are often needed to either remove interfering substances from the sample or implement additional anti-biofouling techniques (Boozer et al. 2006; Campuzano et al. 2019).

Besides direct binding of aptamers on the electrode surface, indirect attachment is also possible through the use of short linkers. One example in literature described the

construction of a sensor where 3-mercaptopropionic acid (MPA) was deposited on the gold surface and used as an intermediate linker. N-(3-dimethylaminopropyl)-N-ethylcarbodiimide hydrochloride (EDC) / N-hydroxy-succinimide (NHS) chemistry was then used to immobilize an amino-modified aptamer to the carboxylic group of the alkanethiol (Ying et al. 2018). Another such example is provided by Chakma et al., who utilized dithiobis(succinimidyl propionate) as a SAM, on which they immobilized an amino-modified aptamer for the detection of histidine rich protein II (Chakma et al. 2018).

The present study will focus on the direct immobilization of a thiolated aptamer on the surface of gold electrodes, in combination with alkanethiols as spacer molecules. The development of the sensors will be monitored and assessed using electrochemical impedance spectroscopy. Alkanethiols will be assessed for their interaction with control standard endotoxin in various buffers, and the binding performance of aptamers will be monitored under various conditions.

#### *3.1.4. Electrochemistry overview*

Across all electrochemical experiments in this study, a three – electrode (classic) electrochemical setup is used (Figure 3.1). It is made up of three electrodes: a working electrode (WE), where the interactions of interest take place, a reference electrode (RE) and a counter electrode (CE) (Colburn et al. 2021). To study the changes occurring on the working electrode, all other electrochemical cell components must be fixed. The reference electrode, which functions as the system's "blank" regarding the changes in potential, ensures that any observed changes in voltage appear at the electrode surface only (Colburn et al. 2021). In an ideal scenario, no current should go through the reference electrode. In this study, a silver-silver chloride (Ag/AgCl) electrode was used.

The current generated at the surface of the working electrode needs to be redirected, otherwise it may affect the voltage of the reference electrode. Therefore, a counter electrode is usually employed to provide an alternative current path. In this study, a platinum (Pt) counter electrode was employed (Colburn et al. 2021).

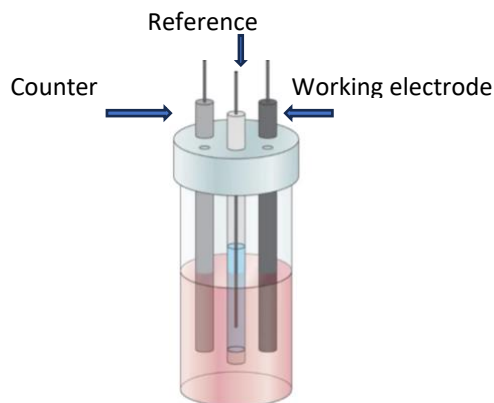


Figure 3.1: A typical electrochemical cell. CE: Counter electrode, RE: Reference electrode, WE: Working electrode (Lee et al. 2017)

### 3.1.4.1 Cyclic voltammetry

Cyclic voltammetry is extensively used by electrochemists to study reduction and oxidation processes. Some of its most common applications include measuring antioxidant levels in biological systems and food products, drug quality assessment in pharmaceuticals and label-free detection of molecules in sensors (Wang et al. 2021a). During CV, the potential is scanned linearly as a function of time, causing the analysed substance to undergo either oxidation or reduction and the resulting current is measured. This can provide information about the quantity of the analyte undergoing oxidation/reduction (Sandford et al. 2019). After completion of the linear sweep, the potential is reversed, returning to the original value. Below in Figure 3.2, a cyclic voltammogram shows the redox behaviour of a clean gold electrode in sulfuric acid ( $H_2SO_4$ ).

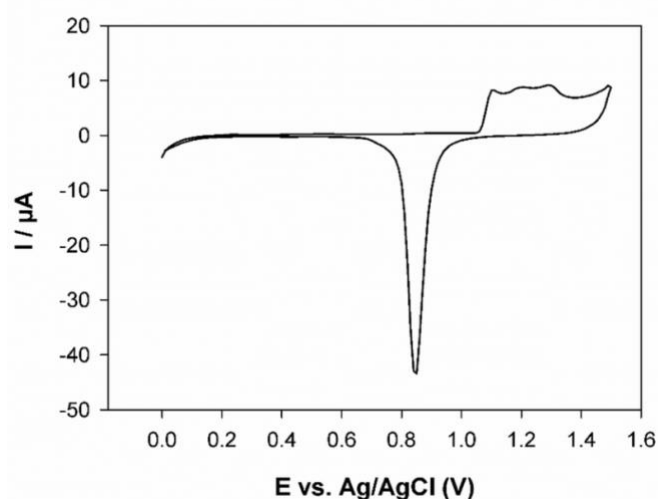


Figure 3.2 Cyclic voltammogram of a bare gold electrode subjected to electropolishing between 0 V and 1.5 V in 0.5M  $H_2SO_4$ . (McCormick et al. 2021).

One of the most commonly used methods for the cleaning of gold electrodes involves performing cyclic voltammetry in H<sub>2</sub>SO<sub>4</sub> (Fakhr et al. 2022). In the area between 1.0 – 1.35 V, three consecutive oxidative peaks can be observed, and in the area around 0.9 V, a single large reduction peak can be observed (Figure 3.2). The sharpness and clarity of each peak is indicative of the cleanliness of the gold and the absence of impurities or scratches on its surface (Fischer et al. 2009).

In this project, cyclic voltammetry is used for the electrochemical cleaning of electrodes, as mentioned before. Moreover, CV is used to confirm the modification of the gold surface, as modification leads to changes in peak current and potential (Steel et al. 1998). Additionally, CV is used to perform electropolymerization of electroactive monomers, a process necessary for the formation of polymer on the gold electrode surface, which also allows control over the growth of the polymer (Gholivand and Torkashvand 2016).

#### 3.1.4.2 Electrochemical Impedance Spectroscopy (EIS)

EIS is one of the most commonly used techniques employed in the development of label-free biosensors (Brett 2022). It can provide valuable information regarding interaction taking place on the surface of an electrode, such as aptamer-target binding, enzyme-substrate reactions and more. EIS-based sensors are economical, easy to fabricate and can be miniaturized, which makes them suitable for use in point-of-care diagnostics (Brett 2022). In EIS, the impedance of the circuit is measured in ohms (as resistance unit), and modification at the electrode surface can increase or decrease its value (Magar et al. 2021). The following section will provide information required to understand the electrochemical aspects of the biosensor and assist with result interpretation.

As mentioned in the previous section, CV is useful in the assessment of reactions taking place at the electrode surface. However, it is not sensitive enough for the detection of biomolecular interactions or the characterization of electrochemical sensors. An alternative electrochemical technique, widely employed in label-free biosensors is EIS. EIS provides valuable information regarding biomolecular interactions, such as antibody–antigen recognition, substrate–enzyme interaction, or whole cell capture (Magar et al. 2021). During EIS, a small (< 5 mV) perturbing potential is applied across an electrode. This is so that the resulting current is pseudo-linear. The ratio between the applied potential and the resulting current is defined as impedance (Z), measured in Ohms (Ω) (Oberhaus et al. 2020). Impedance is similar to resistance (R) and describes a circuit’s ability to resist electron flow. This is described by Ohm’s law (Equation 3.1), which is satisfied when a direct voltage is applied.

Equation 3.1

$$R = \frac{V}{I}$$

Where R is resistance, V is voltage, and I is current.

In EIS, a small, varying sinusoidal potential is applied, which induces an alternating current, which can be seen in Figure 3.3 (Oberhaus et al. 2020). Therefore, it can be said that impedance is resistance that varies in a cyclical manner. Figure 3.3 shows the relationship between a sinusoidally applied potential and the resulting current.

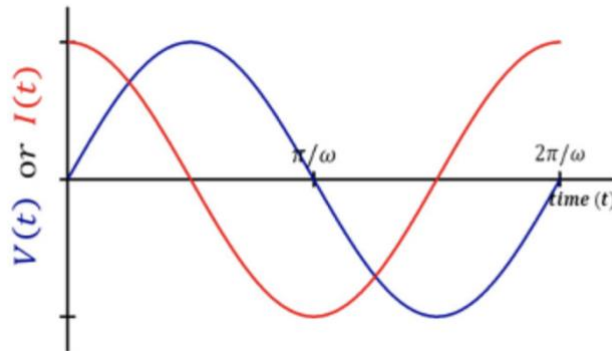


Figure 3.3: The relationship between a sinusoidally applied potential (blue line) and the resulting current measured (red line) as a function of frequency. The measured current is out of phase from the applied potential (Choi et al. 2020).

When an alternating voltage is applied, as is the case in EIS, the resulting impedance  $Z(\omega)$ , where  $\omega = 2\pi f$  is the angular frequency of the applied voltage, can be re-expressed as:

Equation 3.2: 
$$Z(\omega) = \frac{V(\omega)}{i(\omega)}$$

The sinusoidally applied potential and current can be expressed as:

Equation 3.3 
$$V_t = V_m \sin(\omega t)$$

and;

Equation 3.4 
$$I_t = I_m \sin(\omega t + \phi)$$

Where V is the potential,  $V_m$  is the amplitude and  $\omega$  is the radian frequency expressed as  $2\pi f$ . Where I is the current,  $I_m$  is the amplitude and  $\omega$  is the radian frequency expressed as  $2\pi f$ . Same applies to the sinusoidal current which has a phase shift of  $\phi$ .

According to equation 3.2, impedance can now be expressed as:

Equation 3.5 
$$Z = \frac{V_t}{i_t} = \frac{V = V_m \sin(\omega t)}{I = I_m \sin(\omega t + \phi)} = Z_0 = \frac{\sin(\omega t)}{(\omega t + \phi)}$$

A “Lissajous plot” (Figure 3.4), presented as an oval shape is produced when the sinusoidal voltage ( $V_t$ ) is plotted on the X-axis and the resulting sinusoidal current ( $I_t$ ) is plotted on the Y-axis. Before the development of contemporary EIS instrumentation, the standard method for measuring impedance was Lissajous analysis (Magar et al. 2021).

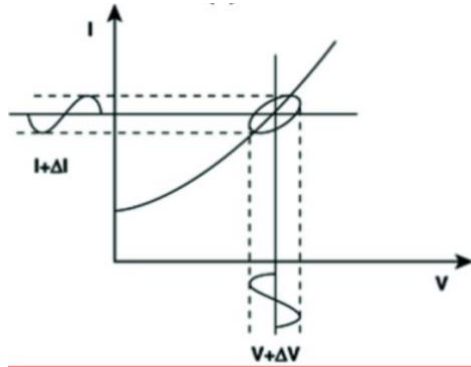


Figure 3.4: Lissajous plot generated by plotting the sinusoidal applied potential and the resulting sinusoidal current. The characteristic oval shape is representative of the phase angle between the two signals, and its shape can change from a perfect circle to a straight line, depending on the phase shift. (Magar et al. 2021).

With Euler’s relationship (a mathematical function):

$$\text{Equation 3.6} \quad \exp j\phi = \cos\phi + j\sin\phi$$

Where  $j$  is an imaginary number. Therefore, impedance can be expressed as a complex function:

$$\text{Equation 3.7} \quad Z(\omega) = \frac{V}{i} = Z_0 \exp(j\phi) = Z_0 (\cos\phi + j\sin\phi) = Z_0 (\cos\phi) + Z_0 j(\sin\phi)$$

$$\text{Equation 3.8} \quad Z(\omega) = Z_{real} + Z_{img}$$

Therefore, total impedance  $Z(\omega)$  is made up of real ( $Z'$ ) and imaginary impedance ( $Z''$ ) and their relationship is described by the following equation:

$$\text{Equation 3.9} \quad Z(\omega) = Z' + jZ''$$

During an EIS experiment, a small voltage is applied over a range of frequencies, ranging from high (kHz) to low (Hz) by the potentiostat, which calculates the resulting time lag  $\phi$  as well as the resulting impedance, which is presented in a Nyquist plot (Figure 3.5), which

shows real impedance on the x axis and imaginary impedance on the y axis.

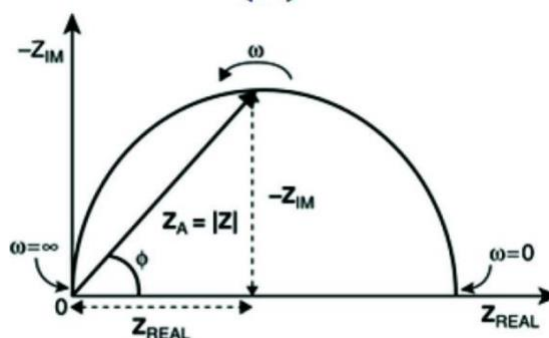


Figure 3.5: A typical Nyquist plot. Real impedance is on the x axis, while imaginary impedance is on the y axis. Impedance is represented as a vector of length (arrow). The phase angle is formed between the vector and the x axis. Impedance at low frequencies is shown on the x axis, on the left, whereas higher frequencies are found at the right of the x axis (Magar et al. 2021).

EIS graphs can provide valuable information on the electrochemical phenomena taking place at the surface of a gold electrode, however, to interpret the results, equivalent circuits are often used. Essentially, it is assumed that an electrochemical cell will exhibit similar behaviour with “real” electrical elements such as capacitors, resistors and inductors that may be connected in parallel or in series with each other (Oberhaus et al. 2020). As the majority of Nyquist plots in biosensing resemble a semicircle with a 45° straight line at the end, the most commonly used equivalent circuit is the Randle’s equivalent circuit (Nejad et al. 2016). Randle’s circuit consists of Solution Resistance ( $R_s$ ) which is found by utilising the high frequency data, while the value for the Charge Transfer Resistance ( $R_{ct}$ ), is defined by low frequency data. During EIS experiments, the potentiostat’s software (Ivium) was used to check the fit of the equivalent circuit and the most suitable one was used for result interpretation.

$\% \Delta R_{ct}$  was determined for all data acquired through EIS following incubation of the electrode with molecules that may cause changes in impedance, and it was determined by the equation:

Equation 3.10

$$\% \Delta R_{ct} = \frac{R_{ct} - R_0}{R_0} \times 100$$

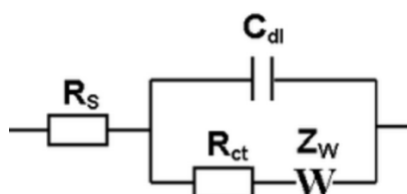
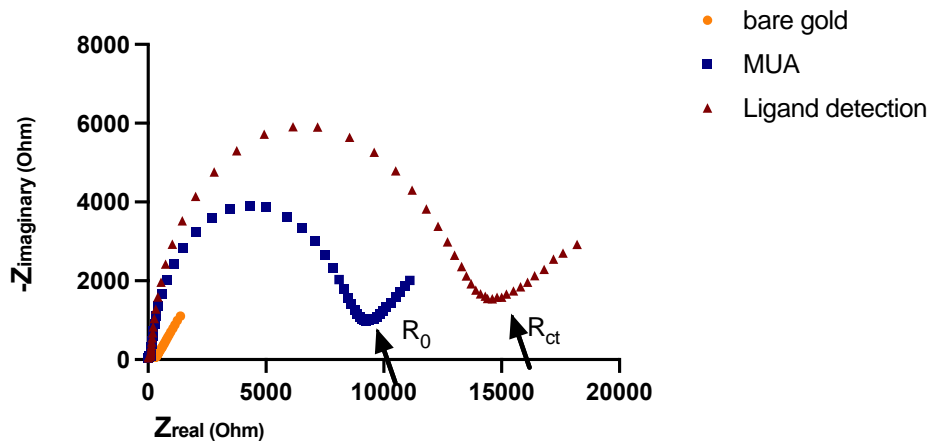


Figure 3.6: Randle’s equivalent circuit consisting of solution resistance ( $R_s$ ), double layer capacitance ( $C_{dl}$ ), charge-transfer resistance ( $R_{ct}$ ) and Warburg’s impedance ( $Z_w$ ).

**Figure 3.7** shows an example EIS graph of a bare gold electrode (gold curve), following incubation and modification with 11-mercaptoundecanoic acid (blue) and a modified surface on to which a ligand has bound (red). The effects of electrode modification can be seen as an increase in charge-transfer resistance ( $R_{ct}$ ).



*Figure 3.7: EIS graphs obtained following assessment of a clean gold electrode (yellow), an electrode surface modified with 11-mercaptoundecanoic acid (blue) and a modified surface on to which a ligand has bound (red). Solution resistance  $R_s$  can be detected at the higher frequencies on the x axis (not visible in graph). Charge-transfer resistance can be seen in lower frequencies ( $R_{ct}$ ). During EIS measurements, a difference in charge-transfer resistance is noted between the modified electrode surface (MUA-modified electrode, blue) and following challenge with ligand (red). Warburg's impedance, a vertical line at the lower frequencies, can be seen, and is used to study diffusion processes.*

In this project, EIS will be used to characterize the gold electrodes and to evaluate the binding performance of the sensors. In particular, EIS will be used to assess the development of self-assembled monolayers, the attachment of aptamers and endotoxin on bare gold, the binding of endotoxin to the aptamer and the molecularly imprinted polymer as well as the hybrid system.

### 3.1.5 Molecularly imprinted polymers (MIPs)

#### 3.1.5.1 General overview

MIPs are synthetic materials that present specific binding, complementary to the target molecule regarding size, shape and functional group orientation (BelBruno 2019). Originally developed as stationary phases for HPLC, they have now found applications in chromatography, solid-phase extraction, binding assays and sensors (Haupt and Mosbach 2000). They have been described as promising alternatives to antibodies and carry the benefits of withstanding environmental conditions as well as being economical to produce, compared to antibodies. (BelBruno 2019). The first approaches towards molecular imprinting

were documented in the 1970s and 1980s, from the works of Günter Wulff in Germany and Klaus Mosbach in Sweden, who utilized covalent and non-covalent approaches for MIP development respectively (Wulff and Sarhan 1972; Arshady and Mosbach 1981). Mosbach in particular, set the groundwork in molecular imprinting by using amino acid derivatives to develop MIPs for the detection of targets in organic solvents (Andersson et al. 1984). MIPs can be produced in various formats, such as membranes, films and beads, to suit different applications (Alexander et al. 2006).

During the production of a MIP, the target molecule (template) is allowed to interact with one or more functional monomers. Polymerisation is initiated, 'locking' these target-monomer complexes in place. Washing of the resultant polymer is performed to disrupt the complexes and allow removal of the template, thus exposing 'binding cavities' that exhibit high specificity and selectivity for the target (Manesiotis et al. 2013). MIPs have been produced for the detection of drugs, environmental pollutants, toxins and even whole cells (Nishino et al. 2006; Sorribes-Soriano et al. 2017; Xiao et al. 2019; Yasmeen et al. 2021). Monomers containing vinyl and acrylic groups are especially popular in molecular imprinting, owing to the wide variety of chemical functionality and the relative ease of polymerization (Haupt and Mosbach 2000). For example commonly used monomers for molecular imprinting include methacrylic acid (MAA), acrylic acid (AA), 2- or 4-vinylpyridine (2- or 4-VP), acrylamide and trifluoromethacrylic acid (Haupt and Mosbach 2000; BelBruno 2019). Throughout the literature, a number of approaches have been described for the production of MIPs, the majority of which are made by free radical-initiated polymerization, electropolymerization or photopolymerization (Sajini and Mathew 2021).

#### *3.1.5.2 Bulk imprinting*

Bulk imprinting is the oldest and most widely used imprinting method for the development of MIPs (Ashley et al. 2017). The first reported bulk imprinted MIPs in literature, developed by Mosbach, were used as a separation method (Arshady and Mosbach 1981). During bulk polymerization, a template molecule is imprinted as a whole in the matrix (Figure 3.8). Following polymerization, the final product is mechanically ground, sieved and washed to produce small particles from which the template is removed (Sajini and Mathew 2021). Bulk polymerization produces readily accessible, template-specific 3D cavities, and this method shows advantages for the recognition of small molecules. Additionally, bulk-imprinted polymers tend to be easily prepared without the need for specific equipment, and the resulting polymers tend to be of high purity (Sajini and Mathew 2021). However, this method shows limitations in the detection of proteins, living cells and microorganisms (Erturk and Mattiasson 2017). Preserving the conformation of protein during the polymerization process is challenging, and additionally, large template molecules can become entrapped into the matrix, leading to low accessibility, and difficulty in removal and rebinding of the template.

Moreover, the re-binding capacity can be limited as a small number of high-quality sites may be produced (Ding and Heiden 2014; Erturk and Mattiasson 2017).



Figure 3.8: The bulk imprinting process. Following the interaction of the template with the monomers in solution, polymerization is initiated which results in the formation of a molecularly imprinted cavity on removal of the template species (BelBruno 2019).

### 3.1.5.3 Surface imprinting

Surface imprinting is an alternative MIP synthesis method, where the target molecule is immobilized, or is in proximity, to a solid support. Surface imprinted MIPs provide more easily accessible cavities with more favorable binding kinetics compared to bulk imprinting, which makes it an attractive choice for the imprinting of proteins, cells and microorganisms (Erturk and Mattiasson 2017). During the surface imprinting step, the template is immobilized on a solid surface, such as a gold electrode. In order to create an imprinting layer with templates, polymerisation is carried out on the solid substrate's surface while initiators and cross-linking agents are present. Finally, the template is washed away, revealing cavities specific to the target molecule (Dong et al. 2021). Surface imprinted MIPs have been employed in sensors, separation and purification and catalysis, thanks to those benefits (Dong et al. 2021). A number of surfaces have been used to assist with template immobilised imprinting, such as activated silica gel,  $\text{Fe}_3\text{O}_4$  magnetic nanoparticles, chitosan and polystyrene beads (Chen et al. 2011). Some techniques used for surface imprinting include template immobilization, self-assembled monolayers, nano-patterning, and soft lithography (Yadav et al. 2022).

Surface imprinting is of particular importance in biosensors, and an increasing number of publications, especially in the field of diagnostics, utilize this methodology (Cui et al. 2017). In literature, this technique has been used in a number of sensor surfaces, including gold coated  $\text{Fe}_3\text{O}_4$  nanoparticles, graphene oxide  $\text{Fe}_3\text{O}_4$  nanoparticles, stainless steel, titanium dioxide nanocomposites, carbon nanotubes, and platinum and gold electrodes (Gao et al. 2011; Li et al. 2013; Cieplak et al. 2015; Duan et al. 2016; Deng et al. 2019; Yu et al. 2019).

Importantly, surface imprinting has been employed in the detection of toxins, bacteria and proteins associated with human disease. Notable templates include Interleukin-1 $\beta$ , human serum albumin, estrone, cholesterol, *Staphylococcus epidermidis*, human papillomavirus derived E7 protein, Zika virus and human immunodeficiency virus p24 (Gao et al. 2011;

Cieplak et al. 2015; Golabi et al. 2017; Ma et al. 2017; Malik et al. 2017; Deng et al. 2019; Shin et al. 2019).

#### 3.1.5.4 Hybrid imprinting

The hybrid approach first described by Allender and Bowen, relies on the use of biological recognition elements such as peptides and aptamers as “super monomers” when creating molecularly imprinted polymers (Bowen, 2011). The hybrid approach has gained popularity, as it allows for the more sensitive detection of molecules, as the incorporation of recognition elements in molecularly-imprinted polymers is hypothesized to result in more homogenous binding sites that are readily accessible by the target, as shown in Figure 3.9 (Jolly et al. 2016). Additionally, the combination of aptamers with high affinity for the target in combination with a suitable monomer results in synergistic recognition with increased binding capacity for the target (Tan et al. 2021a). Furthermore, the incorporation of aptamers is also beneficial, as aptamers are less susceptible to degradation compared to antibodies and they can be developed for a wider range of targets (Abd-Ellatief and Abd-Ellatief 2021).

Hybrid MIPs have been developed for various targets. The researcher’s group has successfully developed an Apta-MIP for the detection of prostate-specific antigen (Jolly et al. 2016). Apta-MIPs have also been developed, by other researchers, for the detection of various other targets such as thrombin, alkaline phosphatase (Li et al. 2019b; Yang et al. 2019).

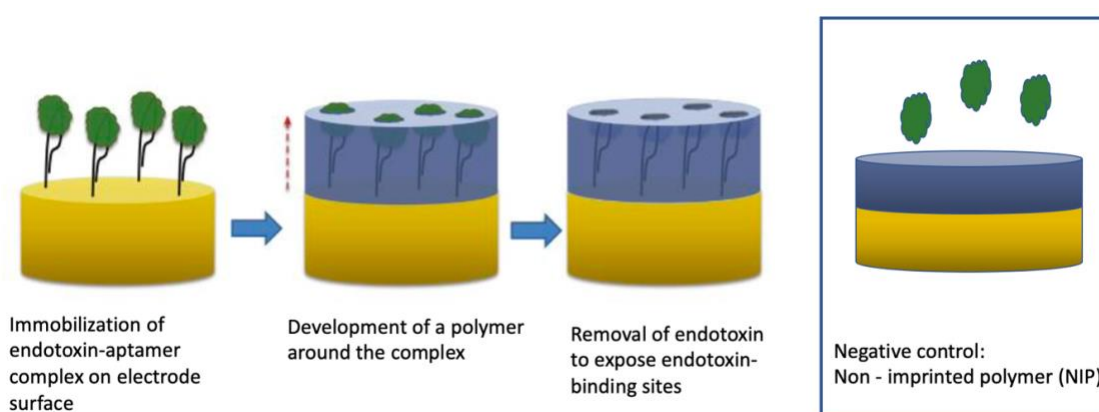


Figure 3.9. MIPs and their formation on gold electrodes. Polymer formation around an immobilised aptamer-endotoxin complex, following the removal of endotoxin, leaves behind an aptamer-lined imprinted site capable of recognizing endotoxin.

#### 3.1.5.5 Monomer selection – APBA

The current project focused on using electropolymerization to generate a molecularly imprinted polymer on the electrode surface. Polymers can be electropolymerized by using commonly used electrochemical techniques. Galvanostatic, potentiostatic or potentiodynamic conditions can be used. Potentiostatic techniques tend to produce thin-film

polymers, whereas galvanostatic techniques produce thicker films (Guchait et al. 2022). Additionally, polymers can be further differentiated into conducting and non-conducting; the former can be divided into proton-conducting, ion-conductive and electronically conductive polymers (Rikukawa and Sanui 2000; Tominaga 2017). For the purposes of this project an electronically conductive polymer, which has been used for the imprinting of endotoxin will be used – 3-aminophenylboronic acid (APBA) (figure 3.10).

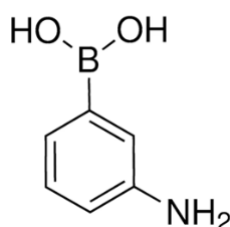


Figure 3.10 aminophenylboronic acid, the monomer of choice in this project.

The boronic acid present in the molecule can reversibly and selectively bind to diols which are present in saccharides (Wannapob et al. 2010). Therefore, they are commonly employed in the design of sensors for the detection of saccharide species, such as blood glucose sensors, cellulose, or complex oligosaccharides such as glycolipids, which are important as blood-type antigens, for example (Williams et al. 2021). In the case of endotoxin, multiple monosaccharides can be found in the O-antigen and core oligosaccharide sections, with each monosaccharide containing at least one *cis*-diol (Ji et al. 2019). Moreover, boronic acids are particularly relevant in endotoxin imprinting, as they have been used in the past for the imprinting of whole bacterial cells, including *E.coli* (Yasmeen et al. 2021). 3-APBA is preferred for the imprinting of bacterial cell imprinted polymers as it demonstrates high affinity and facile template removal (Golabi et al. 2017).

There is little published work on the use of boronic acids for the specific detection of endotoxin. However, 3-APBA has been used as a coating on a magnetic microsphere to facilitate the removal of endotoxin (Ji et al. 2019). A similar application is described by Gomes et al., who used 3-APBA-coated pore glass to adsorb *E.coli* lipopolysaccharides and RNA from plasmid-containing lysates (Gomes et al. 2010). More recently, a modified carbon cloth coated in a porous 3-APBA coating was used to improve biofilm growth of *Shewanella putrefaciens* by promoting bacterial attachment through boronic acid-saccharide interactions (Zhao et al. 2020). Additionally, encapsulated 3-APBA coated quantum dots were used in Janus micromotors for the rapid detection of *Salmonella* (Pacheco et al. 2022). Another recent example includes the use of L-cysteine (Cys) 4-aminophenylboronic acid functionalized quantum dots for the rapid detection of *E.Coli* and *Pseudomonas aeruginosa* (Ye et al. 2022). *As evidenced by literature, there is a recent increasing interest in the use of boronic acids for endotoxin purification or detection, and boronic acids may have promising applications in diagnostics.*



### 3.1.6 Aims and Objectives

Taking into consideration the lack of a rapid clinical detection system for endotoxin, and the successful development of electrochemical endotoxin detection platforms by previous member in the researcher's lab, this chapter will focus on the development and optimization of aptasensors, MIPs and aptaMIPs. The goal of this element of the project is the quantification of endotoxin in aqueous samples, using both aptasensors and hybrid imprinted sensors. Sensors will be replicated as per previous lab member's protocols, and their behaviour under different conditions will be assessed to inform further optimisation.

Therefore, the objectives of this chapter are to:

- Replicate the sensors developed by previous researchers in the researcher's lab, including aptasensors, MIPs and aptaMIPs, and compare their performance in aqueous solutions
- Assess the sensor's performance in various pH and buffers and optimize its performance
- Perform specificity tests using molecules present in blood plasma, such as human serum albumin (HSA).

## 3.2 Materials and Methods

### 3.2.1 Reagents and apparatus

A literature search revealed that despite the availability of several endotoxin-binding aptamers, most of the published work on endotoxin utilizes the aptamer developed by Kim et al, the sequence of which is displayed below (Kim et al. 2012; Ying et al. 2015).

5'- CTT CTG CCC GCC TCC TTC CTA GCC GGA TCG CGC TGG CCA GAT GAT ATA AAG GGT CAG  
CCC CCC AGG AGA CGA GAT AGG CGG ACA CT - 3'

A C6 spacer was introduced into the aptamer, as well as thiol functionality at the 5' end. The aptamer was purchased from Sigma-Aldrich (UK) and stored at -20°C prior to use.

All alkanethiols [6-mercaptohexanol (MCH), 11-mercaptoundecanoic acid (MUA), 4,4-dithiodibutiric acid (DTBA)] and reducing agents [Tris (2-carboxyethyl) phosphine hydrochloride (TCEP)], as well as 3-aminophenylboronic acid and Sodium fluoride (NaF) were purchased from Sigma-Aldrich (UK) and stored under ambient conditions. Endotoxin-free water (Cytiva) was purchased from Fisher Scientific and was stored under ambient conditions. Lipopolysaccharide from *E. coli* (Control Standard Endotoxin) was purchased from Fujifilm Wako Chemicals USA Corporation and following reconstitution with endotoxin free water was stored at -20°C prior to use. Trisodium citrate and glucose were purchased from Sigma-Aldrich (UK) and stored under ambient conditions.

Polishing kits and electrochemistry accessories (Faraday's cage, 2 mm diameter gold disc working electrodes, teflon caps and Pt-wire counter electrodes) were purchased from CH Instruments (UK). Salt bridges and reference electrodes were purchased from Basi Analytical Instruments (UK). Potassium ferrocyanide [ $K_4Fe(CN)_6$ ] was obtained from Fisher Scientific (UK) and potassium ferricyanide [ $K_3Fe(CN)_6$ ] was purchased from Sigma-Aldrich (UK). The MultiWE32 Potentiostat was purchased from Ivium Technologies (The Netherlands).

### 3.2.2. Methods

#### 3.2.2.1 Aptamer handling

All aptamer batches were aliquoted (100  $\mu$ M) in TE buffer (10 mM Tris, 1 mM EDTA) pH 7.5 and kept in a -20 °C freezer, for maximum long-term stability (Leppek and Stoecklin 2014). Prior to use, aptamers were diluted to 10  $\mu$ M in 10 mM PBS pH 7.4 (1x) enriched with 1 mM  $MgCl_2$  (herein referred to as “Folding Buffer”) (Dickey et al. 2016). Subsequently, the vial containing the aptamer solution was immersed in a water bath to heat the aptamer to 90-95 °C for 5 minutes (Dickey et al. 2016). This results in disruption of inter- and intramolecular bonds within or between neighbouring aptamer molecules. All solutions were allowed to cool to room temperature for 15 minutes so that the aptamers can form the appropriate 3D conformation to recognize the ligands.

As thiolated aptamers are oxidized by the manufacturers in order to preserve molecular stability, their reduction prior to use is necessary (Chang et al. 2019a). An aqueous solution of 1 mM TCEP (tris(2-carboxyethyl)phosphine) in TE buffer (10 mM Tris, 1 mM EDTA) containing 100 mM NaCl (herein referred to as “immobilisation buffer”) has been used to activate the aptamer thiol groups and facilitate immobilisation on the gold surface.

#### 3.2.2.2 Cleaning of gold electrodes

The surface of gold electrodes is prone to non-specific adsorption of contaminants such as proteins, cells, lipids and nucleic acids, which can affect electrochemical results and prevent the modification of the electrode surface (Campuzano et al. 2019). The presence of residues on the surface of gold electrodes can disrupt the proper deposition of alkanethiols and biorecognition molecules, interfere with the binding of the target molecule or cause increased background impedance. Therefore, the first step in the experimental process involves the thorough cleaning and polishing of the gold electrodes.

The electrodes were immersed in a beaker containing piranha solution (3:1 ratio of sulfuric acid: hydrogen peroxide) for 10 minutes. Following that, they were immersed in a beaker containing HPLC grade water. A polishing pad soaked with alumina slurry (0.05  $\mu$ M diameter) was used for the polishing process. The electrode was rubbed against the polishing pad in a figure of eight motion for 3 minutes, after which it was rinsed with a mixture of 50:50 water and ethanol. The electrode was then immersed in a beaker containing ethanol and sonicated for 5 minutes. The process was repeated with a beaker containing HPLC grade water. The clean electrodes were then stored in a beaker containing ethanol until ready for use (Fischer et al. 2009).

#### 3.2.2.3 Electrochemical activation of gold working electrodes

A 10mL electrochemistry beaker with a fitting Teflon cap was filled with a solution of 0.5M Sulfuric acid. The salt bridge was rinsed and filled with 10mM PBS pH 7.4 and placed in the beaker. The reference electrode was rinsed with HPLC water and placed inside the salt bridge. The platinum counter electrode was rinsed with HPLC water and placed inside the beaker. Finally, the clean gold electrode was rinsed with HPLC water, dried under nitrogen and placed inside the beaker. All electrodes were connected to the potentiostat and Cyclic Voltammetry was performed until there were no changes observed between consecutive voltammograms (approximately 25 cycles) (Fischer et al. 2009). The potential ranged from 0 to 1.5 V and the scan rate was equal to 100 mV/sec (Fischer et al. 2009). The electrochemically activated gold electrodes were rinsed with HPLC water and dried under nitrogen.

#### *3.2.2.4 Development of self-assembled monolayers (SAMs)*

Following the thorough cleaning and polishing of the gold electrodes, which ensured the surface was residue-free, the next step was the modification of the gold electrodes using aptamers and alkanethiols.

In this study, three alkanethiols were chosen for evaluation -mercaptohexanol (MCH), mercaptoundecanoic acid (MUA) and dithiodibutyric acid (DTBA) -as well as the anti-endotoxin aptamer. All components were dissolved in immobilization buffer enriched with 100 mM NaCl (pH 7.4) (Zhang et al. 2007). In this study, the final aptamer concentration was 1 $\mu$ M. As DTBA exhibits poor aqueous solubility, it was dissolved in a buffer / ethanol solution (50:50). The final TECP concentration was 0.5 mM. Following the preparation of alkanethiols or the aptamer/alkanethiol mixture (1:20 aptamer:DTBA ratio), the electrodes were immersed in 100  $\mu$ L of the solution and incubated either overnight at 2-8°C, or for an hour under ambient conditions.

#### *3.2.2.5 Electropolymerization of 3-aminophenylboronic acid (APBA)*

A 5 mM solution of 3-aminophenylboronic acid (APBA) was prepared in 100 mM PBS pH 5.0 enriched with 120 mM NaF. The applied potential was cycled from -0.2 to 0.7 V with a step of 10 mV and scan rate of 50 mV/sec (38).

Following polymerisation, the modified electrodes were immediately immersed into 10 mM [Fe(CN)<sub>6</sub><sup>3-/4-</sup>] | 10 mM PBS pH 7.4 and allowed to stabilise. CV and EIS were used to confirm growth of a polymer layer. Once a stable baseline reading had been obtained, polymers were incubated with range of endotoxin concentrations (10 fg/mL – 1 ng/mL), with EIS being used to monitor the interaction with the polymer surface.

#### *3.2.2.6 Surface imprinting and development of conventional MIPs*

To create a conventional MIP, bare electrodes were immersed for an hour at room temperature in a 100 pg/ml solution of control standard endotoxin dissolved in HPLC water, allowing endotoxin to deposit on the electrode surface. Before electropolymerization with APBA, the electrodes were rinsed with 10 mM PBS pH 7.4 to remove any non-chemisorbed endotoxin. Endotoxin presence was confirmed by performing EIS and noting an impedance of approximately 2 k $\Omega$ , similar to the values observed by previous lab members (Demertzis, 2019). After being washed, the polymers were then challenged with 10, 20, and 50 pg/ml of endotoxin. The binding performance of the MIP was assessed using EIS. A non-imprinted control was produced in the same manner but in the absence of endotoxin (NIP).

#### *3.2.2.7 Surface imprinting and development of a hybrid MIP*

In accordance with the protocol described in section 3.2.2.1, 10  $\mu$ M of freshly thawed anti-endotoxin aptamer was incubated with 10  $\mu$ M LPS in folding buffer for 45 minutes to allow complex formation. After being diluted to 1  $\mu$ M, the aptamer-endotoxin complex was incubated with 1 mM TCEP in immobilization buffer for 5 minutes. The electrodes were then immersed in this solution overnight at 2-8°C. The electrodes were rinsed with 10 mM PBS pH 7.4 to remove any non-attached complexes and placed into an electrochemistry beaker filled with a degassed solution of APBA plus NaF (5 mM and 120 mM). CV and EIS were used to confirm growth of a polymer layer. A non-imprinted control was produced in the same manner, except that endotoxin was washed away before polymerization (AptaNIP).

#### *3.2.2.8 Polymer washing / regeneration*

The electrodes were subsequently immersed in a solution containing 0.1 % Tween 20 for 5 minutes followed by 10 mM PBS pH 7.4 for another 5 minutes. The electrodes were then stored in 10 mM [Fe(CN)<sub>6</sub><sup>3-/4-</sup>] 10 mM PBS pH 7.4 and left to stabilise, before performing EIS again.

### **3.2.3 Sensor characterization**

#### *3.2.3.1 Electrochemical impedance spectroscopy (EIS)*

The electrochemical impedance spectrum consists of two parts. The first step involves a short pre-treatment period that lasts 30 seconds, during which a potential of 0.2 V is applied. Following that, the potentiostat applies 61 frequencies ranging from 10 kHz to 100 MHz, with a 10m V a.c. voltage superimposed on a bias d.c. voltage of 0.2 V versus an Ag / Ag/Cl reference electrode, in an electrochemical cell containing 10 mM [Fe(CN)<sub>6</sub><sup>3-/4-</sup>] in 10 mM PBS pH 7.4.

To determine baseline impedance, EIS responses of each SAM (alkanethiol +/- anti-LPS aptamer) were recorded at least three times.

### *3.2.3.2 Evaluation of binding performance*

Prior to any characterization process, blank measurements were taken, with a minimum of three readings, separated by a time interval equivalent to that of the incubation process. Each monolayer was challenged with various concentrations of Control Standard Endotoxin (Shah et al.). The SAM-modified electrodes were incubated with 100  $\mu$ L of endotoxin (concentrations vary) in either 10 mM PBS pH 7.4, TE buffer pH 8, or MES buffer pH 5.4. The endotoxin's interactions with the SAMs resulted in changes in impedance at the electrode/electrolyte interface, which were measured using EIS. To detach any loosely associated endotoxin, the electrodes were rinsed with 10 mM PBS pH 7.4 prior to measurement.

For the imprinted systems, again blank measurements were taken, with a minimum of three readings, separated by a time interval equivalent to that of the incubation process. Each system was challenged with various concentrations of Control Standard Endotoxin (Shah et al.) in PBS pH 7.4. To detach any loosely associated endotoxin, the electrodes were gently rinsed with 10 mM PBS pH 7.4.

### 3.3 Results and Discussion

#### 3.3.1 Electrochemical activation of working electrodes

As mentioned before, the cleanliness of the gold electrodes is essential for the generation of reliable and replicable results, as impurities may interfere with gold-thiol bond formation and therefore SAM formation, or endotoxin binding. In literature, Cyclic voltammetry (Kitsios et al.) is commonly used to evaluate and monitor the cleaning and functionalization process of gold electrodes.

During the CV cleaning process, three oxidation peaks can be observed, in the region of 1.35–1.6 V, in addition to a single reduction peak can be observed between 1.0 – 08 V, visible in figure 3.11 (Cherevko et al. 2013). The degree to which the gold surface is residue-free is indicated by the sharpness of each peak. It can be seen from figure 3.11 that the sharpness of the peaks improves with the increase in CV cycles.

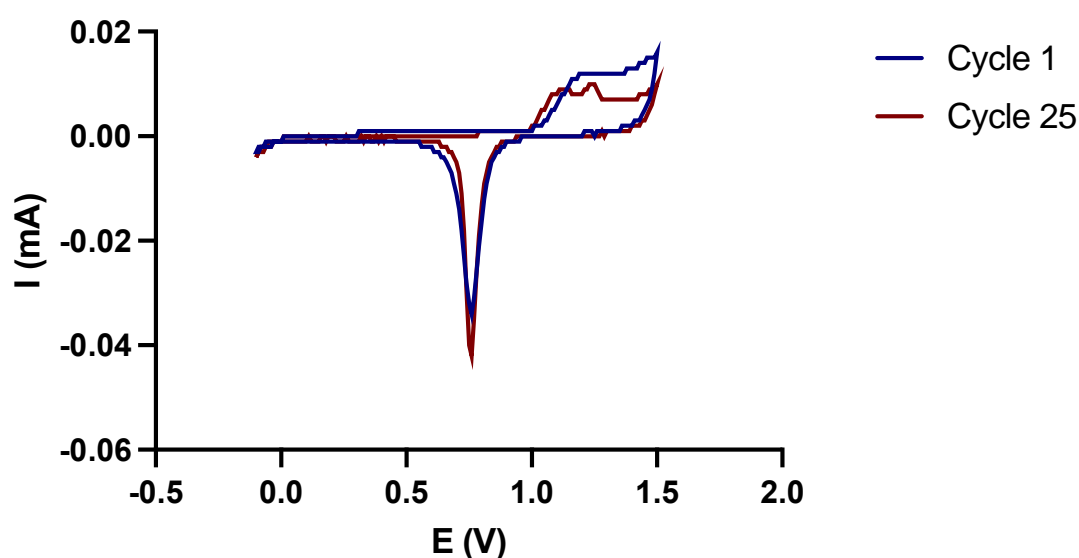


*Figure 3.11: Cyclic voltammogram showing the cleaning process of a gold electrode. The sharpness of the oxidation and reduction peaks improves between cycles 1 – 25. The process was repeated until no further changes in the voltammogram were observed.*

#### 3.3.2 Development of an aptasensor for recognition of endotoxin

The single-stranded aptamer sequence used in this study was developed by Kim et al. and has exhibited its sensitivity and specificity in the detection of endotoxin. This aptamer has also been used by the researcher's group in the past for the development of electrochemical biosensors, where its performance was optimized further, and its sensitivity and specificity were demonstrated (Demertzis, 2019; Kim, 2012). As the main endotoxin used in this study (control standard endotoxin) is different from the endotoxin used in those previous studies,

it was considered worthwhile to assess the behavior of the SAMs and the aptamers with CSE as well as further optimize the sensor.

### 3.3.2.1 Screening of alkanethiols as spacer molecules

While performing a screening process for suitable alkanethiols, it is important to consider the strong negative charge on endotoxin, which is caused by the phosphorylated sugar molecules found in the core and O-antigen regions (Demmer et al. 2003). The alkanethiols chosen for use in this project were 6-mercaptohexanol (MCH), which is neutral at physiological pH, 11-mercaptopundecanoic acid (MUA) and 4,4-dithiodibutyric acid (DTBA), both of which have a negative charge (PubChem, 2023). It was anticipated that a negatively charged surface would prevent non-specific adsorption of endotoxin on the gold electrode surface but it is also important that it does not interfere with the binding of the endotoxin on the aptamer. It was considered likely that the length of the alkanethiol may have an impact on aptamer binding, hence the selection of two different negatively charged molecules; one with 11 carbons and the other with four.

Figure 3.12 shows the EIS results obtained from the monolayers formed by each alkanethiol. DTBA, MCH and MUA were used at concentrations of 40mM, 25mM and 1mM. The results were similar to those obtained by the researcher's group in the past (Demertzis, 2020). More specifically, MCH was expected to show the lowest impedance, since it is made up of six carbons and a hydroxyl group (PubChem, 2023). In contrast, DTBA was expected to show a higher impedance compared to MCH, as it is a larger molecule comprising two butyric acid molecules connected by a disulphide which is reduced upon interaction with the gold surface (PubChem, 2023). DTBA is well known for forming highly ordered, closely packed monolayers, which explains the increase in impedance (Jang and Keng 2008). Finally, MUA exhibited the highest impedances, which was expected, as MUA consists of 11 carbons and a negatively charged carboxylic acid head group (Jang and Keng 2008).

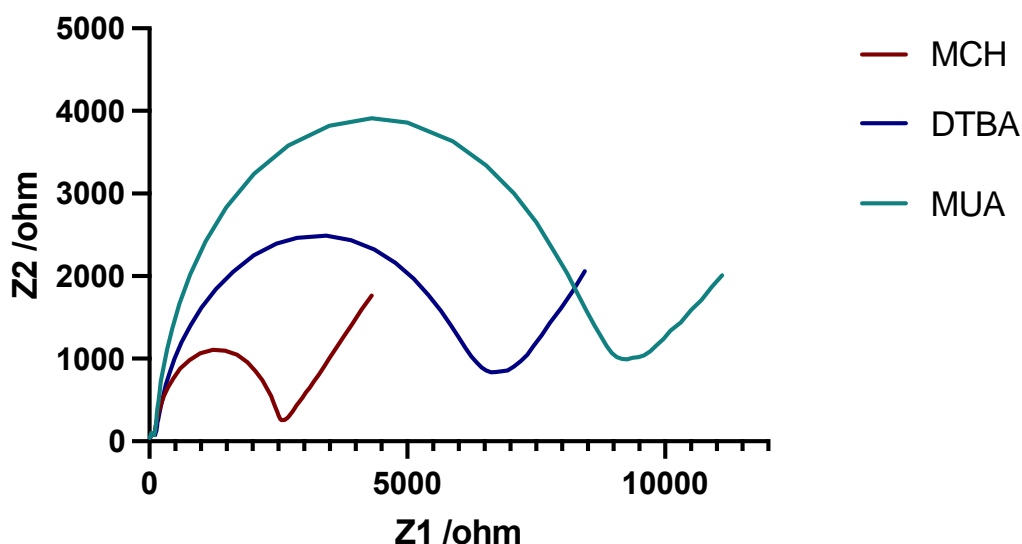


Figure 3.12: Electrochemical impedance spectra of 6-mercaptohexanol (MCH), 4,4-dithiodibutyric acid (DTBA) and 11-mercaptoundecanoic acid (MUA) modified gold electrodes.  $N=3$  for each alkanethiol. EIS curves are exemplar for each molecule.

Additionally, it was considered worthwhile to assess the interactions between the three alkanethiols and the reduced (“activated”) aptamers. Clean gold electrodes were incubated with the relevant alkanethiol in triplicate at ambient temperature for 1hr, away from direct sunlight. The modified electrodes were rinsed with endotoxin-free water and baseline EIS measurements were performed. Subsequently, the modified electrodes were incubated with the reduced aptamer (1 $\mu$ M) for 5 minutes at ambient temperature. Electrodes were then rinsed with endotoxin-free water and EIS measurements were performed.

According to figure 3.13, DTBA shows little interaction with the reduced aptamer, whereas MCH and MUA both show a small degree of interaction. MCH, although widely used in biosensors, shows a number of drawbacks such as less ordered monolayers which may contain defects or gaps which may allow for aptamer attachment at the gold surface (Oberhaus et al. 2020). This is well-reported in the literature and could provide an explanation regarding the increase in impedance (Lao et al. 2005; Keighley et al. 2008). MCH-based sensors have also shown susceptibility to biofouling, although mostly by proteins (Jolly et al. 2015). DTBA and MUA contain a carboxyl group that provides negative surface charge, which provides electrostatic repulsion against negatively charged DNA (Meng et al. 2018). This may explain the relatively low interaction with the aptamer by those alkanethiols. The greater interaction observed with MUA may be explained by the fact that larger alkanethiols, such as MUA, are prone to leaving gaps on the electrode surface where the aptamers may attach (Richards et al. 2010).

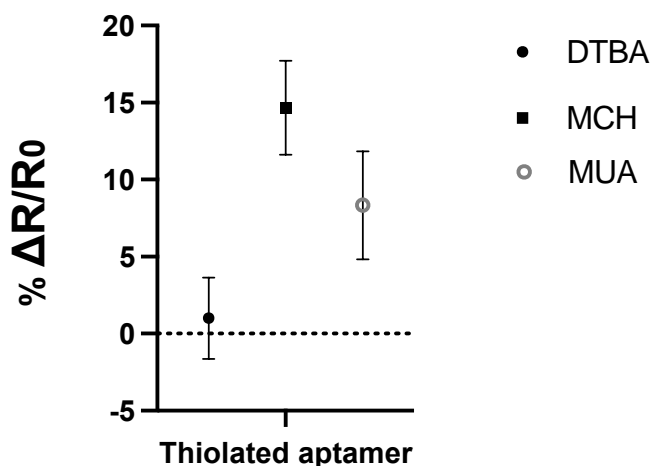


Figure 3.13: SAMs were challenged with reduced (“activated”) aptamers. DTBA shows very little interaction, whereas an increase in impedance can be observed with MCH and MUA.

### 3.2.2.2 Evaluation of alkanethiol interaction with endotoxin

A screening process was performed to assess the suitability of the three alkanethiols under various pH. As non-specific adsorption is an issue in the development of biosensors, especially those targeting endotoxin, it was important that the chosen alkanethiol would exhibit minimal binding to endotoxin. Therefore, alkanethiol-only SAMs were developed and were subsequently challenged with 0.1, 1, 10, 100 and 1000 pg/mL of endotoxin. To explore effects of pH and charge on the interaction, screening experiments were performed in 10mM PBS pH 7.4, TE buffer pH 8 (10 mM Tris, 1 mM EDTA), 50mM MES buffer pH 4.9 (Figures 3.14, 3.15 and 3.16 respectively).

Across all buffers used in this experiment, MUA demonstrated the highest interaction with endotoxin, especially at higher concentrations (> 10 pg/mL). In *PBS*, at endotoxin concentrations higher than 10 pg/mL, an average increase of approximately 37% is observed (Figure 3.14). Similarly, in TE buffer, an average increase of 20% is seen for the same alkanethiol (Figure 3.15). In *MES* buffer, a lower increase in impedance of approximately 8% is noted (Figure 3.16). Beyond the simple increase in size of MUA compared to the other two alkanethiols investigated, it is known that larger molecules are prone to forming disordered monolayers which may contain gaps at the electrode surface where endotoxin may bind (Richards et al. 2010). Additionally, it has been reported that carboxylic acid terminating alkanethiols tend to form more disordered monolayers, which may also affect MUA impedances (Kepley et al. 1992).

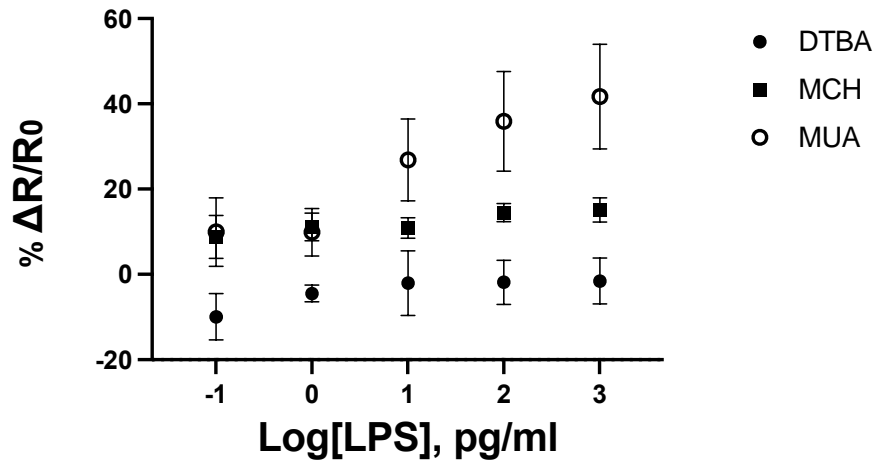


Figure 3.14. DTBA, MCH and MUA SAMs were challenged with endotoxin concentrations ranging from 0.1 to 1000 pg/mL in **PBS pH 7.4**. MCH and DTBA show little interaction with endotoxin whereas MUA shows significant interaction with endotoxin at higher concentrations (10, 100 and 1000 pg/mL)

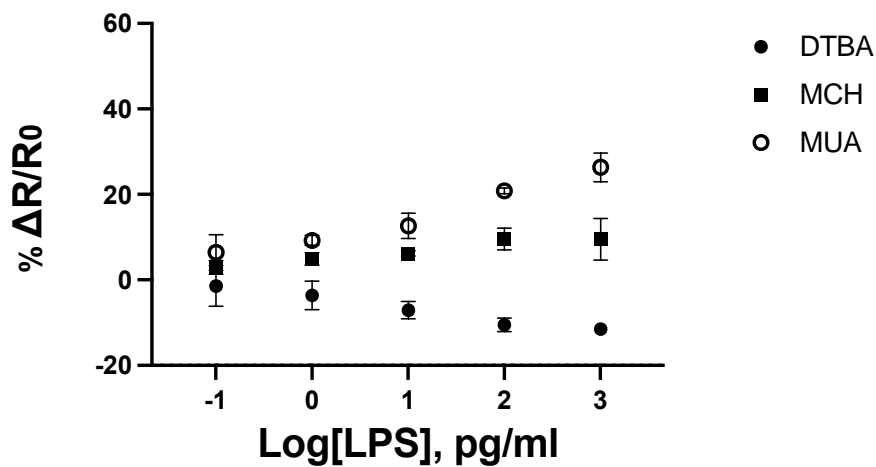


Figure 3.15. DTBA, MCH and MUA SAMs were challenged with endotoxin concentrations ranging from 0.1 to 1000 pg/mL in **TE buffer pH 8**. MCH and DTBA show little interaction with endotoxin whereas MUA shows significant interaction with endotoxin at higher concentrations (1, 10, 100 and 1000 pg/mL)

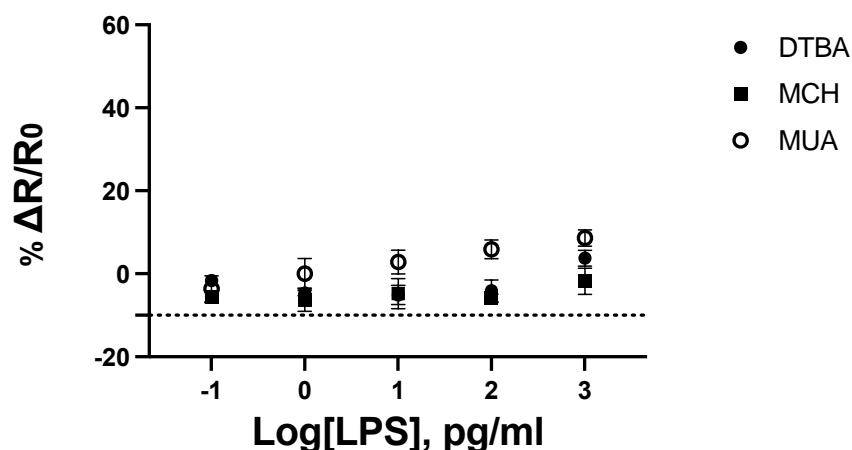


Figure 3.16: DTBA, MCH and MUA SAMs were challenged with endotoxin concentrations ranging from 0.1 to 1000 pg/mL in MES buffer pH 4.9. MCH and DTBA show little interaction with endotoxin whereas MUA shows significant interaction with endotoxin at higher concentrations (1, 10, 100 and 1000 pg/mL)

According to literature, MCH is the most commonly used alkanethiol in biosensors, and was used by the group who developed the aptamer used in this project (Kim et al. 2012). MCH contains 6 carbon atoms and a hydroxyl group, making it a neutral spacer molecule, which may explain the small degree of interaction with endotoxin throughout all three graphs (Figure 3.15 – 3.16). There is also less variation in response between the different buffer systems for this alkanethiol. Previous work in the researcher’s group has shown that MCH interacts strongly with endotoxin, with an average increase in impedance of approximately 50% (Demertzis, 2019). The results presented here show an increase in impedance of approximately 17% in PBS (figure 3.14), 8% in TE buffer (figure 3.15) and very little change in impedance in MES buffer (figure 3.16), suggesting some interaction with endotoxin in neutral and alkaline pH. The difference in interaction may be partly explained by the different endotoxins used. (FITC-conjugated endotoxin by Demertzis vs CSE endotoxin in this study).

It is evident from this data that pH plays a role in the interaction between endotoxin and the SAMs. Changes in pH affect not only the charge of the alkanethiols but also the charge on endotoxin. In physiological conditions or in alkaline pHs, such as when PBS or TE buffer is used, the negatively charged electrolytes present in the solution used for EIS ( $\text{Fe}(\text{CN})_6^{3-/4-}$ ) cannot access the surface of the gold electrode due to the negative charge associated with deprotonated carboxyl groups present in DTBA and MUA. This gives rise to larger impedances. When the negative charge on the surface of the gold electrode is reduced, through protonation of the carboxyl groups at pHs below the pKa of the alkanethiol, then the electrolytes can more readily access the surface of the gold electrode, leading to lower impedances, as is evident in Figure 3.16 (Kim et al. 2012). Moreover, the charge of endotoxin needs to be taken into account. Endotoxin has an isoelectric point of approximately 2, which results in a strong negative charge at most pHs (Reich et al. 2019). This was the reason that a

positively charged alkanethiol was not selected as part of the screening process, as strong charge-charge interactions were foreseen. Tris, which is present in TE buffer, contains a primary amine that is positively charged at  $\text{pH} < 8.06$ , which was the case in this study ( $\text{pH} 8$ ). Tris has been shown to interact with carboxylic acids (Šípová-Jungová et al. 2021). In particular, this interaction has been shown to reduce the negative charge of the carboxylic acids, which leads to the generation of lower impedances (figure 3.15).

Overall, it can be concluded that regardless of the buffer used, DTBA consistently shows the least interaction with endotoxin. DTBA carries two carboxylic acid groups, which provides a stronger negative charge, which may inhibit the interaction with endotoxin, causing little to no increase in impedance. Additionally, this effect may be enhanced by the better packing of the monolayer, caused by the short length of the molecule, as well as the disulphide bond in the center of the chain which, when reduced at the gold surface, leaves two butyric acid molecules in close proximity to one another (Jang and Keng 2008). Therefore, it will be the alkanethiol taken forward in the development of the aptasensor.

### **3.3.3 Endotoxin sensor characterization**

Previous work in the researcher's lab has determined that the optimal working ratio between the aptamer and DTBA is  $1 \mu\text{M}$  of aptamer to  $20 \mu\text{M}$  of DTBA (Demertzis, 2020). As DTBA is reduced at the gold surface to produce two spacer molecules, an aptamer:DTBA ratio of 1:20 corresponds to an aptamer:spacer ratio of 1:40. Indeed, this ratio of aptamer:DTBA produced a sensor with similar characteristics as the one developed in the past by the researcher's group.

During the development of a biosensor, there are several parameters that need to be evaluated, such as reproducibility, sensitivity and dynamic range (Thevenot et al. 2001):

#### **3.3.3.1 Sensor stability, reproducibility and sensitivity**

Three important features that affect the sensor's performance are stability, reproducibility, and sensitivity.

Aptasensors were produced in triplicate to determine their reproducibility. A baseline impedance of  $12.39 \text{ k}\Omega$ , with a standard deviation (SD) of  $0.088$  (CV of  $0.71\%$ ) was observed. Although it varies with analyte and assay methodology, a CV (Coefficient of Variation) of  $5\%$  (intra-assay) or  $10\%$  (inter-assay) is considered acceptable from a biosensing / diagnostics perspective (Chatziharalambous et al. 2016). The system's noise is defined as the standard deviation, therefore an increase in impedance would be considered significant only if the higher than  $0.264 \text{ k}\Omega$  ( $3 \times \text{SD}$ ).

The aptasensor was challenged with a variety of endotoxin concentrations ranging from 10 fg/mL up to 100 ng/mL, with 3 replicates for each concentration to ascertain the sensor's sensitivity and enable the estimation of the limit of detection. The EIS results are presented in figure 3.17 below. The lowest endotoxin concentration that the aptasensor was capable of detecting was 50 fg/mL, which gave rise to an increase in Rct of > 2 kΩ, which is greater than the 3 x SD limit of 0.264 kΩ. Increasing concentrations of endotoxin resulted in higher impedances. However, satisfactory linearity is only shown between endotoxin concentrations of 0.5 pg/mL and 1 ng/mL, with an  $r^2$  of 0.9810 and  $r$  of 0.9904 (Figure 3.18).

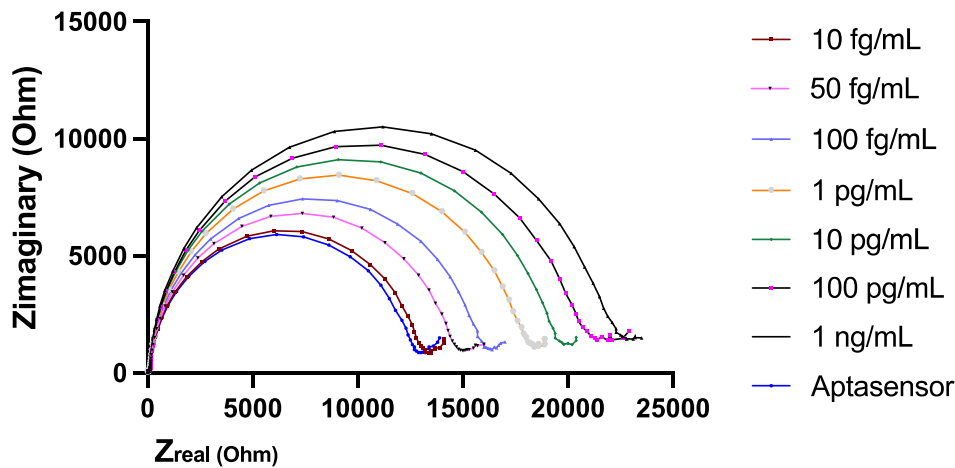


Figure 3.17: Exemplar EIS graph showing the impedances of the aptasensor in PBS (N=3) following challenge with various concentrations of endotoxin (0.01 pg/mL up to 1000 pg/mL).

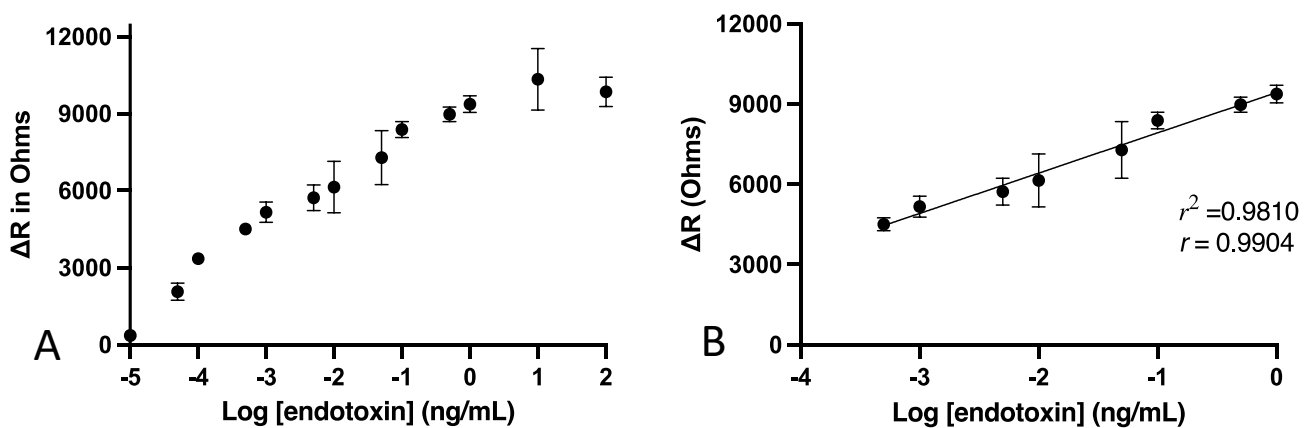


Figure 3.18.A and 3.18.B. Figure A shows the sensor's differences in impedance following challenge with various concentrations of endotoxin (from 10 fg/mL up to 100 ng/mL). Figure B shows the dynamic range of the sensor, exhibiting good linearity between 0.5 pg/mL up to 1 ng/mL ( $r^2=0.9810$ ).

The results generated from this study are comparable with other studies found in literature that utilize the same aptamer. Kim et al., who developed the aptamer used in this study and used MCH as a spacer, reported a limit of detection of 10 pg/mL (Kim et al. 2012). Su et al.,

who employed 3-mercaptopropionic acid as a spacer and EDC/NHS chemistry to attach the aptamer determined a LOD of 1 pg/mL (Su et al. 2012). Those two studies, where the aptamer was used without any sensitizers, report similar results and LOD with the results of this project.

Other sensors utilizing different methodologies using the same aptamer have been described in the literature, the majority of which employ sensitizers or alternative detection methods. Duan et al. have constructed a sandwich signal amplification aptasensor with a LOD of 0.05 pg/mL. To amplify the signal generated by the aptamer, a copper ion-mediated gold nanoparticle aggregate was used, and differential pulse voltammetry was used to determine endotoxin binding. Despite the remarkable detection limit, the fabrication process is more complicated and time-consuming (Wang et al. 2019).

Bai et al. have developed a sensor using a three-way DNA junction-aided enzymatic recycling system in combination with graphene and toluidine blue nanohybrid plus gold nanoparticles for amplification. The sensor had a LOD of 8.7 pg/mL, however the process of developing the sensitizers is complicated and laborious and includes a long incubation time (>48hrs) (Bai et al. 2014).

Ma et al. used polyethylenimine coated magnetic nanoparticles to which the aptamer conjugated to a fluorophore was attached to capture and detect endotoxin through fluorescence measurements. A detection range from 35 ng/mL up to 10 $\mu$ g/mL was reported (Ma et al. 2018b).

More recently, Tian et al. developed a sensitive platform for the detection of endotoxin. In this platform, a silver-nanoparticle decorated titanium dioxide nanotube was modified with polydiallyldimethylammonium chloride (PDDA) functionalized reduced graphene oxide to form a new nanohybrid with a large surface area, on to which the aptamer was immobilized. Cyclic voltammetry was used to determine endotoxin binding and a LOD of 5 fg/mL was determined (Tian et al. 2021). The same group, a year later, developed a sandwich-type electrochemical endotoxin sensor utilizing the same aptamer with a LOD of 0.55 fg/mL. Specifically, nitrogen-doped carbon nanotubes were functionalized with polydiallyldimethylammonium chloride, forming a nanocomposite. Following that, an iron-based metal-organic framework and silver nanoparticles were functionalized with the previously formed nanocomposite. Differential pulse voltammetry was used for the electrochemical measurements (Mu et al. 2022).

Posha et al. developed an electrochemical aptasensor that utilizes aptamers immobilized on gold clusters, which allows for sensitive detection of endotoxin through differential pulse voltammetry and EIS. In this method, the aptamer was immobilized on the surface of the gold clusters and then on the gold electrodes. A remarkable detection limit of 7.94 zM, with a dynamic range of 0.01 aM to 1pM was reported (Posha et al. 2018). Despite the impressive

detection limit, it is important to emphasize that oversensitive detection isn't necessarily a priority in clinical sample detection. A background endotoxin level of approximately 0.001 – 0.01 EU/mL is always present in blood samples, which means that oversensitivity may not provide valuable clinical information (Pearson et al. 1985; Nadhazi et al. 2002). Additionally, many sensors cannot be used in blood plasma, as it is one of the most challenging sample matrices or require extensive preparation time and expensive reagents. Therefore, an ideal sensor needs to be sufficiently sensitive as well as applicable to clinical samples.

Interestingly, a shear horizontal surface acoustic wave biosensor utilizing the same aptamer was developed by Ji et al., with a LOD of 3.53 ng/mL, however the fabrication process was lengthy and complicated (Ji et al. 2020). Finally, Zamani et al. used aptamer conjugated magnetic Fe<sub>3</sub>O<sub>4</sub> nanoparticles that were modified with the addition of gold. The aptamer sequence was chemically modified and thiourea was used to attach the sequence to the nanoparticles. Methylene blue was used as a sensitizer to enhance sensitivity. Electrochemical methods were used to characterize the sensor and the final aptasensor had a LOD of 0.2 fg/mL (Zamani et al. 2022).

In general, the sensor developed in this study exhibits satisfactory performance. A main advantage of this aptasensor is the ease of fabrication, as the thiolated end of the aptamer provides a straightforward attachment method. Additionally, provided that the electrodes are sufficiently cleaned and polished beforehand, the sensor can be fabricated in about 1 ½ hours under ambient conditions.

Using a one site total binding model in GraphPad Prism (Version 9) a dissociation constant ( $K_d$ ) for the developed system has been estimated (Figure 3.19). To calculate this parameter, the endotoxin concentrations has been converted to pM. Using this model, an apparent  $K_d$  of 6.5 pM has been determined. The  $r^2$  value is 0.9443. The sensor's maximum response is determined at 81%, which is achieved at 200 pM endotoxin. The buffer used in this study was PBS at pH 7.4.

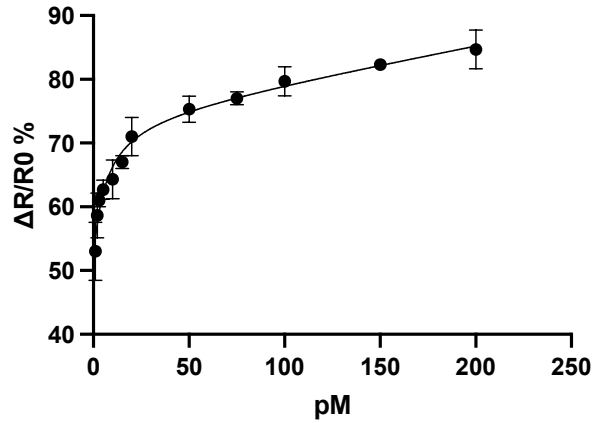


Figure 3.19: The aptasensor was challenged with a range of endotoxin concentrations, ranging from 0.002pM (0.01 pg/mL) up to 200 pM (1 ng/mL) to determine its binding performance. A one site-total model was used, showing a good fit with a  $R^2$  of 0.9443.

### 3.3.3.2 Performance in MES and TRIS buffers

Given the use of acid / base treatment in the sample pre-treatment protocol developed in Chapter 2, it was decided to explore the performance of the aptasensor in acidic or alkaline pH conditions. The aptasensor was therefore challenged with a series of endotoxin concentrations ranging from 10 fg/mL up to 100 ng/mL, in either MES buffer (pH 5.4) or TE buffer (pH 8). Figures 3.20 and 3.21 show the sensor's behaviour in MES and TRIS buffer respectively.

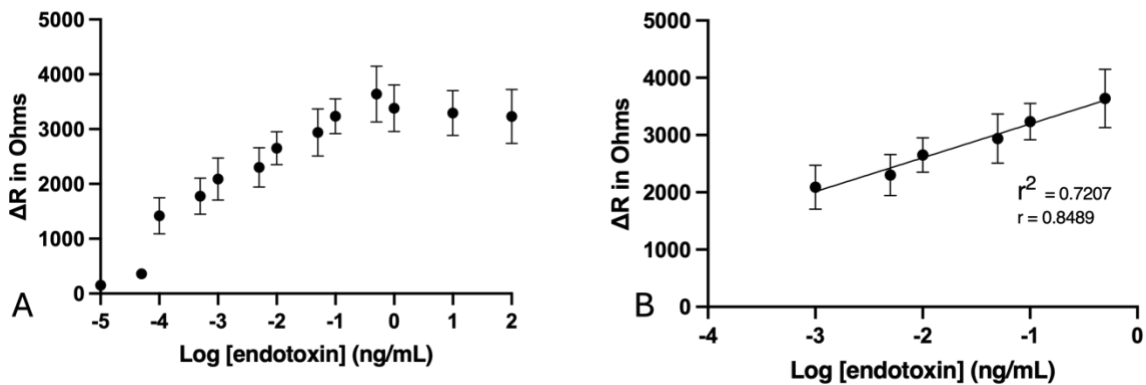


Figure 3.20 A and B: Figure A shows the sensor's differences in impedance in MES buffer pH 4.9 following challenge with various concentrations of endotoxin (from 10 fg/mL up to 100 ng/mL). Figure B shows the dynamic range of the sensor, exhibiting linearity between 1 pg/mL and 500 pg/mL.

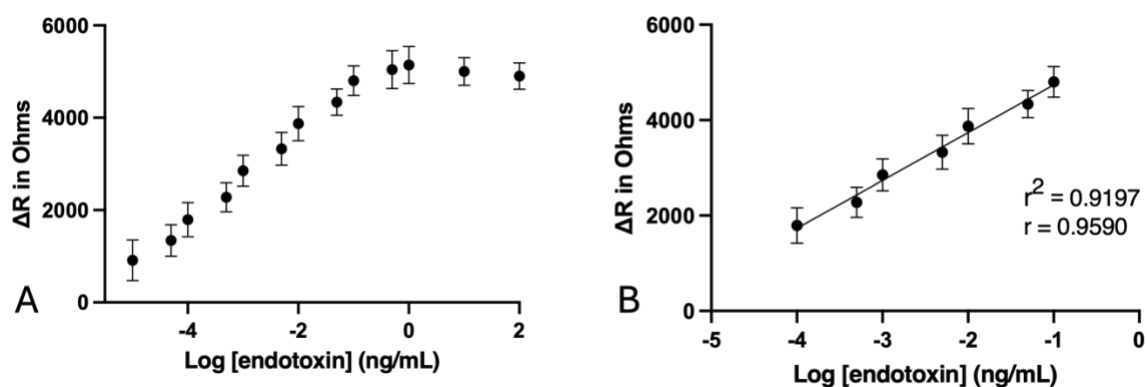


Figure 3.21 A and B: Figure A shows the sensor's differences in impedance in **TRIS buffer pH 8** following challenge with various concentrations of endotoxin (from 10 fg/mL up to 100 ng/mL). Figure B shows the dynamic range of the sensor, exhibiting linearity between 0.1 pg/mL and 100 pg/mL.

According to figures 3.20 and 3.21, endotoxin detection in both MES and TRIS buffers is feasible, however larger error bars, in comparison with detection in PBS, can be noted. Moreover, in MES, a decrease in the dynamic range (1 pg/mL – 500 pg/mL compared to 0.5 pg/mL – 1 ng/mL in PBS) is observed.

It has been reported in the literature that Tris buffer interacts with carboxylic groups on SAMs, as well as short DNA molecules (Šípová-Jungová et al. 2021). The same study also found that Tris buffer can also interact with either single-stranded or double-stranded DNA, which may also affect the results presented in this study. Interestingly, the dynamic range of the sensor in TRIS buffer retains relatively good linearity and sensitivity (0.1 pg/mL to 100 pg/mL).

One issue often faced with aptamers is the lack of information regarding their molecular interaction with the target. Neither the group that designed the aptamer, nor any studies utilizing it have explored its binding with endotoxin. Compared to protein-protein interactions, where *in silico* methods can provide valuable information, very few published workflows are available to study aptamer-target interactions. The researcher attempted to use online computational modelling servers (3DRNA and HDOCK) to understand molecular level interactions, with no success, as the complicated and non-defined structure of endotoxin compared with the limited available tools for aptamer modelling posed a challenge. Methods that can be used to assess aptamer-target interaction include Isothermal titration calorimetry (ITC), which can provide a complete set of the thermodynamic binding parameters (Slavkovic, 2023). Mass spectroscopy, combined with ion mobility MS, can also be used to examine aptamer-ligand interactions and conformational changes (Daems et al. 2021). Other techniques include fluorescence anisotropy, x-ray crystallography (mostly on aptamer-protein interactions) and solution- state Nuclear Magnetic Resonance (NMR), which provides information on binding at a molecular level and the location of the interactions (Zhao, 2020, Bottari, 2020).

### 3.3.5 Development and optimization of a hybrid molecularly imprinted polymer

#### 3.3.5.1 APBA polymerization

Previous work in this lab had focused on the development and optimization of a hybrid-MIP, where 50mM 3-aminobenzoic acid (APBA) was used to create a hybrid recognition system for the sensitive detection of endotoxin in aqueous solutions. However, upon the introduction of serum spiked with endotoxin, even after significant dilution (1 in 100,000) resulted in very high background “noise” levels, high levels of biofouling and low levels of endotoxin detection (Demertzis, 2019). Therefore, work in this section will be focused on recreating and optimizing the hybrid-MIP system for use in clinical samples.

In the previous sections, the fabrication and testing of an electrochemical aptasensor for the detection of endotoxin was described. Despite the encouraging results, there was room for improvement regarding the sensitivity and dynamic range of the sensor. Previous work in the researcher’s lab had focused on the development of a molecularly imprinted polymer for endotoxin, as well as the implementation of a hybrid imprinting strategy utilizing aptamers in conjunction with polymers, with remarkable results in aqueous solutions (Demertzis, 2019).

To electrochemically polymerize the APBA, the working electrode was immersed in a degassed solution of APBA and up to 10 cycles of polymerization were performed. Based on previous research, it was assumed that 10 cycles would result in the formation of a complete polymer layer on the working electrode surface (Demertzis, 2019). Figure 3.22 shows the electropolymerization of APBA.

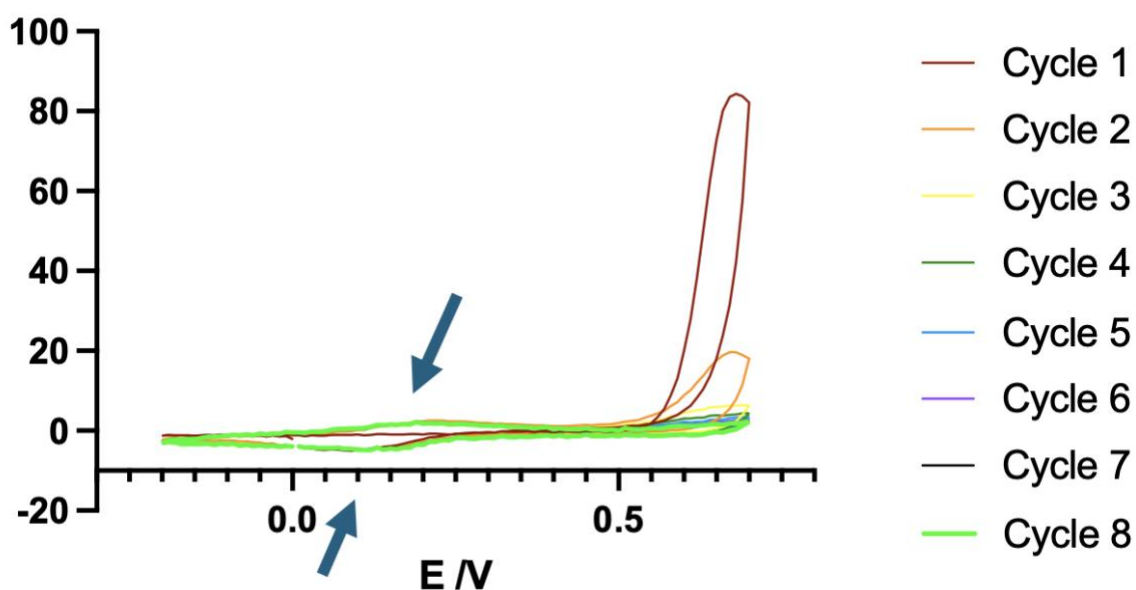
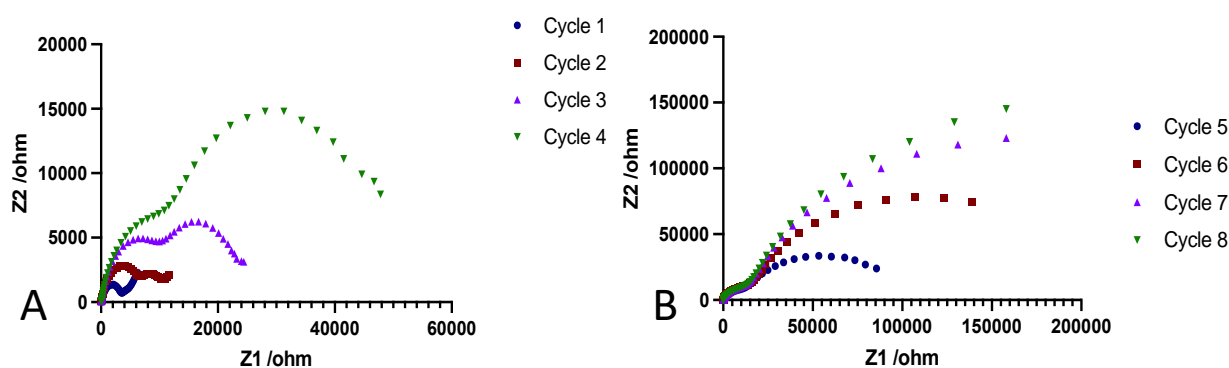


Figure 3.22: Voltammogram obtained following the polymerization of APBA (10 cycles). PAPBA is conducting in nature, as indicated by the increasing redox peaks, indicated by arrows.

PAPBA is a conducting polymer, which is evidenced by the presence of increasing redox peaks with each polymerization cycle (Ciftci et al. 2014). In figure 3.22, two increasing peaks in the polymerization voltammogram can be observed, close to 0.2 V.

Figures 3.23 A and B show the EIS spectra of each polymer layer developed on the working electrode from the electropolymerization of 50 mM APBA. From cycles 1-4, a gradual increase in impedance can be observed, associated with the growth of the polymer layer. From cycles 4-5, impedances began to increase steeply, with values reaching over 100 kΩ. As impedance values after 5 cycles of endotoxin were too high to work with, it was decided to reduce the working concentration of APBA down to 25mM for all future experiments.



Figures 3.23 A and B: EIS graphs showing the impedances obtained after each cycle (1-4) of APBA (50mM) polymerization. An increase in impedance is noted with each subsequent cycle.

Figure 3.24 shows the EIS spectra of polymer growth following 5, 7 and 10 cycles of polymerization, using an APBA concentration of 25mM. Compared to figures 3.23, lower impedances were noted for the recorded cycles, and better control was obtained over the thickness of the polymer.

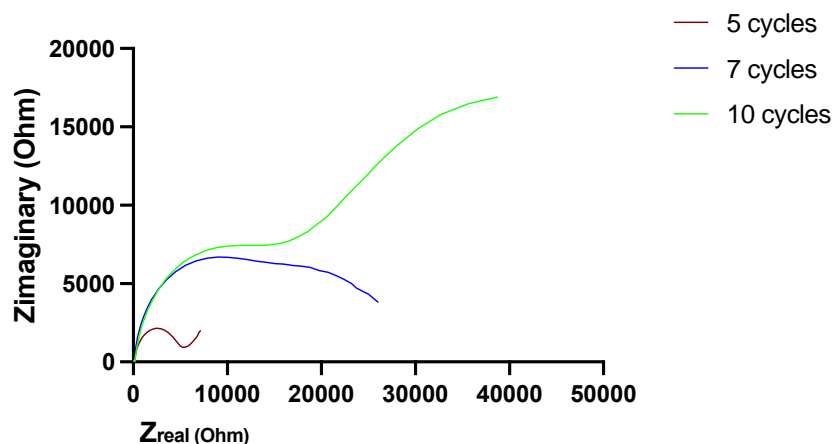
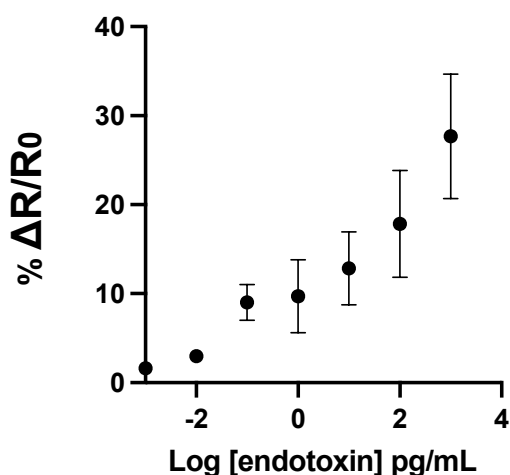


Figure 3.24: EIS graphs showing the impedances obtained after cycles 5, 7 and 10 of APBA electropolymerization (25mM). An increase in impedance is noted with each subsequent cycle.

### 3.3.5.2 Development of APBA non-imprinted polymer

Having optimized polymer formation, non-imprinted polymers (NIPs) consisting of only PAPBA on the surface of the gold electrodes, at a concentration of 25mM, were fabricated. Following thorough cleaning and polishing, the electrode was immersed into the degassed monomer solution and polymerization was performed for 7 cycles. The electrodes were then rinsed carefully with PBS and incubated in PBS until a stable reading was achieved. NIPs were produced in triplicate to determine their reproducibility, and an average baseline impedance of 16.1 k $\Omega$  was noted, with a standard deviation of 0.8735 (CV of 3.67%).

The NIPs were incubated in ambient conditions for 5 minutes with a variety of endotoxin concentrations ranging from 1 fg/mL up to 1 ng/mL, with 3 replicates for each concentration. EIS responses following incubation with increasing concentrations of endotoxin were small and fairly indistinguishable from one another until concentrations exceeded 10 pg/mL (Figure 3.25).



*Figure 3.25 Dose response graph of the NIP when challenged with a variety of endotoxin concentrations, ranging from 1 fg/mL to 100 pg/mL. The NIP shows a moderate interaction with endotoxin at higher concentrations.*

According to figure 3.25, the NIP shows a moderate response to endotoxin, which is attributed to the interaction of the boronic acid with the diol groups present in the saccharides of endotoxin. The results are similar to those obtained by a previous researcher in the group (Demertzis, 2019).

### 3.3.5.3 Development of 'conventional' APBA molecularly imprinted polymer

Having optimized polymer formation and having developed non-imprinted polymers consisting of only PAPBA on the gold electrode surface, it was decided to fabricate a conventional molecularly imprinted polymer using endotoxin as a template molecule.

Endotoxin was incubated with the electrode surface overnight to allow for non-specific adsorption to the surface. Following rinsing with PBS to remove any loosely associated endotoxin, EIS was performed to confirm the presence of endotoxin at the surface, which was indicated by an average impedance of 1.8-2.0 k $\Omega$  (compared to 0.2-0.6 for a blank electrode). Subsequently, the electrode was immersed into the degassed monomer solution and polymerization was performed for 7 cycles. The electrodes were then rinsed carefully with PBS, then with 0.05% Tween 20 to remove the endotoxin from the matrix, before being re-incubated in PBS to remove the Tween along with any loosely associated polymer or endotoxin, as shown in figure 3.26, where a small decrease in impedance (2 k $\Omega$ ) was noted after washing.

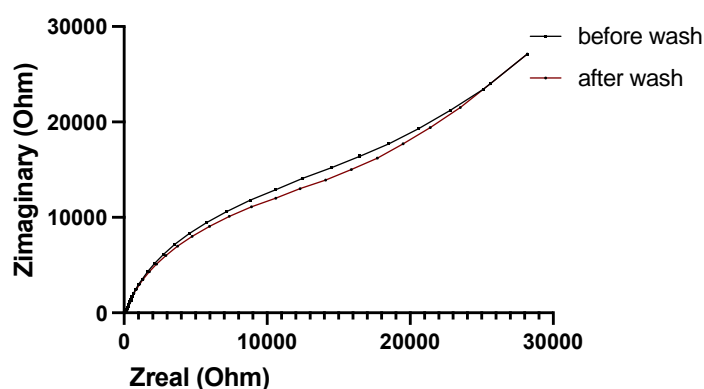


Figure 3.26: EIS graph showing the impedance of a MIP before washing (black curve) vs the impedance obtained following washing with 0.05% tween (red). A small decrease in impedance can be noted, indicative of endotoxin removal.

MIPs were produced in triplicate to determine their reproducibility, and a baseline impedance of 6.8k $\Omega$ , with a standard deviation (SD) of 0.61 k $\Omega$  was recorded. The system's noise is defined as the standard deviation, therefore an increase in impedance would be considered significant only if the higher than 1.83 k $\Omega$  (3x SD).

The MIP was challenged with a variety of endotoxin concentrations ranging from 1pg/mL up to 1 ng/mL, with 3 replicates for each concentration. The system only showed a response with concentrations higher than 1 pg/mL. EIS curves are shown in Figure 3.27 with the extracted % R/R<sub>0</sub> data given in Figure 3.28. The lowest endotoxin concentration that the MIP was capable of detecting was 10 pg/mL as an increase in Rct of 1.9 k $\Omega$  was noted, which is greater than the 3 x SD limit of 1.83 k $\Omega$ . Increasing concentrations of endotoxin resulted in higher impedances. A linear response was observed between endotoxin concentrations of 1 pg/mL and 1 ng/mL, with an r<sup>2</sup> of 0.7587. The sensor's maximum response is determined at 81%. In comparison, the aptasensor has a LOD of 0.5 pg/mL, and a dynamic range of 0.5 pg/mL up to 1 ng/mL. This suggests that the conventional MIP shows a similar sensitivity and dynamic range to the conventional aptasensor.

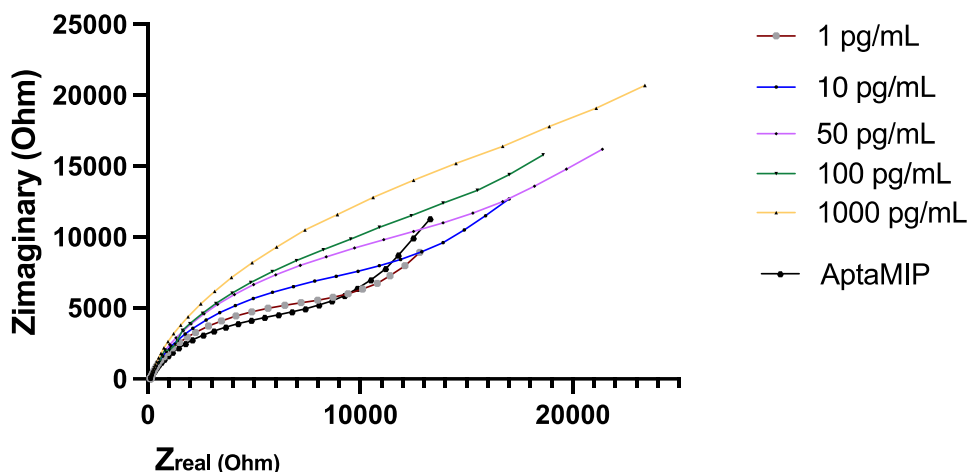


Figure 3.27: Exemplar EIS graph of an APBA molecularly imprinted polymer, showing a dynamic range of 1pg/mL up to 1 ng/mL

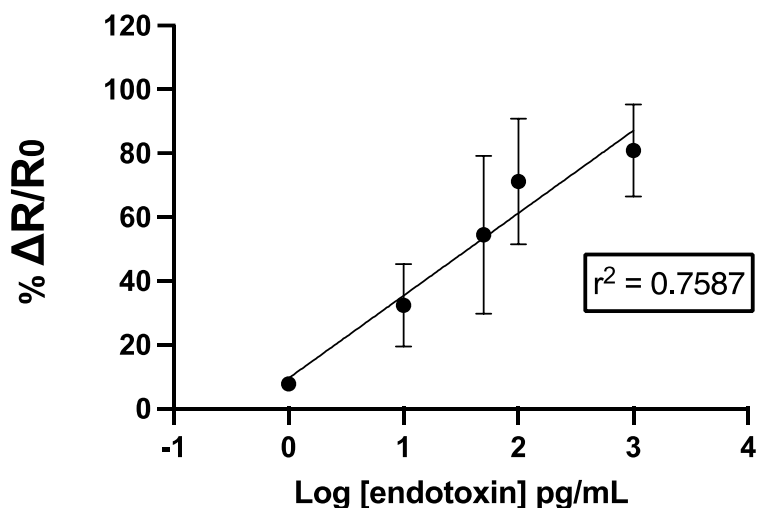


Figure 3.28: Following incubation with endotoxin, the MIP sensor showed a linear response between 1 pg/ml and 1 ng/ml ( $R^2 = 0.7587$ ).

### 3.3.5.4 Development of APBA Hybrid molecularly imprinted polymer

Having developed non-imprinted polymers and a conventional MIP which showed a similar LOD compared to the aptasensor (1 pg/mL vs 0.5 pg/mL), it was decided to proceed with the development of a hybrid MIP which combines the anti-endotoxin aptamer and the imprinted sites. In accordance with previous research which utilized the same aptamer, 7 polymerization cycles of 25mM APBA were performed, which has been shown to provide sufficient polymer growth as to entrap the aptamer-endotoxin complex whilst allowing

efficient release and rebinding of endotoxin (Demertzis, 2019). The CV results for the hybrid-MIP system are presented in figure 3.29. Modification of the clean gold electrode with the endotoxin-aptamer complex resulted in a large reduction in peak current, as shown by the green line. Polymerization of APBA resulted in a further decrease in peak current (red line) with washing producing a small increase in peak current (blue).

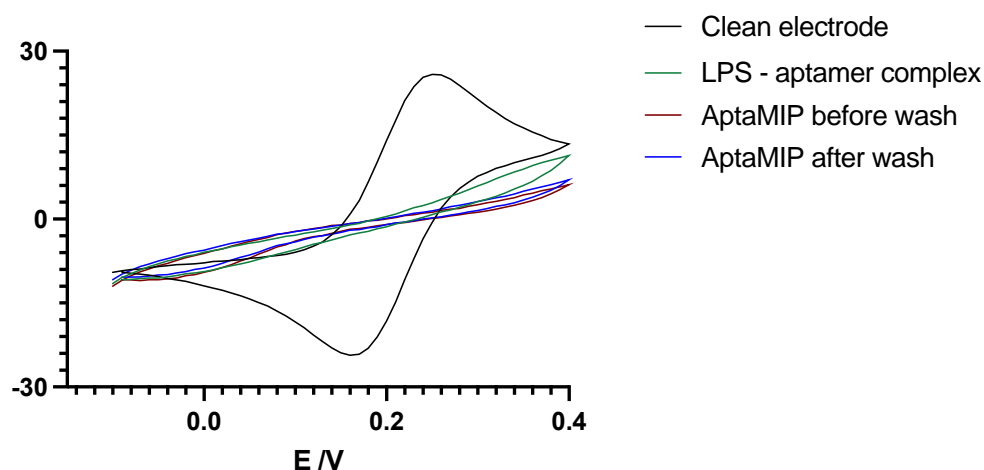


Figure 3.29: CV graph showing the CV of a clean electrode (black), compared to the CV of a gold electrode modified by the attachment of endotoxin-aptamer complexes on its surface, prior to polymerization (green), which results in a decrease in peak current. The formation of a polymer layer results in a further decrease in peak current, indicated by the red CV curve. Following the washing step in 0.05% tween, a small increase in peak current can be noted (blue line).

A hybrid apta-NIP was also developed, where the immobilized aptamer-endotoxin complex was washed with 0.05% tween to remove the bound endotoxin prior to polymerization. Immobilization of the aptamer-endotoxin complex ensures similar aptamer spacing and density on the electrode surface between the aptaMIP and the aptaNIP.

Apta-MIPs and NIPs were produced in triplicate to determine their reproducibility. A baseline impedance of 25.1k $\Omega$ , with a standard deviation (SD) of 0.941 (CV of 4.5%) was recorded for the aptaMIP. Similar values were recorded for the aptaNIP, with a baseline impedance of 22.5 k $\Omega$ , with a standard deviation (SD) of 1.043.

The Apta-MIP was then challenged with a variety of endotoxin concentrations ranging from 10 fg/mL up to 1 ng/mL, with 3 replicates for each concentration (figure 3.30 A and B). The lowest endotoxin concentration that the apta-MIP was capable of detecting was 10 fg/mL, as an increase in Rct of > 2.8 k $\Omega$  was noted, which is greater than the 3 x SD limit. Increasing concentrations of endotoxin resulted in higher impedances. Satisfactory linearity is shown between 10 fg/mL and 1 ng/mL, with an  $r^2$  of 0.9300 and  $r$  of 0.9643. The sensor's maximum response is determined at 110%. Compared to the Apta-NIP (figure 3.31), which shows little response across the same endotoxin concentration range, the AptaMIP demonstrates high

affinity for endotoxin, strongly supporting the hypothesis of the generation of aptamer-lined imprinted sites.

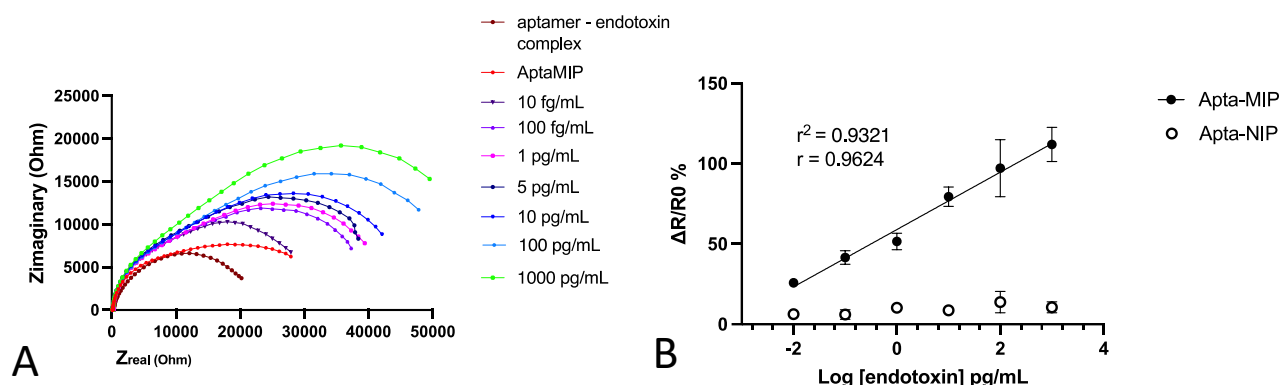


Figure 3.30 A and B: EIS graph showing the impedances of the hybrid-MIP sensor. A dynamic range between 10 fg/mL and 1 ng/mL is demonstrated. Figure 3.30 B: Dose-response graphs of the apta-MIP and aptaNIP when challenged with a variety of LPS concentrations, ranging from 10 fg/ml to 1 ng/ml. The sensor shows a linear response between 10 fg/ml and 100 pg/ml ( $R^2 = 0.9321$ ), with a high increase in impedance (approx. 27% for 10 fg/mL) showing the best sensitivity so far in the study.  $N=3$  for each data point.

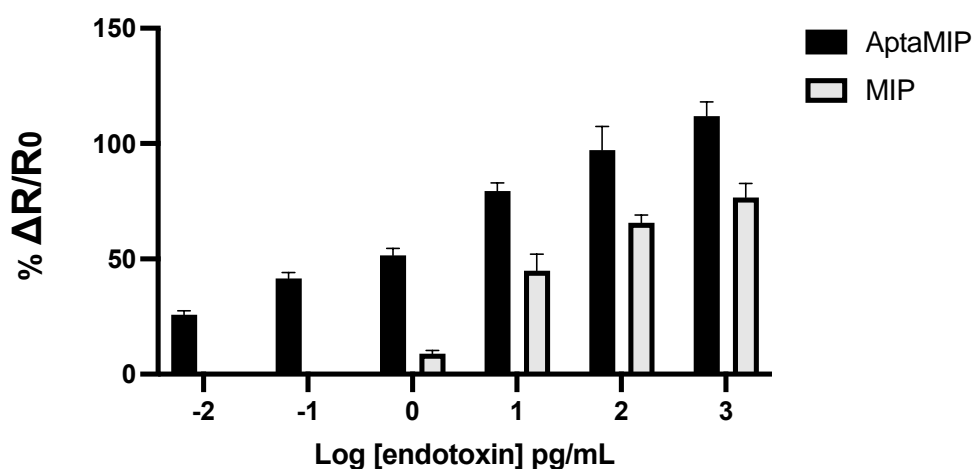


Figure 3.31: Comparison of the two MIP systems developed in this study. A significant difference in the dynamic range and sensitivity between the two systems can be observed, with the hybrid system displaying superior performance.  $N=3$  for all values.

The previous researcher that developed the aptaMIP platform used RuHex, a complex that binds selectively to DNA and chronocoulometry to estimate the number of aptamers bound to the electrode surface (Demertzis, 2019). It was found that the unwashed aptaMIP contained  $6.37E+10$  aptamers, whereas the washed system contained  $5.46E+10$  aptamers. As the sensor in this project was developed using the same protocol, it is anticipated that a similar number of aptamers were bound on the surface of the electrode. Other techniques that could be used to characterize the sensor's surface include transmission electron

microscopy, which has been used in literature to characterize imprinted polymers (Korol et al. 2023). Additionally, atomic force microscopy has been used by previous lab members to characterize the polymer thickness of an aptaMIP developed for prostate-specific antigen (Jolly, 2016).

#### **3.3.5.5 Comparison with gold-standard LAL assay**

The current gold standard in endotoxin detection, the LAL assay, can detect endotoxin down to 0.015 EU/ml (approximately 1 pg/mL) in the gel-clot assay, down to 0.001 EU/mL (0.1 pg/mL) in the kinetic turbidimetric assays (Piehler et al. 2020) and down to 0.0005 EU/mL (50 fg/mL) in the chromogenic assays (Wako Pyrostar, 2023). However, despite its wide use in the detection of endotoxin in the pharmaceutical sector, the LAL assay faces a number of drawbacks. First of all, the activation cascade of the assay can be activated by beta-glucans, commonly found in the cell wall of fungi, which can lead to false positives (Piehler et al. 2020). Secondly, the LAL assay, as an enzymatic cascade, is sensitive to sample conditions such as pH and temperature, therefore particular attention needs to be paid to these factors to prevent assay inhibition, which can be an issue when a sample preparation protocol is implemented (Aketagawa et al. 1993). Finally, none of the available LAL assay methods are routinely used to determine endotoxin levels in clinical samples, due to interference from sample constituents or low endotoxin recovery, both of which were covered in more depth in Chapter 2.

The AptaMIP outperforms the gold-standard LAL assay, being capable of detecting endotoxin at levels as low as 1 fg/mL. Additionally, the sensor has been shown by previous work in the researcher's lab, to exhibit low cross-reactivity to molecules that cause false-positives in LAL samples such as beta-glucan, and lipoteichoic acid (Demertzis, 2019).

#### **3.5.5.6 Comparison with literature**

Very little published work was found regarding the development of imprinted polymers for the detection of endotoxin. This is probably attributed to the challenging nature of endotoxin as a target molecule for imprinting, as it exhibits poor solubility, a non-defined structure and complicated behaviour under varying conditions (Gorman and Golovanov 2022). Altintas et al. used itaconic acid, methacrylic acid and acrylamide as functional monomers to imprint lipid A to develop nano-membranes in a microplate, with a reported LOD of 0.44 ng/mL (Altintas et al. 2016). In a similar method, Liu et al. used dopamine to develop nano-membranes, in combination with an antibody specific for the lipid A region, with similar results (Liu et al. 2019). An interesting approach using solid-phase synthesis is described by Abdin et al., who immobilized endotoxin on glass beads and used itaconic acid to develop the MIPs, and surface plasmon resonance was used to determine endotoxin concentration. A LOD of 15.6 ng/mL was observed (Abdin et al. 2015). Another study used acryloyl lysine (A-Lys)

and acryloyl phenylalanine (A-Phe), as functional monomers to entrap Lipid A, and FITC-labelled endotoxin was used to determine binding. However, this MIP exhibited poor selectivity and no LOD was reported (Ogawa et al. 2012). Finally, Sulc et al. developed a MIP utilizing a lipid A analogue (phosphatic acid dimer). Two monomers were used, urea and bis-imidazolium. The MIP showed high affinity for *E.coli* endotoxin, but was only capable of detecting endotoxin in the mg/mL range (Sulc et al. 2017).

No published work utilizing APBA or apta-MIP approaches for the detection of endotoxin was found in literature. However, the results in this chapter are comparable to those produced in the researcher's lab, which indicates that the sensors have good reproducibility (Demertzis, 2019).

In order to determine the binding kinetics of the AptaMIP, GraphPad Prism was used. The Langmuir-Freundlich model ("one site-total"), describing specific and non-specific binding phenomena was used, as the endotoxin may bind to either the polymer, the aptamer or the hybrid imprinted site. The endotoxin concentration was converted into pM to allow estimation of the  $K_d$ . Figure 3.32 shows the dose-response graph generated using the one site-total model.

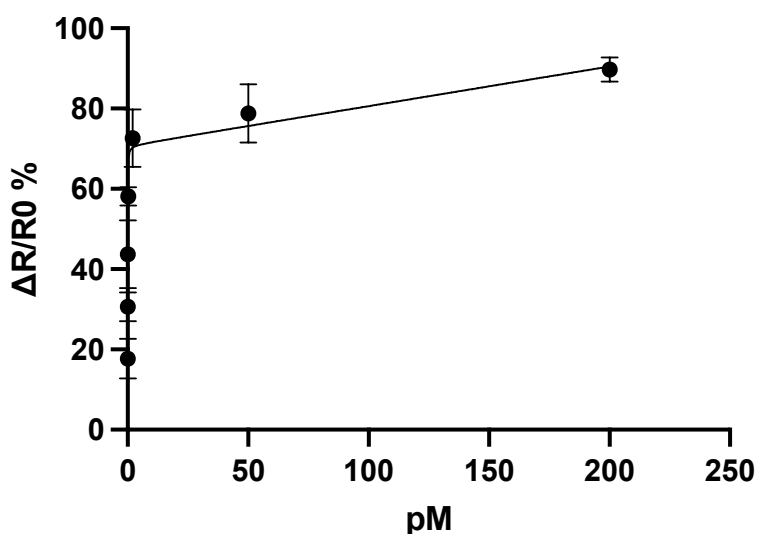


Figure 3.32: Dose-reponses graph for the AptaMIP. GraphPad prism was used to calculate the binding kinetics and the Langmuir-Freundlich binding model ("one site-total") was chosen. A  $R^2$  of 0.9246 was determined, and the system displays a  $K_d$  of 1.006 pM.

The Langmuir-Freundlich binding model provided a good fit for the data, as a  $R^2 = 0.9246$  was determined and a  $K_d$  of 1.006 pM was calculated. There is very little published data that the  $K_d$  can be compared with, however the values are similar to those reported by previous work in the researcher's group, which showed a  $K_d$  of 1.68 pM for the AptaMIP (Demertzis, 2019).

Figure 3.33 summarizes the performance of all the systems developed in the project so far for the detection of endotoxin (conventional MIP, aptasensor and AptaMIP, along with NIP controls). Across all endotoxin concentrations, the Apta-NIP and NIP display consistently low detection levels and little difference in impedance when challenged with endotoxin, especially at higher concentrations (0.1 – 100 pg/mL). Overall, the hybrid system significantly outperforms both the conventional MIP and aptasensor, exhibiting the lowest LOD so far at 10 fg/mL, compared to the aptasensor's 0.5 pg/mL and the conventional MIP's 10 fg/mL.

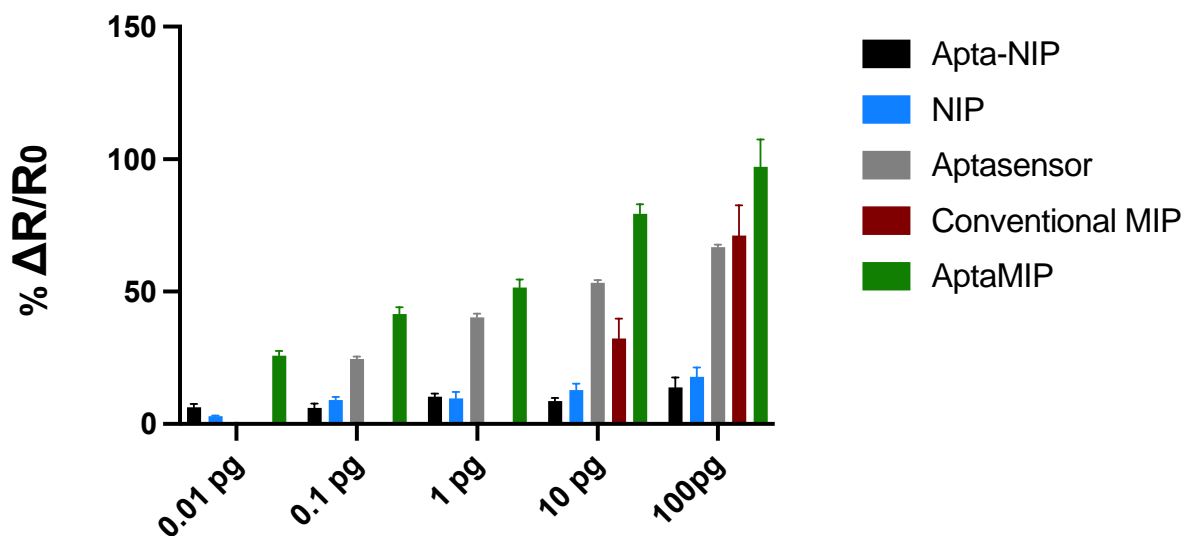


Figure 3.33 Comparison of the changes in  $\Delta R$  between the generated systems. The progression of the study, starting from the aptasensor and finishing with the apta-MIP, demonstrates a continuous improvement in performance. All systems used the model  $Rs((RctW)Qdl)$  to characterise the circuit.

Figure 3.33 provides important information for the aptaMIP when compared to the aptaNIP. Across all endotoxin concentrations tested, the aptaNIP exhibits a consistently low response, never exceeding a 35% increase in impedance. This indicates a small, non-specific response to endotoxin, which is attributed to the interaction of the boronic acid with the diol groups present in the saccharides of endotoxin.

In comparison to the aptaNIP, the aptaMIP shows a large difference in  $\% \Delta R/R_0$ , even at 10 fg/mL. This is observed across all concentrations tested, where the aptaMIP outperforms the aptaNIP. Although the aptaNIP and the aptaMIP both contain the aptamer, in the case of the aptaNIP the endotoxin was removed, leaving only the aptamer on the surface prior to polymerization. It is anticipated that the removal of endotoxin as a template molecule prevents the formation of cavities and effectively entraps the aptamer into the polymer matrix. The difference in performance demonstrated by the two systems supports the imprinting hypothesis.

### 3.3.6 Biofouling studies

The ultimate goal of this project is to develop a biosensor for the detection of endotoxin in clinical samples, and in particular blood plasma. It is well-known that endotoxin binds to blood components such as cells, proteins, lipoproteins and nucleic acids (Harm et al. 2021). Additionally, the biofouling effect of blood plasma components is well documented in the literature (Campuzano et al. 2019). Previous attempts focused on the development of an electrochemical LPS aptasensor showed that introduction of serum to the sensor, even after significant dilution (1 in 100,000) resulted in very high background “noise” levels, high levels of biofouling and low levels of endotoxin detection (Demertzis, 2019). Therefore, as a first step in the identification of blood plasma constituents that cause biofouling, the sensors were challenged with various concentrations and combinations of human serum albumin (HSA), which is the dominant protein in blood, interleukin 6 and 10 and lastly a combination of HSA and endotoxin.

#### 3.3.6.1 Human serum albumin (HSA) challenge

HSA is the most abundant protein in blood plasma, with concentrations varying between 35 and 50 mg/mL (Mishra and Heath 2021). Proteins are well known for their biofouling properties in electrochemical sensors, as they contain numerous hydrogen bond donors and acceptors. As a first step in clinical sample preparation, the samples are diluted in order to reduce interference from sample matrix components. Therefore, a range of dilutions were prepared, in order to assess the effect of HSA on the sensor. Figure 3.34 presents the changes in impedance following incubation with HSA.

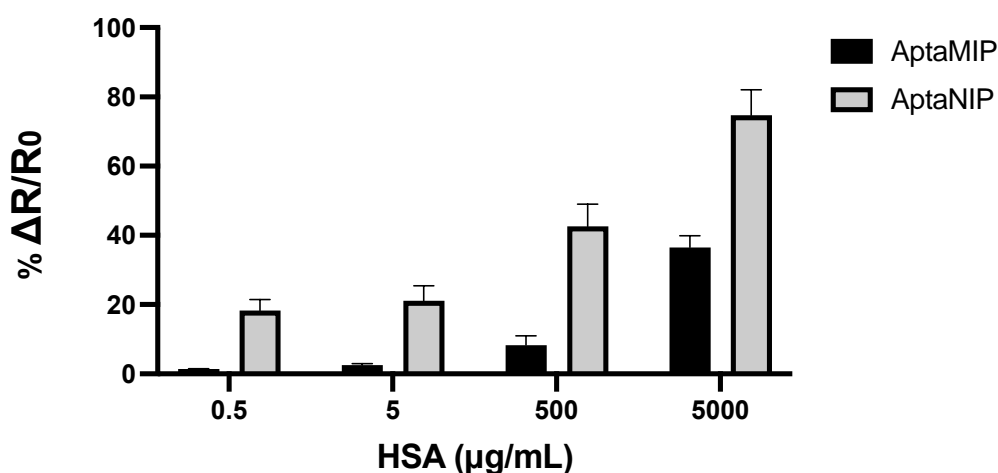


Figure 3.34: Comparison of the changes in impedance following incubation of the aptaMIP and AptaMIP with various concentrations of HSA. Results indicate a concentration-dependent effect on biofouling.

Figure 3.34 shows that the aptaMIP shows the lowest susceptibility to biofouling compared to the aptaNIP. More specifically, very little changes in impedance are noted for low concentrations of HSA (0.5 – 50  $\mu\text{g}/\text{mL}$ ). At 500  $\mu\text{g}/\text{mL}$ , a small but noticeable increase in average impedance of 8.3% is noted. At high concentrations (> 5,000  $\mu\text{g}/\text{mL}$ , equivalent to a 1/10 dilution of plasma), the effects of biofouling are more apparent, suggesting that sample dilution is a necessary step to reduce non-specific adsorption. The low amount of non-specific interaction may be attributed to the fact that HSA is negatively charged at physiological pH, which may cause electrostatic repulsion when in proximity with the negatively charged aptamer (Jansen et al. 1993). In the case of the AptaNIP, the lack of an endotoxin ‘template’ during the polymerisation process likely leads to entrapment / overgrowth of the aptamer with polymer. Therefore, a greater degree of non-specific adsorption would be expected, especially as aminophenyl boronic acid has been used to bind to HSA (Bonini et al. 2007).

### 3.3.6.2 Challenge with HSA and endotoxin

As endotoxin is known for binding to proteins, it was considered worthwhile assessing whether pre-incubation (10 minutes at RT) of endotoxin with HSA would impact response (Reich et al. 2019; Harm et al. 2021).. Figure 4.35 shows the  $\% \Delta R/R_0$  results of the aptaMIP, aptaNIP and aptasensor following addition of endotoxin spiked HSA samples.

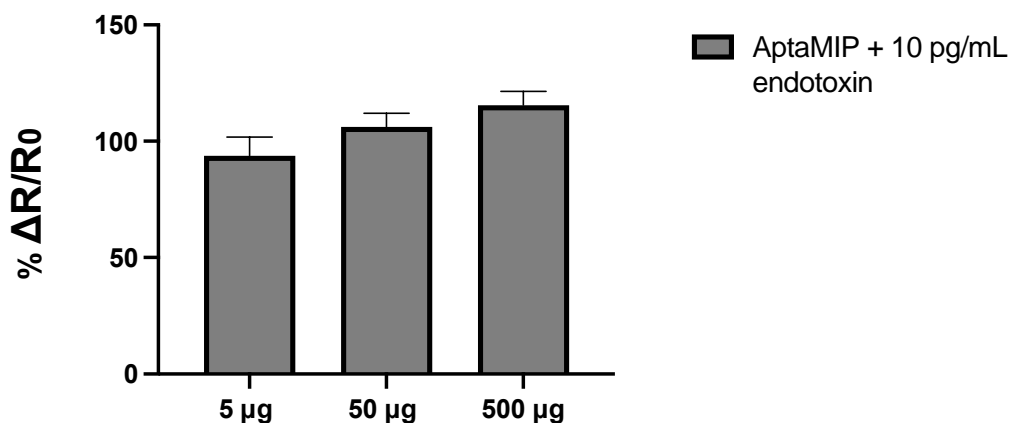


Figure 3.35: Comparison of the changes in impedance following incubation of the AptamIP with various concentrations HSA + 10 pg/mL of endotoxin. Results indicate that the combination of HSA with endotoxin leads to higher impedances compared with HSA alone, suggesting a synergistic effect.

From figure 3.35, it can be observed that the combination of endotoxin with HSA leads to a large increase in impedance compared to HSA alone (figure 3.32). When challenged with endotoxin alone, at a concentration of 10 pg/mL, the AptamIP shows an increase in impedance of approximately 80%; when the same concentration of endotoxin was added to 5  $\mu\text{g}/\text{mL}$  of HSA an impedance increase of approximately 93% is noted. Increasing concentrations of HSA, at 50 and 500  $\mu\text{g}/\text{mL}$  resulted in increases in impedance of 106% and

115%, respectively. The increased responses of endotoxin or HSA alone, provides further evidence that the sensor is able to detect its target even when complexed to other plasma components.

### 3.3.6.3 Interleukin 6 challenge

As one of the aims of the project was the detection of interleukins in plasma samples it was decided to challenge the aptaMIP and NIP with interleukin-6. IL-6 is found elevated in the plasma of pneumonia patients, especially in pediatric cases, which makes them relevant to this study (Khattab et al. 2018). Plasma IL-6 levels during sepsis can be found in high concentrations (300-500 pg/mL) (Ortqvist et al. 1995). Figure 3.36 shows the results obtained following incubation of the aptaMIP, AptaNIP and aptasensor with three different concentrations of IL-6 (0.5, 5 and 50 pg/mL). Only a small degree of interaction was noted across both systems across the concentrations investigated. It was anticipated that some non-specific binding would be observed as IL-6 is a glycosylated protein which will bind to the boronic acid functional group of APBA (Oliveira et al. 2022).

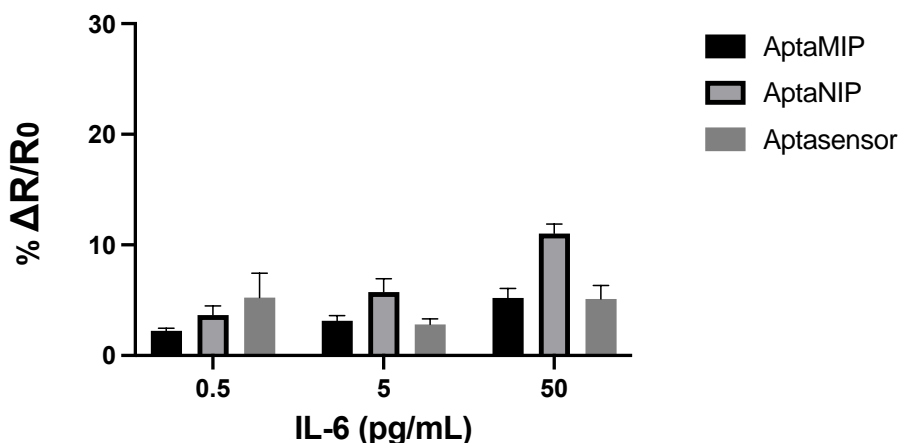


Figure 3.36: Comparison of the changes in impedance following incubation of the MIP and AptaMIP with various concentrations of IL-6. Results indicate that out of all systems tested, the aptaMIP showed the lowest levels of interaction.

It is evident from figure 3.36 that across all three systems, very little interaction with IL-6 was noted. A low response was expected from the aptasensor, as previous work in the lab as well as published literature have demonstrated that the aptamer used in this study exhibits high selectivity against endotoxin (Demertzis, 2019; Kim et al. 2012; Su et al. 2012; Ma et al. 2018; Jiang et al. 2022). The aptaNIP displayed slightly higher levels of interaction, possibly owing to the non-specific binding of IL-6 to the boronic acid functional group of APBA (Oliveira et al. 2022). Compared to the other two systems, the aptaMIP showed similar levels of IL-6

interaction to the aptasensor, which further provides evidence for the generation of aptamer lined imprinted sites.

### 3.3.6.4 AptaMIP response to glucose and citrate

An important consideration for the aptaMIP is its non-specific interaction with other molecules. Moving away from the LAL assay means the introduction of new factors that need to be taken into consideration, such as boronic acid and its interaction with plasma constituents. As boronic acids are known for their high affinity interaction with sugars through the formation of boronates with cis-diols that are present in blood glucose, it was also decided to test the aptaMIP response when challenged with glucose (Zhao et al. 2017). Additionally, as the plasma samples used in future experiments will be generated from venous blood drawn into vacutainers containing citrate as an anticoagulant, it was decided to test the sensor's response to the presence of trisodium citrate. A concentration of 3.5 mM for glucose, representative of levels present in fasting blood plasma was chosen (Koobotse et al. 2020). A concentration of 3.2% w/v trisodium citrate, representative of the concentration found in the blood collection tubes was used. The resulting EIS are presented below in figure 3.37.

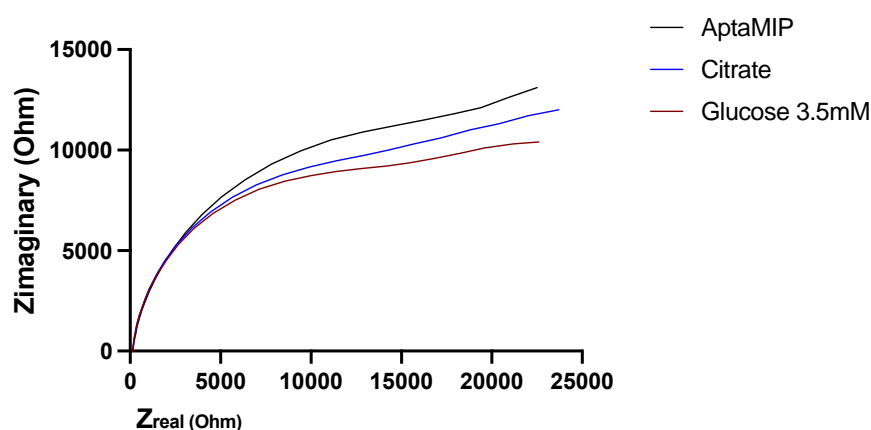


Figure 3.37: EIS graph showing the response of the aptaMIP (black) following incubation with trisodium citrate 3.2% (blue) and 3.5mM glucose (red). Very little change in impedance was noted across both samples. N=1 as this was a screening experiment.

Figure 3.37 shows that the neither the addition of sodium citrate nor glucose resulted in an increase in impedance. In fact, a small reduction in impedance was noted, possibly caused by the removal of non-attached monomers following the washing of the aptaMIP in-between experiments. Additionally, as stated above boronic acid are known to bind to sugars, including glucose. It is possible that the binding of glucose, which results in the formation of boronate esters, reduces the negative charge at the surface of the electrode, which translates to a decrease in impedance (Zhao et al. 2017). This suggests that the aptaMIP is not affected by neither the anticoagulant at the concentration used in blood collection tubes nor blood glucose.

### 3.4 Conclusions and future work

Three electrochemical biosensors for the detection of endotoxin have been developed -an aptasensor, a conventional MIP and a hybrid aptaMIP, along with the relevant controls. The aptasensor has a LOD of 0.5 pg/mL, whereas the MIP has a LOD 1 pg/mL and the aptaMIP has a LOD of 10 fg/mL. The performance of the sensors described in this Chapter are comparable to those developed by Demertzis et al., which attests to their reproducibility. With the exception of the conventional MIP, which has a relatively high LOD and displays poor linearity across endotoxin concentrations, both the aptasensor and the aptaMIP display competitive LODs (50 fg/mL and 10 fg/mL, respectively). The aptaMIP outperforms all LAL assays (gel-clot, kinetic turbidimetric and chromogenic), whereas the aptasensor displays similar performance to the chromogenic assay. As previous research has demonstrated that both sensors show low levels of cross-reactivity with beta glucan and lipoteichoic acid, both sensors can be viable alternatives for the LAL assay in aqueous samples (Demertzis, 2019). However, specificity studies showed that the aptaMIP demonstrates superior performance when challenged with competing samples.

The specificity studies in this Chapter further support the hypothesis of the development of imprinted sites. HSA specificity studies showed that compared to the apta-NIP, the aptaMIP showed very little interaction with HSA, up to a concentration of 500 µg/mL, which supports the imprinted sites hypothesis. Moreover, incubation with IL-6 showed that the specificity of the aptaMIP is comparable to the aptasensor, which has been assessed in literature for its specificity to endotoxin, which further provides evidence for the generation of aptamer lined imprinted sites. Incubation of endotoxin with HSA resulted in the formation of conjugated complexes, as evidenced by figure 3.35. This resulted in a further increase in impedance across all systems. Although the aptaMIP demonstrated the lowest further increase in impedance, this finding highlights the need for a sample preparation protocol in order to counteract this increase in impedance caused by endotoxin complexation, something which will be explored in depth in the next Chapter.

The sensitivity of the AptaMIP is remarkable when challenged with aqueous solutions, and the next major step in this project is the transfer of the sample preparation protocol, described in Chapter 2, to the aptaMIP sensor to enable the efficient and sensitive detection of endotoxin from clinical samples.

### 3.5 Bibliography

Abd-Ellatief, R. and Abd-Ellatief, M. R. 2021. Electrochemical Aptasensors: Current Status and Future Perspectives. *Diagnostics (Basel)* 11(1), doi: 10.3390/diagnostics11010104

Aketagawa, J. et al. 1993. Activation of limulus coagulation factor G by several (1→3)-beta-D-glucans: comparison of the potency of glucans with identical degree of polymerization but different conformations. *J Biochem* 113(6), pp. 683-686. doi: 10.1093/oxfordjournals.jbchem.a124103

Aljohani, M. M. et al. 2022. Aptamers: Potential Diagnostic and Therapeutic Agents for Blood Diseases. *Molecules* 27(2), doi: 10.3390/molecules27020383

Bai, L. et al. 2014. A signal-on electrochemical aptasensor for ultrasensitive detection of endotoxin using three-way DNA junction-aided enzymatic recycling and graphene nanohybrid for amplification. *Nanoscale* 6(5), pp. 2902-2908. doi: 10.1039/c3nr05930h

BelBruno, J. J. 2019. Molecularly Imprinted Polymers. *Chemical Reviews* 119(1), pp. 94-119. doi: 10.1021/acs.chemrev.8b00171

Bottari, F. et al. 2020. Do Aptamers Always Bind? The Need for a Multifaceted Analytical Approach When Demonstrating Binding Affinity between Aptamer and Low Molecular Weight Compounds. *J Am Chem Soc* 142(46), pp. 19622-19630. doi: 10.1021/jacs.0c08691

Bowen JL. Detection of Lipopolysaccharide Pyrogens by Molecularly Imprinted Polymers. 2011.

Campuzano, S. et al. 2019. Antifouling (Goodman et al.)materials for Electrochemical (Goodman et al.)sensing. *Int J Mol Sci* 20(2), doi: 10.3390/ijms20020423

Chakma, B. et al. 2018. Development of Electrochemical Impedance Spectroscopy Based Malaria Aptasensor Using HRP-II as Target Biomarker. *Electroanalysis* 30(8), pp. 1847-1854. doi: <https://doi.org/10.1002/elan.201800142>

Chang, C. et al. 2019. Optimization of tris(2-carboxyethyl) phosphine reduction conditions for fast analysis of total biothiols in mouse serum samples. *Heliyon* 5(5), p. e01598. doi: 10.1016/j.heliyon.2019.e01598

Chatziharalambous, D. et al. 2016. Analytical Performance of ELISA Assays in Urine: One More Bottleneck towards Biomarker Validation and Clinical Implementation. *PLoS ONE* 11(2), p. e0149471. doi: 10.1371/journal.pone.0149471

Chen, L. et al. 2011. Recent advances in molecular imprinting technology: current status, challenges and highlighted applications. *Chemical Society Reviews* 40(5), pp. 2922-2942. doi: 10.1039/C0CS00084A

Cherevko, S. et al. 2013. Gold Dissolution: Towards Understanding of Noble Metal Corrosion. *RSC Advances* 3, pp. 16516-16527. doi: 10.1039/c3ra42684j

Choi, W. et al. 2020. Modeling and Applications of Electrochemical Impedance Spectroscopy (EIS) for Lithium-ion Batteries. *Journal of electrochemical science and technology* 11, pp. 1-13.

Ciftci, H. et al. 2014. Development of poly(3-aminophenylboronic acid) modified graphite rod electrode suitable for fluoride determination. *Talanta* 126, pp. 202-207. doi: 10.1016/j.talanta.2014.03.018

Colburn, A. W. et al. 2021. Lifting the lid on the potentiostat: a beginner's guide to understanding electrochemical circuitry and practical operation. *Phys Chem Chem Phys* 23(14), pp. 8100-8117. doi: 10.1039/d1cp00661d

Daems, E. et al. 2021. Aptamer-ligand recognition studied by native ion mobility-mass spectrometry. *Talanta* 224, p. 121917. doi: 10.1016/j.talanta.2020.121917

Demmer, W. et al. 2003. Chapter 14 - Economic production of biopharmaceuticals by high-speed membrane adsorbers. In: Bhattacharyya, D. and Butterfield, D.A. eds. *Membrane Science and Technology*. Vol. 8. Elsevier, pp. 283-295.

Dickey, D. D. et al. 2016. 744. Optimizing Conditions for Aptamer Folding Using a High-Throughput Aptamer Fluorescence Binding and Internalization (AFBI) Assay. *Molecular Therapy* 24, p. S293. doi: 10.1016/S1525-0016(16)33552-3

Ding, X. and Heiden, P. A. 2014. Recent Developments in Molecularly Imprinted Nanoparticles by Surface Imprinting Techniques. *Macromolecular Materials and Engineering* 299(3), pp. 268-282. doi: <https://doi.org/10.1002/mame.201300160>

Ellington, A. D. and Szostak, J. W. 1990. In vitro selection of RNA molecules that bind specific ligands. *Nature* 346(6287), pp. 818-822. doi: 10.1038/346818a0

Erturk, G. and Mattiasson, B. 2017. Molecular Imprinting Techniques Used for the Preparation of Biosensors. *Sensors (Basel)* 17(2), doi: 10.3390/s17020288

- Fakhr, M. H. et al. 2022. Cleaning of LTCC, PEN, and PCB Au electrodes towards reliable electrochemical measurements. *Sci Rep* 12(1), p. 20431. doi: 10.1038/s41598-022-23395-3
- Feng, C. et al. 2014. Optical aptasensors for quantitative detection of small biomolecules: a review. *Biosens Bioelectron* 59, pp. 64-74. doi: 10.1016/j.bios.2014.03.014
- Fischer, L. M. et al. 2009. Gold cleaning methods for electrochemical detection applications. *Microelectronic Engineering* 86(4), pp. 1282-1285. doi: <https://doi.org/10.1016/j.mee.2008.11.045>
- Golabi, M. et al. 2017. Electrochemical bacterial detection using poly(3-aminophenylboronic acid)-based imprinted polymer. *Biosens Bioelectron* 93, pp. 87-93. doi: 10.1016/j.bios.2016.09.088
- Gomes, A. G. et al. 2010. Clearance of host cell impurities from plasmid-containing lysates by boronate adsorption. *Journal of Chromatography A* 1217(15), pp. 2262-2266. doi: <https://doi.org/10.1016/j.chroma.2010.02.015>
- Guchait, A. et al. 2022. 8 - Conjugated polymers in bioelectronics. In: Kumar, V. et al. eds. *Conjugated Polymers for Next-Generation Applications*. Vol. 1. Woodhead Publishing, pp. 239-272.
- Ikebukuro, K. et al. 2004. Electrochemical Detection of Protein Using a Double Aptamer Sandwich. *Analytical Letters* 37(14), pp. 2901-2909. doi: 10.1081/AL-200035778
- Ilgü, M. and Nilsen-Hamilton, M. 2016. Aptamers in analytics. *Analyst* 141(5), pp. 1551-1568. doi: 10.1039/c5an01824b
- Jang, L. S. and Keng, H. K. 2008. Modified fabrication process of protein chips using a short-chain self-assembled monolayer. *Biomed Microdevices* 10(2), pp. 203-211. doi: 10.1007/s10544-007-9126-7
- Ji, J. et al. 2020. An aptamer-based shear horizontal surface acoustic wave biosensor with a CVD-grown single-layered graphene film for high-sensitivity detection of a label-free endotoxin. *Microsyst Nanoeng* 6, p. 4. doi: 10.1038/s41378-019-0118-6
- Ji, Y. et al. 2019. Development of boronic acid-functionalized mesoporous silica-coated core/shell magnetic microspheres with large pores for endotoxin removal. *Journal of Chromatography A* 1602, pp. 91-99. doi: <https://doi.org/10.1016/j.chroma.2019.06.004>

- Jiang, J. et al. 2022. Simple and fast colorimetric detection of lipopolysaccharide based on aptamer and SYBR Green I mediated aggregation of gold nanoparticles. *Int J Biol Macromol* 223(Pt A), pp. 231-239. doi: 10.1016/j.ijbiomac.2022.10.276
- Jolly, P. et al. 2015. Label-free impedimetric aptasensor with antifouling surface chemistry: A prostate specific antigen case study. *Sensors and Actuators B: Chemical* 209, pp. 306-312. doi: <https://doi.org/10.1016/j.snb.2014.11.083>
- Keighley, S. D. et al. 2008. Optimization of DNA immobilization on gold electrodes for label-free detection by electrochemical impedance spectroscopy. *Biosens Bioelectron* 23(8), pp. 1291-1297. doi: 10.1016/j.bios.2007.11.012
- Kepley, L. J. et al. 1992. A selective SAW-based organophosphonate chemical sensor employing a self-assembled, composite monolayer: a new paradigm for sensor design. *Analytical Chemistry* 64(24), pp. 3191-3193. doi: 10.1021/ac00048a018
- Kim, S. E. et al. 2012. Harnessing aptamers for electrochemical detection of endotoxin. *Anal Biochem* 424(1), pp. 12-20. doi: 10.1016/j.ab.2012.02.016
- Korol, D. et al. 2023. Synthesis of conducting molecularly imprinted polymer nanoparticles for estriol chemosensing. *Sensors and Actuators B: Chemical* 382, p. 133476. doi: <https://doi.org/10.1016/j.snb.2023.133476>
- Lao, R. et al. 2005. Electrochemical interrogation of DNA monolayers on gold surfaces. *Anal Chem* 77(19), pp. 6475-6480. doi: 10.1021/ac050911x
- Lee, K. J. et al. 2017. Electrochemical and spectroscopic methods for evaluating molecular electrocatalysts. *Nature Reviews Chemistry* 1(5), p. 0039. doi: 10.1038/s41570-017-0039
- Leff, D. V. et al. 1996. Synthesis and Characterization of Hydrophobic, Organically-Soluble Gold Nanocrystals Functionalized with Primary Amines. *Langmuir* 12(20), pp. 4723-4730. doi: 10.1021/la960445u
- Leppek, K. and Stoecklin, G. 2014. An optimized streptavidin-binding RNA aptamer for purification of ribonucleoprotein complexes identifies novel ARE-binding proteins. *Nucleic Acids Res* 42(2), p. e13. doi: 10.1093/nar/gkt956
- Li, Z. et al. 2021. Advances in Screening and Development of Therapeutic Aptamers Against Cancer Cells. *Front Cell Dev Biol* 9, p. 662791. doi: 10.3389/fcell.2021.662791

Ma, L. et al. 2018. Harnessing the affinity of magnetic nanoparticles toward dye-labeled DNA and developing it as an universal aptasensor revealed by lipopolysaccharide detection. *Analytica Chimica Acta* 1036, pp. 107-114. doi: <https://doi.org/10.1016/j.aca.2018.06.060>

Magar, H. S. et al. 2021. Electrochemical Impedance Spectroscopy (EIS): Principles, Construction, and Biosensing Applications. *Sensors (Basel)* 21(19), doi: 10.3390/s21196578

Mandler, D. and Kraus-Ophir, S. 2011. Self-assembled monolayers (SAMs) for electrochemical sensing. *Journal of Solid State Electrochemistry* 15(7), pp. 1535-1558. doi: 10.1007/s10008-011-1493-6

Manesiotis, P. et al. 2013. Molecularly imprinted polymers for the extraction of imiquimod from biological samples using a template analogue strategy. *ANALYTICAL METHODS* 5, pp. 3122-3128. doi: 10.1039/c3ay40239h

McCormick, W. et al. 2021. Covalent Immobilisation of a Nanoporous Platinum Film onto a Gold Screen-Printed Electrode for Highly Stable and Selective Non-Enzymatic Glucose Sensing. *Catalysts* 11, doi: 10.3390/catal11101161

Meng, L. et al. 2018. 11-Mercaptoundecanoic acid capped gold nanoclusters as a fluorescent probe for specific detection of folic acid via a ratiometric fluorescence strategy. *RSC Adv* 8(17), pp. 9327-9333. doi: 10.1039/c8ra00481a

Morita, Y. et al. 2018. Aptamer Therapeutics in Cancer: Current and Future. *Cancers (Basel)* 10(3), doi: 10.3390/cancers10030080

Mu, Z. et al. 2022. A new electrochemical aptasensor for ultrasensitive detection of endotoxin using Fe-MOF and AgNPs decorated P-N-CNTs as signal enhanced indicator. *Applied Surface Science* 573, p. 151601. doi: <https://doi.org/10.1016/j.apsusc.2021.151601>

Nejad, S. et al. 2016. A systematic review of lumped-parameter equivalent circuit models for real-time estimation of lithium-ion battery states. *Journal of Power Sources* 316, pp. 183-196. doi: <https://doi.org/10.1016/j.jpowsour.2016.03.042>

Nimjee, S. M. et al. 2017. Aptamers as Therapeutics. *Annu Rev Pharmacol Toxicol* 57, pp. 61-79. doi: 10.1146/annurev-pharmtox-010716-104558

Nishino, H. et al. 2006. Selective protein capture by epitope imprinting. *Angew Chem Int Ed Engl* 45(15), pp. 2392-2396. doi: 10.1002/anie.200503760

Oberhaus, F. V. et al. 2020. Immobilization Techniques for Aptamers on Gold Electrodes for the Electrochemical Detection of Proteins: A Review. *Biosensors (Basel)* 10(5), doi: 10.3390/bios10050045

Pacheco, M. et al. 2022. Transition metal dichalcogenide-based Janus micromotors for on-the-fly Salmonella detection. *Mikrochim Acta* 189(5), p. 194. doi: 10.1007/s00604-022-05298-2

Pendergrast, P. S. et al. 2005. Nucleic acid aptamers for target validation and therapeutic applications. *J Biomol Tech* 16(3), pp. 224-234.

Piebler, M. et al. 2020. Comparison of LAL and rFC Assays-Participation in a Proficiency Test Program between 2014 and 2019. *Microorganisms* 8(3), doi: 10.3390/microorganisms8030418

Posha, B. et al. 2018. Gold atomic cluster mediated electrochemical aptasensor for the detection of lipopolysaccharide. *Biosensors and Bioelectronics* 101, pp. 199-205. doi: <https://doi.org/10.1016/j.bios.2017.10.030>

Reich, J. et al. 2019. Low Endotoxin Recovery-Masking of Naturally Occurring Endotoxin. *Int J Mol Sci* 20(4), doi: 10.3390/ijms20040838

Richards, D. et al. 2010. Assessment of the passivation capabilities of two different covalent chemical modifications on GaP(100). *Langmuir* 26(11), pp. 8141-8146. doi: 10.1021/la904451x

Rikukawa, M. and Sanui, K. 2000. Proton-conducting polymer electrolyte membranes based on hydrocarbon polymers. *Progress in Polymer Science* 25(10), pp. 1463-1502. doi: [https://doi.org/10.1016/S0079-6700\(00\)00032-0](https://doi.org/10.1016/S0079-6700(00)00032-0)

Sajini, T. and Mathew, B. 2021. A brief overview of molecularly imprinted polymers: Highlighting computational design, nano and photo-responsive imprinting. *Talanta Open* 4, p. 100072. doi: <https://doi.org/10.1016/j.talo.2021.100072>

Sandford, C. et al. 2019. A synthetic chemist's guide to electroanalytical tools for studying reaction mechanisms. *Chem Sci* 10(26), pp. 6404-6422. doi: 10.1039/c9sc01545k

Šípová-Jungová, H. et al. 2021. Interaction of Tris with DNA molecules and carboxylic groups on self-assembled monolayers of alkanethiols measured with surface plasmon resonance. *Applied Surface Science* 546, p. 148984. doi: <https://doi.org/10.1016/j.apsusc.2021.148984>

Slavkovic, S. and Johnson, P. E. 2023. Analysis of Aptamer-Small Molecule Binding Interactions Using Isothermal Titration Calorimetry. *Methods Mol Biol* 2570, pp. 105-118. doi: 10.1007/978-1-0716-2695-5\_8

Su, W. et al. 2012. Determination of endotoxin through an aptamer-based impedance biosensor. *Biosensors and Bioelectronics* 32(1), pp. 32-36. doi: <https://doi.org/10.1016/j.bios.2011.11.009>

Thevenot, D. R. et al. 2001. Electrochemical biosensors: recommended definitions and classification. *Biosens Bioelectron* 16(1-2), pp. 121-131. doi: 10.1016/s0956-5663(01)00115-4

Tian, J. et al. 2021. Electrochemical aptasensor for ultrasensitive detection of lipopolysaccharide using silver nanoparticles decorated titanium dioxide nanotube/functionalized reduced graphene oxide as a new redox nanoprobe. *Microchimica Acta* 188(2), p. 31. doi: 10.1007/s00604-020-04695-9

Tominaga, Y. 2017. Ion-conductive polymer electrolytes based on poly(ethylene carbonate) and its derivatives. *Polymer Journal* 49(3), pp. 291-299. doi: 10.1038/pj.2016.115

Tricase, A. et al. 2021. Surface composition of mixed self-assembled monolayers on Au by infrared attenuated total reflection spectroscopy. *Applied Surface Science* 559, p. 149883. doi: <https://doi.org/10.1016/j.apsusc.2021.149883>

Tsai, T. C. et al. 2019. In situ study of EDC/NHS immobilization on gold surface based on attenuated total reflection surface-enhanced infrared absorption spectroscopy (ATR-SEIRAS). *Colloids Surf B Biointerfaces* 175, pp. 300-305. doi: 10.1016/j.colsurfb.2018.12.009

Wang, H.-W. et al. 2021. Cyclic Voltammetry in Biological Samples: A Systematic Review of Methods and Techniques Applicable to Clinical Settings. *Signals* 2(1), pp. 138-158.

Wang, N. et al. 2019. Copper ion-assisted gold nanoparticle aggregates for electrochemical signal amplification of lipopolysaccharide sensing. *Biosens Bioelectron* 126, pp. 529-534. doi: 10.1016/j.bios.2018.11.021

Wannapob, R. et al. 2010. Affinity sensor using 3-aminophenylboronic acid for bacteria detection. *Biosens Bioelectron* 26(2), pp. 357-364. doi: 10.1016/j.bios.2010.08.005

Williams, G. T. et al. 2021. Molecular Boronic Acid-Based Saccharide Sensors. *ACS Sens* 6(4), pp. 1508-1528. doi: 10.1021/acssensors.1c00462

Yadav, A. K. et al. 2022. Molecularly imprinted polymer-based nanodiagnostics for clinically pertinent bacteria and virus detection for future pandemics. *Biosensors and Bioelectronics: X* 12, p. 100257. doi: <https://doi.org/10.1016/j.biosx.2022.100257>

Yan, Z. et al. 2013. Rational design of a thrombin electrochemical aptasensor by conjugating two DNA aptamers with G-quadruplex halves. *Anal Biochem* 442(2), pp. 237-240. doi: 10.1016/j.ab.2013.06.021

Yasmeen, N. et al. 2021. Molecularly imprinted polymer as a synthetic receptor mimic for capacitive impedimetric selective recognition of Escherichia coli K-12. *Analytica Chimica Acta* 1188, p. 339177. doi: <https://doi.org/10.1016/j.aca.2021.339177>

Ye, S. et al. 2022. Wulff-type boronic acid-functionalized quantum dots for rapid and sensitive detection of Gram-negative bacteria. *Sensors and Actuators B: Chemical* 356, p. 131332. doi: <https://doi.org/10.1016/j.snb.2021.131332>

Ying, G. et al. 2018. Construction and application of an electrochemical biosensor based on an endotoxin aptamer. *Biotechnology and Applied Biochemistry* 65(3), pp. 323-327. doi: <https://doi.org/10.1002/bab.1610>

Ying, G. et al. 2015. Selecting DNA aptamers for endotoxin separation. *Biotechnology Letters* 37(8), pp. 1601-1605. doi: 10.1007/s10529-015-1839-8

Zamani, M. et al. 2022. A novel labeled and label-free dual electrochemical detection of endotoxin based on aptamer-conjugated magnetic reduced graphene oxide-gold nanocomposite. *Journal of Electroanalytical Chemistry* 908, p. 116116. doi: <https://doi.org/10.1016/j.jelechem.2022.116116>

Zhang, J. et al. 2007. A gold nanoparticle-based chronocoulometric DNA sensor for amplified detection of DNA. *Nat Protoc* 2(11), pp. 2888-2895. doi: 10.1038/nprot.2007.419

Zhao, Q. et al. 2020. Aptamer binding assays and molecular interaction studies using fluorescence anisotropy - A review. *Anal Chim Acta* 1125, pp. 267-278. doi: 10.1016/j.aca.2020.05.061

Zhao, X. et al. 2020. Promoting electricity generation of shewanella putrefaciens in a microbial fuel cell by modification of porous poly(3-aminophenylboronic acid) film on carbon anode. *Electrochimica Acta* 354, p. 136715. doi: <https://doi.org/10.1016/j.electacta.2020.136715>



# Chapter 4

## **AptaMIP sensor – Detection in blood plasma**

---

## 4.1 Introduction

### 4.1.1. General overview

Aptamers are synthetic nucleic acid sequences (20 – 50 nucleotides long) capable of specifically interacting with the analyte of choice, which can range from ions to whole cells (Jiang et al. 2022). Since the selection of an endotoxin-binding aptamer by Kim et al., an increasing number of aptamer-based sensors for the detection of endotoxin have been developed (Kim et al. 2012; Su et al. 2012; Ma et al. 2018b; Jiang et al. 2022). However, the majority of aptamer-based endotoxin sensors reported in the literature, including the aptasensor and hybrid imprinted sensors developed previously by the researcher's group, have demonstrated their performance in aqueous solution and not in clinical samples, which limits their real-life application. The gold standard LAL assay, whilst validated for use in the testing of pharmaceutical samples is not routinely used in clinical applications. The endotoxin activity assay (EEA), developed by Spectral Diagnostics, is the only FDA approved test for endotoxin detection in blood (Yaguchi et al. 2012). It uses human neutrophils primed with endotoxin-antibody complexes coupled with the oxidation of luminol to semi-quantify endotoxin (low, medium and high levels of endotoxin) With the exception of EEA, there is no standard test nor standard sample preparation protocol for the detection of endotoxin in clinical samples (Yaguchi et al. 2012; Reich et al. 2019).

As mentioned in *Chapter 2*, the detection of endotoxin in clinical matrices is especially challenging. Components of the sample matrix as well as additives, such as anticoagulants, can interfere with the detection assays (Harm et al. 2021). *Chapter 2* demonstrated the need for an extensive sample preparation protocol to enable endotoxin detection in citrated blood plasma, highlighting the challenges faced with the recovery of endotoxin in blood samples.

The overarching aim of this chapter is to combine and build upon previous research (Demertzis, 2019) and the work of *Chapter 2*. More specifically, to transfer, assess and optimize the sample preparation approaches, allowing endotoxin recovery using the LAL assay in *Chapter 2*, to the promising aptaMIP developed by previous lab members, which is described in *Chapter 3*.

The work presented in this chapter describes the successful development of a sample preparation protocol which allows the recovery of endotoxin concentrations as low as 10 fg/mL from citrated blood plasma.

### 4.1.2 Shortcomings of biosensors in clinical matrices

One of the most important shortcomings of novel sensors is their application in complex sample matrices, and in particular blood. One of the major issues to overcome is non-specific

binding of sample constituents, such as proteins, lipids and nucleic acids. Many label-free systems are susceptible to pH, temperature and ionic strength changes, and molecules other than the target molecule may cause false-positive signals. (Sin et al. 2014).

Additionally, it is well-known that endotoxin binds to blood components such as cells, proteins, lipoproteins and nucleic acids, causing the masking of endotoxin (Harm et al. 2021). Previous attempts focused on the development of an electrochemical LPS aptasensor, showed that introduction of serum to the sensor, even after significant dilution (1 in 100,000) resulted in very high background “noise” levels, high levels of biofouling and low levels of endotoxin detection, which confirms this (Demertzis, 2019). *Chapter 3* showed that the aptaMIP exhibited high specificity against endotoxin, and little interaction with other proteins, which is an encouraging observation regarding applications in clinical samples.

#### **4.1.3 AptamIP – role in improving specificity and biofouling prevention**

It is hypothesized that the polymer layer prevents biofouling by the formation of specific binding cavities following template extraction, which exhibit high specificity and selectivity for the target molecule (Manesiotis et al. 2013). Additionally, it is hypothesized that the MIP may “lock” the aptamer in a target-detecting conformation, improving sensitivity by increasing specificity for the target molecule and preventing the non-specific binding of sample matrix components. Finally, the polymer layer by itself acts as a barrier between the gold electrode surface, which is well-known for its susceptibility to non-specific binding (Campuzano et al. 2019). Biofouling is often prevented through the use of polymers, such as polyethylene glycol (Bonini et al.) polymers, which are considered the “gold standard” in biofouling prevention, as the polymer layer cannot be readily displaced by sample matrix components, e.g., proteins (Campuzano et al. 2019).

Additionally, conducting polymers, which include aminophenylboronic acid, have gained attention for their biofouling-preventing properties and many MIPs have been developed from both conducting and non-conducting polymers for use in blood samples. Conducting polymers form dense polymer layers which provide a large surface area with greater diffusivity compared to non-conductive polymers, leading to improved biofouling prevention compared to non-conducting polymers (Campuzano et al. 2019). Additionally, electropolymerization can fine-tune the thickness of polymer, leading to optimized polymer thicknesses for improved biofouling prevention (Saxena et al. 2024). For example, a polyaniline molecularly imprinted electrochemical sensor for the detection of phenobarbital was prepared, which exhibited good performance in blood and urine samples (Velayati et al. 2022). Another polyaniline-based sensor has shown a detection limit of 40 fg/mL for Cardiac troponin T, in addition to good performance in dilute human plasma (Phonklam et al. 2020). Polydopamine-based hybrid aptaMIP have also been developed for the detection of prostate specific antigen, with promising results observed in human plasma (Tamboli et al. 2016).

Another example of a PSA-detecting MIP utilizing toluidine blue, with good sensing capabilities in plasma (LOD 0.5 pg/mL) has been described in literature (Abbasy et al. 2020).

Overall, imprinted polymers appear to provide an effective platform with detection limits rivalling commercial immunoassays, with many sensors in literature displaying good biofouling resistance and applications in clinical samples, including blood samples (Cabaleiro-Lago et al. 2023).

#### **4.1.4 Recovery of endotoxin from plasma**

Endotoxin masking is known to be a time-dependent phenomenon. As a result, regulatory authorities require that complex pharmaceutical samples e.g., biopharmaceuticals and those drug products known to contain materials likely to interfere with recovery of endotoxin, are tested in hold-time studies (Reich et al. 2019). It is known that endotoxin is usually found bound to sample matrix constituents, such as enzymes, proteins, lipids, antibodies, platelets, and nucleic acids (Reich et al. 2019). Additionally, sepsis patients usually present themselves at the hospital at the later stages of infection, which suggests prolonged presence of elevated levels of endotoxin in the bloodstream (Paoli et al. 2018). Furthermore, blood samples are often not processed immediately after collection, but are often refrigerated or transported, which may affect the masking of endotoxin (Wu et al. 2017).

*Chapter 2* presented evidence of endotoxin masking in plasma samples, even immediately after spiking ( $t=0$ ), as well as evidence of increased masking over time which was found to be irreversible past day 3 of incubation at either room temperature or refrigeration. Therefore, it is worthwhile investigating whether the development of an endotoxin detection system other than the LAL assay opens up new sample preparation options, improving endotoxin recovery, and allowing endotoxin detection following prolonged incubation.

#### 4.1.5 Aims and objectives

Given the lack of a rapid clinical detection system for endotoxin, the complexity of plasma as a sample matrix and the challenges in endotoxin detection, this chapter will present efforts to overcome the issues around endotoxin detection, using a novel detection platform based on a hybrid imprinted polymer as an alternative to the 'gold standard' LAL assay. The goal of this chapter is to demonstrate the sensitive and rapid detection of endotoxin in plasma, combined with a study of endotoxin masking kinetics under different storage conditions (fridge vs room temperature). Additionally, in *Chapter 3*, recovery of endotoxin was shown to be possible for up to three days of storage at both room temperature and fridge; therefore, one of the questions to be answered in this chapter is whether recovery is possible following prolonged storage (>7 days) by using an alternative detection method.

Thus, the objectives of this chapter are:

- To build upon the sample preparation protocol developed in Chapter 2, exploring further pre-treatment approaches not previously feasible with a LAL-based assay
- To optimize the sample preparation protocol to allow endotoxin recovery from spiked samples following prolonged storage periods (> 7 days).
- To develop a more sensitive endotoxin detection system compared to the LAL assay which has a current detection limit 100 fg/mL for kinetic chromogenic and the turbidimetric assays (Piehler et al. 2020; Pasqua et al. 2021). Clinical samples often require dilution ahead of testing, therefore a low LOD is beneficial (Dagur and McCoy 2015)

## 4.2 Materials and methods

### 4.2.1 Reagents and apparatus

Sodium fluoride (NaF), 3-aminophenylboronic acid, magnesium chloride, sodium deoxycholate, trisodium citrate and hydrochloric acid were purchased from Sigma-Aldrich (UK) and stored under ambient conditions. Sodium hydroxide was purchased from Fisher Scientific and was stored under ambient conditions. Lipopolysaccharide from *E. coli* (Control Standard Endotoxin) was purchased from Fujifilm Wako Chemicals USA Corporation and following reconstitution with endotoxin free water was stored at -20°C prior to use. Endotoxin-free water (Cytiva) was purchased from Fisher Scientific and was stored under ambient conditions. BD Vacutainer blood collection tubes were purchased from MediSupplies (UK). Depyrogenated borosilicate glass tubes and glassware were purchased from Fujifilm Wako Chemicals USA Corporation. The endotoxin aptamer and electrochemical equipment were as described in Chapter 3.

### 4.2.2 Aptamer handling

Aptamer was prepared as described in Chapter 3 section 3.2.2.1.

### 4.2.3 Depyrogenation of equipment

Pyrogen-free centrifuge tubes and pipette tips were purchased from Fisher scientific. Glass test tubes used for blood plasma treatment were depyrogenated by pipetting 100µL of 1M sodium hydroxide into the wells and sealed with parafilm, followed by 2hr incubation at room temperature and rinsing with endotoxin-free water. The tubes were dried using dry heat. Endotoxin-free water was used for the preparation of all solutions and materials in this study. Solutions were tested for the presence of endotoxin using the aptasensor or aptaMIP, where possible.

### 4.2.4 *Blood extraction, storage, and endotoxin spiking*

Venous blood was extracted (following informed consent) into a blue BD Vacutainer citrate tube containing 3.2% trisodium citrate. Immediately after extraction, the blood was centrifuged for 10 minutes at 3000 rpm (Lesche et al. 2016). The resultant plasma supernatant was aliquoted into depyrogenated HPLC vials, sealed with parafilm and stored in a freezer at -20°C until ready to use.

Plasma samples were then either thawed, aliquoted into glass tubes and spiked with endotoxin to determine endotoxin recovery at t=0 or spiked with 10µL of 10 pg/mL endotoxin stock (final endotoxin concentration following sample prep protocol = 100fg/mL), sealed with

parafilm and incubated at either ambient conditions or 2 - 8°C to study endotoxin recovery and masking kinetics.

#### *4.2.5 Spike-hold study*

According to regulators, the spike volume should be minimized to avoid changing the concentration of the undiluted sample (Eur. Pharm. Rev., 2017). In spike-hold studies, 10µL of 10 pg/mL endotoxin stock were added to 90µL of plasma to give an endotoxin concentration of 1 pg/mL. During sample preparation, 40µL of this plasma sample was diluted to a final volume of 400µL resulting in an endotoxin concentration of 100 fg/mL.

Plasma samples were spiked as mentioned above, sealed with parafilm and incubated at either ambient conditions or 2 - 8°C to study endotoxin masking kinetics. Samples were assessed for endotoxin recovery at 24hr intervals after spiking.

#### 4.2.6 Electrochemical characterization of sensors

The electrochemical methodology and techniques used to develop and characterize the sensors and their performance are as described in Chapter 3.

#### 4.2.7 Final sample preparation protocol

Following addition of 40µL of plasma into depyrogenated glass tubes, 40µL of 10mM sodium deoxycholate (NaDOC) was added. Immediately after, 60µL of 0.1M HCl and 200µL of endotoxin-free water were added to give a final volume of 340µL. The tubes were sealed with parafilm, heated at 82.5°C for 10 minutes and cooled down in ice-cold water for 1 minute. Following cooling, 60µL of 0.1M NaOH was added before transferring 200µL of the treated plasma to a pyrogen-free centrifuge tube. The sample was centrifuged for 2 minutes at 9000 x g. The supernatant (10µL) was diluted with 90µL of PBS prepared in endotoxin-free water.

### 4.3 Results and Discussion

Endotoxin levels in this Chapter are reported as mass per volume concentrations (i.e., pg/mL or fg/mL). To allow comparisons with the LAL assay and literature, it is reminded that 1 EU (endotoxin unit) is equal to 0.1-0.2 ng (Sigma-Aldrich, 2023).

#### 4.3.1 Requirement of a sample preparation protocol

Previous work in the researcher's group has shown that despite the aptaMIP's impressive performance in aqueous solutions, upon addition of dilute spiked serum samples, significantly reduced performance was observed making endotoxin quantification almost impossible (Demertzis, 2019). While biofouling may have played a role in the generation of high impedance values, endotoxin's ability to bind and attach itself to sample matrix components, such as proteins, lipids and nucleic acids, also plays an important role in the generation of high impedances. This may be possible by the formation of complexes with plasma components which is known to render endotoxin undetectable by the LAL assay, and possibly by said complexes adding large masses on the surface of the aptaMIP (Harm et al. 2021).

This was well documented in *Chapter 2*, where an extensive sample preparation protocol was developed to render endotoxin detectable by the LAL assay. However, the LAL assay requires the activation of the coagulation cascade, which is inhibited by sodium citrate, an anticoagulant present in blood-collection tubes. As the aptaMIP utilizes a different detection pathway, it is possible that reversal of anticoagulation caused by citrate may not be necessary.

It is well known that plasma lipoproteins bind and neutralize endotoxins, and that lipid shedding from LDL and VLDL cholesterol to form HDL following prolonged storage in ambient conditions may explain the phenomenon of endotoxin masking over time (Pinto et al. 2014; Harm et al. 2021). In *Chapter 2*, it was demonstrated that despite the extensive sample preparation protocol, complete endotoxin recovery was impossible with the passage of time, possibly owing to challenges caused by the presence of lipoproteins. Failing heat and acid denaturation, it was hypothesized that the addition of a lipid-solubilizing detergent may assist with endotoxin recovery, however as discussed in previous Chapters, the LAL assay is sensitive to sample temperature and pH fluctuations, and its activity is severely hindered by the addition of surfactants and detergents, such as polysorbate and sodium deoxycholate (NaDOC) (Harm et al. 2021).

NaDOC is an ionic detergent with lipid-solubilizing properties that has a well-known effect on human plasma lipoproteins, which are notorious endotoxin binders (Aketagawa et al. 1993; Harm et al. 2021). Due to the beforementioned susceptibilities of the LAL assay, the researcher was limited regarding possible sample preparation approaches. However, the use of an alternative detection platform, utilizing aptamers and MIPs may provide the

opportunity to explore alternative sample preparation approaches, including the use of lipid-solubilizing detergents such as NaDOC.

In this Chapter, the key factors in sample preparation were systematically explored. Starting with the approaches presented in Chapter 2, a series of experiments exploring the effects of individual modifications to the LAL plasma protocol on endotoxin recovery, such as heating, modified acid-base treatment, filtration, centrifugation and addition of NaDOC.

#### 4.3.1.1 Effect of simple plasma dilution

Dilution in endotoxin-free water is often one of the first approaches used when dealing with low endotoxin recovery, as interferences are often caused by high concentrations of endotoxin-binding compounds or matrix components (Cooper 1990). Given the high number of potential biofouling and endotoxin-masking agents present in blood plasma, it often the first solution suggested by LAL manufacturers (Associates of Cape Cod, 2005; Lonza, 2012). Although in *Chapter 2* it was discovered that dilution had little to no effect in improving endotoxin recovery using the LAL assay, it was considered worthwhile to assess its effects using the aptaMIP, as it would provide insights on the factors causing biofouling/LER.

Figure 4.1 shows the EIS spectra obtained following incubation of the AptaMIP with various dilutions of citrated plasma. The addition of undiluted plasma caused a massive increase in impedance of approximately 225%, suggesting high levels of biofouling. Plasma dilution appears to be effective at reducing biofouling, with higher dilution factors leading to lower impedances. Still, even at 1 in 10 dilution, an unacceptably large increase in impedance (88%) was observed suggesting that further sample preparation is required and that biofouling cannot be resolved by dilution alone.

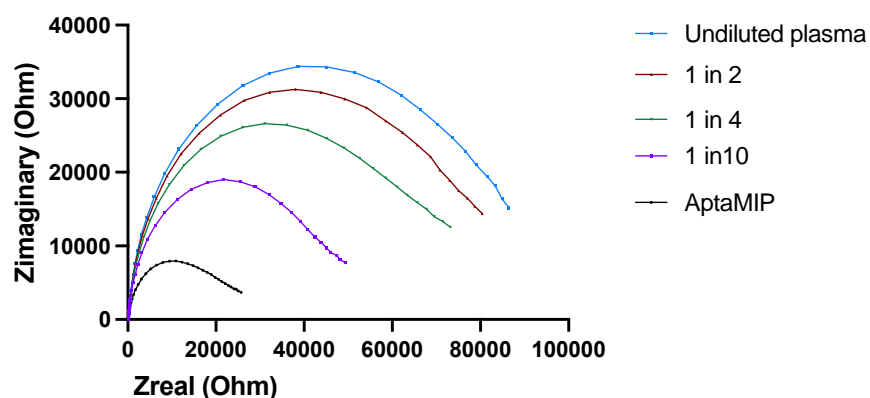


Figure 4.1: EIS results showing the response of the aptaMIP following incubation with various dilutions of unspiked plasma (N=3). Incubation with tenfold diluted plasma caused a large increase in impedance (approximately 88%), and increased plasma concentrations resulted in further increases in impedance, suggesting high levels of biofouling that cannot be resolved by dilution alone.

To assess the effect of simple dilution on endotoxin recovery, plasma samples were spiked and then diluted spiked with endotoxin to give a final concentration of 10 fg/mL. Figures 4.2 A-C shows the EIS spectra obtained following incubation of the AptamIP with various dilutions of spiked citrated plasma. As described in Chapter 3, incubation of the AptamIP with 10 fg/mL endotoxin in water resulted in an average increase in impedance of 28% (figure 3.29).

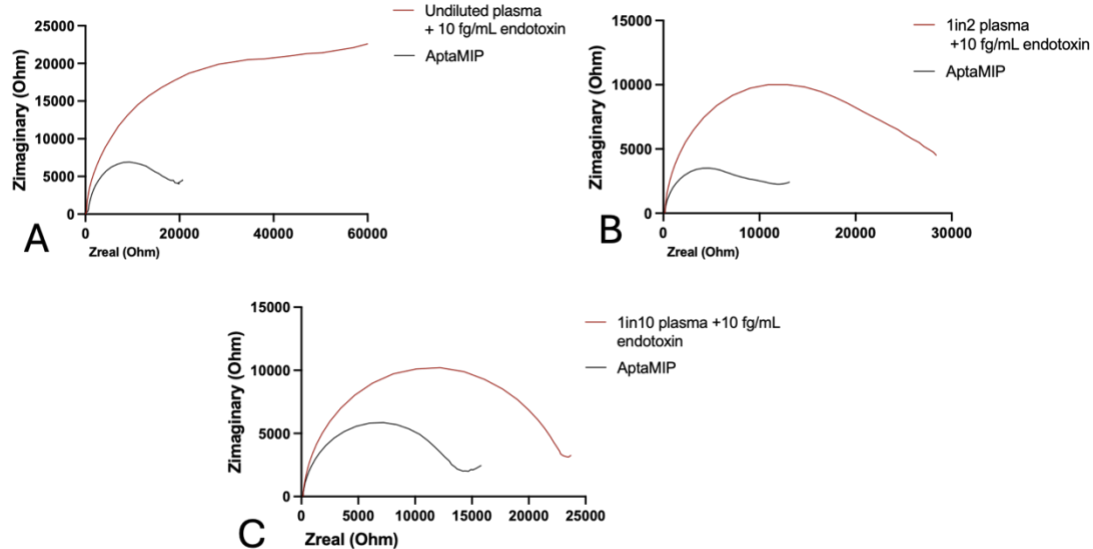


Figure 4.2 A-C: EIS results showing the response of the aptaMIP following incubation of the AptamIP (black lines) with various dilutions of spiked citrated plasma (red lines). Figure 4.2 A shows the results following incubation with spiked undiluted plasma, B shows the results following incubation with spiked twofold diluted plasma, and C shows the results following incubation with spiked tenfold diluted plasma.

Figure 4.2 A shows that incubation with undiluted plasma spiked with 10 fg/mL results in a large increase in impedance of approximately 155%, and that twofold diluted spiked plasma resulted in a similar increase in impedance of approximately 140%. Tenfold diluted, spiked plasma resulted in an increase in impedance of approximately 77%. Despite tenfold dilution being moderately effective at biofouling reduction, the impedances recorded were still significantly higher than that observed with the same concentration of endotoxin in water, suggesting that further sample preparation was required.

Overall, compared to the results in the previous graph (figure 4.1), lower impedances were noted in the spiked samples compared to the unspiked ones, especially across undiluted and twofold diluted samples (239% vs 155%, and 192% vs 140%). This is an interesting observation and may suggest that the system may still exhibit selectivity for endotoxin, even in minimally treated samples, with the binding of endotoxin to the apta-MIP at the electrode surface serving to decrease non-specific interaction with other plasma components. Regardless, the results suggested that further sample preparation was necessary.

#### 4.3.1.2 Effect of acid / base treatment and modifications (Chapter 2 protocol)

Based on the successful application of the sample preparation protocol developed in *Chapter 2*, it was decided to evaluate its efficiency using the aptaMIP sensor. Following addition of 40 $\mu$ L unspiked plasma into depyrogenated glass tubes, 40 $\mu$ L of endotoxin free water and 60 $\mu$ L of 1M hydrochloric acid were added, followed by 200 $\mu$ L of magnesium chloride at a concentration of 5mM. The tubes were sealed with parafilm, heated at 82.5 $^{\circ}$ C for 10 minutes and cooled down in ice-cold water for 1 minute. Sodium hydroxide (1M, 60 $\mu$ L) was added to give a total volume of 400 $\mu$ L. The samples did not undergo centrifugation. Figure 4.3 shows the EIS spectra obtained following addition of the treated plasma to the aptaMIP. A decrease in impedance (approximately -47%) was observed.

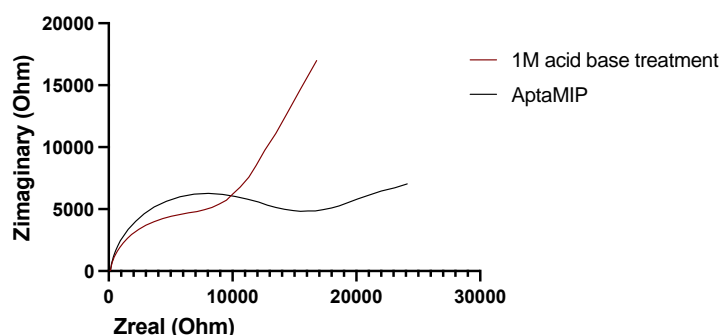


Figure 4.3: EIS results showing the response of the aptaMIP (black curve) following incubation with plasma treated according to the Chapter 2 protocol (red curve). A decrease in impedance (approximately -47%) was observed.

Interestingly, the use of the original sample preparation protocol (red line), which included the acid / base treatment using 5mM MgCl<sub>2</sub>, 1M HCl and 1M NaOH caused a drop in impedance. This may be caused by a pH imbalance affecting either the polymer or the aptamers, or both. DNA is known for its stability between pH 5 and 9, so it is possible that pH fluctuations may affect the sensor (Thaplyal and Bevilacqua 2014). It was decided to reduce the HCl and NaOH concentrations to 0.1M. Figure 4.4 shows the system's response following addition of the treated plasma to the aptaMIP. An increase in impedance (approximately 80%) was observed.

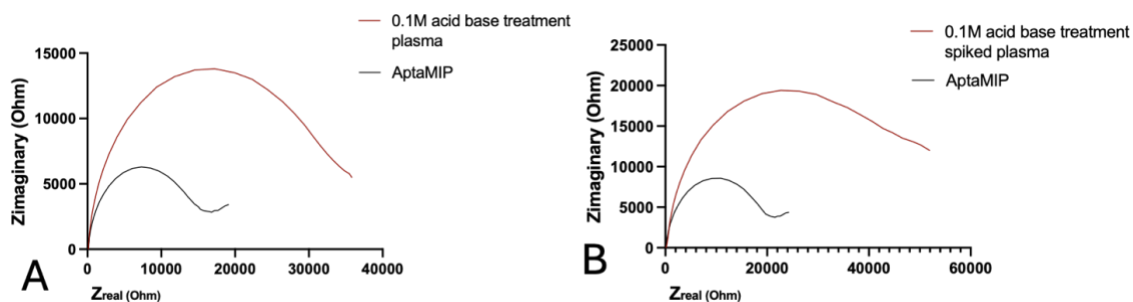


Figure 4.4 A and B: EIS results showing the response of the aptaMIP (black curve) following incubation with **unspiked** (A) and **spiked with 10 fg/mL** plasma (B) treated according to the Chapter

2 protocol, with a lower concentration of HCl and NaOH (0.1 M), as well as **5mM MgCl<sub>2</sub>** (red curve). An increase in impedance (approximately 80% for unspiked plasma and approximately 115% for spiked) was observed for both samples.

The use of 0.1M HCl and NaOH solutions resolved the impedance decrease issue, however the impedances noted following the treatment were similar to those observed with a simple tenfold dilution of plasma (figure 4.1), suggesting that further refinement is necessary. The use of acids to denature proteins is well documented in literature, with acidic environments known to lower the denaturation temperature of blood proteins (Fink et al. 1994; Baler et al. 2014).

However, the impedances noted so far in treated plasma were still high, suggesting that further modifications to the treatment protocol were required. It was hypothesized that the addition of MgCl<sub>2</sub>, which is known to promote aggregation of endotoxin, may lead to the generation of high impedances brought about by the binding of large endotoxin aggregates on the sensor's surface (Szermer-Olearnik and Boratynski 2015; Harm et al. 2021).

Figure 4.5 A shows the system's response following addition of the treated plasma, this time without MgCl<sub>2</sub>, to the aptaMIP. An increase in impedance (approximately 57%) was observed. Figure 4.5 B shows the response obtained following addition of plasma spiked with 10 fg/mL, subjected to the same protocol. An increase in impedance of 68% was observed.

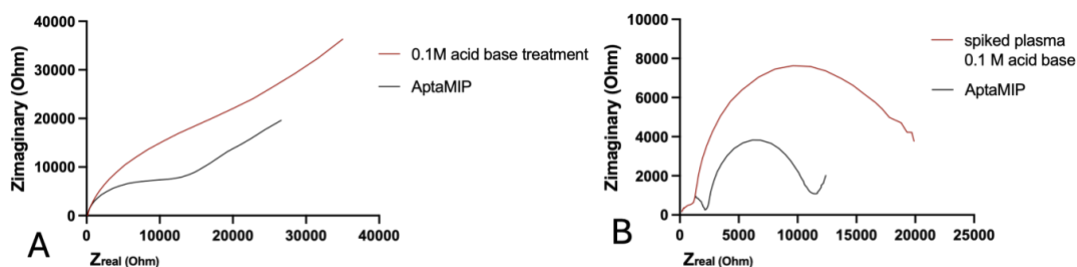


Figure 4.5 A: EIS results showing the response of the aptaMIP (black curve) following incubation with plasma treated according to the Chapter 2 protocol, with a lower concentration of HCl and NaOH (0.1 M each) **and without MgCl<sub>2</sub>** (red curve). An increase in impedance (approximately 55%) was observed. Figure 4.5 B shows the response of the aptaMIP (black line) following incubation with plasma **spiked with 10 fg/mL**, following the same preparation protocol

It is not known whether the aptamer used in this study interacts with the Lipid A portion of endotoxin, or the O-antigen. Neither the paper published by the group that engineered the aptamer, nor subsequent papers utilizing this aptamer mention the exact detection mechanism for endotoxin (Kim et al. 2012; Su et al. 2012; Jiang et al. 2022). Moreover, it is not known whether the conformation of the endotoxin (monomer or aggregate form) affects the interaction with the aptamer. Figures 4.4 A and B shows that the inclusion of MgCl<sub>2</sub> in the sample pretreatment, both the control plasma sample and the spiked plasma sample caused

an increase in impedance of approximately 80% and 115%. It is known that the addition of  $MgCl_2$  causes the formation of endotoxin aggregates. This is well-documented in literature; addition of divalent cations has been associated with formation of multilamellar structures, and in the presence of  $Mg^{2+}$ , the negatively charged lipid A regions of endotoxin react with the cations to form aggregates. The binding of endotoxin aggregates on the aptaMIP surface may cause an increase in impedance, as endotoxin aggregates carry a strong negative charge (endotoxin has an isoelectric point of 2). This increases the steric barrier, inhibiting the passage of electrons to the electrode's surface, resulting in an increase in impedance (Reich et al. 2018). When endotoxin is found in aggregate form, the hydrophobic lipid A regions are hidden inside the core of the structure, while the hydrophilic O-antigen is fully exposed (Harm et al. 2021).

It can be hypothesized that the aptamer developed by Kim et al. detects the O-antigen portion of endotoxin. However, it is important to note that the structure of Lipid A is highly conserved across bacterial species, whereas the O-antigen is more variable (Gorman and Golovanov 2022). The group that engineered the aptamer used endotoxin from *E. coli* 055:B5 (Kim et al. 2012). Control standard endotoxin is extracted from *E. coli* O113:H10, sharing similar O-antigens with *E. coli* 055:B5, which may support the O-antigen recognition hypothesis. Literature is poor on the application of the aptamer developed by Kim et al. on sensors, so comparisons with literature are challenging.

This comes into agreement with previous findings in *Chapter 3*, and in particular Figure 3.35. Figure 3.35 showed that endotoxin incubated with HSA resulted in higher-than-normal impedances. According to literature, HSA binds to lipid A with high affinity (Gioannini et al. 2002). Therefore, combined with the observation in Figure 3.35, the hypothesis that the aptamer detects the O-antigen portion of endotoxin becomes stronger. This may be confirmed by the use of endotoxin lacking the O-antigen (lipooligosaccharide), which was not possible in this project due to time constraints. Published studies using the aptamer used in this project have used either *Pseudomonas aeruginosa* or *Escherichia coli* endotoxins, which contain the O-antigen, and similar responses were noted between those two endotoxins (Kim et al. 2012; Su et al. 2012; Ma et al. 2018b; Jiang et al. 2022). Given the interest in diseases caused by lipooligosaccharide-containing bacteria such as *Haemophilus influenzae* and *Campylobacter jejuni*, this may provide insights for future sensor development.

#### **4.3.1.3 Physical separation (centrifugation and filtration)**

Although centrifugation provided a small improvement in terms of minimizing biofouling, it was considered worthwhile assessing whether filtration would prove beneficial. Cellulose was the filter of choice, as studies have shown that it allows passage of endotoxin (Vanhaecke et al. 1989). Whilst cellulose filters are also known for their interference with the LAL assay by causing false-positives through contamination with beta-glucans, it was anticipated that the

use of a non-LAL assay approach would allow their use in sample preparation (Ikemura et al. 1989). Previous research in the researcher's group has presented evidence that the AptaMIP does not cross-react with beta-glucan (Demertzis, 2019). Other filters, such as positively-charged Nylon and PTFE membranes are known for their ability to effectively remove endotoxin from samples and were therefore not included in this study (Gerba and Hou 1985; Dahlman-Hoglund et al. 2016). Figure 4.6 A shows the system's response following addition of plasma filtered using a cellulose syringe filter, and figure 4.6 B shows the response following incubation with spiked plasma subjected to the same protocol. No change in impedance was observed with the control plasma, while a small increase of 4% was noted for the plasma spiked with 10 fg/mL endotoxin. This is considerably lower than the 26% change in impedance observed for the same concentration of endotoxin in water.

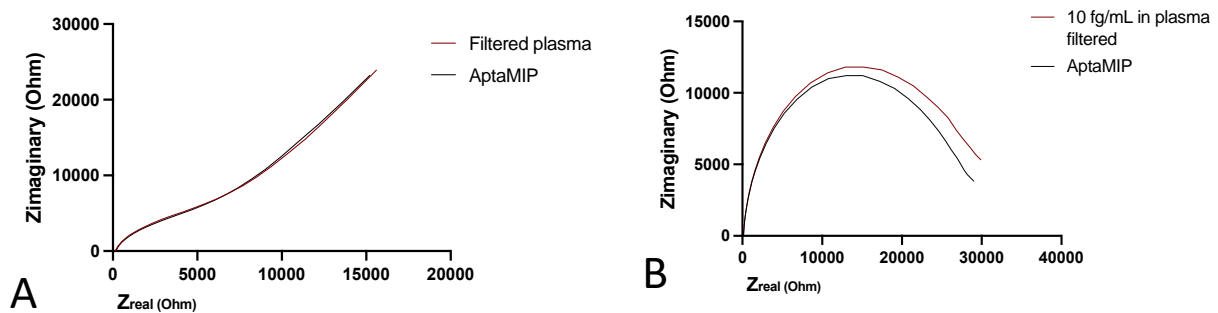


Figure 4.6 A: EIS results showing the response of the aptaMIP (black curve) following incubation with plasma filtered using a cellulose syringe filter (red curve). No changes in impedance were observed.

Figure 4.6 B shows the response of the aptaMIP (black curve) following incubation with spiked plasma filtered using a cellulose syringe filter (red curve). A 4% change in impedance was observed.

Whilst filtration allowed for a good baseline response to be achieved with the control plasma, it also adversely affected the recovery of endotoxin. To assess whether this was down to removal of free endotoxin or endotoxin bound to plasma constituents, a water sample spiked with 10 fg/mL endotoxin was subjected to filtration and analysed. The results are shown in figure (4.7).

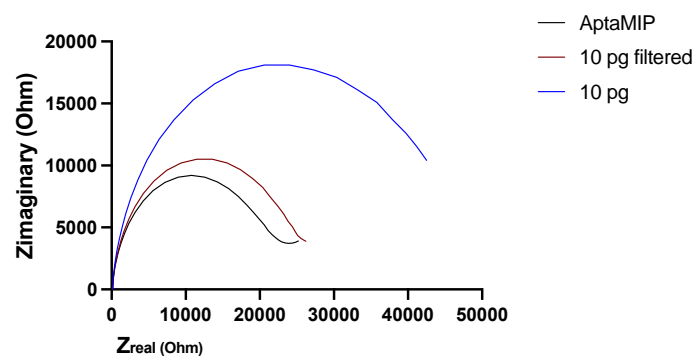


Figure 4.7: EIS graph showing the aptaMIP (black line) response following incubation with a water sample spiked with 10 pg/mL endotoxin and then subjected to filtration through a cellulose syringe

filter (red line) and the same solution without filtration (blue line).  $N=1$  as this was a screening experiment.

Interestingly, as shown in figure 4.7, filtration using a cellulose syringe filter resulted in approximately 80% of endotoxin (10 pg/mL) being filtered out. Therefore, it was decided to exclude filtration from the sample preparation protocol.

In Chapter 2, centrifugation was found to be effective at further improving endotoxin recovery, through the physical separation of denatured proteins and other interfering plasma components. Therefore, it was decided to assess the effect of centrifugation in the reduction of biofouling. Figure 4.8 shows the system's response following addition of the treated plasma, without  $MgCl_2$ , plus centrifugation, to the aptaMIP. An increase in impedance (approximately 47%) was observed.

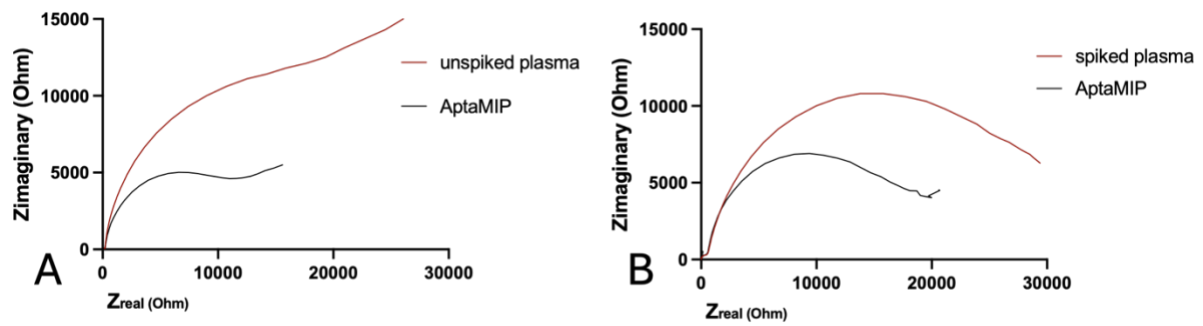


Figure 4.8: EIS results showing the response of the aptaMIP (black curve) following incubation with plasma treated according to the Chapter 2 protocol, with a lower concentration of HCl and NaOH (0.1 M each) **without  $MgCl_2$  and including centrifugation** (red curve). An increase in impedance (approximately 47%) was observed for the unspiked plasma, with an increase of 52% noted following addition of plasma spiked with 10 fg/mL endotoxin.

Figure 4.8 shows that centrifugation resulted in a further decrease in impedance compared to the previous step (approximately 8% difference). Centrifugation is commonly used in sample preparation, especially in serum and plasma, to deplete samples of lipoproteins and protein contaminants (Brennan et al. 2020). In combination with the dilution, heating and acid / base treatment steps, it may help improve recoveries of endotoxin by preventing rebinding to plasma components (Lu et al. 2012; Sneek et al. 2012).

#### 4.3.1.4. Effect of sodium deoxycholate (NaDOC) on endotoxin recovery

Despite the notable reduction in impedance brought about by the modification of the acid / base treatment protocol developed in Chapter 2, following an extensive preparation protocol including centrifugation, it was apparent that there were other plasma constituents bound to endotoxin or causing biofouling that needed to be addressed.

It is well known that plasma lipoproteins bind and neutralize endotoxins (Pinto et al. 2014). Sodium deoxycholate (NaDOC) has been long used for the solubilization of lipids and lipoproteins including LDL and HDL present in human blood (Robern 1982; Walsh and Atkinson 1983). However, the LAL assay is severely hindered by the addition of surfactants and detergents, such as sodium deoxycholate (NaDOC). It was hypothesized that the use of a different detection system may allow its successful application in sample preparation.

According to the literature, various NaDOC concentrations have been used for lipoprotein solubilization, with good dissolution being observed at 1mM (Oeswein and Chun 1983). Additionally, DNA and aptamers show good tolerance to neutral and anionic surfactants, however it is important to keep its concentration low so as to preserve the aptamer's secondary structure and binding capacity. It was therefore decided to prepare a 10mM NaDOC stock solution to give a final sample concentration of 1mM (Peterson et al. 2015).

The final protocol consisted of 40  $\mu$ L of spiked plasma into depyrogenated glass tubes, 40 $\mu$ L of 10mM sodium deoxycholate (NaDOC) (10 mM), 60 $\mu$ L of 0.1M HCl and 200 $\mu$ L of endotoxin-free water, heating at 82.5°C for 10 minutes and 60 $\mu$ L of 0.1M NaOH. By the end of the process, the plasma had been diluted 1 in 10. Figure 4.9 shows the EIS spectra of the AptaMIP following addition of control plasma subjected to the optimized pre-treatment protocol.

The responses observed with water and plasma samples spiked with endotoxin and subjected to the final protocol are shown in Figure 4.10. Figure 4.9 shows that incubation of the aptaMIP with unspiked plasma subjected to the final protocol resulted in the lowest increase in impedance across all treatments screened in this study (approximately 15%). The data shows that the addition of NaDOC to spiked plasma samples resulted in EIS spectra closely resembling those obtained from water samples containing the same concentration of endotoxin, subjected to the same protocol, suggesting that lipoproteins may be responsible for the majority of biofouling or endotoxin binding.

Figure 4.10 shows that incubation of the aptaMIP with spiked plasma subjected to the final protocol resulted in an increase in impedance (approximately 32%) similar to the values recorded with endotoxin in water, subjected to the same protocol (approximately 26%).

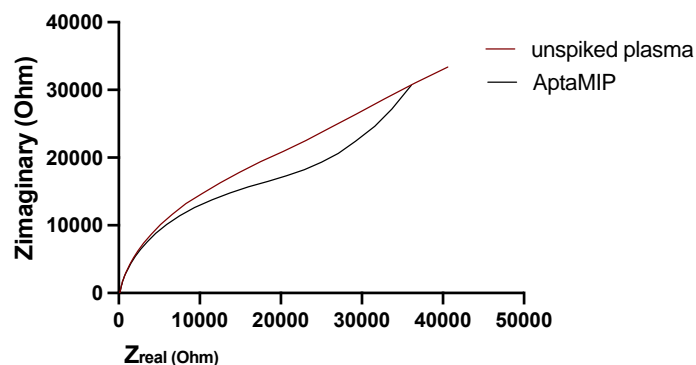


Figure 4.9: EIS results showing the response of the aptaMIP (black curve) following incubation with unspiked plasma treated according to the Chapter 2 protocol, with a lower concentration of HCl and NaOH (0.1 M each) **including NaDOC, without MgCl<sub>2</sub> and including centrifugation** (red curve). An increase in impedance (approximately 15%) was observed.

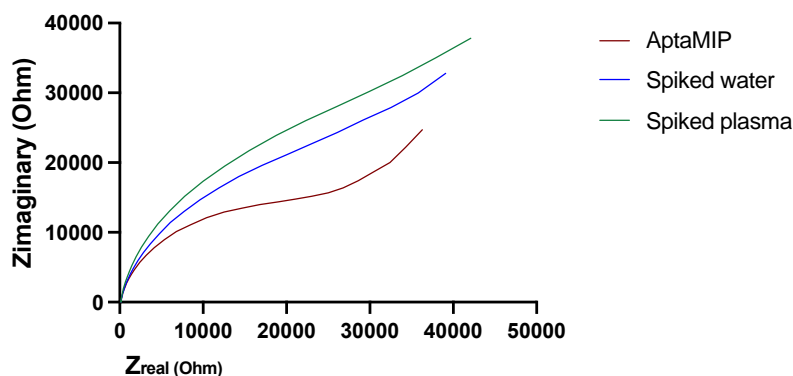


Figure 4.10: EIS graph showing the response of the aptaMIP following incubation with water and plasma samples spiked with 10 fg/mL endotoxin and subjected to treatment with the optimised sample treatment protocol, including dilution, acid-base treatment, NaDOC addition and centrifugation. N=1 as this was a screening experiment.

It was noted that the combination of NaDOC with acid-base treatment resulted in the formation of precipitate, as shown in Figure 4.11. NaDOC addition by itself results in the sample becoming cloudy, however no precipitate was observed following centrifugation. HCl alone doesn't lead to a visual change.



Figure 4.11: Photo showing the formation of white precipitate at the bottom of a centrifuge tube, following the completion of the finalized sample preparation protocol.

#### 4.1.3.5 Summary of various plasma treatments in unspiked plasma

So far, several sample preparation approaches have been explored. Simple dilution, often recommended as a first approach to sample preparation, was found ineffective regarding biofouling prevention. The use of 1M HCl and NaOH as part of an acid-base protein denaturation step was found to be incompatible with the sensor, resulting in sharp drops in impedance. Between filtration and centrifugation, only centrifugation provided a viable improvement in biofouling prevention, as filtration also found to remove endotoxin from the sample. Finally, the addition of NaDOC and centrifugation to the existing protocol resulted in the lowest levels of biofouling in this study, as evidenced by figure 4.12 below.

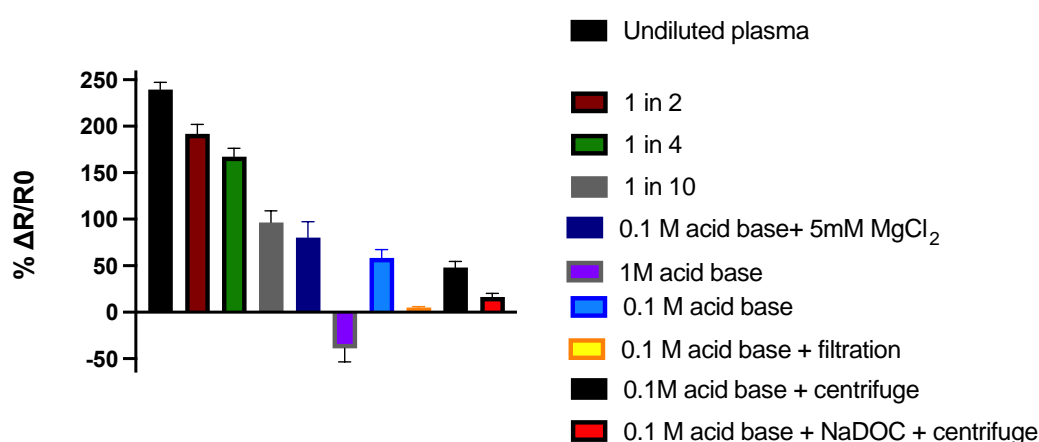


Figure 4.12. Percentage change following incubation of the aptaMIP with unspiked plasma following various sample preparation treatments

Figure 4.13 below summarises the aptaMIP response following incubation of the sensor with spiked (10 fg/mL) plasma samples subjected to the various pre-treatment protocols. When compared to the water control (water spiked with 10 fg/mL endotoxin), it is evident that the addition of NaDOC and centrifugation to the pre-treatment protocol produces a response most similar to the control (37% vs. 26%, respectively). All other pre-treatment approaches resulted in responses some 2.5 - 3.5-fold greater than the control, which is assumed to be a consequence of a combination of biofouling and endotoxin aggregation, either with itself or with other plasma components. Such an exaggerated response is likely to diminish the working range of the sensor.

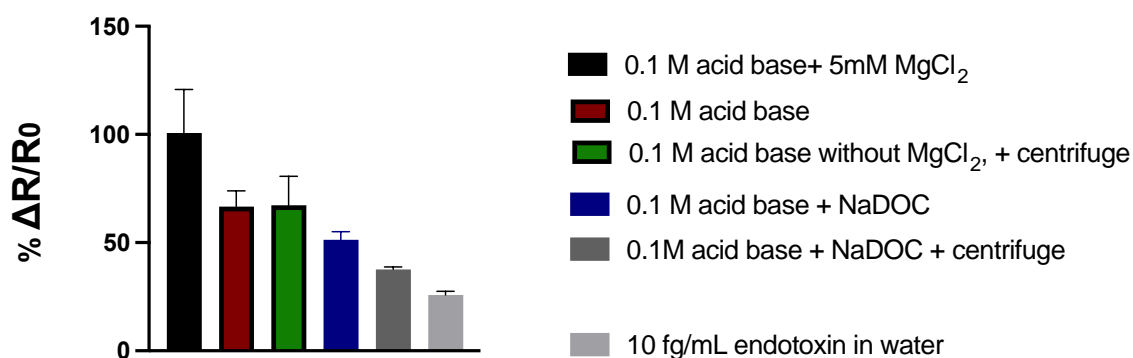


Figure 4.13 Percentage change following incubation of the aptaMIP with plasma spiked with 10 fg/mL following various sample preparation treatments. The response obtained with 10 fg/mL endotoxin in water is added for comparison (light grey bar, rightmost side).

From start to finish, the total sample preparation time is approximately 15 minutes, which is 5 minutes shorter than the protocol proposed in *Chapter 2* due to reduced cooling times following the heating step (1 minute vs 3) and a faster centrifugation step (2 minutes vs 5). Similarly to as described in *Chapter 2*, it is understandable that the numerous steps involved are less than ideal, however the shorter preparation time may be beneficial for a “near-patient” detection system. It is reminded that citrated blood plasma is an especially challenging sample matrix, and that to the best of the researcher’s knowledge, no successful recovery of endotoxin from citrated plasma has been presented in literature (Harm et al. 2021).

#### 4.1.3.6 Further refinement of the pre-treatment protocol

Taking forward the ‘final’ protocol described above, the sensor was challenged with plasma samples spiked with between 10 fg/mL and 100 pg/mL endotoxin. Figure 4.14 shows the EIS spectra obtained from this study, demonstrating a clear dose-response relationship thus supporting the application of the pre-treatment protocol.

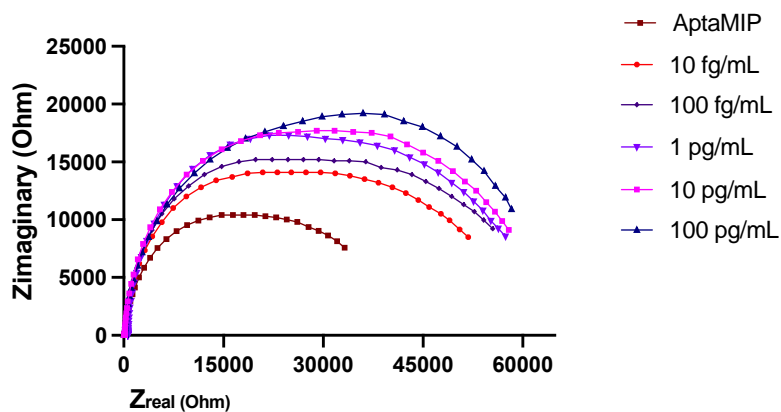


Figure 4.14. EIS graph showing the response of the aptaMIP to spiked plasma samples subjected to the optimised pre-treatment protocol described in 4.3.1.4. N=1 as this was a screening experiment.

Despite the successful recovery of endotoxin, the system exhibited poor replicability across sensors and instability, observed as EIS shifts, following incubation with treated plasma, possibly explained by a pH imbalance from the acid/base treatment. It was therefore decided to dilute the treated plasma in PBS (10mM, pH 7.4) to ensure return to a neutral pH and hopefully improve the stability of the sensor.

The final sample preparation protocol consists of the addition of NaDOC to spiked plasma, addition of 0.1M HCl, dilution in endotoxin free water, heating, pH balancing with 0.1M NaOH, resulting in a 1 in 10 dilution, centrifugation for two minutes and a further 1 in 10 dilution in endotoxin-free PBS, resulting in a 1 in 100 overall dilution. Figure 4.15 shows the EIS spectra obtained following incubation of the aptaMIP with increasing concentrations of spiked plasma.

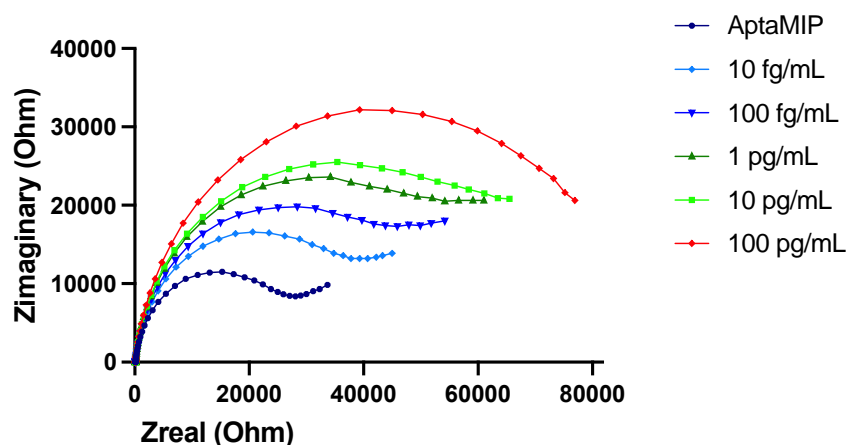


Figure 4.15: EIS graph showing the dynamic range of the aptaMIP (dark blue line) following incubation with a range of treated plasma spiked with endotoxin (10 fg/mL – 100 pg/mL). An increase in impedance is noted with increasing concentrations.

Figure 4.16 shows the sensor's linearity when challenged with treated plasma comparing it with the sensor's performance in water. The aptaMIP exhibits satisfactory linearity in both

media, with an  $r^2 = 0.9321$  across all endotoxin concentrations tested in plasma, although a higher  $r^2$  value is observed between the ranges of 10 fg/mL and 10 pg/mL ( $R^2 = 0.961$ ,  $R = 0.9803$ ).

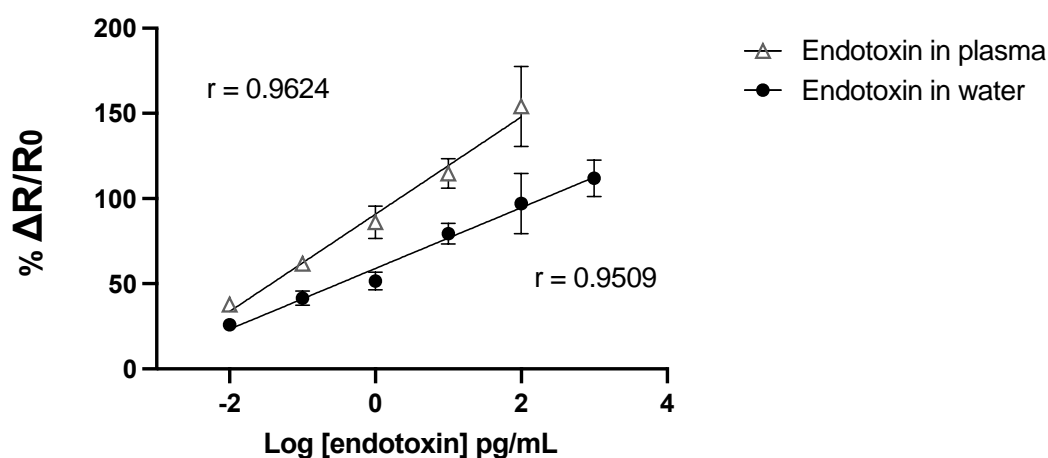


Figure 4.16: Dose-response graph of the aptaMIP when challenged with a variety of endotoxin concentrations in both water and treated plasma, ranging from 10 fg/ml to 100 pg/ml. The sensor shows a good linear response in plasma between 10 fg/ml and 100 pg/ml ( $r^2 = 0.9321$   $r = 0.9654$ ).

Overall, higher  $\% \Delta R$  values are noted for all plasma samples compared to water, with a greater deviation in  $\% \Delta R/R_0$  values between the two sample matrices being observed as the concentration of endotoxin increased. It is possible that at higher endotoxin concentrations, relatively more endotoxin is able to bind to residual plasma components which manifests as higher impedances and also more variability in response, as indicated by the larger error bars. However, larger error bars were also recorded for endotoxin in water, which suggests that plasma components may not be solely responsible for the increase in error. It is possible that in larger concentrations, endotoxin arranges itself in aggregates or supramolecular structures. It is known that in physiological conditions, such as the ones in this experiment, endotoxin forms non-lamellar cubic structures, which also increase the bioactivity of endotoxin (Gorman and Golovanov 2022).

No published work utilizing APBA or apta-MIP approaches for the detection of endotoxin, especially in clinical matrices, was found in literature, and very little published work exists on the recovery of endotoxin from blood samples, especially citrated plasma (Harm et al. 2021). Therefore, it is difficult to compare the results of this project to existing literature, and comparisons will be made with general MIP approaches. Çimen et al. developed an endotoxin imprinted surface plasmon resonance sensor, using 2-hydroxyethylmethacrylate as a functional monomer (Cimen et al. 2021). A LOD of 0.023 ng/mL was reported. Another SPR platform which utilized MIPs was developed by Abdin et al., who used itaconic acid as a monomer and reported a LOD of 15.6 ng/mL (Abdin, 2015). Altintas et al. used itaconic acid, methacrylic acid and acrylamide as functional monomers to imprint lipid A to develop nano-

membranes in a microplate, with a reported LOD of 0.44 ng/mL (Altintas et al. 2016). In a similar method, Liu et al. used dopamine to develop nano-membranes, in combination with an antibody specific for the lipid A region, with similar results (Liu et al. 2019). Compared to the published MIP work in literature, the system developed in this study displays a low LOD of 10 fg/mL as well as the ability to detect endotoxin in plasma samples.

### 4.3.1 Spike-hold studies

#### 4.3.1.1 Unspiked plasma stored at room temperature or in the refrigerator

In *Chapter 2*, spike-hold studies were performed in spiked plasma and evidence of endotoxin masking over time was presented. Therefore, it was considered worthwhile to investigate whether *unspiked* plasma underwent any changes that would result in changes in impedance following storage over time, at both room temperature (RT) and refrigeration. Figure 4.17 A shows the EIS spectra of unspiked plasma stored at RT for up to 15 days. Figure 4.17 B shows the impedance change, expressed as  $\% \Delta R$ , following incubation with unspiked plasma stored at *ambient* conditions and subjected to treatment with the finalized sample preparation protocol, including addition of NaDOC, centrifugation and tenfold dilution in endotoxin-free PBS.

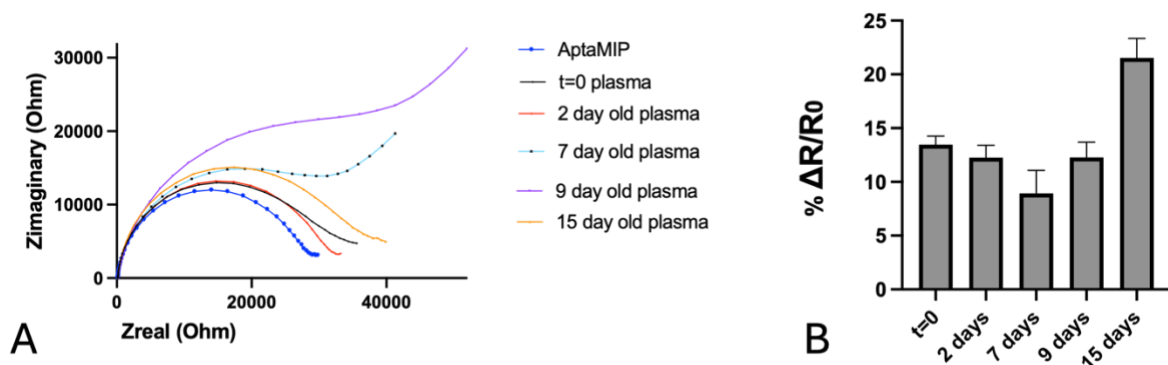


Figure 4.17 A: EIS graph showing the impedances of unspiked plasma ( $N=3$ ) following prolonged storage at **room temperature**, for up to 15 days. 4.17 B shows the  $\% \Delta R$  corresponding to figure 4.17 A.

Overall, similar impedances were noted for plasma stored at room temperature when stored for up to 9 days, suggesting no major changes in plasma composition. Interestingly, an increase in impedance was noted at day 15. A possible reason for this is described below.

Figure 4.18 A shows the EIS spectra of unspiked plasma stored in the refrigerator for up to 15 days and subjected to the finalized sample preparation protocol, with Figure 4.18 B showing the impedance change, expressed as  $\% \Delta R$ .

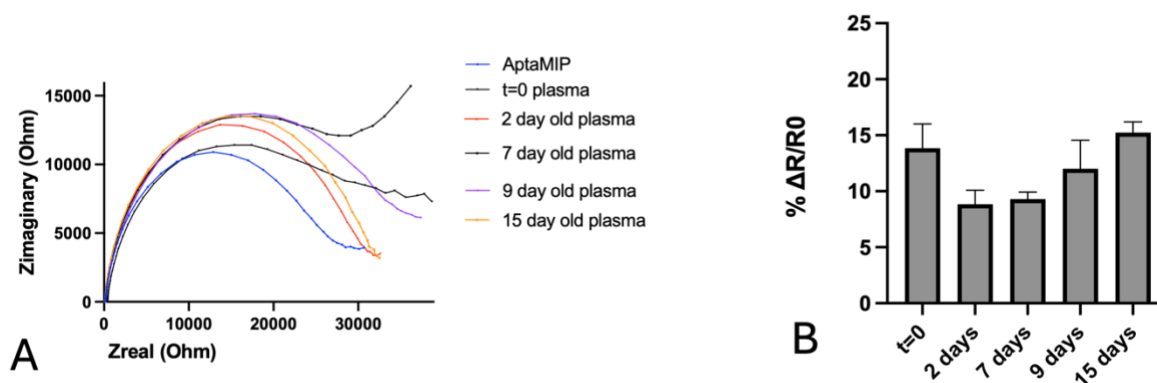


Figure 4.18: EIS graph showing the impedances of unspiked plasma (N=3) following prolonged storage in the fridge, up to 15 days. 4.18 B shows the % $\Delta R/R_0$  corresponding to figure 4.18 A.

Overall, similar impedances were noted for plasma stored in the fridge across all days tested, suggesting good stability for up to 15 days of storage.

There are several studies reporting the stability of plasma and the biochemical markers contained within under different conditions, including prolonged storage. Regarding the increase in impedance on day 15 at room temperature it is hypothesized that any changes noted in unspiked plasma were probably caused by either metabolic changes in blood plasma or peptides resulting from protein degradation (Kaisar et al. 2016; Kapuruge et al. 2022). It is also possible that prolonged storage may lead to denaturation of proteins, enzymes and lipids, some of which may be able to interact with the aptamip (Kaisar et al. 2016).

LDL, VLDL and cholesterol have been shown to undergo significant changes following prolonged storage (Pinto et al. 2014; Holzer et al. 2017). In particular, the study of Pinto et al. has shown that LDL/VLDL begin discarding phospholipids to form HDL after 2.5hrs incubation at room temperature (Pinto et al. 2014). A study by Shimizu and Ichihara found a 9% increase in plasma HDL at room temperature after day 3 of storage, and interestingly, a decrease of 8.5% on day 28, but no changes across plasma lipids stored at 4°C (Shimizu and Ichihara 2019). This increase in HDL may be explained by the results of a study which found that in serum stored at room temperature, LCAT (lecithin:cholesterol acyltransferase) acted on HDL to increase its levels (Pini et al. 1990). No other studies were found in literature regarding the effect of sample storage on LCAT function. Additionally, literature is divided on the effect of prolonged storage of plasma at room temperature, with some studies reporting little to no changes in clinically relevant protein markers (Aguilar-Mahecha et al. 2012; Pasella et al. 2013; Kaisar et al. 2016), while others report changes only after > 96 hrs (Kapuruge et al. 2022), therefore it is difficult to pinpoint the exact mechanism behind the observations made here.

It is possible that refrigeration slows down the lipid shedding from VLDL and LDL to HDL. According to clinical guidelines lipoproteins remain stable for 24hrs at 4°C, and damage to refrigerated HDL is noted between week 1 and 4 of refrigeration (Holzer et al. 2017). This partially comes in agreement by a study by Zivkovic et al., where blood lipids exhibited stability following storage at either 4°C, -20°C and -70°C for a week (Zivkovic et al. 2009). However the stability of HDL is controversial, as the same work has shown that freezing of isolated HDL irreversibly disrupts its structure with effects on its function, with the addition of cryoprotectants such as glycerol having a beneficial effect (Holzer et al. 2017). This comes in contrast with some published work, which indicates that at lower temperatures (4°C) an increase in plasma HDL is noted. Given HDL is known to inactivate endotoxin, this may provide an explanation for the lack of recovery observed in *Chapter 2* (Cohn et al. 2004). The significant improvements in endotoxin recovery observed following addition of NaDOC, which has been demonstrated to dissolve lipoproteins including HDL, to the pretreatment protocol further supports the endotoxin masking by lipoprotein inactivation hypothesis (Robern 1982).

Additionally, after 48-96 hrs, a reduction in serum albumin and fragmentation of complement system proteins has been observed, which may affect plasma samples (Kaisar et al. 2016; Kapuruge et al. 2022). Another protein, bilirubin, which is responsible for the yellow colour of plasma, is known for being stable at either room temperature or refrigeration for up to 48 hrs, and may be subjected to degradation following prolonged storage (Sofronescu et al. 2012).

It should be noted that in this project, plasma was frozen at -20°C without the use of any cryoprotectants and was used for up to 6 months after initial storage. Individual plasma aliquots were only subject to one freeze-thaw cycle.

#### **4.3.1.2 Spiked plasma stored at room temperature or in the refrigerator**

In *Chapter 2*, the endotoxin-masking phenomenon was described in detail and evidence of endotoxin masking over time in plasma samples was presented. According to Figure 3.17B, endotoxin recovery using the LAL assay was possible only up to day 3, following incubation at either ambient temperature or fridge. Given the sensitivity of the LAL assay to temperature and pH variations, as well as assay interferences caused by alternative sample preparation steps, such as the addition of NaDOC, it was anticipated that the use of an aptamer-based platform would allow recovery following prolonged incubation. It is recommended that spike-hold studies are undertaken for at least 7 days to ensure the presence / absence of masking kinetics (Bech Orving et al. 2020).

For the spike-hold study, 10µL of 10 pg/mL endotoxin stock were added to 90µL of plasma to give an endotoxin concentration of 1 pg/mL. Samples were assessed for endotoxin recovery after storage for 2, 6, 9 and 15 days at either room temperature or in the fridge. During sample

preparation, 40 $\mu$ L of this plasma sample was diluted to a final volume of 400 $\mu$ L resulting in an endotoxin concentration of 100 fg/mL.

Endotoxin recovery was calculated using the following formula:

$$\% \text{ spike recovery} = \frac{\% \Delta R \text{ of spiked sample} - \% \Delta R \text{ of unspiked sample}}{\% \Delta R \text{ of added endotoxin}}$$

Figure 4.19 A shows the EIS spectra of spiked plasma (final endotoxin concentration: 100 fg/mL) stored at RT for up to 15 days. Figure 4.19 B shows the calculated endotoxin recoveries per day tested, following plasma treatment with the finalized protocol. Plasma samples were stored at *ambient* conditions and subjected to treatment with the finalized sample preparation protocol, including addition of NaDOC, centrifugation and tenfold dilution in endotoxin-free PBS.

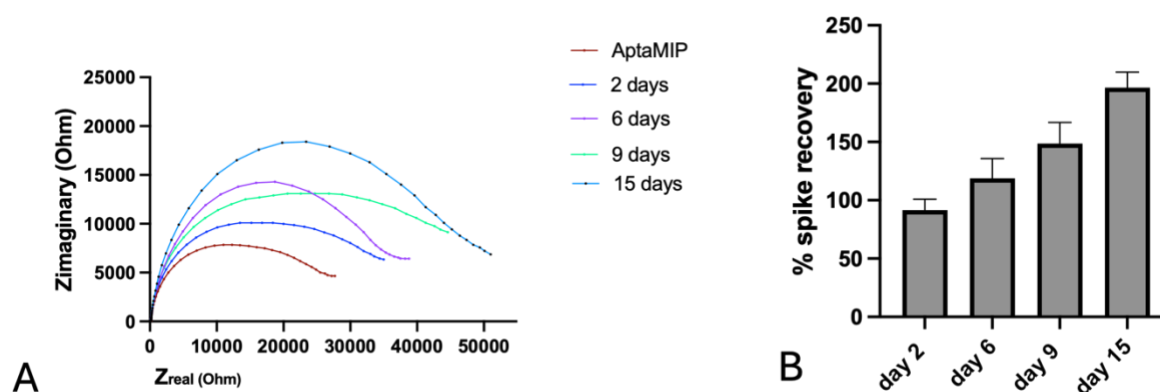
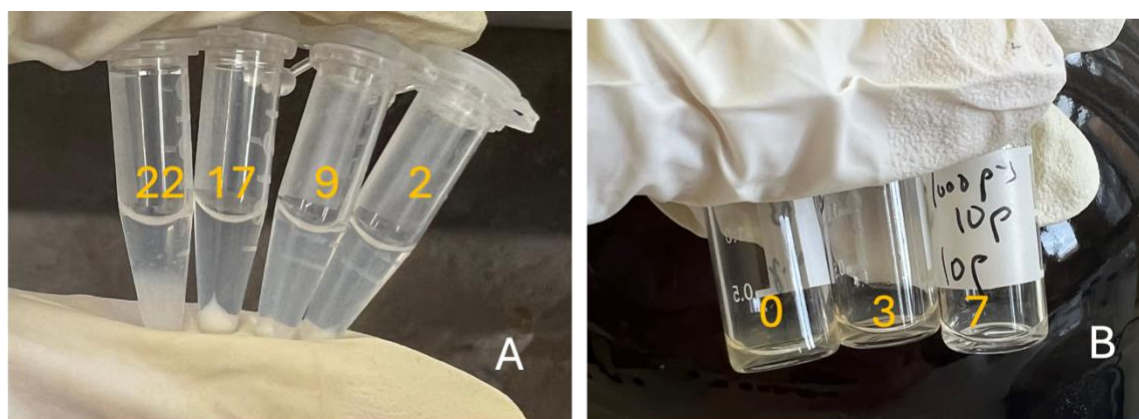


Figure 4.19 A: EIS graph showing the impedances of plasma spiked with 100 fg/mL endotoxin (N=3) following prolonged storage in the fridge, up to 15 days. 4.19 B shows the calculated spike recoveries for each day tested.

Figure 4.20 A shows the treated spiked plasma samples, immediately after centrifugation but before tenfold dilution with PBS. From left to right, samples were incubated for 22, 17, 9 and 2 days, respectively. Increasing white precipitates are observed from day 2 to day 17. At day 22 this precipitate is notably more diffuse, giving rise to a hazy layer at the bottom of the sample rather than a formed pellet.

Figure 4.20 B shows parafilm-sealed plasma samples incubated at room temperature. From left to right, samples were incubated for t=0 (immediately thawed, spiked and re-sealed), 3 days and 7 days. A visual change in viscosity, transparency and colour can be observed, with older samples becoming more transparent and paler in appearance.



Figures 4.20 A and B show photos of plasma following prolonged storage. Figure 4.20 A and B show the treated spiked plasma samples, following incubation for 22, 17 9 and 2 days respectively, immediately after centrifugation. Figure 4.20 B shows sealed, untreated plasma samples, following incubation for t=0, 2 days and 7 days at room temperature

An impressive recovery of endotoxin is noted, until an average recovery of 196% for day 15 is observed, after which endotoxin recoveries were calculated to be above the 200% cutoff limit set by European Pharmacopoeia (European pharmacopoeia - Bacterial Endotoxins, Ph. Eur. method 2.6.14). Therefore, it can be concluded that endotoxin can be recovered up to day 15 (borderline) of storage at room temperature. This is a significant improvement over the recoveries noted using the LAL assay in *Chapter 2*, where recovery was only possible up to day 3. Incubation for longer time periods (17 and 22 days) resulted in higher impedances (224% and 240%, respectively), and high endotoxin recoveries in levels exceeding those set by regulatory authorities (higher than 200%).

Analysing the data presented in figure 4.19 B above, it could be concluded that increased storage periods are associated with improved endotoxin recoveries. However, it is important to differentiate between endotoxin recovery as observed by the LAL assay, and as presented in *Chapter 2*, versus the observations made using the aptaMIP. When using the LAL assay to assess endotoxin masking by plasma components, a decrease in reactivity is associated with high levels of endotoxin masking. This is most evident in untreated plasma samples, where no response was recorded (section 2.3.3) and in treated plasma samples over time, where lower responses were noted with each passing day (sections 2.3.3 and 2.3.4). This is explained by the fact that once endotoxin is bound to plasma components, it is no longer free to react with the enzymatic cascade, resulting in a reduced response (Harm et al. 2021). However, when using the aptaMIP to assess endotoxin recovery, it would appear that the endotoxin can still be recognized by the aptamer, even when complexed with other sample components. Endotoxin bound to plasma components can be recognized by the aptamer which increases the steric barrier, inhibiting the passage of electrons to the electrode's surface, resulting in an increase in impedance (Reich et al. 2018). This gives rise to an increase in impedance over time that falsely suggests an increased recovery, which is in contrast with the results obtained

with the LAL assay. No published studies on this subject, utilizing aptamers, were found in literature,

Figure 4.20 A shows the treated spiked plasma samples, immediately after centrifugation but before tenfold dilution with PBS. From left to right, samples were incubated for 22, 17, 9 and 2 days, respectively. An increase in precipitate can be associated with longer storage times. This precipitate may be caused by degradation of plasma proteins, lipids and enzymes over time. As mentioned before, published work is divided on the stability of plasma proteins over time at room temperature. Kapuruge et al. noted a decrease in plasma  $\Delta$ S-Cys-Albumin after 96 h (4 days) at 23 °C, and Kaisar et al. found an increase in complement-cascade derived peptide fragments after 48 hrs at room temperature. A study in human serum stored at various temperatures for more than 7 days found a significant decrease in plasma proteins stored at room temperature, including complement proteins C3 and C4,  $\alpha$ 2-macroglobulin and Zn- $\alpha$ 2-glycoprotein (Lee et al. 2010a). The same study also noted an increase in low molecular weight proteins, possibly as a result of protein degradation. These observations may partly explain the increase in precipitate. Additionally, it is possible that some of the peptides produced may irreversibly bind to endotoxin, which may explain the increase in endotoxin recovery, as presented in figures 4.19 A and B. As mentioned before, the most likely explanation for this false increase in recovery is endotoxin binding to peptides formed over time at ambient conditions, as well as HDL shedding over time, both of which form complexes with endotoxin that can still be recognised by the system, resulting in increases in impedance (Pinto et al. 2014).

Figure 4.20 B shows sealed plasma samples incubated at room temperature. From left to right, samples were incubated for t=0 (immediately thawed and spiked), 3 days and 7 days. A visual change in viscosity, transparency and colour can be observed, with older samples becoming more transparent and paler in appearance. As mentioned before, after 48-96 hrs, reduction in serum albumin and fragmentation of complement system proteins has been observed, which may partly explain the transparency and viscosity changes (Kaisar et al. 2016; Kapuruge et al. 2022). Additionally bilirubin, which is responsible for the yellow colour of plasma, is known for being stable at either room temperature or refrigeration for up to 48 hrs (Sofronescu et al. 2012). This may explain the loss of colour in samples stored for 3 and 7 days at room temperature, respectively.

Figure 4.21 A shows the EIS spectra of spiked plasma (final endotoxin concentration: 100 fg/mL) stored at the **fridge** for up to 15 days. Figure 4.21 B shows the calculated endotoxin recoveries per day tested, following plasma treatment with the finalized protocol (final endotoxin concentration: 100 fg/mL). Plasma samples were stored at *the fridge* and subjected to treatment with the finalized sample preparation protocol, including addition of NaDOC, centrifugation and tenfold dilution in endotoxin-free PBS.

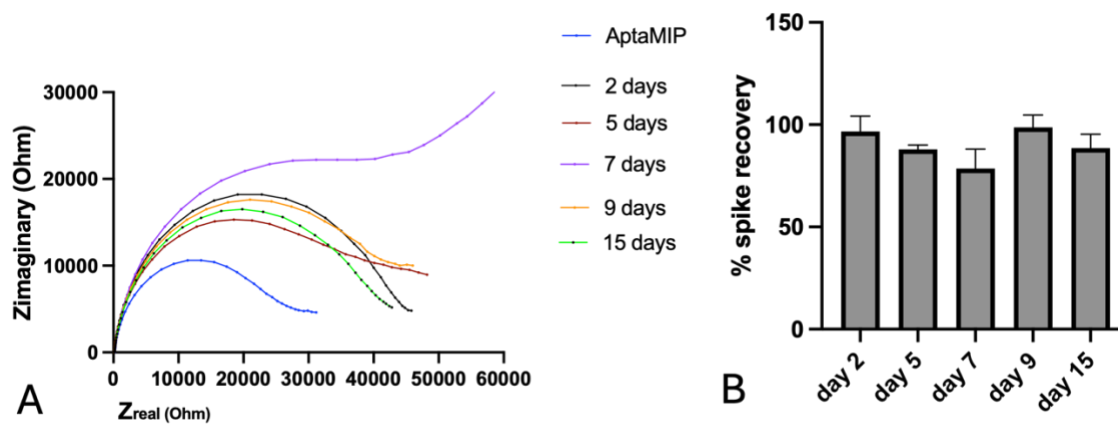
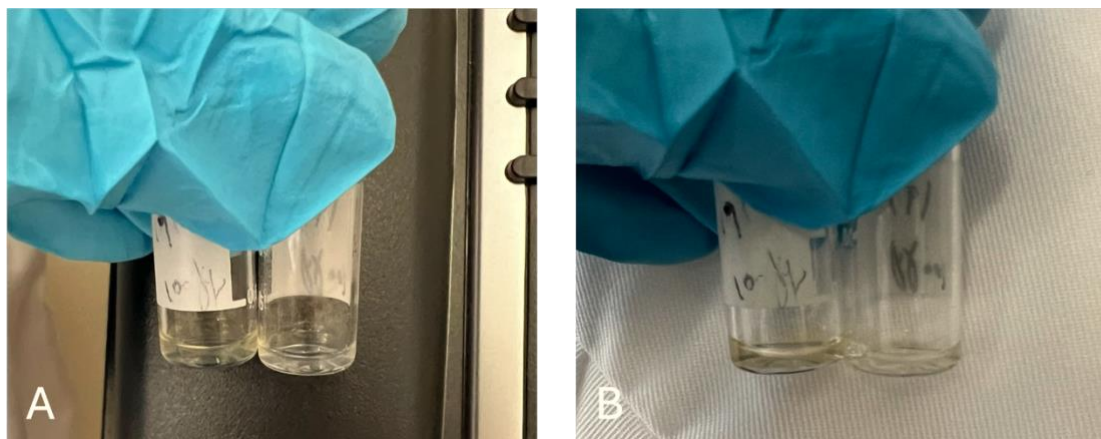


Figure 4.21 A: EIS graph showing the impedances of plasma spiked with 100 fg/mL endotoxin (N=3) following prolonged storage in the fridge, up to 15 days. 4.21 B shows the calculated spike recoveries for each day tested.

Figure 4.22 A below compare sealed plasma samples stored at different temperatures for 15 days. The sample on the left was stored in the fridge while sample on the right was kept at ambient temperature. A visual difference in colour and transparency can be noted, with the refrigerated sample displaying retention of yellow colour similar to freshly thawed plasma. According to literature, blood sample refrigeration is an effective method of retaining sample integrity (Basu and Kulkarni 2014). The visual changes noted here may support the hypothesis that plasma undergoes changes when stored at ambient temperature.



Figures 4.22 A and B show two sealed plasma samples incubated for 15 days, against two different backgrounds. Left sample was incubated in the fridge, right sample was incubated at room temperature.

Overall, satisfactory endotoxin recovery similar to freshly spiked plasma was noted across all days tested. Unlike plasma incubated at room temperature, where an increase in impedance was noted with longer incubation times, refrigerated samples showed consistently similar

impedances across days tested. This contrasts the observations made for plasma samples stored at room temperature in terms of recoveries. As plasma degradation and complex formation with endotoxin is slower at lower temperatures, it is more likely that endotoxin alone is detected, rather than aggregated material, which translates in more consistent recoveries over time, as shown in figure 4.21 A and B (Reich et al. 2019).

In *Chapter 2* where the LAL assay was used, a reduction in endotoxin recovery was noted in both refrigerated and room temperature samples (figure 4.21). In particular, in refrigerated samples a small increase in recovery was noted, and it was hypothesized that cold-activated plasma coagulation through activation of coagulation factor VII or the complement system was responsible for the change recovery (Morrissey et al. 1993; Kaisar et al. 2016). Cold-activated coagulation may cause interference with the LAL assay, which is coagulation-based (Levin and Bang 1968). It is possible that cold-activated coagulation may take place in refrigerated samples, possibly causing an increase in viscosity, which may interfere with the viscosity change of the LAL reagent. As the aptaMIP utilizes an alternative detection pathway, this may explain the lack of interference in refrigerated samples.

#### 4.3.3. Regeneration of AptamIP following use in plasma

In *Chapter 3* the sensor's regeneration following immersion for 5 minutes in 0.05% tween 20 was demonstrated. As the sensor can be regenerated when used in aqueous samples, it was considered worthwhile assessing whether it can be reused following incubation with plasma samples. Figure 4.23 shows the EIS data of the washed aptaMIP, using the protocol established in Chapter 3 (0.05% tween 20 wash), and the resulting EIS data following incubation with 10 fg/mL endotoxin in water.

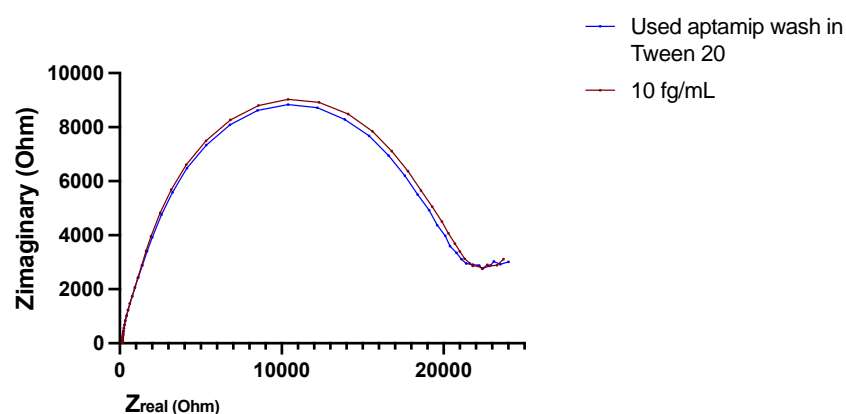


*Figure 4.23 EIS graph showing impedances following 1 hr incubation in 0.05% tween 20 (blue line) and subsequent incubation with 10 fg/mL (red line). No significant response was noted.*

A prolonged incubation time of 1 hour was required in order to bring the impedances down to their usual values (approximately 21-24 kΩ). In Chapter 3, it was demonstrated that a 5-minute incubation in tween 20 post aptamer production is sufficient for endotoxin removal.

However, following use in plasma, even after 1 hr of incubation the sensor's performance couldn't be restored. This suggests that the sensor is still subject to biofouling, despite the extensive sample preparation protocol. Following 10 minutes of incubation with 10 fg/mL endotoxin in endotoxin-free water, a very small increase in impedance was noted. Increased incubation times did not result in any further increase in impedance. This suggests that sample matrix components were able to irreversibly bind to the aptaMIP and compromise its performance, or that residual endotoxin was still bound to the sensor.

Given the limited success noted when using 0.05% tween, it was decided to use an alternative regeneration method different to a detergent, as higher detergent concentrations were found to be detrimental to the aptaMIP (Demertzis, 2019). Previous work in the researcher's lab, focused on the development of an aptaMIP for prostate-specific antigen detection, used a 5% v/v acetic acid wash in water to denature PSA (Tamboli, 2017). Figure 4.24 shows the EIS data obtained following washing of the aptaMIP in 5% acetic acid, and the resulting EIS data following incubation with 10 fg/mL in endotoxin free water.

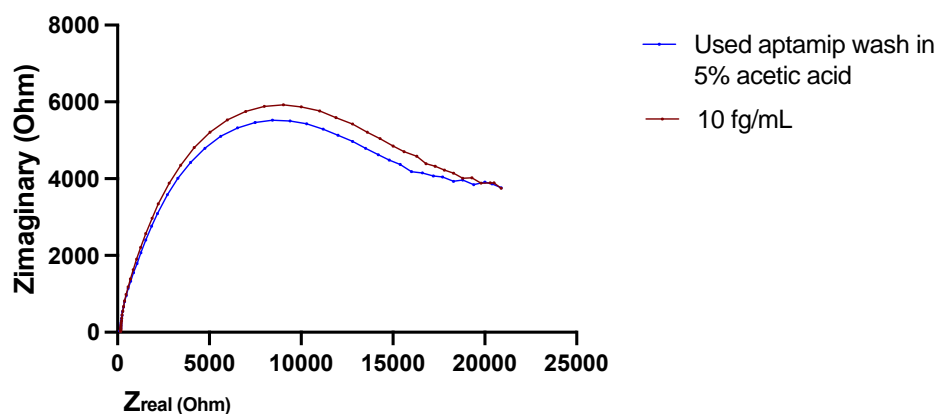


Figure 4.24 EIS showing impedances following 1 hr incubation in 5% acetic acid and subsequent incubation with 10 fg/mL. No significant response was noted.

Use of 5% acetic acid further decreased the aptaMIP's impedance well below the values of a regenerated aptaMIP (21-24k $\Omega$ ), suggesting a detrimental effect on the aptamer or the polymer. Following incubation with 10 fg/mL, a larger change in impedance was noted compared to tween20 (figure 4.23), but was still well below the response noted with a fresh aptaMIP. This suggests that biofouling caused by treated plasma is irreversible, and that further washing techniques can be detrimental to the sensor.

Despite the unsuccessful attempts at sensor regeneration following use in plasma samples, this is not a worrying observation, as biosensors intended for clinical samples are often intended for single use applications. Given the relatively low cost of developing the current aptaMIP, the reusability of gold electrodes and the potential for miniaturization of electrochemical sensors, the sensor has potential for application in a near-patient scenario.

#### 4.3.4 Application of finalized sample preparation protocol to simple aptasensor

Section 4.2.1 describes the finalized sample preparation protocol required to allow endotoxin recovery from citrated plasma samples using the developed aptaMIP sensor. It is reminded that the finalized protocol included a tenfold dilution in PBS in order to ensure a neutral pH and the stability of the system. It was decided to evaluate the performance of the simple aptasensor (no MIP) when challenged with plasma sample treated in the same manner. There was no storage of these samples – they were spiked, subjected to the pre-treatment protocol and analysed immediately. The EIS data are presented in figure 4.25 below.

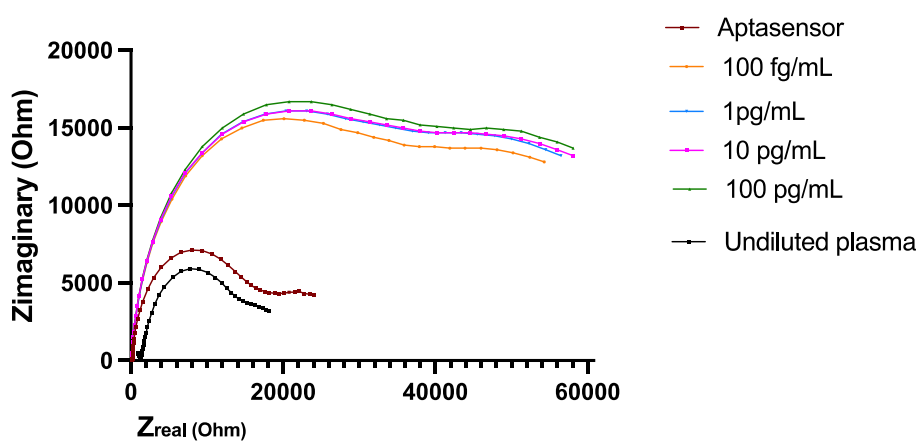


Figure 4.25: EIS graph showing the response of the aptasensor following the addition of spiked plasma subjected to the plasma preparation protocol used for the aptaMIP.

Figure 4.25 shows that addition of undiluted plasma resulted in a decrease in impedance. Incubation with plasma subjected to the finalized sample prep protocol resulted in a large increase in impedance following incubation with even the lowest concentration of endotoxin in plasma. Higher concentrations resulted in further small increases in impedance, showing poor resolution between endotoxin concentrations. This suggests that either plasma components or specific sample preparation steps were causing interference with the sensor. A number of other sample preparation steps (e.g., dilution, heating, addition of  $MgCl_2$ , acid base treatment) were applied to the aptasensor, all of which resulted in large drops in impedance (data not shown). Considering the aptasensor's poor performance in citrated blood samples, coupled with the enhanced performance of the aptaMIP when challenged with simple water based endotoxin samples (Section 3.3.5.4) it can be concluded that the aptaMIP performance is also superior when analysing clinical samples. It is likely that the polymer layer provides stability to the system, preventing biofouling / interference from other sample components which results in a more sensitive and efficient sensor.

#### 4.4 Conclusions and future work

In this chapter, the development and optimization of a sample preparation protocol for citrated blood plasma has been described.

Despite the LAL assay being the gold standard in endotoxin detection in pharmaceuticals and manufactured products, its use in blood has been held back by the presence of various inhibitors, proteins, lipids and interferents in the sample matrix (Harm et al. 2021). Although encouraging results were observed with the sample prep protocol for the LAL assay in *Chapter 2*, the limitations of the LAL assay such as sensitivity to pH, temperature and detergents, limited the sample treatment refinement options, which resulted in a limited endotoxin recovery for samples incubated for up to 3 days at room temperature/fridge.

The results in this chapter suggest that sample dilution by itself is not enough to overcome biofouling or endotoxin binding to plasma components, and that further sample treatments are necessary, including heating, acid / base treatment and centrifugation. In contrast with the LAL assay, where the addition of  $MgCl_2$  was necessary to overcome inhibition as it is a coagulation-based assay, the aptaMIP does not require the addition of salts. Moreover, results in this Chapter further support the endotoxin masking by lipoproteins hypothesis, as the addition of NaDOC allowed for improved endotoxin recoveries, especially in refrigerated samples. Importantly, the LAL assay is incompatible with detergents, including NaDOC (Harm et al. 2021). As demonstrated in this Chapter, the addition of NaDOC was invaluable for the successful recovery of endotoxin, something which would not be possible by using the LAL assay. However, the aptaMIP is not immune to sample pH fluctuations, with the acid / base treatment resulting in an unstable system, requiring an additional tenfold dilution with PBS to produce a sensor system with good reproducibility.

Spike-hold studies showed that recovery of endotoxin from samples stored at both room temperature and fridge was possible following storage for up to 15 days. A steady increase in endotoxin 'recovery' was noted over time in samples stored at ambient temperature, most likely owing to protein breakdown and endotoxin complexation with plasma components over time resulting in the detection of aggregates at the sensor surface. In contrast, similar endotoxin recovery levels were observed (approximately 100%) across all samples stored in the fridge, regardless of timeframe, suggesting that refrigeration slowed the breakdown of plasma components / endotoxin complexation

When the simple aptasensor was challenged with samples subjected to the optimized pre-treatment protocol, a large increase in impedance was observed for even the lowest spike concentration, with higher endotoxin concentration samples being poorly resolved. The aptaMIP demonstrated a clear advantage over the aptamer only sensor.

#### 4.5 Bibliography

Abbasy, L. et al. 2020. Development of a reliable bioanalytical method based on prostate specific antigen trapping on the cavity of molecular imprinted polymer towards sensing of PSA using binding affinity of PSA-MIP receptor: A novel biosensor. *J Pharm Biomed Anal* 188, p. 113447. doi: 10.1016/j.jpba.2020.113447

Aguilar-Mahecha, A. et al. 2012. The effect of pre-analytical variability on the measurement of MRM-MS-based mid- to high-abundance plasma protein biomarkers and a panel of cytokines. *PLoS ONE* 7(6), p. e38290. doi: 10.1371/journal.pone.0038290

Aketagawa, J. et al. 1993. Activation of limulus coagulation factor G by several (1-->3)-beta-D-glucans: comparison of the potency of glucans with identical degree of polymerization but different conformations. *J Biochem* 113(6), pp. 683-686. doi: 10.1093/oxfordjournals.jbchem.a124103

Baler, K. et al. 2014. Electrostatic unfolding and interactions of albumin driven by pH changes: a molecular dynamics study. *J Phys Chem B* 118(4), pp. 921-930. doi: 10.1021/jp409936v

Basu, D. and Kulkarni, R. 2014. Overview of blood components and their preparation. *Indian J Anaesth* 58(5), pp. 529-537. doi: 10.4103/0019-5049.144647

Bech Orving, R. et al. 2020. Bacterial Endotoxin Testing-Fast Endotoxin Masking Kinetics in the Presence of Lauryldimethylamine Oxide. *Microorganisms* 8(11), doi: 10.3390/microorganisms8111728

Bonini, F. et al. 2007. Surface imprinted beads for the recognition of human serum albumin. *Biosensors and Bioelectronics* 22(9), pp. 2322-2328. doi: <https://doi.org/10.1016/j.bios.2006.12.034>

Cabaleiro-Lago, C. et al. 2023. Recent Advances in Molecularly Imprinted Polymers and Their Disease-Related Applications. *Polymers (Basel)* 15(21), doi: 10.3390/polym15214199

Campuzano, S. et al. 2019. Antifouling (Bio)materials for Electrochemical (Bio)sensing. *Int J Mol Sci* 20(2), doi: 10.3390/ijms20020423

Cohn, J. S. et al. 2004. Storage of human plasma samples leads to alterations in the lipoprotein distribution of apoC-III and apoE. *J Lipid Res* 45(8), pp. 1572-1579. doi: 10.1194/jlr.D300041-JLR200

Cooper, J. F. 1990. Resolving LAL Test interferences. *J Parenter Sci Technol* 44(1), pp. 13-15.

Dagur, P. K. and McCoy, J. P., Jr. 2015. Collection, Storage, and Preparation of Human Blood Cells. *Curr Protoc Cytom* 73, pp. 5 1 1-5 1 16. doi: 10.1002/0471142956.cy0501s73

Dahlman-Hoglund, A. et al. 2016. Endotoxin in Size-Separated Metal Working Fluid Aerosol Particles. *Ann Occup Hyg* 60(7), pp. 836-844. doi: 10.1093/annhyg/mew036

Fink, A. L. et al. 1994. Classification of acid denaturation of proteins: intermediates and unfolded states. *Biochemistry* 33(41), pp. 12504-12511. doi: 10.1021/bi00207a018

Garidel, P. et al. 2005. Divalent cations affect chain mobility and aggregate structure of lipopolysaccharide from *Salmonella minnesota* reflected in a decrease of its biological activity. *Biochim Biophys Acta* 1715(2), pp. 122-131. doi: 10.1016/j.bbamem.2005.07.013

Gerba, C. P. and Hou, K. 1985. Endotoxin removal by charge-modified filters. *Appl Environ Microbiol* 50(6), pp. 1375-1377. doi: 10.1128/aem.50.6.1375-1377.1985

Gioannini, T. L. et al. 2002. An essential role for albumin in the interaction of endotoxin with lipopolysaccharide-binding protein and sCD14 and resultant cell activation. *J Biol Chem* 277(49), pp. 47818-47825. doi: 10.1074/jbc.M206404200

Gorman, A. and Golovanov, A. P. 2022. Lipopolysaccharide Structure and the Phenomenon of Low Endotoxin Recovery. *European Journal of Pharmaceutics and Biopharmaceutics* 180, pp. 289-307. doi: <https://doi.org/10.1016/j.ejpb.2022.10.006>

Harm, S. et al. 2021. An in vitro study on factors affecting endotoxin neutralization in human plasma using the Limulus amoebocyte lysate test. *Sci Rep* 11(1), p. 4192. doi: 10.1038/s41598-021-83487-4

Holzer, M. et al. 2017. HDL structure and function is profoundly affected when stored frozen in the absence of cryoprotectants. *J Lipid Res* 58(11), pp. 2220-2228. doi: 10.1194/jlr.D075366

Ikemura, K. et al. 1989. False-positive result in Limulus test caused by Limulus amoebocyte lysate-reactive material in immunoglobulin products. *J Clin Microbiol* 27(9), pp. 1965-1968. doi: 10.1128/jcm.27.9.1965-1968.1989

Jiang, J. et al. 2022. Simple and fast colorimetric detection of lipopolysaccharide based on aptamer and SYBR Green I mediated aggregation of gold nanoparticles. *Int J Biol Macromol* 223(Pt A), pp. 231-239. doi: 10.1016/j.ijbiomac.2022.10.276

Kaisar, M. et al. 2016. Plasma degradome affected by variable storage of human blood. *Clin Proteomics* 13, p. 26. doi: 10.1186/s12014-016-9126-9

Kapuruge, E. P. et al. 2022. Tracking the Stability of Clinically Relevant Blood Plasma Proteins with Delta-S-Cys-Albumin-A Dilute-and-Shoot LC/MS-Based Marker of Specimen Exposure to Thawed Conditions. *Mol Cell Proteomics* 21(11), p. 100420. doi: 10.1016/j.mcpro.2022.100420

Kim, S. E. et al. 2012. Harnessing aptamers for electrochemical detection of endotoxin. *Anal Biochem* 424(1), pp. 12-20. doi: 10.1016/j.ab.2012.02.016

Lee, D. H. et al. 2010. Proteomic analysis of the effect of storage temperature on human serum. *Ann Clin Lab Sci* 40(1), pp. 61-70.

Lesche, D. et al. 2016. Does centrifugation matter? Centrifugal force and spinning time alter the plasma metabolome. *Metabolomics* 12(10), p. 159. doi: 10.1007/s11306-016-1109-3

Levin, J. and Bang, F. B. 1968. Clottable protein in Limulus; its localization and kinetics of its coagulation by endotoxin. *Thromb Diath Haemorrh* 19(1), pp. 186-197.

Lu, M. et al. 2012. Kinetic analysis of thermal stability of human low density lipoproteins: a model for LDL fusion in atherogenesis. *J Lipid Res* 53(10), pp. 2175-2185. doi: 10.1194/jlr.M029629

Ma, L. et al. 2018. Harnessing the affinity of magnetic nanoparticles toward dye-labeled DNA and developing it as an universal aptasensor revealed by lipopolysaccharide detection. *Analytica Chimica Acta* 1036, pp. 107-114. doi: <https://doi.org/10.1016/j.aca.2018.06.060>

Manesiotis, P. et al. 2013. Molecularly imprinted polymers for the extraction of imiquimod from biological samples using a template analogue strategy. *ANALYTICAL METHODS* 5, pp. 3122-3128. doi: 10.1039/c3ay40239h

Morrissey, J. H. et al. 1993. Quantitation of Activated Factor VII Levels in Plasma Using a Tissue Factor Mutant Selectively Deficient in Promoting Factor VII Activation. *Blood* 81(3), pp. 734-744. doi: <https://doi.org/10.1182/blood.V81.3.734.734>

Oeswein, J. Q. and Chun, P. W. 1983. Human serum low density lipoprotein-sodium deoxycholate interaction. *J Biol Chem* 258(6), pp. 3645-3654.

- Paoli, C. J. et al. 2018. Epidemiology and Costs of Sepsis in the United States-An Analysis Based on Timing of Diagnosis and Severity Level. *Crit Care Med* 46(12), pp. 1889-1897. doi: 10.1097/CCM.0000000000003342
- Pasella, S. et al. 2013. Pre-analytical stability of the plasma proteomes based on the storage temperature. *Proteome Sci* 11(1), p. 10. doi: 10.1186/1477-5956-11-10
- Pasqua, S. et al. 2021. Complete intra-laboratory validation of a LAL assay for bacterial endotoxin determination in EBV-specific cytotoxic T lymphocytes. *Mol Ther Methods Clin Dev* 22, pp. 320-329. doi: 10.1016/j.omtm.2021.05.002
- Peterson, A. M. et al. 2015. Modulating the Substrate Selectivity of DNA Aptamers Using Surfactants. *Langmuir* 31(43), pp. 11769-11773. doi: 10.1021/acs.langmuir.5b02818
- Phonklam, K. et al. 2020. A novel molecularly imprinted polymer PMB/MWCNTs sensor for highly-sensitive cardiac troponin T detection. *Sensors and Actuators B: Chemical* 308, p. 127630. doi: <https://doi.org/10.1016/j.snb.2019.127630>
- Piehler, M. et al. 2020. Comparison of LAL and rFC Assays-Participation in a Proficiency Test Program between 2014 and 2019. *Microorganisms* 8(3), doi: 10.3390/microorganisms8030418
- Pini, C. et al. 1990. Effects of serum storage on the determination of cholesterol. *Ric Clin Lab* 20(1), pp. 37-44. doi: 10.1007/BF02910147
- Pinto, J. et al. 2014. Human plasma stability during handling and storage: impact on NMR metabolomics. *Analyst* 139(5), pp. 1168-1177. doi: 10.1039/c3an02188b
- Reich, J. et al. 2018. Investigation of the kinetics and mechanism of low endotoxin recovery in a matrix for biopharmaceutical drug products. *Biologicals* 53, pp. 1-9. doi: 10.1016/j.biologicals.2018.04.001
- Reich, J. et al. 2019. Low Endotoxin Recovery-Masking of Naturally Occurring Endotoxin. *Int J Mol Sci* 20(4), doi: 10.3390/ijms20040838
- Robern, H. 1982. The application of sodium deoxycholate and Sephacryl-200 for the delipidation and separation of high density lipoprotein. *Experientia* 38(4), pp. 437-439. doi: 10.1007/BF01952626

Saxena, S. et al. 2024. Anti-Fouling Polymer or Peptide-Modified Electrochemical Biosensors for Improved Biosensing in Complex Media. *Advanced Sensor Research* 3(5), p. 2300170. doi: <https://doi.org/10.1002/adsr.202300170>

Shimizu, Y. and Ichihara, K. 2019. Elucidation of stability profiles of common chemistry analytes in serum stored at six graded temperatures. *Clin Chem Lab Med* 57(9), pp. 1388-1396. doi: 10.1515/cclm-2018-1109

Sin, M. L. et al. 2014. Advances and challenges in biosensor-based diagnosis of infectious diseases. *Expert Rev Mol Diagn* 14(2), pp. 225-244. doi: 10.1586/14737159.2014.888313

Sneck, M. et al. 2012. Conformational changes of apoB-100 in SMase-modified LDL mediate formation of large aggregates at acidic pH. *J Lipid Res* 53(9), pp. 1832-1839. doi: 10.1194/jlr.M023218

Snyder, S. et al. 1999. Lipopolysaccharide bilayer structure: effect of chemotype, core mutations, divalent cations, and temperature. *Biochemistry* 38(33), pp. 10758-10767. doi: 10.1021/bi990867d

Sofronescu, A. G. et al. 2012. Effects of temperature and light on the stability of bilirubin in plasma samples. *Clin Chim Acta* 413(3-4), pp. 463-466. doi: 10.1016/j.cca.2011.10.036

Su, W. et al. 2012. Determination of endotoxin through an aptamer-based impedance biosensor. *Biosensors and Bioelectronics* 32(1), pp. 32-36. doi: <https://doi.org/10.1016/j.bios.2011.11.009>

Szermmer-Olearnik, B. and Boratynski, J. 2015. Removal of endotoxins from bacteriophage preparations by extraction with organic solvents. *PLoS ONE* 10(3), p. e0122672. doi: 10.1371/journal.pone.0122672

Tamboli, V. K. et al. 2016. Hybrid Synthetic Receptors on MOSFET Devices for Detection of Prostate Specific Antigen in Human Plasma. *Anal Chem* 88(23), pp. 11486-11490. doi: 10.1021/acs.analchem.6b02619

Thaplyal, P. and Bevilacqua, P. C. 2014. Experimental approaches for measuring pKa's in RNA and DNA. *Methods Enzymol* 549, pp. 189-219. doi: 10.1016/B978-0-12-801122-5.00009-X

Vanhaecke, E. et al. 1989. Endotoxin removal by end-line filters. *J Clin Microbiol* 27(12), pp. 2710-2712. doi: 10.1128/jcm.27.12.2710-2712.1989

Velayati, S. et al. 2022. Fabrication and evaluation of a molecularly imprinted polymer electrochemical nanosensor for the sensitive monitoring of phenobarbital in biological samples. *Microchemical Journal* 174, p. 107063. doi: <https://doi.org/10.1016/j.microc.2021.107063>

Walsh, M. T. and Atkinson, D. 1983. Solubilization of low-density lipoprotein with sodium deoxycholate and recombination of apoprotein B with dimyristoylphosphatidylcholine. *Biochemistry* 22(13), pp. 3170-3178. doi: 10.1021/bi00282a021

Wu, D. W. et al. 2017. How Long can we Store Blood Samples: A Systematic Review and Meta-Analysis. *EBioMedicine* 24, pp. 277-285. doi: 10.1016/j.ebiom.2017.09.024

Yaguchi, A. et al. 2012. Combining intermediate levels of the Endotoxin Activity Assay (EAA) with other biomarkers in the assessment of patients with sepsis: results of an observational study. *Crit Care* 16(3), p. R88. doi: 10.1186/cc11350

Zivkovic, A. M. et al. 2009. Effects of sample handling and storage on quantitative lipid analysis in human serum. *Metabolomics* 5(4), pp. 507-516. doi: 10.1007/s11306-009-0174-2

# Chapter 5

## Development of electrochemical sensors for the detection of Interleukin 6 and beta-globin

---

## **5.1 Introduction**

### *5.1.1 General overview*

As mentioned in Chapter 1, the overarching aim of this project is the development of protocols allowing the detection of different types of biomarkers; ideally a protein target, a nucleic acid target and an endotoxin (a lipid-polysaccharide conjugate). It is anticipated that the protocols developed in this thesis can be applied across a variety of detection platforms, such as miniaturized electrochemical systems, and devices employing electron paramagnetic resonance (EPR).

In Chapter 1, the roles of IL-6 and beta globin in sepsis secondary to pneumonia were described. Briefly, interleukin 6, a protein marker often elevated in the first stages of sepsis, and beta globin, a DNA marker often elevated in septic patients, have shown potential in the risk evaluation of pediatric patients and can provide insights regarding patient outcome or disease progression (Pietrzak et al. 2023).

Chapters 3 and 4 describe the successful development of sensors for endotoxin, using aptamer and hybrid imprinting approaches. In particular, initial attempts to develop an immunosensor for IL-6 utilizing antibodies will be presented, followed by the development of aptasensors for the detection of IL-6 and beta-globin. Finally, the successful development of sensitive aptasensors for both IL-6 and beta-globin utilizing DNA sensitizers, plus the successful application of those sensors in citrated blood plasma following minimal sample preparation will be described.

### **5.1.2 Interleukin 6 detection**

The gold standard in IL-6 detection is set by enzyme-linked immunoassays (ELISAs) and chemiluminescent immunoassays (CLIAs), both of which have demonstrated specificity and reliability in clinical samples (McCrae et al. 2023). However, such assays often require large sample volumes, long preparation and incubation times, execution by skilled technicians and often need to be processed in centralized labs, further increasing result turnaround time (McCrae et al. 2023). In the case of sepsis, where rapid diagnosis is paramount and early diagnosis can lead to improved patient outcomes, the need to develop an economical, easy-to-fabricate and rapid sensor becomes apparent (Dolin et al. 2018). IL-6 can be found overexpressed in various acute, chronic, and communicable diseases. For example, IL-6 over expression has been observed in Alzheimer's, cancer and cardiovascular disease. Research has shown that detection and quantification of IL-6 plays an important role in the management of sepsis in paediatric patients, as elevated levels of IL-6 in children are associated with disease severity and poor prognosis (Michelow et al. 2007; Khatlab et al. 2018; Vasconcellos et al. 2018).

As described in previous chapters, electrochemical sensors provide the benefit of rapid detection combined with miniaturization and relatively low set-up costs (Khan and Mujahid 2020). There are numerous published studies of electrochemical sensors utilizing aptamers, antibodies and imprinted polymers as recognition elements in the literature, many of which have been applied to sample matrices such as sweat, saliva, urine and tears (McCrae et al. 2023). However, this section will be focused on sensors tested on blood samples.

The majority of reported IL-6 sensors in literature which have been applied to clinical samples are antibody-based. The sensor with the lowest LOD in human blood samples was developed by Lou et al., who utilized electrochemically reduced graphene oxide and gold–palladium bimetallic nanoparticles together with anti-IL6 antibodies, which resulted in a LOD of 0.4 pg/mL in serum samples (Lou et al. 2014). Another sensitive sensor is described by Tanak et al., who used a nanofilm semiconducting/metal electrode interface in conjunction with antigens and demonstrated a LOD of 0.1 pg/mL from undiluted human plasma (Tanak et al. 2021). Another immunosensor built on gold interdigitated electrode arrays showed a LOD of 11.84 pg/mL in human serum, while a sensor using a similar approach on a gold needle-shaped microelectrode showed a LOD of 20 pg/mL (Russell et al. 2019; Oh et al. 2021). Finally, Tan et al. used direct laser scribing on polyimide tapes, functionalized with anti IL-6 antibodies and demonstrated a LOD of 5.1 pg/mL in fetal bovine serum (Tan et al. 2021b).

The most sensitive sensors reported in literature utilize alternative recognition moieties, such as aptamers, imprinted polymers or receptors. Tertiş et al., who developed the IL-6 aptamer used in this chapter, fabricated an aptasensor based on gold electrodes modified with p-aminobenzoic acid, p-aminothiophenol and gold nanoparticles, reporting a LOD of 1.6 pg/mL (Tertis et al. 2019). Figure 5.1 shows a schematic representation of the group’s aptasensor fabrication process.

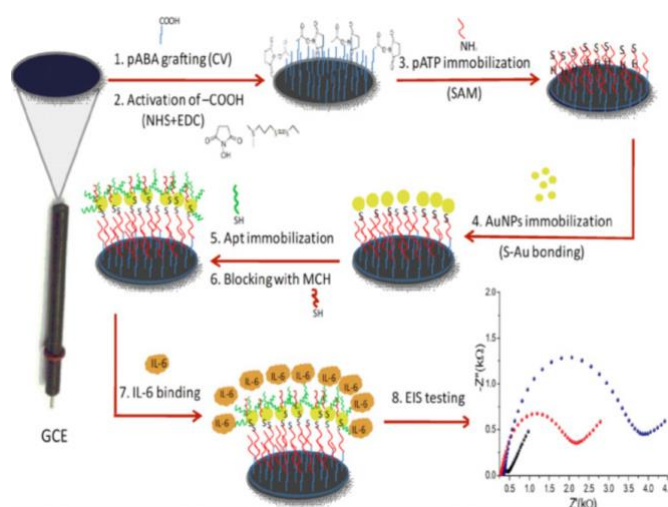


Figure 5.1: Schematic representation of the aptasensor fabrication process, as described in the Tertiş et al paper (Tertis et al. 2019).

An aptasensor using an aptamer developed by the group, modified with methylene blue, and a sensor utilizing graphene–gold nanoparticles allowed the electrochemical monitoring of IL-6 levels in wounds (up to 30 ng/mL) (Gao et al. 2021). Aydin et al. utilized pyrrole containing epoxy side groups on tin oxide electrodes, to achieve a LOD of 6 fg/mL in human serum, following simple PBS dilution (Aydin 2020). The same group developed another sensor based on acetylene black (AB)/epoxy-substituted-poly(pyrrole) polymer with an impressive LOD of 3.2 fg/mL, including in human serum (Aydin et al. 2021). Additionally, there are examples of MIPs allowing sensitive IL-6 detection, such as the work of Özcan et al., who developed a pyrrole-based MIP on graphene quantum dots, with a LOD of 3 pg/mL (Özcan et al. 2020). Another MIP sensor based on pyrrole and carboxylated pyrrole exhibited a LOD of 0.02 pg/mL in spiked serum (Gonçalves et al. 2021).

In this Chapter, antibodies and the aptamer developed by Tertiş et al. will be used to develop sensors for the detection of IL-6 in citrated blood plasma.

### **5.1.3 DNA sensors and Beta-globin**

Currently, the gold standard for DNA detection in clinical samples is the Polymerase Chain Reaction (PCR), as it provides specific detection of microbial and host DNA in clinical samples (Lorente et al. 2000). However, similar to ELISAs, PCR often needs to be performed in centralized labs by specialized technicians. PCR often has prolonged run times of approximately one hour, which can increase turnaround times (Lorente et al. 2000). Therefore, there is significant interest in the development of so-called label-free, point of care biosensors for the detection of single-stranded DNA (Trotter et al. 2020). The low developmental cost, simplicity and quick result turnaround time makes them attractive to researchers (Hai et al. 2020).

One of the aims in this project is to develop a sensing platform which allows the detection of nucleic acid sequences, especially single-stranded DNA. During the literature review process, a number of nucleic acid sequences overexpressed in sepsis were identified, and the sequence for human beta-globin was chosen for the development of a proof-of-concept sensor. In this Chapter, the aim is to develop a label-free DNA sensor based on complementary strand hybridization.

There are many label-free DNA sensors reported in literature, however our focus will be on hybridization-based sensors. Han et al. used carbon nanotube-gold nanoparticle conjugates to develop an electrochemical sensor for a complementary DNA sequence with a dynamic detection range of 0.1 pM –10 nM (Han et al. 2020). A sensitive microRNA sensor based on RNA-DNA hybridization was developed, based on functionalized metal–organic frameworks, with a LOD of 8.2 fM (Chang et al. 2019b). Luo et al. used 1-aminopyrene/graphene hybrids to detect target DNA via hybridization, which was monitored via EIS, with a LOD of 0.45 pM

(Luo et al. 2013). A molybdenum disulfide-based sensor, modified with gold nanoparticles and DNA as a capture probe was developed for the detection of miR-155, with a LOD of 0.26 pM (Zhu et al. 2017).

In this Chapter, the human beta-globin capture sequence and its complementary strand will be used to develop label-free hybridization-based sensors for the detection of beta globin in citrated blood plasma.

#### **5.1.4 Use of sensitizing molecules in electrochemical sensors**

The focus in this section will be on electrochemical detection, rather than spectroscopic detection. Label-free methods have been used throughout the project so far, and their advantages (shorter processing times, fewer steps) are well reported in literature and covered in Chapter 1. However, there is increasing interest from researchers on the optimization and development of sensitive label-free DNA sensors, which has led to the implementation of methods such as nanostructures, nanoparticles, conducting polymers and DNA intercalators (Yang et al. 2016).

DNA intercalators, in particular, have long been used for the assessment of DNA hybridization, including applications in electrochemical sensors (Regan et al. 2014). Some examples of DNA intercalators include cationic metal complexes, antibiotics, anti-cancer drugs such as epirubicin, redox-active molecules, such as methylene blue and DNA- intercalating dyes such as SYBR green (Jiang et al. 2012; Regan et al. 2014; Abi and Safavi 2021). Metal complexes, such as Hexaammineruthenium(III),  $\text{RuHex}^{3+}$ , are routinely used to determine DNA concentrations in electrochemical sensors (Abi and Safavi 2021). Additionally, gold nanoparticles or carbon nanotubes, both of which are redox active may be modified with nucleic acids to allow signal amplification of DNA hybridization (Bonanni and del Valle 2010).

Numerous sensors utilizing sensitizers have been developed, the majority of which have been assessed for their performance in aqueous samples. Li et al. developed a SS-DNA sensor and utilized  $[\text{Cu}(\text{dmp})(\text{H}_2\text{O})\text{Cl}_2]$  (dmp = 2,9-dimethyl-1,10-phenanthroline) as an indicator to develop a sensitive platform for Hepatitis B detection, with a LOD of  $7.0 \times 10^{-8}$  M (Li et al. 2007).

To the best of our knowledge, no sensors utilizing DNA intercalating sensitizers in plasma samples have been described in literature. Therefore, one of the aims in this Chapter were to not only develop sensitive sensors using metal complex sensitizers, but also assess their performance in blood samples following minimal preparation.

Through collaboration with the IDTH at Cardiff University, it was decided to test a variety of Co(III) cobalt complexes for their DNA affinity by using the aptasensor developed in Chapter 3 as an example.

The sensitizer is a cobalt complex designed to intercalate ds-DNA. The collaborators were interested in assessing the sensitizer's effect on impedance following binding to aptamers, both before and after the introduction of the target molecule. Therefore, the sensitizer was trialed in two ways: Introduction of the molecule to the system before the addition of endotoxin versus introduction following binding of endotoxin to the aptamer.

As no studies had been carried out in electrochemical systems, it was hypothesized that binding of the molecule to the aptamer-endotoxin complex would result in an increase in impedance, allowing for signal amplification.

## 5.2 Aims and Objectives

As mentioned before, there are challenges faced with the rapid and sensitive detection of protein and nucleic acid biomarkers, and literature is poor regarding the use of sensitizing molecules, especially in plasma samples. Therefore, the aims and objective of this Chapter are:

- To develop a sensor for IL-6 and assess whether the introduction of the sensitizer allows for more sensitive detection in both aqueous and plasma samples.
- To develop a sensor for beta-globin DNA detection and assess whether the introduction of the sensitizer allows for more sensitive detection in both aqueous and plasma samples.
- To assess the use of the sensitizer in an aptasensor designed for endotoxin detection, as described in Chapter 3.
- To perform specificity tests, in order to assess the sensitizer's specificity for the target molecules.

### 5.3. Materials and methods

#### 5.3.1 Materials overview

An aptamer sequence capable of binding to IL-6 was identified in a paper by Tertis et al. (Tertis et al. 2019). A 3' thiol C6 spacer was added to the aptamer by the aptamer manufacturer (Eurogentec, Belgium), similar to the paper by Tertis et al.

5'-GTC TCT GTG TGC GCC AGA GAC ACT GGG GCA GAT ATG GGC CAG CAC AGA ATG AGG CCC-3'

The human beta-globin capture sequence, and its complementary beta-globin strand were identified in the work of Steube et al. (Steube et al. 2003). A 5' thiol C6 spacer was added to the capture strand by the manufacturer (Eurogentec, Belgium). Both strands, were synthesized by Eurogentec (Belgium).

Capture strand            5'-CAA GAC AGG TTT AAG GAG ACC A- 3'  
Complementary strand    **GTT CTG TCC AAA TTC CTC TGG T**

Both IL-6 aptamer and beta-globin complementary strand utilize the same C6-thiol linker as was used to attach the endotoxin aptamer (Chapter 3). Upon arrival, aptamers and DNA were aliquoted into 10 µM aliquots and stored frozen at -20 °C.

Human IL-6 (recombinant) and anti-IL6 antibodies were purchased from R&D biosystems and were kept refrigerated at 2-5 °C. Human IL-6 was aliquoted into the desired concentrations in endotoxin-free PBS and kept refrigerated at 2-5 °C.

The endotoxin aptamer was prepared as described in Chapter 3 section 3.2.2.1.

*N*-hydroxysuccinimide (NHS) and *N*-(3-(dimethylamino)propyl)-*N'*-ethylcarbodiimide hydrochloride (EDC) were purchased from Sigma-Aldrich and were stored in a fridge. 2-(*N*-morpholino)ethanesulfonic acid (MES) was purchased from Sigma-Aldrich and stored at ambient temperature. TE buffer was prepared as a solution 10 mM Tris and 1 mM EDTA. EDTA and TCEP were purchased from Sigma-Aldrich and stored at ambient temperature. 4,4-dithiodibutyric acid (DTBA) and mercaptoundecanoic acid (MUA) were purchased from Sigma-Aldrich and stored at ambient temperature. Streptococcal Protein G was purchased from Sigma-Aldrich and stored at the fridge (-20 °C).

The DNA Co(III) complex was synthesized by Dr Emily-Judd Cooper at the School of Chemistry, Cardiff University

### 5.3.2 Methods

The majority of methods in this Chapter are analogous to those in Chapters 3 and 4, with the exception of EDC/NHS coupling, which will be described below. Any minor changes will be described in the results/discussion sections of this Chapter.

#### 5.3.2.1 EDC/NHS coupling

Gold electrodes were cleaned as described in section 3 and incubated in MUA solution (1  $\mu$ M in ethanol) for an hour. MES buffer (50 mM, pH 5) was prepared in distilled water, and its pH was adjusted using 0.1M NaOH, guided by a pH meter. The modified electrodes were then immersed in a solution of 200 mM EDC and 200 mM NHS in MES buffer for 30 minutes. The modified electrode was then rinsed with distilled water and immersed in a PBS solution containing 25  $\mu$ g/mL anti-IL6 capture antibodies, or Protein G (1 mg/mL) for 1 hour. Electrodes were washed with distilled water to remove unbound antibodies. Following electrode modifications, measurements were performed in a 50 mM ferro/ferricyanide solution in PBS (1x concentration).

#### 5.3.2.2 Use of DNA sensitizers developed by collaborators in the School of Chemistry

A DNA-binding Co(III) complex (Figure 5.2), which has demonstrated its affinity and performance in Chapter 4, was chosen for the development of IL-6 and beta globin sensors. The sensitizer (5 mg) was dissolved in 5 ml TE buffer prepared in endotoxin-free water. The mixture was covered with aluminum foil and stirred overnight, before being filtered using a 0.2-micron PTFE syringe filter. The solution was wrapped in aluminum foil and kept refrigerated before use.

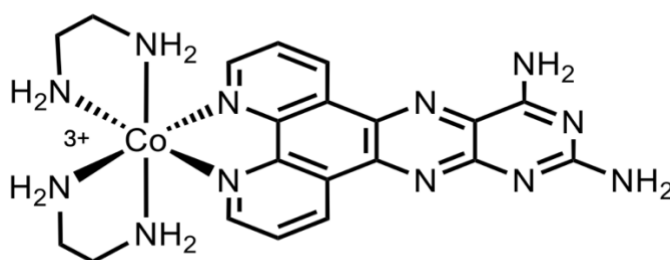


*Figure 5.2: The compound chosen to be taken forward for experiments with the IL-6 aptamer and beta globin.*

Similar to section 4.2.2, following electrode modification with aptamers and thiol spacers, the electrodes were rinsed with endotoxin free water and subsequently incubated with 100  $\mu$ L of 1 mg/mL sensitizer in TE buffer for 10 minutes, away from direct sunlight. The sensors were then incubated with various concentrations of target molecules.

## 5.4 Results and discussion

We set out to develop two sensors, viz. one for IL-6 and one for DNA detection in both aqueous samples and blood plasma.

### 5.4.1 Use of EDC/NHS to develop an IL-6 immunosensor

Development of a sensor of IL-6 was the first objective. As antibody-based systems such as ELISAs are the gold-standard in protein detection and are routinely used in clinical samples, it was decided to begin with the development of a simple immunosensor based upon unmodified anti-IL6 antibodies, utilizing EDC/NHS for immobilization (Lou et al. 2014). MUA was selected as the alkanethiol of choice due to literature suggesting that longer alkanethiol chain lengths are associated with improved sensor performance when used for EDC/NHS coupling, by preventing steric hindrance (Bhadra et al. 2015). In contrast, a densely packed thiol such as DTBA causes steric hindrance between the immobilized antibodies, which severely limits sensor functionality (Bhadra et al. 2015).

Figure 5.3 shows the EIS data obtained following formation of a MUA SAM (black line) and the reduction in impedance following EDC/NHS coupling and incubation with anti-IL-6 antibodies (red line).

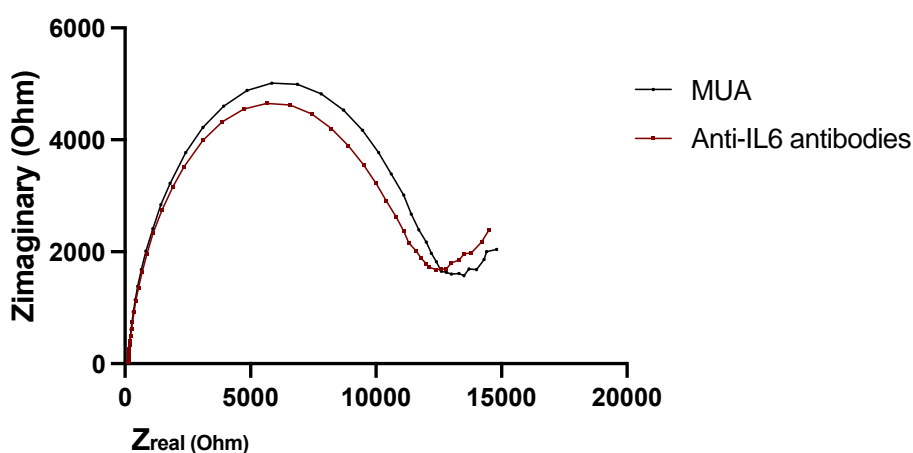


Figure 5.3: EIS graph showing the impedance of MUA following EDC/NHS coupling (black line) and following 1hr incubation with anti-IL6 antibodies (red line).

Figure 5.3 shows a decrease in impedance following the attachment of antibodies. Decreases in impedance have been observed in a number of published studies, including with IL-6 antibodies immobilized through EDC/NHS chemistry (Russell et al. 2019; Oh et al. 2021). It is

hypothesized that the binding of the IL-6 protein, which has a size of 21-26 kDa, opens up the monolayer structure, allowing electron passage to the gold surface, resulting in a decrease in impedance (Jolly et al. 2016; Russell et al. 2019).

Following the attachment of the anti-IL-6 antibodies, the next step was the assessment of the sensor's functionality and its characterization. The sensor was incubated with a range of aqueous samples of IL-6 with concentrations, ranging from 5 pg/mL to 150 pg/mL, and the resulting EIS graph is presented in figure 5.4.

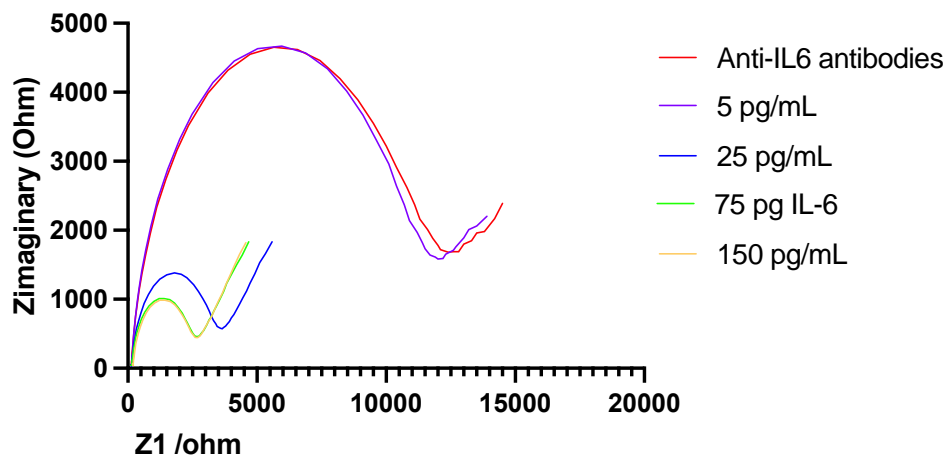


Figure 5.4: EIS graph showing the dynamic range of a simple IL-6 immunosensor, following incubation with IL-6 (5 pg/m – 150 pg/mL). A decrease in impedance is noted following IL-6 binding.

Figure 5.4 shows that the impedance decreases slightly upon addition of 5 pg/mL of IL-6 and then decreases significantly upon addition of 25 pg/mL. A further reduction in impedance is observed when the concentration is increased to 75 pg/mL with no further change observed when the sensor was challenged with 150 pg/mL.

The sensor's poor performance is attributed to the non-targeted nature of the coupling method resulting in disordered immobilisation. EDC / NHS chemistry is used to facilitate amide bond formation between the carboxylate group on the SAM and any primary amine on the antibody. Consequently, the orientation of the antibody is random which may hinder access to the Fab region resulting in sub-optimal binding of the antigen (Bhadra et al. 2015). Targeted thiolation of the Fc domain of the antibody can help provide a single point of attachment to gold surfaces (Oliveira, 2019), however orientation can still prove problematic given the bulkiness of the antibody structure and the ability of many other chemical functionalities to non-specifically interact with gold surfaces. An alternative approach is to use Protein G to facilitate oriented immobilisation (Bae et al. 2005).

#### 5.4.2 Use of protein G to improve IL-6 immunosensor performance.

Given the sensor's poor performance, it was decided to use Streptococcal Protein G to assess whether an improvement in performance will be noted. Protein G is known for its ability to bind to mammalian antibodies, often being used for antibody purification (Akerstrom et al. 1985). Protein G binds with high affinity to the Fc region of the antibody and helps to orient the antibodies away from the sensor's surface, providing easier access the Fab domain thus facilitating efficient antigen recognition (Bae et al. 2005).

Similar to 5.3.1, EDC/NHS coupling was used to immobilize unmodified Streptococcal Protein G on MUA-modified gold electrodes. Following the immobilization of Protein G, the electrode was incubated with anti-IL6 antibodies for 1 hr, rinsed, and incubated with various concentrations of IL-6 and EIS was carried out. The results are presented in figure 5.x below. Although the sensor was challenged with an IL-6 concentration of 5 pg/mL, it did not result in an increase in impedance, so data is presented from a concentration of 12.5 pg/mL onward.

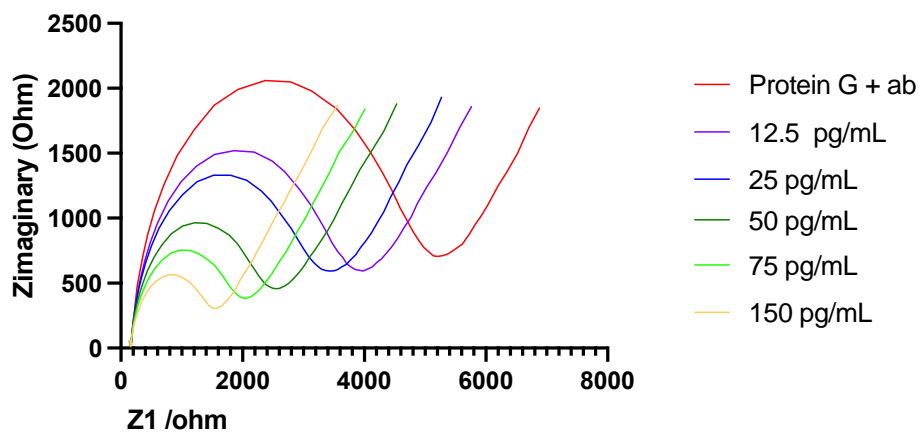
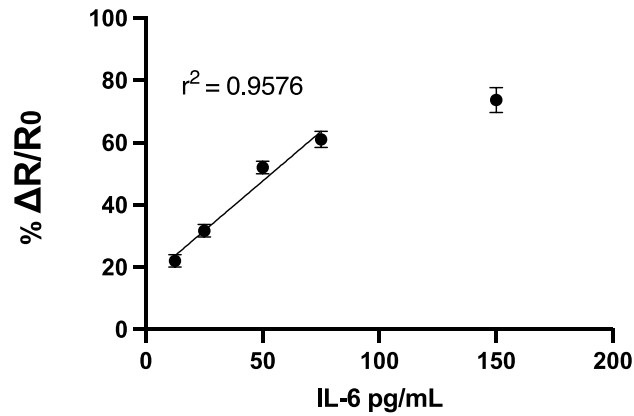


Figure 5.5: EIS graph showing the dynamic range of a Protein G IL-6 immunosensor, following incubation with IL-6 (12.5 pg/m – 150 pg/mL). A decrease in impedance is noted following IL-6 binding.

Figure 5.5 shows that, analogous to the results observed with direct immobilisation of the antibody onto the SAM, a decrease in impedance was noted following incubation with increasing concentrations of IL-6. The percentage change in impedance,  $\Delta R/R_0$ , was plotted as a function of IL-6 concentration in the sample, with this data provided in Figure 5.6.



*Figure 5.6: Dose-response graph showing the absolute response of the Protein G sensor following incubation with IL-6 (12.5 pg/mL – 150 pg/mL) in PBS. The sensor shows a limited linear response in PBS between 12.5 pg/mL and 75 pg/mL, with a  $r^2$  value of 0.9576.*

Despite an improvement in performance being noted with the Protein G immobilisation strategy as a consequence of better orientation of the antibody at the sensor surface, the sensor still displays a very limited detection range. As clinical samples are often highly diluted prior to analysis, the development of a more sensitive sensor with a lower LOD is important. Therefore, in pursuit of a more sensitive IL-6 sensor, it was decided to employ a different detection strategy with aptamers.

### 5.4.3 Evaluation of IL-6 aptamer functionality

#### 5.4.3.1 Aptamer-only monolayer

When using aptamers as the capture elements in biosensors, limiting the interaction between the SAM and the target molecule is crucial, in order to reduce non-specific binding (Campuzano et al. 2019). Prior to the development of the aptasensor, it was decided to screen DTBA and MCH monolayers for their affinity for IL-6. Mercaptohexanol is neutral at physiological pH, and DTBA has a negative charge (PubChem, 2024). IL-6 has an isoelectric point of 6.96, so in PBS buffer it was anticipated that it would have a neutral charge (PubChem, 2024).

To assess the interaction between IL-6 and the thiolated monolayers, gold electrodes were cleaned and incubated with either DTBA or MCH for 1 hour, in order to develop a stable monolayer. Subsequently, the electrodes were rinsed with distilled water and incubated with 25 pg/mL IL-6. EIS measurements were performed and the results, expressed as  $\% \Delta R/R_0$ , are presented below in figure 5.7.

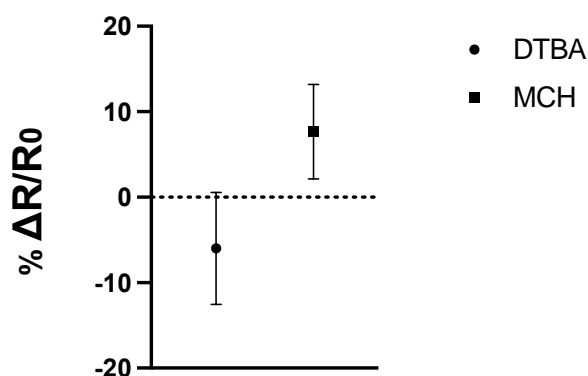


Figure 5.7: Shows the  $\% \Delta R/R_0$  of alkanethiol SAMs following incubation with 25 pg/mL IL-6.

Figure 5.7 shows that, similar to endotoxin in section 3.3.2.1, DTBA shows no interaction with IL-6 at all. There may even be a small reduction in impedance, albeit within error margins, something which was also noted in Chapter 3. A small reduction in impedance may be attributed to the washing steps between incubation and measurement. Additionally, DTBA is known for forming tightly-packed SAMs, which may prevent non-specific binding of IL-6 (Jang and Keng 2008). MCH, which is widely used in the development of sensors, showed little interaction with IL-6 (approximately 7% increase in impedance). As both alkanethiols exhibited low levels of interaction with IL-6, experiments were carried out using both molecules.

For the next step, it was decided to assess the function of a simple aptasensor consisting of aptamer layer, backfilled with MCH to fill any gaps on the gold surface and displace any misaligned aptamers.

A SAM consisting of only aptamer was formed, by incubating clean gold electrodes with the aptamer for 1 hr. at room temperature. The electrode was rinsed with dH<sub>2</sub>O and EIS was performed. The same electrode was immersed in a solution consisting of 40mM MCH for 30 minutes. The electrode was rinsed with dH<sub>2</sub>O, and EIS was performed again. The EIS results are presented in figure 5.8.

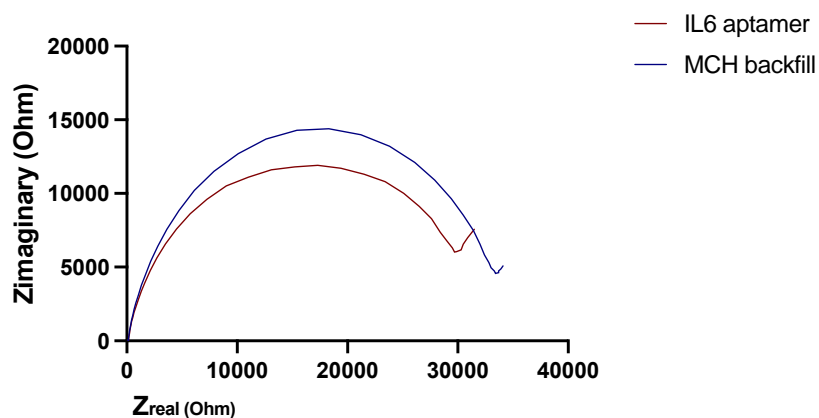


Figure 5.8: EIS graph showing the impedance of an IL6 aptamer monolayer (red) followed by MCH backfilling (blue).

Figure 5.8 above shows that an aptamer-only monolayer resulted in very high impedances (approximately 28 kΩ). Backfilling with MCH (blue curve) showed a small further increase in impedance, which suggests the filling of gaps of the aptamer-only SAM by MCH.

Following the MCH backfilling step, it was decided to assess the sensor's behaviour after incubation with a modest concentration of IL-6 (5 pg/mL). The sensor presented in figure 5.8 above was incubated with 5 pg/mL IL-6 and the resulting EIS graph is presented below in figure 5.9.

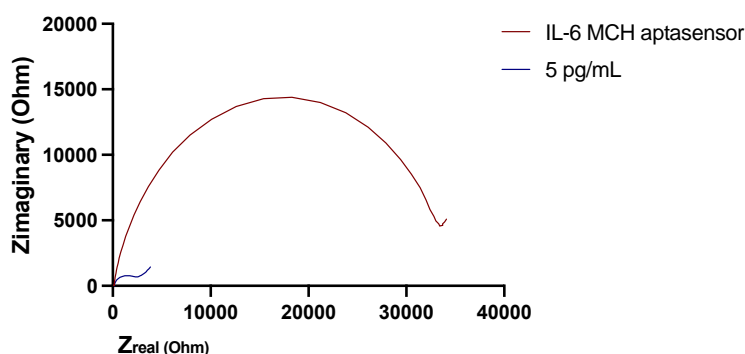


Figure 5.9: EIS graph showing the impedance of an IL6 aptamer monolayer following MCH backfilling (red) followed by incubation with 5 pg/mL IL-6 (blue). A large reduction in impedance is noted.

Figure 5.9 shows that incubation of the MCH-backfilled aptasensor with 5 pg/mL IL-6 resulted in a large decrease in impedance. Previous work in the researcher's group observed that the binding of prostate-specific antigen to aptamers also caused a reduction in impedance (Jolly et al. 2016). It was hypothesized that the binding of the protein to the negatively charged aptamer, caused less DNA charge to be exposed to the solution, resulting in a decrease in impedance. As this system resulted in a large decrease in impedance following incubation with a relatively low IL-6 concentration, it was decided to reproduce the sensor and incubate it with lower concentrations of IL-6 (Figure 10).

The aptasensor was reproduced by following the same protocol (IL-6 aptamer SAM, MCH backfilling), and incubated with various concentrations of IL-6 (0.1 pg/mL – 10 pg/mL), to better assess its dynamic range. The resulting EIS are presented in figure 5.10.

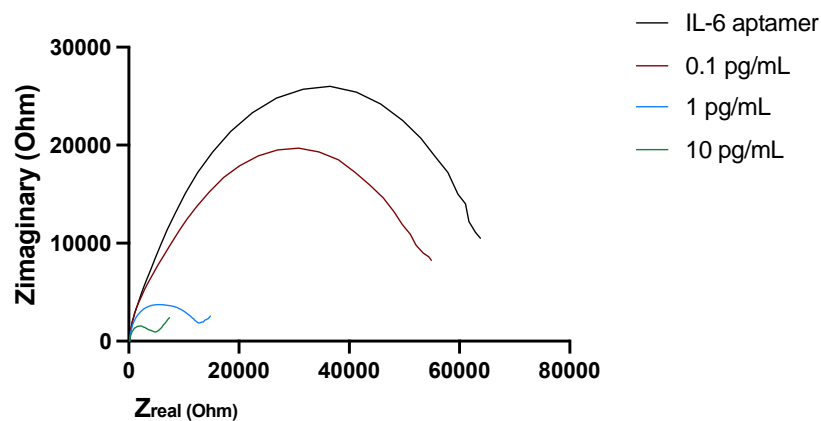


Figure 5.10: EIS graph showing the impedance of an IL6 aptamer monolayer following MCH backfilling (black) followed by incubation with a range of IL-6 concentrations (0.1 – 10 pg/mL).

Figure 5.10 above shows that incubation of the aptasensor (black line) with 0.1 pg/mL IL-6 resulted in a moderate decrease in impedance (1.3 k $\Omega$ ), suggesting an improvement in performance. A further sharp decrease in impedance was observed when the sensor was challenged with 1 pg/mL IL-6. However, comparison of Figures 5.8 and 5.9 shows that the backfilled sensor resulted in inconsistent starting impedances, which varied between 30 and 60 k $\Omega$ . This is incompatible with development of a robust and reproducibly operating biosensor system. It was thought this may be due to the initial immobilisation of the aptamer alone (followed by backfilling with MCH) producing somewhat disordered surfaces. Therefore, it was decided to explore a co-immobilization strategy with MCH and DTBA.

#### 5.4.3.2 DTBA IL6 aptasensor

It was hypothesized that one of the reasons behind the sensor's inconsistent results was the high aptamer concentration when the aptamer is immobilized by itself (1  $\mu$ M). Therefore, it

was anticipated the co-immobilization with an alkanethiol would provide an improvement as a result of lower surface density of the aptamer on the electrode.

A mixture of 1  $\mu\text{M}$  IL-6 aptamer (activated with TCEP) with 40  $\mu\text{M}$  DTBA was applied to gold electrodes and following incubation, various IL-6 concentrations were tested. However, the sensor only showed a positive response within a narrow IL-6 range (100 fg/mL to 3 pg/mL), which is displayed in the figure below (figure 5.11).

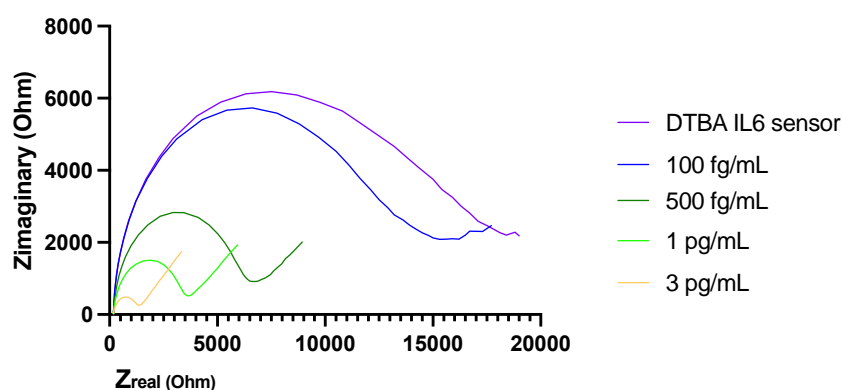


Figure 5.11: EIS graph showing the response of a DTBA-IL-6 aptasensor following incubation with IL-6 (100 fg/mL – 3 pg/mL). A decrease in impedance is noted following IL-6 binding.

Compared to the MCH-backfilled aptasensor (figure 5.10), the DTBA sensor displayed a lower starting impedance of approximately 18 k $\Omega$ , and the sensors displayed consistently similar starting impedances, suggesting an improvement in replicability compared to the MCH-backfilled sensor. This improvement in replicability may be attributed to fact that DTBA is well known for forming highly ordered, closely packed monolayers (Jang and Keng 2008).

Figure 5.11 shows that the mixed DTBA-aptamer sensor exhibited similar sensitivity (100 fg/mL), but a smaller decrease in impedance was observed (-22% vs. -18%). Incubation with higher IL-6 concentrations resulted in larger decreases in impedance. The sensor hit a plateau at 3 pg/mL, and incubation with higher concentrations resulted in negligible changes in impedance.

Despite the sensor exhibiting a poor dynamic range and rapid saturation with IL-6, further attempts to use alternative alkanethiols (MCH, 3-MPA) (data not shown) resulted in underperforming sensors. The DTBA co-immobilized aptasensor showed the best reproducibility in terms of starting impedance so far, and so it was the sensor selected to be taken forward in experiments focused on integrating the sensitizer strategy.

#### 5.4.4 Use of sensitizer on IL-6 aptasensor

Clean gold electrodes were incubated with an aptamer:DTBA mix (1:20) in TE buffer for one hour under ambient temperature. Following that, the electrode was rinsed with endotoxin-free water to remove any non-attached molecules. Then, the electrode was incubated with 100  $\mu$ L of a 1 mg/mL solution of the sensitizer, away from direct sunlight (the sensitizer is labelled **091** across graphs) before measurements were performed. The effect of addition of the sensitizer was evaluated first and is presented in figure 5.12

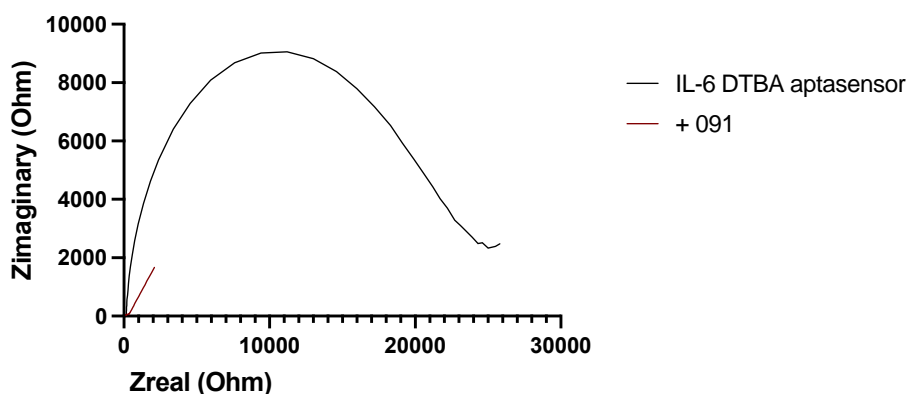


Figure 5.12: EIS graph showing the impedances of the mixed DTBA-aptamer sensor (black) and the same sensor following incubation with the sensitizer (red). A sharp decrease in impedance is noted.

Figure 5.12 shows that, similar to observations for the endotoxin aptasensor, the addition of the sensitizer resulted in a significant decrease in impedance (-98%). This decrease is believed to be attributed to the cancellation of the aptamer's negative charge by the positive charge on the sensitizer. Additionally, it is possible that the binding of the sensitizer to the aptamer may bring about a conformational change. For example, if a partial collapse of the aptamer onto itself were to occur, the resultant reduction in steric barrier might allow the passage of electrons from the ferro/ferricyanide solution to the electrode's surface. A reduction in negative charge will similarly reduce the electrostatic barrier to electron transfer, resulting in a decrease in impedance being observed.

The interaction of the sensitizer with the aptamer was further explored using cyclic voltammetry, with the data presented in Figure 5.13.

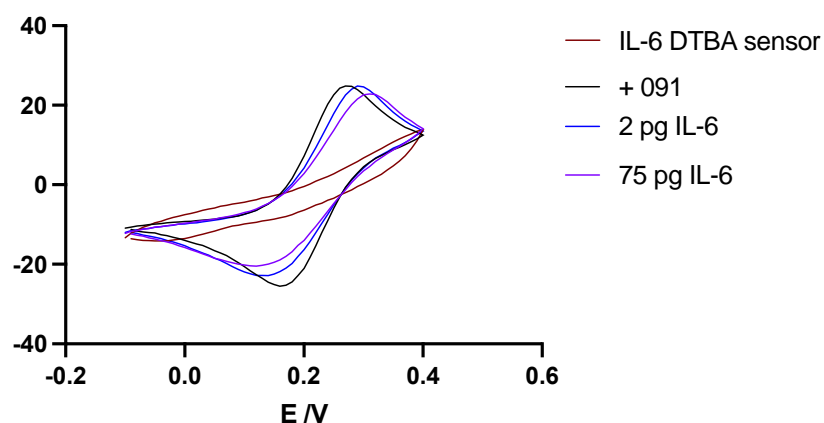


Figure 5.13: CVs of the aptasensor following incubation with sensitiser and further addition of IL-6 at 2 and 75 pg/mL.

The CVs recorded in figure 5.13 show that the addition of the sensitizing complex causes a new peak in the CV for both the oxidative and reductive wave, associated with an increase in current flow. This observation is attributed to binding of the complex to the aptamer, placing the complex in proximity of the electrode so that the redox processes associated with the sensitizer are observed. Addition of IL-6 results in a decrease in current and a slight increase in the potential at which the maximum currents occur. Both figures 5.12 and 5.13 suggest the effective intercalation of the sensitizer with the aptamer.

#### 5.4.4.1 Use of sensitized IL-6 aptasensor in water samples

Following addition of the sensitizer, the aptasensor was challenged with a variety of IL-6 concentrations in water ranging from 10 fg/mL up to 150 pg/mL, with 3 replicates produced for each concentration, to ascertain the sensor's sensitivity and enable the estimation of the limit of detection. The resultant EIS data is shown in Figure 5.14, with the correlation between correlation and %R/R0 provided in Figure 5.15.

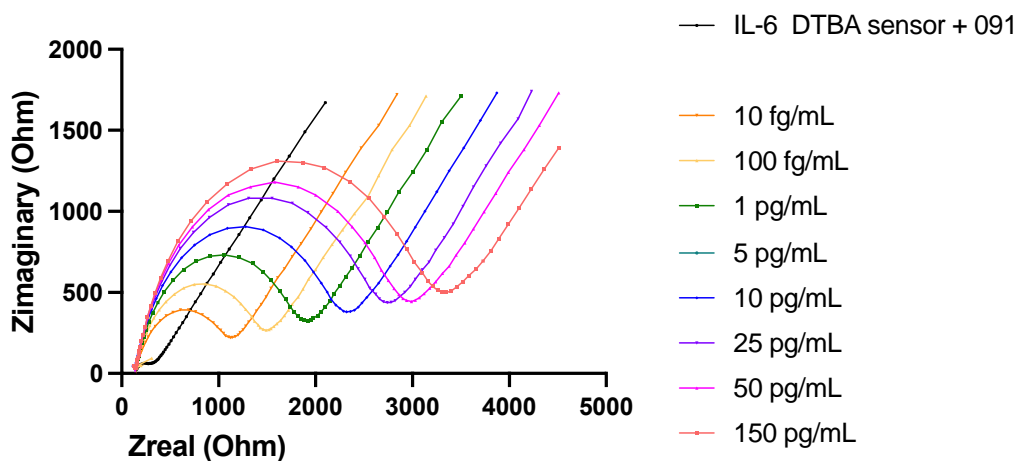


Figure 5.14 EIS graph showing the detection range of the aptamer following incubation with sensitizer and various concentrations of IL-6 in water.

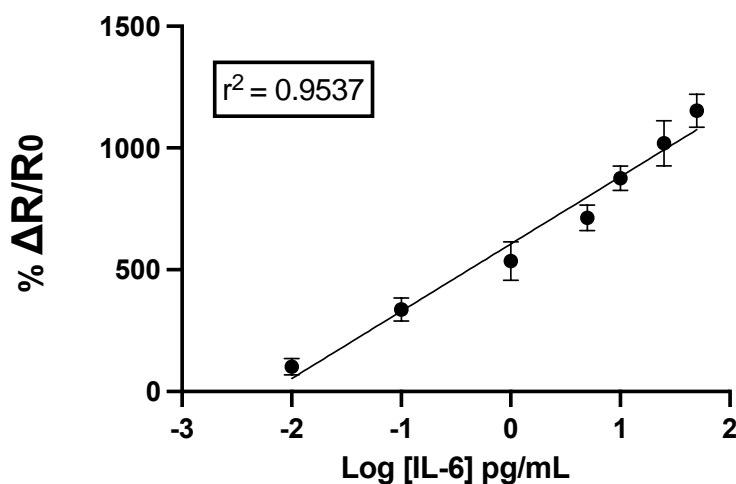


Figure 5.15: Shows the  $\% \Delta R/R_0$  of the sensor following incubation with sensitizer and various concentrations of IL-6 in water.

Figure 5.14 shows the sensor's response in water from 10 fg/mL up to 50 pg/mL, expressed as  $\% \Delta R/R_0$ . A linear response was observed, with an  $R^2$  of 0.9537.

Overall, a significant improvement was observed in the sensitized sensor compared to the regular aptasensor. The sensitized system had a LOD of 10 fg/mL, whereas the aptasensor had a LOD of 100 fg/mL. Most importantly, however, the sensitizer improved the sensor's dynamic range, with the sensitised system capable of detecting up to 150 pg/mL, compared to the 3 pg/mL maximum observed with the conventional aptasensor.

Of interest is the sensitizer's mode of action. The aptasensor without the sensitizer showed a decrease in impedance following IL-6 binding (section 5.4.3.2). In contrast, the sensitized system showed an increase in impedance. The addition of the sensitizer resulted in an initial significant decrease in impedance, which suggests negation of the aptamer's negative charge

and / or conformational change. The binding of IL-6, which has an isoelectric point of 6.96 and therefore a neutral charge in water, adds mass at the electrode surface thus increasing the steric barrier and hence impedance (PubChem, 2024) but is not expected to result in an increase in the electrostatic barrier. In percentage terms, the effect of IL-6 on the sensitized aptasensor is significantly higher than for the non-sensitized aptasensor but this needs to be considered in light of the fact that the baseline impedance is significantly lower for the sensitized system. Nevertheless, the measured impedance of the sensitized system exceeds the measured impedance of the non-sensitized system, which is suggestive of the sensitizers remaining involved in the complex formed on the electrode.

#### 5.4.4.2 Use of sensitized IL-6 aptasensor in plasma samples

The sensitizer showed promising results for the detection of IL-6 in water, therefore it was decided to assess its functionality in citrated blood plasma, which is the sample matrix used throughout this project. Blood components are not known to interfere with IL-6 detection, and ELISAs are routinely used for the detection of IL-6 in blood samples (McCrae et al. 2023). Previous work in the researcher's lab showed that a tenfold dilution of plasma allowed detection of procalcitonin and c-reactive protein in plasma using aptasensors (Demertzis, 2019).

The sensitized aptasensors were prepared as per section 5.3.4. The aptasensor was challenged with a variety of IL-6 concentrations in tenfold diluted (in endotoxin free water) citrated blood plasma ranging from 10 fg/mL up to 50 pg/mL, with 3 replicates produced for each concentration, to ascertain the sensor's sensitivity and enable the estimation of the limit of detection. The resultant EIS data is shown in Figure 5.16, with the correlation between concentration and %R/R<sub>0</sub> provided in Figure 5.17.

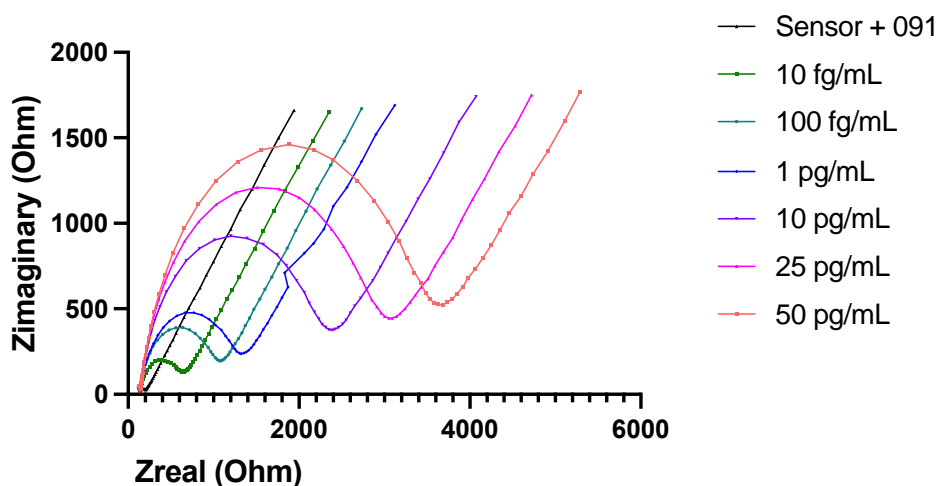


Figure 5.16: EIS graph showing the detection range of the aptamer following incubation with sensitizer and various concentrations of IL-6 in citrated blood plasma.

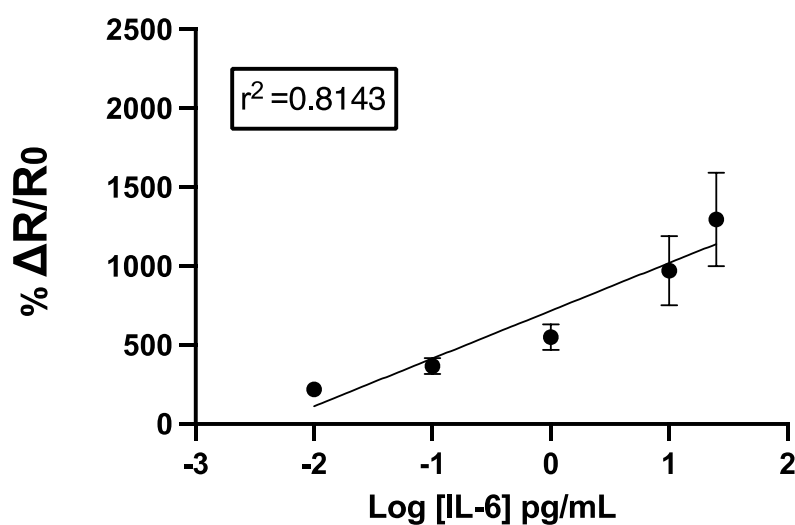


Figure 5.17: Shows the  $\% \Delta R/R_0$  of the sensor following incubation with sensitizer and various concentrations of IL-6 in citrated blood plasma. A linear range is noted between 10 fg/mL and 25 pg/mL.

Figure 5.17 shows the sensor's response in plasma from 10 fg/mL up to 25 pg/mL, expressed as  $\% \Delta R/R_0$ . A linear response was observed, with an  $R^2$  of 0.8143. Overall, the sensor retained its performance, showing consistent sensitive detection of IL6 from 10 fg/mL, up to 25 pg/mL. Compared to detection in water, higher  $\% \Delta R/R_0$  were noted, which may be attributed to non-specific binding of plasma components, such as proteins, lipids or other nucleic acids (Harm et al. 2021). A control including plasma diluted in tenfold was performed, and the results are presented in the next section (section 5.3.4.2).

The retention of efficiency of the sensor upon going from an aqueous sample to a plasma sample is an encouraging observation, as it demonstrates the successful application of a DNA intercalating complex as a sensitizer in aptamers and its successful application in blood plasma. Moreover, assuming the electrodes are cleaned beforehand, the aptasensors can be set up in about an hour, which allows the quick and efficient preparation of sensors and detection. There are few aptasensors that utilize sensitizing molecules in literature, and literature is scarce on the application of such sensors in clinical samples.

#### 5.4.4.3 Specificity tests on IL-6 aptasensor

Given the impressive detection range produced by the use of the sensitizer, it was considered worthwhile assessing the sensitized sensor's affinity for components of diluted blood plasma by itself, as well as proteins and endotoxin. Therefore, the sensor was incubated with various

concentrations of HSA, IL-10 and endotoxin. Figures 5.18 A-D show the sensitized sensor's response following incubation with tenfold diluted plasma, HSA, IL-10 and endotoxin.

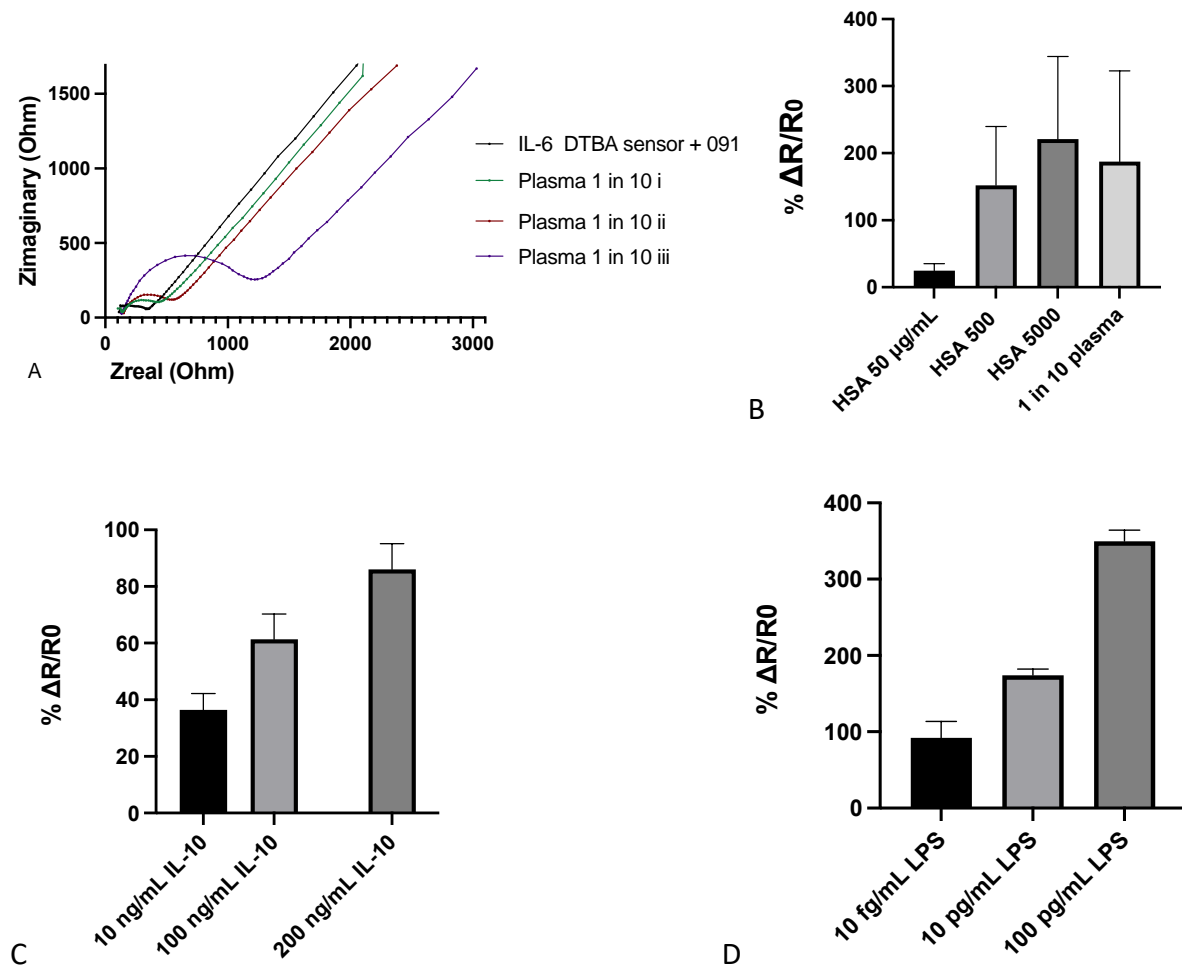


Figure 5.18: A shows the sensor's (black) response following incubation with citrated plasma following tenfold dilution. 5.18 B shows the  $\% \Delta R/R_0$  of the sensor following incubation with various HSA concentrations and tenfold diluted plasma. 5.18 C and D show the  $\% \Delta R/R_0$  of the sensor following incubation with various concentrations of IL-10 and endotoxin.

Figure 5.18 B shows that a HSA concentration of 50  $\mu\text{g/mL}$  showed the lowest response (avg increase of 25%, standard error 6%), whereas concentrations of 500 and 5000  $\mu\text{g/mL}$  resulted in approximate increases of 152% (standard error 50%) and 221% (standard error 71%) respectively. Incubation with tenfold diluted citrated plasma resulted in an average increase in impedance of 184%. Incubation with IL-6 in water and plasma at a concentration of 10 fg/mL resulted in increase of 101% and 254%, respectively.

Figure 5.18 C shows the responses following incubation with high concentrations of IL-10. Interestingly, across all molecules tested, IL-10 resulted in the lowest increases in impedance, even at very high concentrations (200 ng/mL). The isoelectric point of IL-10 has been found

to be 8.2 – 9.0, which results in a positively charged molecule in neutral solutions (Bondoc et al. 1997). This is an interesting observation, as it suggests that the sensitized sensor may show higher affinity for molecules with negative or neutral surface charge.

Finally, figure 5.18 D shows the responses following incubation with endotoxin. Incubation with 10 fg/mL produced an increase of 92%, which is similar to the response following incubation with 10 fg/mL IL-6. According to the figure, the system shows an affinity for endotoxin, which may be attributed to the molecule's strong negative charge in physiological conditions. The background level of endotoxin has been estimated to be around 1-10 fg/mL in this project (Chapter 2).

Interestingly, despite the sensor's positive responses following incubation with HSA, IL-10 and endotoxin, the system produced a linear response in diluted plasma, with increases in impedance significantly exceeding those noted in specificity studies. This suggests selectivity for IL-6 in the presence of other molecules, including other proteins, nucleic acids, lipids and low amounts of endotoxin (1-10 fg/mL). Moreover, with the exception of endotoxin, the observed signals upon exposure to IL-6 are significantly higher than the observed signals upon exposure to HSA and IL-10. Given the complexity in target molecule detection in clinical samples and in particular blood, this is an encouraging observation.

#### **5.4.5 Initial experiments to develop a beta globin sensor**

Following the successful development of an aptasensor for IL-6 detection in both aqueous solutions and blood plasma, it was decided to develop a sensor for the detection of single-stranded DNA, which was one of the targets of this project. As mentioned in the introductory section of this chapter, a thiolated ss-DNA sequence, complementary to the beta-globin strand was chosen as the recognition element for the sensor.

As a first step in the sensor fabrication process, a DNA-only monolayer was developed. Clean gold electrodes were incubated with thiolated beta-globin ss-DNA complementary strand in TE buffer for one hour under ambient conditions. Following that, electrodes were rinsed with endotoxin-free water to remove any non-attached DNA strands and then challenged with the target beta globin DNA strand at a 1 $\mu$ M concentration, for 1 hour under ambient conditions (Figure 5.19).

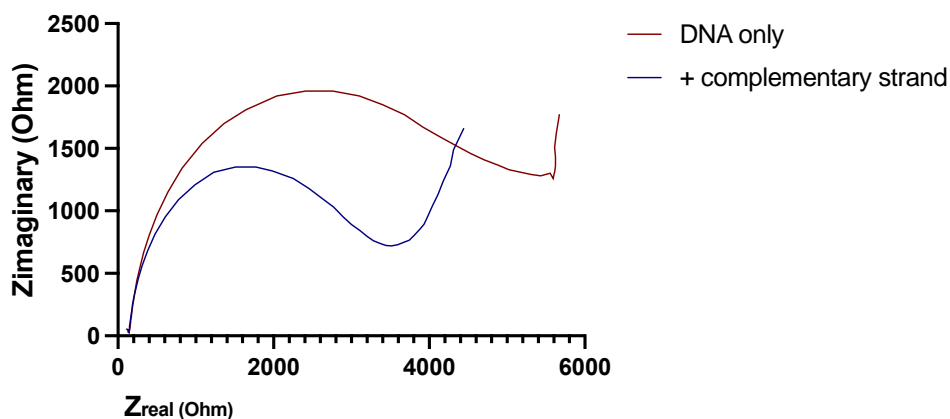


Figure 5.19: EIS graph showing the response of a capture-DNA strand without any spacers. A reduction in impedance was observed on addition of the complementary strand.

Figure 5.19 shows that without surface passivation through the use of spacer molecules, a reduction in impedance of -36% is noted when the complementary strand of DNA is added. This is unexpected and may be suggestive of a lack of selective binding / duplex DNA formation, possibly due to steric hindrance caused by DNA overcrowding. The reduction in impedance may be brought about by the washing step following incubation with the target DNA.

The sensor was recreated but this time, following immobilisation of the capture strand, 20 mM MCH was added to backfill the surface. As is evident from Figure 5.20, the use of a back filling approach results in a baseline impedance of the sensor of 13.5 k $\Omega$  compared to 4.8 k $\Omega$  when the capture strand was immobilised without back filling. This increase in impedance is attributed to more complete coverage of the sensor surface brought about by the addition of the MCH spacer molecules. The back filled sensor was subsequently challenged with three concentrations (0.1, 0.5 and 1  $\mu$ M) of the complementary beta-globin strand. The EIS results are shown in Figure 5.20.

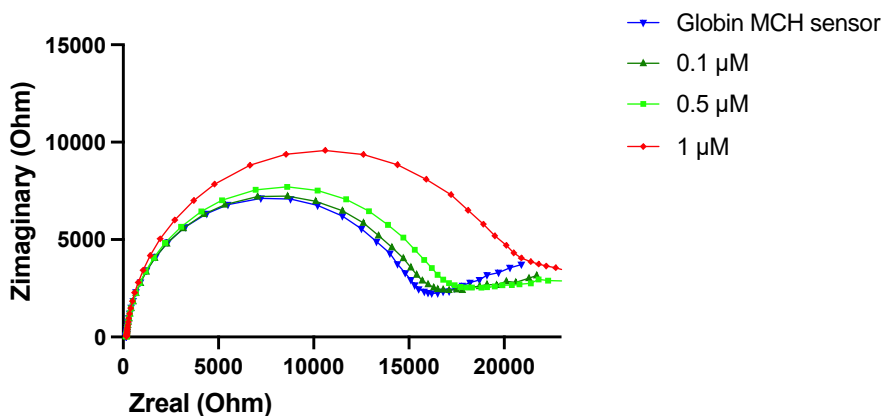


Figure 5.20: EIS graph showing the MCH-backfilled DNA sensor following incubation with various concentrations of target DNA.

Figure 5.20 shows that backfilling with MCH resulted in an improvement in target DNA binding, manifest as a small increase in impedance following incubation with 0.1 and 0.5  $\mu\text{M}$  globin DNA (2% and 5%, respectively). A larger change in impedance (29%) was observed following incubation with 1  $\mu\text{M}$  globin DNA. Despite the positive response at higher DNA concentrations, the sensor was still far from applicable. Although plasma DNA levels in sepsis tend to be found in ng/mL concentrations, the development of a sensitive sensor is still important as clinical samples are often diluted as per protocol (Rhodes et al. 2006).

The development of the beta globin DNA sensor was challenging. Out of all spacers used (DTBA, MCH, 3-MPA, (data not shown)), only backfilling with MCH resulted in a small increase in impedance, and only following incubation with a high concentration of target DNA (1  $\mu\text{M}$ ). Co-immobilization with MCH also resulted in poor sensor performance. Out of all approaches used, the formation of a target DNA monolayer followed by MCH backfilling was the only way to produce a sensor which generated a positive response. It was therefore decided to take this sensor forward into experiments utilizing the same sensitizer molecule as described in the IL-6 sensor studies.

#### 5.4.6 Use of sensitizer in the beta-globin sensor

The sensitizer used in this study is based on a cobalt complex and designed to intercalate ds-DNA. At the time this experiment was carried out, it hadn't been used in ss-DNA systems before. Some DNA intercalating dyes, such as methylene blue and SYBR green are known for their action on ss-DNA, although to a lesser degree compared to ds-DNA (Zipper et al. 2004; Trantakis et al. 2010; Miao et al. 2016). Thus, it was considered worthwhile assessing the sensitizer's binding efficiency to ss-DNA.

First, the interaction of **91** with an electrode carrying the beta globin capture strand backfilled with MCH was studied. EIS data is presented in Figure 5.21.

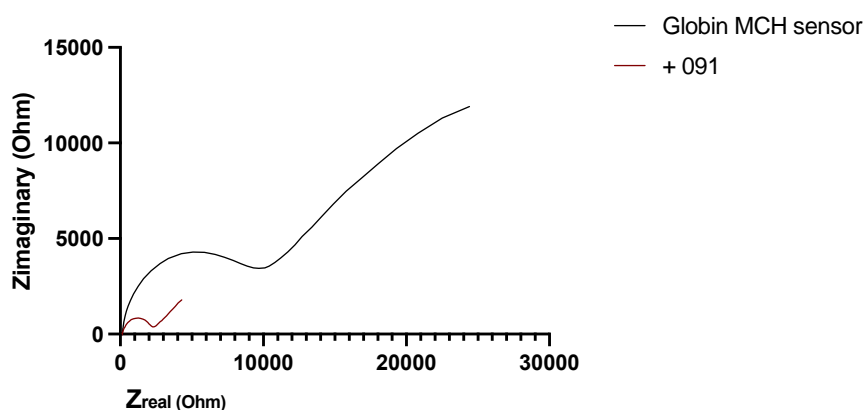


Figure 5.21: EIS graph showing the impedances of the MCH backfilled ss-DNA sensor (black) and the same sensor following incubation with the sensitizer (red). A sharp decrease in impedance is noted.

Figure 5.21 shows that incubation of the ss-DNA modified electrode with the sensitizer caused a decrease in impedance (-75 %), similar to the response noted with the IL-6 aptasensor. This is an interesting observation, as it was assumed that the sensitizer functioned by intercalation in DNA duplex regions. The observation in figure 5.21 suggests that the complex can bind to ss-DNA, possibly by attraction to the negative charge of DNA. Another possible explanation may be intercalation in partially folded GC regions, which is observed with methylene blue (Miao et al. 2016).

As for the IL-6 sensor, the interaction of molecule **91** with the sensor was evaluated using CV (Figure 5.22).

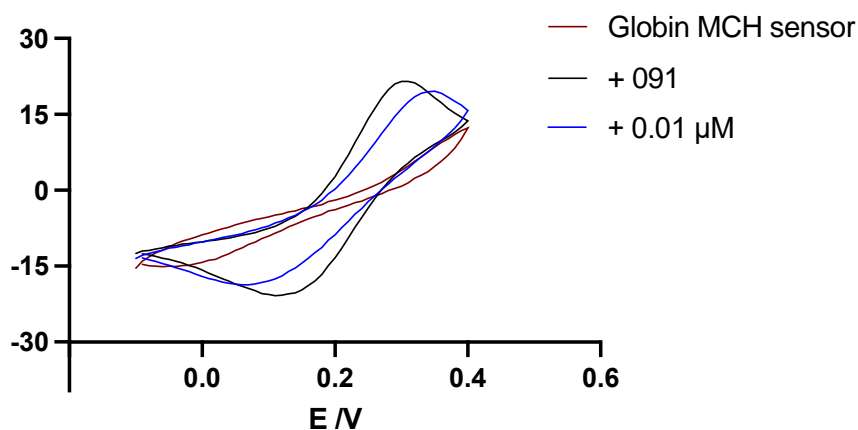


Figure 5.22: CVs of the MCH backfilled ss-DNA sensor following incubation with the sensitizer and further addition of beta-globin DNA at 0.01  $\mu\text{M}$ .

Figure 5.22 shows that, similar to figure 5.13 showing the CVs of the IL6 sensor, the addition of the sensitizing complex causes a large increase in current flow. The new peaks are again attributed to the redox properties of the cobalt complex. Incubation with 0.01  $\mu\text{M}$  beta globin resulted in a decrease in current flow, suggesting effective DNA binding.

It was therefore decided to evaluate the sensitized sensor for beta globin using EIS. The aptasensor was challenged with a variety of beta globin DNA concentrations in water ranging from 0.01  $\mu\text{M}$  up to 10  $\mu\text{M}$ , with 3 replicates produced for each concentration, to ascertain the sensor's sensitivity and enable the estimation of the limit of detection. The resultant EIS data is shown in Figure 5.23, with the correlation between concentration and  $\%R/R_0$  provided in Figure 5.24.

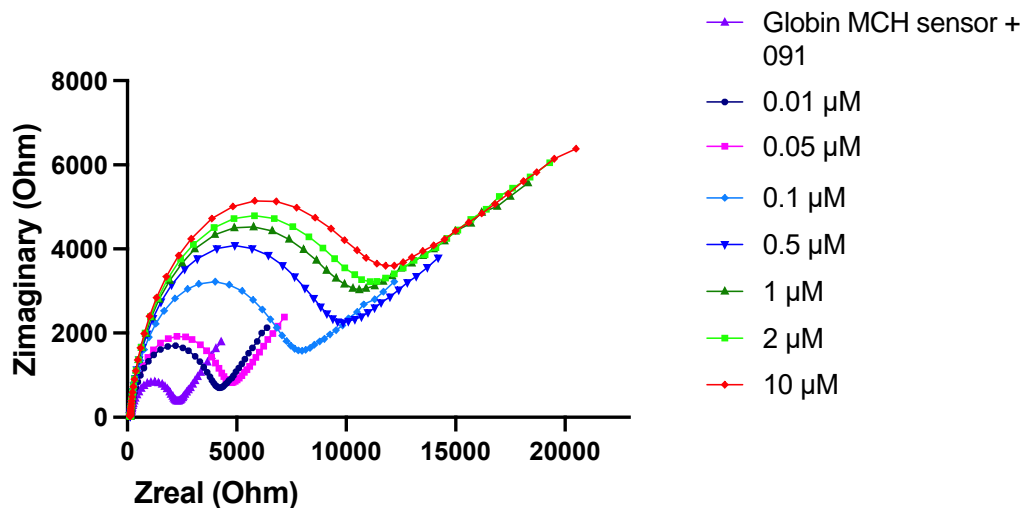


Figure 5.23 EIS graph showing the detection range of the MCH DNA sensor following incubation with sensitizer and various concentrations of beta globin in water.

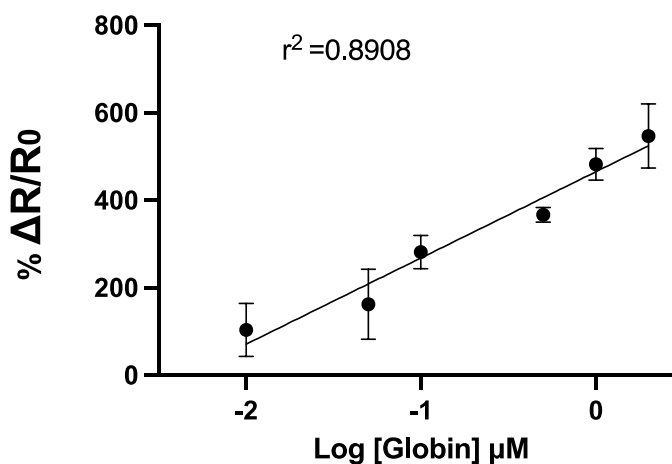


Figure 5.24: Shows the  $\% \Delta R/R_0$  of the sensor following following incubation with sensitizer and various concentrations of beta globin in water. A linear range is noted between 0.01 and 2  $\mu\text{M}$ .

Figure 5.24 shows the sensor's response in water from 0.01  $\mu\text{M}$  up to 2  $\mu\text{M}$  beta globin, expressed as  $\% \Delta R/R_0$ . A linear response was observed, with an  $R^2$  of 0.8908.

Overall, a significant improvement was observed in the sensitized sensor compared to the regular DNA sensor, which exhibited poor performance. The sensitized system had a LOD of 0.01  $\mu\text{M}$ , whereas the DNA sensor without added sensitizer only showed a significant

response above baseline at 1  $\mu\text{M}$ . Most importantly, the sensitizer significantly improved the sensor's detection range, allowing DNA detection from 0.01  $\mu\text{M}$  up to 10  $\mu\text{M}$ .

#### 5.4.6.1 Use of sensitized beta globin sensor in plasma samples

Given the promising results for the detection of beta globin in water, it was decided to assess the sensor's performance when challenged with tenfold diluted (in endotoxin free water) citrated blood plasma spiked with beta-globin. The aptasensor was challenged with a variety of beta globin concentrations in plasma ranging from 0.01 $\mu\text{M}$  up to 10  $\mu\text{M}$ , with 3 replicates produced for each concentration, to ascertain the sensor's sensitivity and enable the estimation of the limit of detection. The resultant EIS data is shown in Figure 5.25, with the correlation between concentration and %R/R0 provided in Figure 5.26.

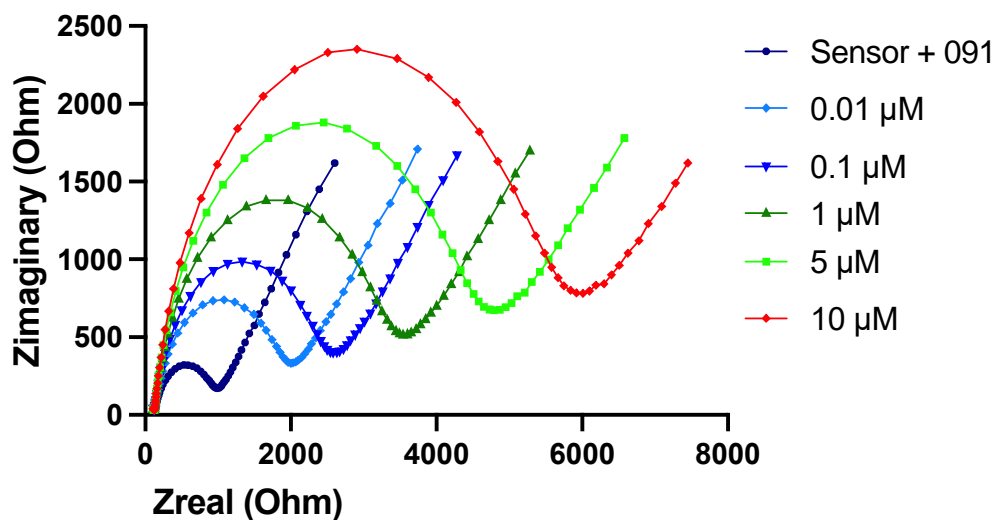


Figure 5.25: EIS graph showing the detection range of the aptamer following incubation with sensitizer and various concentrations of beta globin in citrated blood plasma.

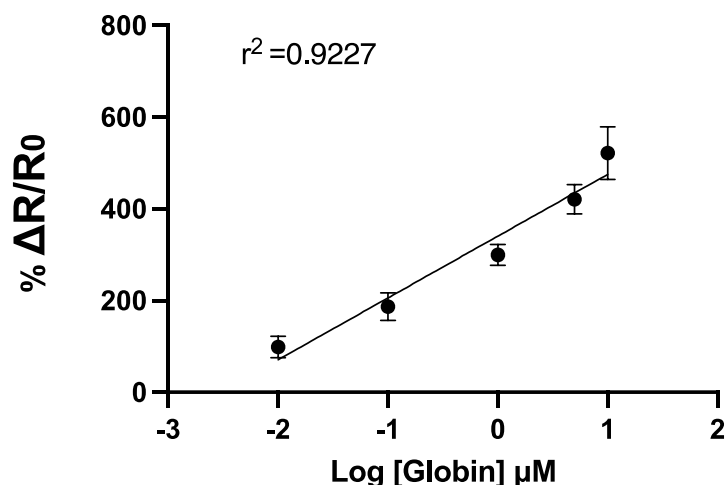


Figure 5.26: Shows the  $\% \Delta R/R_0$  of the sensor following following incubation with sensitizer and various concentrations of beta globin in citrated blood plasma. A linear range is noted between 0.01 and 10  $\mu\text{M}$ .

Figure 5.26 shows the sensor's response in citrated blood plasma from 0.01  $\mu\text{M}$  up to 10  $\mu\text{M}$  beta globin, expressed as  $\% \Delta R/R_0$ . A linear response was observed, with an  $R^2$  of 0.9227.

Overall, the sensor retained its performance, showing consistent sensitive detection of beta globin from 0.01  $\mu\text{M}$  up to 10  $\mu\text{M}$  with good linearity, similar LOD and sensitivity to beta globin in both matrices. Interestingly, the change in impedance is smaller in plasma compared to water, for the same DNA concentrations. It is possible that interaction with plasma components may hinder the binding of the DNA, and that a more thorough plasma preparation protocol may counter this. Regardless, this is an encouraging observation, as it demonstrates the successful application of a DNA intercalating complex as a ss-DNA sensitizer for sensing applications in blood plasma.

#### 5.4.6.2 Specificity tests on beta globin sensor

Finally, the specificity of the beta globin sensor was explored through exposure to HSA, diluted plasma, IL-10 and endotoxin to evaluate the risk of false positives. Figures 5.27 A-C show the sensitized sensor's response following incubation with tenfold diluted plasma, HSA, IL-10 and endotoxin.

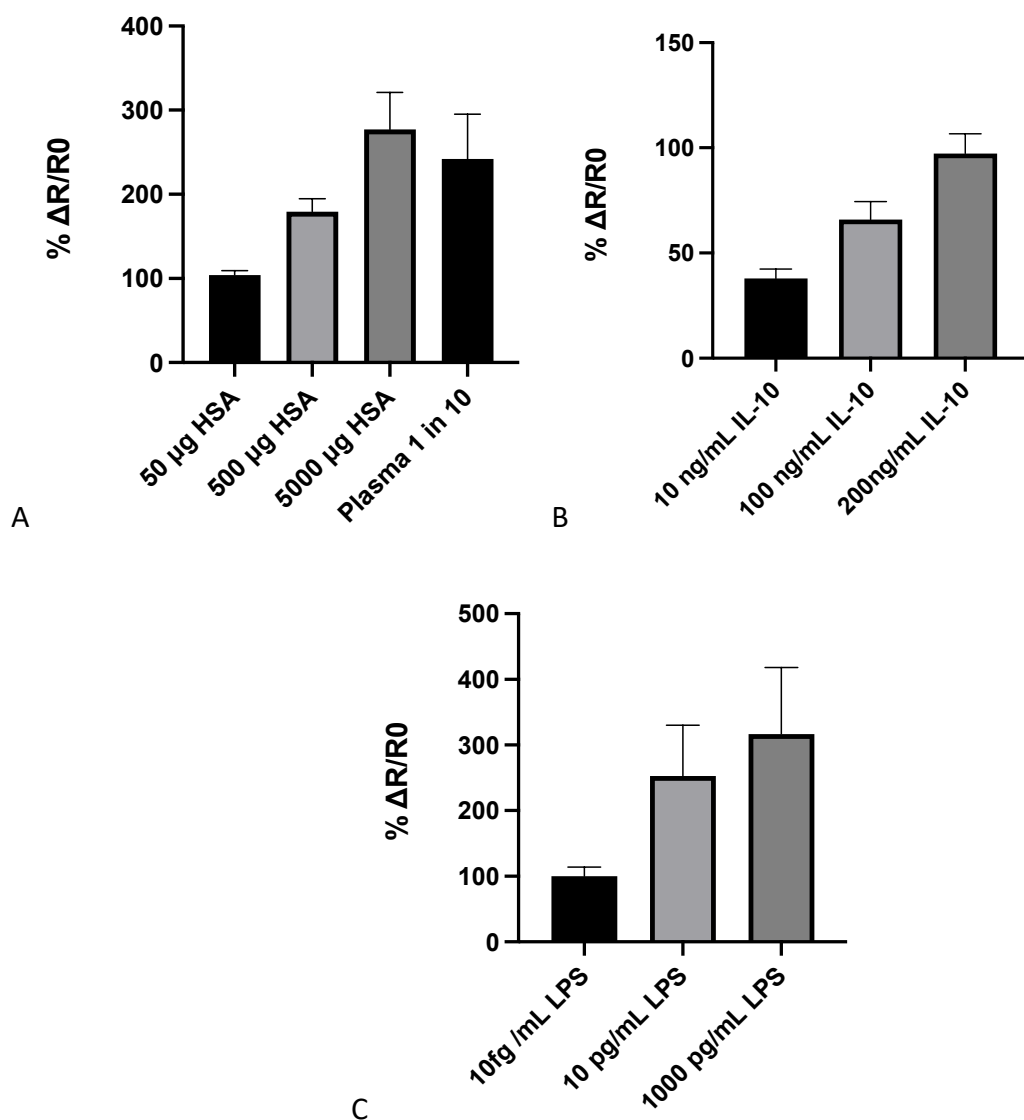


Figure 5.27 A shows the % $\Delta R/R_0$  of the sensor following incubation with various HSA concentrations and tenfold diluted plasma. 5.27 B and C show the % $\Delta R/R_0$  of the sensor following incubation with various concentrations of IL-10 and endotoxin respectively.

Figure 5.27 A shows that a HSA concentration of 50  $\mu\text{g}/\text{mL}$  showed the lowest response (avg 104%), whereas concentrations of 500 and 5,000  $\mu\text{g}/\text{mL}$  resulted in approximate increases of 179% and 277%, respectively. Incubation with tenfold diluted citrated plasma resulted in an average increase in impedance of 242%. Compared to the IL-6 sensitized sensor, higher % $\Delta R/R_0$  were observed. This may be caused by reduced binding of the sensitizer to ss-DNA, which may lead to increased biofouling.

Figure 5.27 B shows the responses following incubation with high concentrations of IL-10. Similar to the IL-6 sensor, across all molecules tested, IL-10 resulted in the lowest increases in impedance, even at very high concentrations (200 ng/mL). The isoelectric point of IL-10 has

been found to be 8.2 – 9.0, which results in a positively charged molecule in neutral solutions (Bondoc et al. 1997). This may explain the sensor's lesser affinity for IL-10 and may further support the charge-attraction hypothesis.

Finally, figure 5.27 C shows the responses following incubation with endotoxin. Incubation with 10 fg/mL produced an increase of 92%, which is similar to the response seen with the IL-6 sensor. According to the figure, the system shows an affinity for endotoxin, which may be attributed to the molecule's strong negative charge in physiological conditions.

Interestingly, throughout the experiments, following incubation with the sensitizer, the IL-6 sensor showed lower impedances (0.2-0.5 k $\Omega$ ) compared to the globin sensor (2 – 5 k $\Omega$ ). This may be attributed to the sensitizer's affinity for double-stranded DNA. This makes sense, as aptamers are known for forming duplexes and loops (Aljohani et al. 2022). Moreover, the aptamer is a longer DNA sequence compared to the globin sequence, which may also explain the increased binding.

One of the most important observations in this section is that the sensitized system was still capable of detecting the beta-globin sequence with minimally treated plasma (tenfold dilution) as shown in figure 5.27, with surprisingly acceptable linearity ( $r^2 = 0.9227$ ). It is possible that further refinement of the plasma treatment protocol may further improve linearity and detection limits. This is an encouraging observation that may prompt further investigation into the application of the sensitizer in DNA sensing applications.

## 5.5 Conclusions

This Chapter describes the successful development of two sensors, one for IL-6 and one for DNA detection, in both aqueous samples and blood plasma.

Initial attempts to fabricate an IL-6 sensor did not produce viable sensors, with EDC/NHS chemistry resulting in poorly performing sensors with a high LOD (pg/mL) and poor dynamic ranges. The introduction of Protein G to enable oriented antibody immobilisation resulted in a modest improvement in sensor performance, with a LOD of 0.1 pg/mL, however the poor dynamic range remained. Immobilization of the aptamer by itself led to the generation of very high impedances with high variance between sensors. Incubation with 100 fg/mL IL-6 resulted in a massive drop in impedance, and incubation with further IL-6 concentrations resulted in further, smaller drops in impedance. Attempts were made to improve the aptasensor's performance, through co-immobilization with various alkanethiols, where it was observed that co-immobilization with DTBA improved performance by allowing the detection of IL-6 from 100 fg/mL up to 3 pg/mL. However, overall, the sensor performance remained poor, and it was decided to use the sensitizer complex to assess its effect on the aptasensor.

The introduction of the sensitizer resulted in a considerable expansion of the dynamic range, allowing detection of IL-6 from 10 fg/mL up to 50 pg/mL. The sensor retained its activity when challenged with spiked citrated plasma, with a dynamic range of 10 fg/mL up to 25 pg/mL being observed. Specificity tests on the sensor showed an interaction with HSA and endotoxin, however the sensor displayed good performance in blood plasma, which may suggest a strong affinity for the target molecule.

Similar to the IL-6 aptasensor, the development of the beta globin sensor was challenging. Following a screening process, it was discovered that backfilling with MCH was the only way to produce a sensor with a positive response, but only at high beta globin concentrations (1  $\mu\text{M}$ ). The introduction of the sensitizer resulted in an improved detection range of 0.01  $\mu\text{M}$  - 2  $\mu\text{M}$  in water, and 0.01  $\mu\text{M}$  – 10  $\mu\text{M}$  in blood plasma. Similarly to the sensitized IL-6 sensor, the beta globin sensor showed an interaction with HSA and endotoxin. However the sensor displayed good performance in blood plasma, which may suggest a strong affinity for the target molecule.

The results generated in this Chapter show the potential of DNA intercalating molecules in the development of rapid detection systems. Both systems require less than 1.5 hrs to set up, relying on a 5-minute incubation time with the sensitizer and a sample incubation time of less than 10 minutes. These short incubation times, coupled with the performance data obtained using spiked blood plasma samples, demonstrate the potential for these sensors in real-life applications.

Due to time constraints, as those experiments were carried out near the end of the project, it wasn't possible to challenge the sensor with other molecules. Additionally, it wasn't possible to plan experiments aiming to assess the sensitizer's mode of action, kinetics and interactions with molecules. Finally, given the encouraging results presented in this chapter, it would be interesting to construct an AptaMIP platform for the detection of IL-6, in combination with the sensitizer presented in this study. It is anticipated that the addition of the polymer would reduce/prevent the non-specific binding with other competitors (HSA, IL-10, endotoxin) seen in section 5.3.4.2.

The researcher hopes that the results presented in this chapter will inspire future investigations towards the use of these interesting molecules into diagnostic applications.

## 5.6 Bibliography

- Abi, A. and Safavi, A. 2021. Determination of the binding site size of hexaammineruthenium(iii) inside monolayers of DNA on gold. *Analyst* 146(2), pp. 547-557. doi: 10.1039/d0an01685c
- Akerstrom, B. et al. 1985. Protein G: a powerful tool for binding and detection of monoclonal and polyclonal antibodies. *J Immunol* 135(4), pp. 2589-2592.
- Aljohani, M. M. et al. 2022. Aptamers: Potential Diagnostic and Therapeutic Agents for Blood Diseases. *Molecules* 27(2), doi: 10.3390/molecules27020383
- Aydin, E. B. 2020. Highly sensitive impedimetric immunosensor for determination of interleukin 6 as a cancer biomarker by using conjugated polymer containing epoxy side groups modified disposable ITO electrode. *Talanta* 215, p. 120909. doi: 10.1016/j.talanta.2020.120909
- Aydin, E. B. et al. 2021. A novel electrochemical immunosensor based on acetylene black/epoxy-substituted-polypyrrole polymer composite for the highly sensitive and selective detection of interleukin 6. *Talanta* 222, p. 121596. doi: 10.1016/j.talanta.2020.121596
- Bae, Y. M. et al. 2005. Study on orientation of immunoglobulin G on protein G layer. *Biosens Bioelectron* 21(1), pp. 103-110. doi: 10.1016/j.bios.2004.09.003
- Bai, L. et al. 2014. A signal-on electrochemical aptasensor for ultrasensitive detection of endotoxin using three-way DNA junction-aided enzymatic recycling and graphene nanohybrid for amplification. *Nanoscale* 6(5), pp. 2902-2908. doi: 10.1039/c3nr05930h
- Bonanni, A. and del Valle, M. 2010. Use of nanomaterials for impedimetric DNA sensors: a review. *Anal Chim Acta* 678(1), pp. 7-17. doi: 10.1016/j.aca.2010.08.022
- Bondoc, L. L., Jr. et al. 1997. Resolution of recombinant human interleukin 10 from variants by recycling free flow focusing. *Anal Biochem* 246(2), pp. 234-238. doi: 10.1006/abio.1997.2023
- Campuzano, S. et al. 2019. Antifouling (Bio)materials for Electrochemical (Bio)sensing. *Int J Mol Sci* 20(2), doi: 10.3390/ijms20020423

Chang, J. et al. 2019. Nucleic Acid-Functionalized Metal-Organic Framework-Based Homogeneous Electrochemical Biosensor for Simultaneous Detection of Multiple Tumor Biomarkers. *Anal Chem* 91(5), pp. 3604-3610. doi: 10.1021/acs.analchem.8b05599

Dolin, H. H. et al. 2018. A Novel Combination of Biomarkers to Herald the Onset of Sepsis Prior to the Manifestation of Symptoms. *Shock* 49(4), pp. 364-370. doi: 10.1097/SHK.0000000000001010

Gao, Y. et al. 2021. A flexible multiplexed immunosensor for point-of-care in situ wound monitoring. *Sci Adv* 7(21), doi: 10.1126/sciadv.abg9614

Gonçalves, M. d. L. et al. 2021. Electrochemical Point-of Care (PoC) Determination of Interleukin-6 (IL-6) Using a Pyrrole (Py) Molecularly Imprinted Polymer (MIP) on a Carbon-Screen Printed Electrode (C-SPE). *Analytical Letters* 54(16), pp. 2611-2623. doi: 10.1080/00032719.2021.1879108

Hai, X. et al. 2020. DNA-based label-free electrochemical biosensors: From principles to applications. *TrAC Trends in Analytical Chemistry* 133, p. 116098. doi: <https://doi.org/10.1016/j.trac.2020.116098>

Han, S. et al. 2020. Label-Free and Ultrasensitive Electrochemical DNA Biosensor Based on Urchinlike Carbon Nanotube-Gold Nanoparticle Nanoclusters. *Anal Chem* 92(7), pp. 4780-4787. doi: 10.1021/acs.analchem.9b03520

Harm, S. et al. 2021. An in vitro study on factors affecting endotoxin neutralization in human plasma using the Limulus amoebocyte lysate test. *Sci Rep* 11(1), p. 4192. doi: 10.1038/s41598-021-83487-4

Hu, Q. et al. 2023. Dually Amplified Electrochemical Aptasensor for Endotoxin Detection via Target-Assisted Electrochemically Mediated ATRP. *Anal Chem* 95(12), pp. 5463-5469. doi: 10.1021/acs.analchem.3c00741

Jang, L. S. and Keng, H. K. 2008. Modified fabrication process of protein chips using a short-chain self-assembled monolayer. *Biomed Microdevices* 10(2), pp. 203-211. doi: 10.1007/s10544-007-9126-7

Jiang, D. et al. 2012. Development of a Cyclic Voltammetry Method for DNA Electrochemical Detection on Microfluidic Gene Chip. *International Journal of Electrochemical Science* 7(11), pp. 10607-10619. doi: [https://doi.org/10.1016/S1452-3981\(23\)16887-8](https://doi.org/10.1016/S1452-3981(23)16887-8)

Jolly, P. et al. 2016. Aptamer–MIP hybrid receptor for highly sensitive electrochemical detection of prostate specific antigen. *Biosensors and Bioelectronics* 75, pp. 188-195. doi: <https://doi.org/10.1016/j.bios.2015.08.043>

Khan, M. A. and Mujahid, M. 2020. Recent Advances in Electrochemical and Optical Biosensors Designed for Detection of Interleukin 6. *Sensors (Basel)* 20(3), doi: 10.3390/s20030646

Khattab, A. A. et al. 2018. Clinical study of serum interleukin-6 in children with community-acquired pneumonia. *Egyptian Pediatric Association Gazette* 66(2), pp. 43-48. doi: <https://doi.org/10.1016/j.epag.2018.03.003>

Li, X. M. et al. 2007. Nucleic acid biosensor for detection of hepatitis B virus using 2,9-dimethyl-1,10-phenanthroline copper complex as electrochemical indicator. *Anal Chim Acta* 582(1), pp. 158-163. doi: 10.1016/j.aca.2006.09.004

Lorente, M. L. et al. 2000. Diagnosis of pneumococcal pneumonia by polymerase chain reaction (PCR) in whole blood: a prospective clinical study. *Thorax* 55(2), pp. 133-137. doi: 10.1136/thorax.55.2.133

Lou, Y. et al. 2014. A competitive electrochemical immunosensor for the detection of human interleukin-6 based on the electrically heated carbon electrode and silver nanoparticles functionalized labels. *Talanta* 122, pp. 135-139. doi: 10.1016/j.talanta.2014.01.016

Luo, L. Q. et al. 2013. Label-free electrochemical impedance genosensor based on 1-aminopyrene/graphene hybrids. *Nanoscale* 5(13), pp. 5833-5840. doi: 10.1039/c3nr01237a

McCrae, L. E. et al. 2023. Advancing electrochemical biosensors for interleukin-6 detection. *Biosensors and Bioelectronics: X* 13, p. 100288. doi: <https://doi.org/10.1016/j.biosx.2022.100288>

Miao, X. et al. 2016. Ultrasensitive electrochemical detection of protein tyrosine kinase-7 by gold nanoparticles and methylene blue assisted signal amplification. *Biosens Bioelectron* 83, pp. 39-44. doi: 10.1016/j.bios.2016.04.032

Michelow, I. C. et al. 2007. Systemic cytokine profile in children with community-acquired pneumonia. *Pediatr Pulmonol* 42(7), pp. 640-645. doi: 10.1002/ppul.20633

Mu, Z. et al. 2022. A new electrochemical aptasensor for ultrasensitive detection of endotoxin using Fe-MOF and AgNPs decorated P-N-CNTs as signal enhanced indicator. *Applied Surface Science* 573, p. 151601. doi: <https://doi.org/10.1016/j.apsusc.2021.151601>

Oh, C. et al. 2021. Electrochemical Immunosensing of Interleukin-6 in Human Cerebrospinal Fluid and Human Serum as an Early Biomarker for Traumatic Brain Injury. *ACS Meas Sci Au* 1(2), pp. 65-73. doi: 10.1021/acsmesuresciau.1c00013

Özcan, N. et al. 2020. A Novel Molecularly Imprinting Biosensor Including Graphene Quantum Dots/Multi-Walled Carbon Nanotubes Composite for Interleukin-6 Detection and Electrochemical Biosensor Validation. *ECS Journal of Solid State Science and Technology* 9, doi: 10.1149/2162-8777/abd149

Pietrzak, B. et al. 2023. Circulating Microbial Cell-Free DNA in Health and Disease. *Int J Mol Sci* 24(3), doi: 10.3390/ijms24033051

Regan, E. M. et al. 2014. A novel cobalt complex for enhancing amperometric and impedimetric DNA detection. *Electrochimica Acta* 128, pp. 10-15. doi: <https://doi.org/10.1016/j.electacta.2013.10.028>

Russell, C. et al. 2019. Development of a needle shaped microelectrode for electrochemical detection of the sepsis biomarker interleukin-6 (IL-6) in real time. *Biosens Bioelectron* 126, pp. 806-814. doi: 10.1016/j.bios.2018.11.053

Steube, K. G. et al. 2003. A simple method using beta-globin polymerase chain reaction for the species identification of animal cell lines--a progress report. *In Vitro Cell Dev Biol Anim* 39(10), pp. 468-475. doi: 10.1290/1543-706X(2003)039<0468:ASMUGP>2.0.CO;2

Tan, P. S. et al. 2021. Laser Scribing Fabrication of Graphitic Carbon Biosensors for Label-Free Detection of Interleukin-6. *Nanomaterials (Basel)* 11(8), doi: 10.3390/nano11082110

Tanak, A. S. et al. 2021. Multiplexed cytokine detection using electrochemical point-of-care sensing device towards rapid sepsis endotyping. *Biosens Bioelectron* 171, p. 112726. doi: 10.1016/j.bios.2020.112726

Tertis, M. et al. 2019. Impedimetric aptasensor for the label-free and selective detection of Interleukin-6 for colorectal cancer screening. *Biosens Bioelectron* 137, pp. 123-132. doi: 10.1016/j.bios.2019.05.012

Trantakis, I. A. et al. 2010. Ultrafast fluorescence dynamics of Sybr Green I/DNA complexes. *Chemical Physics Letters* 485(1), pp. 187-190. doi: <https://doi.org/10.1016/j.cplett.2009.12.030>

- Trotter, M. et al. 2020. Review: Electrochemical DNA sensing - Principles, commercial systems, and applications. *Biosens Bioelectron* 154, p. 112069. doi: 10.1016/j.bios.2020.112069
- Vasconcellos, A. G. et al. 2018. Systemic cytokines and chemokines on admission of children hospitalized with community-acquired pneumonia. *Cytokine* 107, pp. 1-8. doi: 10.1016/j.cyto.2017.11.005
- Yang, L. et al. 2016. [Cu(phen)<sub>2</sub>](<sup>2+</sup>) acts as electrochemical indicator and anchor to immobilize probe DNA in electrochemical DNA biosensor. *Anal Biochem* 492, pp. 56-62. doi: 10.1016/j.ab.2015.09.011
- Zamani, M. et al. 2022. A novel labeled and label-free dual electrochemical detection of endotoxin based on aptamer-conjugated magnetic reduced graphene oxide-gold nanocomposite. *Journal of Electroanalytical Chemistry* 908, p. 116116. doi: <https://doi.org/10.1016/j.jelechem.2022.116116>
- Zhu, D. et al. 2017. Label-Free Electrochemical Sensing Platform for MicroRNA-21 Detection Using Thionine and Gold Nanoparticles Co-Functionalized MoS<sub>2</sub> Nanosheet. *ACS Appl Mater Interfaces* 9(41), pp. 35597-35603. doi: 10.1021/acsami.7b11385
- Zipper, H. et al. 2004. Investigations on DNA intercalation and surface binding by SYBR Green I, its structure determination and methodological implications. *Nucleic Acids Res* 32(12), p. e103. doi: 10.1093/nar/gnh101

# Chapter 6

## General discussion, concluding remarks and future outlook

---

## 6.1 General overview of thesis

At the beginning of the project, due to lab inaccessibility for the first six months due to COVID-19, a comprehensive literature review was performed, which is presented as **Chapter 1** of this thesis. Emphasis was placed on the development of sepsis secondary to pneumonia, and its consequences as a leading cause of mortality and morbidity worldwide in children between the ages of 28 days and 5 years (de Benedictis et al. 2020). Moreover, sepsis is a major cause of economic burden for health systems worldwide, and a leading cause of hospitalization (Chalmers et al. 2017). With a mortality rate between 5% and 15%, an annual cost of 2 billion GBP to the NHS and eventually 29000 annual deaths in the UK, it is evident that rapid and accurate diagnosis and management of sepsis is of paramount importance (Lim et al. 2009; Chalmers et al. 2011; Chalmers et al. 2017).

To date, the “gold-standard” in the detection of sepsis secondary to pneumonia still requires chest x-rays as a diagnostic method, which pinpoints lung damage but cannot identify the causative pathogen, or the stage of the disease (Pahal et al. 2021). PCR is often performed to try and identify the infective cause, however it is held back by false-positive results and the risk of contamination from other pathogens (Radstrom et al. 2004). However, PCR does not provide information regarding disease severity nor the underlying immunological response of the patient, which is what ultimately leads to multi-organ failure and death. Furthermore, the equipment and the reagents required for performing PCR analysis can be costly, reducing its application in remote areas or limited-resource settings (Radstrom et al. 2004). Therefore, the need for a rapid, specific and accessible diagnostic platform for the diagnosis of sepsis secondary to pneumonia is evident.

During the **literature review** phase of the project, suitable platforms for the development of sensors were presented. Such platforms included optical, electrochemical, magnetic, piezoelectric, thermometric, and more. As previous work in the lab largely focused on electrochemical methods, it was decided to focus on their applications as sensing platforms. Electrochemical sensors are easy to use, can be prepared relatively quickly, do not require expensive or complicated equipment or reagents, and have potential for miniaturization and transfer into POC devices (Campuzano et al. 2017). Therefore, focus was paid on the applications of electrochemical sensors, as well as methods to prevent biofouling, which is often a challenge.

One of the aims of the literature review was the identification and selection of suitable biomarkers for the diagnosis of sepsis. As one of the overarching objectives of this project was the development of protocols allowing the detection of multiple biomarker classes, it was decided to focus on the detection of three types: A protein marker, a nucleic acid marker and endotoxin. As previous work in the lab had focused on the detection of procalcitonin and C-reactive protein, both of which are associated with sepsis, it was decided to choose IL-6, a

predominantly pro-inflammatory protein, beta globin, a DNA sequence, and endotoxin, as targets in this project.

**Chapter 2** focused on the assessment of endotoxin activity in human plasma with evaluation of masking kinetics and development of a sample preparation protocol to allow for detection of endotoxin from clinical samples. It was decided to initiate experiments using a magneto-optical platform utilizing the LAL assay, which is considered the “gold standard” in endotoxin detection. Despite the LAL assay being the gold standard in endotoxin detection in pharmaceuticals and manufactured products, its use in blood has been held back by the presence of various inhibitors, proteins, lipids and interferences in the sample matrix (Harm et al. 2021). In Chapter 2, a number of sample preparation protocols were evaluated for their effects on endotoxin recovery, and following a screening process, a finalized protocol which included dilution, heating, addition of 5mM MgCl<sub>2</sub>, acid base treatment and centrifugation was developed. This protocol allowed for satisfactory endotoxin recovery, up to 3 days of incubation for plasma samples stored in either room temperature or fridge. To date, successful endotoxin recovery has only been performed in heparinized plasma, with no success in citrated plasma (Harm et al. 2021). This Chapter also provided initial insights in endotoxin masking by plasma components over time, with results showing that endotoxin masking is time and temperature dependent, as well as forming the hypothesis of endotoxin masking by lipoproteins. Given the sensitivity of the LAL assay to temperature and pH variations, as well as assay interferences caused by alternative sample preparation steps, such as the addition of NaDOC, it was anticipated that the use of an aptamer-based platform would allow the use of protocols incompatible with the LAL assay and allow recovery following prolonged incubation, something which was explored in Chapter 3.

The main focus of **Chapter 3** was the development and optimization of electrochemical sensors for the detection of endotoxin in aqueous solutions, based on protocols developed by previous lab members. The aptasensor displayed performance similar to the results reported by previous lab members, with a LOD of 0.5 pg/mL. Additionally, adoption of a hybrid imprinting strategy led to the recreation of an aptaMIP endotoxin sensor. Further optimization of the previously developed protocol improved control over polymer thickness and produced more reproducible results. A conventional MIP was also developed, which exhibited a similar LOD to the aptasensor, although linearity was poor across endotoxin concentrations tested (1 pg/mL and 1 ng/mL). An aptaNIP was also prepared as a control, which displayed negligible interaction with endotoxin at concentrations up to 10 pg/mL.

The optimized aptaMIP displayed similar performance to the aptaMIP developed by Demertzis, highlighting the reproducibility of the system. Specifically, a LOD of 10 fg/mL was detected, with a sensor displaying an upper limit of 1 ng/mL. Good linearity ( $r = 0.9694$ ) was reported. As published literature is scarce on aptaMIP systems, comparisons with conventionally imprinted platforms with LODs in the ng/mL scale show that the aptaMIP

displays superior performance (Altintas et al. 2016). The LOD was also significantly lower than that observed with the conventional aptasensor. This highlights the strengths of the hybrid system, and further supports the hypothesis that the aptamer assists the formation of imprinted cavities with increased sensitivity and selectivity for the target molecule.

Importantly, the aptaMIP outperforms the LAL assay, which has a LOD of 1 pg/mL in the gel-clot assay, down to 100 fg/mL in the kinetic turbidimetric assays (Piehler et al. 2020) and down to 50 fg/mL in the chromogenic assays (Wako Pyrostar, 2023). Additionally, previous work in the lab demonstrated the aptaMIP does not display cross-reactivity with beta-glucan and lipoteichoic acid, which can cause false positives in the LAL assay (Demertzis, 2019). Finally, specificity studies showed that preincubation of HSA with endotoxin resulted in the formation of endotoxin-protein complexes that resulted in a further increase in impedance, highlighting the need for a sample preparation protocol for plasma samples, the development process of which can be found in Chapter 4.

**Chapter 4** focused on the development of a suitable sample preparation protocol for the detection of endotoxin in citrated blood plasma, this time using the aptaMIP as a detection platform. Similar to Chapter 2, a screening process was performed where various sample preparation treatments were assessed for their effects on endotoxin recovery. Through this process, the existing sample preparation protocol was further developed to include sodium deoxycholate (NaDOC) addition. The use of NaDOC was not possible with the LAL assay, as is the lysate is incompatible with detergents (Harm et al. 2021). As it is well known that plasma lipoproteins, especially HDL, bind and neutralize endotoxins, and HDL concentration in stored plasma increases over time, it is hypothesized that they play a role in the time-dependent masking of endotoxin (Pinto et al. 2014). Indeed, the use of NaDOC significantly improved endotoxin recoveries; Spike-hold studies showed recovery for up to 15 days post-spike in samples stored at both room temperature and fridge. Importantly, almost 100% recovery was noted across all days tested for samples stored in the fridge, which further evidences the time and temperature dependency of endotoxin masking.

In **Chapter 5**, electrochemical sensors for the detection of IL-6, a protein biomarker, and beta-globin ss-DNA, which is associated with elevated sepsis risk, were developed. The development of an IL-6 immunosensor based on an anti-IL-6 antibody and EDC/NHS chemistry faced challenges from the beginning, as all attempts resulted in sensors with very limited detection ranges and high LODs (25 pg/mL). The introduction of Protein G, with the hope of orienting the anti-IL6 antibodies, offered a small improvement in LOD (12.5 pg/mL), however a limited dynamic range remained. Therefore, it was decided to use an aptamer developed by Tertic et al., using DTBA as a passivation layer. The use of the aptamer allowed for more sensitive IL-6 detection, with a LOD of 100 fg/mL, however the sensor's range was still limited, similar to the results obtained with the immunosensors.

A collaboration with the School of Chemistry through the Interdisciplinary Doctoral Training Hub programme allowed access to DNA intercalating sensitizer molecules. Introduction of a cobalt based sensitizer to the IL-6 aptasensor resulted in a massive decrease in impedance, explained by the sensitizer's positive charge cancelling out the aptamer's negative charge. The use of the sensitizer allowed for a significant improvement in IL-6 detection, dropping the LOD of the sensor down to 10 fg/mL, and allowing detection of IL-6 at concentrations of up to 150 pg/mL. The sensitized system displayed similar responses in spiked plasma, subjected only to tenfold dilution with water. Specificity tests showed that although the sensitized system interacted with other molecules, such as HSA, IL-10 and endotoxin, the system produced a linear response in diluted plasma, with increases in impedance significantly exceeding those noted in specificity studies. This suggests selectivity for IL-6 in the presence of other molecules, and potential for application in diagnostics.

For the development of the beta-globin sensor, initial attempts at a sensor used a DNA strand complementary to the target sequence. Despite optimization efforts using different alkanethiols as spacer / backfilling molecules, which only slightly improved binding, no significant responses were noted even following incubation with high DNA concentrations (1  $\mu$ M). Application of the same sensitizer as used in the IL-6 studies allowed for a significant improvement in beta globin DNA detection, with the sensitized system demonstrating a LOD of 0.01  $\mu$ M, and detection of beta globin DNA up to 2  $\mu$ M. Like the IL-6 sensitized sensor, the system displayed similar responses in spiked plasma, subjected only to tenfold dilution with water. Additional specificity studies showed that the sensitized globin sensor shows selectivity for the DNA in the presence of other molecules.

This wraps up the other two aims of this project, which was the development of sensing platforms for a protein and a nucleic-acid target. Additionally, the sensitizer work brings together the work of IDTH members from the School of Chemistry, which was also one of the overarching goals of the project.

At the very end of this PhD project a further 'proof-of-principle' study was carried out using the sensitizer with the endotoxin aptasensor. The system was prepared according to section 3.2.2.4 in Chapter 3. The sensitized aptasensor was challenged with a variety of endotoxin spiked samples, with concentrations ranging from 0.001 fg/mL up to 1 pg/mL, with 3 replicates produced for each concentration, to ascertain the sensor's sensitivity and enable the estimation of the limit of detection. The resultant EIS data is presented in Figure 6.1, with the correlation between concentration and  $\% \Delta R/R_0$  shown in Figure 6.2.

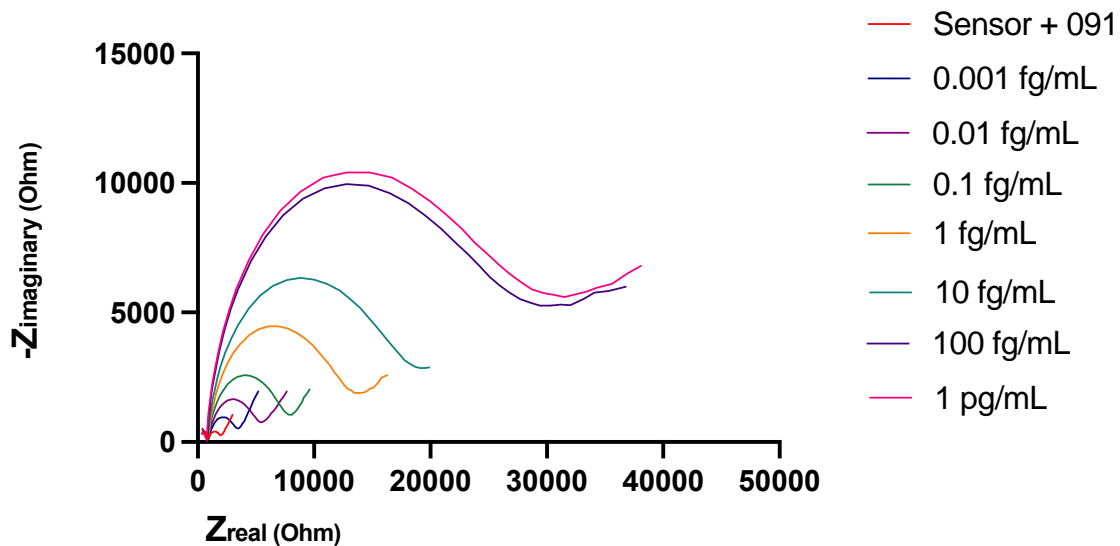


Figure 6.1: EIS graph showing the detection range of the endotoxin aptasensor following incubation with sensitizer and various concentrations (0.001 fg/mL – 1 pg/mL) of endotoxin in water.

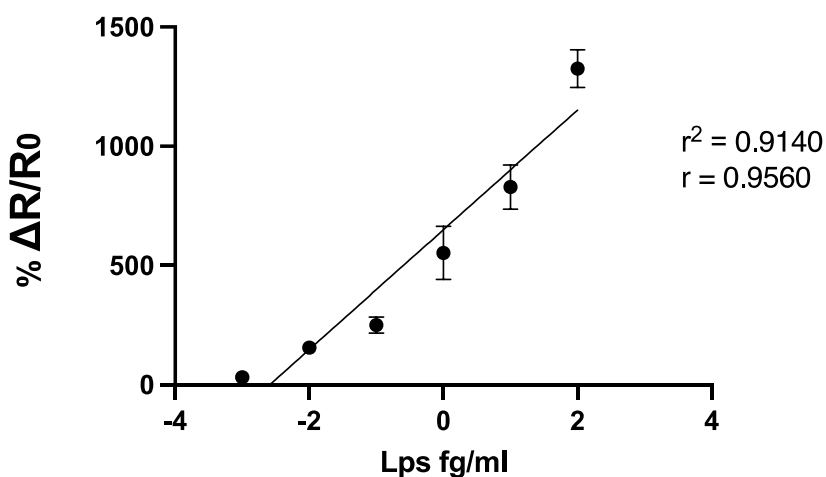


Figure 6.2: Shows the % $\Delta R/R_0$  of the sensor following incubation with sensitizer and various concentrations of endotoxin in water. A linear range is noted between 0.001 fg/mL and 100 fg/mL.

Figures 6.1 and 6.2 show an impressive detection limit of 0.001 fg/mL, which outperforms the LAL assay, aptasensor and aptaMIP. This is an interesting observation, as very few endotoxin sensors in literature report such low levels of detection. The only reported system in literature with a lower detection limit has been reported by Posha et al., where the aptamer was immobilized on the surface of the gold clusters and then on the gold electrodes, which resulted in remarkable detection limit of 7.94 zM, with a dynamic range of 0.01 aM to 1pM (Posha et al. 2018).

Due to time constraints, only limited experiments were performed, and the impressive results obtained using the sensitizer couldn't be assessed in more detail. It is possible that the sensitizer, combined with a DNA-based platform, may allow for even more sensitive endotoxin detection. Therefore, it would be interesting if interdisciplinary future work unveiled the sensitizer's mode of action and combined it with a suitable detection platform to develop even more sensitive and rapid sensors.

## **6.2 Conclusion and future outlook**

In conclusion, the current work presents the challenges faced with endotoxin detection using LAL and electrochemical approaches, as well as the challenges faced with endotoxin detection in clinical matrices. Importantly, this work showcases the advantages of a hybrid imprinted sensor, especially regarding detection of challenging molecules, or molecules found in low concentrations in complex clinical matrices. It is anticipated that this work inspires the development of hybrid imprinted sensors for the detection of other important biomarkers.

As this work showcases the advantages of the aptaMIP and its successful application in spiked plasma samples, it would be interesting to use as part of a clinical study using plasma samples from real sepsis patients, or hospitalized pneumonia patients. Moreover, there is potential for the further simplification of the sample preparation protocol. Some of the sample preparation steps, such as dilution, heating and centrifugation could potentially become automated. Additionally, the use of microwaves could potentially shorten the heating step.

One of the benefits of electrochemical sensors, as mentioned in the introduction, is their potential for miniaturization. It would be interesting to see whether the use of screen-printed electrodes or microfluidics could potentially assist the transition of the aptaMIP from a near-patient sensor to a POC sensor.

The sensitizer chapter showcases the potential for novel discoveries through collaboration, and it is anticipated that it may inspire future investigations towards the use of these interesting molecules into diagnostic applications. One possibility is the development of a hybrid imprinting strategy combining aptamers and sensitizers to achieve ultra-sensitive molecule detection. It is anticipated that the sensitivity provided by the sensitizer, combined with the biofouling controlling properties of the MIP will lead to superior biosensor performance. To date, no such sensors can be found in literature, so the development of such a sensor would be an interesting project.

### 6.3 Bibliography

Altintas, Z. et al. 2016. Ultrasensitive detection of endotoxins using computationally designed nanoMIPs. *Analytica Chimica Acta* 935, pp. 239-248. doi: <https://doi.org/10.1016/j.aca.2016.06.013>

Campuzano, S. et al. 2017. Molecular Biosensors for Electrochemical Detection of Infectious Pathogens in Liquid Biopsies: Current Trends and Challenges. *Sensors (Basel)* 17(11), doi: 10.3390/s17112533

Chalmers, J. et al. 2017. Community-acquired pneumonia in the United Kingdom: a call to action. *Pneumonia (Nathan)* 9, p. 15. doi: 10.1186/s41479-017-0039-9

Chalmers, J. D. et al. 2011. Severity assessment tools to guide ICU admission in community-acquired pneumonia: systematic review and meta-analysis. *Intensive Care Med* 37(9), pp. 1409-1420. doi: 10.1007/s00134-011-2261-x

de Benedictis, F. M. et al. 2020. Complicated pneumonia in children. *Lancet* 396(10253), pp. 786-798. doi: 10.1016/S0140-6736(20)31550-6

Harm, S. et al. 2021. An in vitro study on factors affecting endotoxin neutralization in human plasma using the Limulus amoebocyte lysate test. *Sci Rep* 11(1), p. 4192. doi: 10.1038/s41598-021-83487-4

Lim, W. S. et al. 2009. BTS guidelines for the management of community acquired pneumonia in adults: update 2009. *Thorax* 64 Suppl 3, pp. iii1-55. doi: 10.1136/thx.2009.121434

Pahal, P. et al. 2021. Typical Bacterial Pneumonia. *StatPearls*. Treasure Island (FL).

Piehler, M. et al. 2020. Comparison of LAL and rFC Assays-Participation in a Proficiency Test Program between 2014 and 2019. *Microorganisms* 8(3), doi: 10.3390/microorganisms8030418

Pinto, J. et al. 2014. Human plasma stability during handling and storage: impact on NMR metabolomics. *Analyst* 139(5), pp. 1168-1177. doi: 10.1039/c3an02188b

Posha, B. et al. 2018. Gold atomic cluster mediated electrochemical aptasensor for the detection of lipopolysaccharide. *Biosensors and Bioelectronics* 101, pp. 199-205. doi: <https://doi.org/10.1016/j.bios.2017.10.030>

Radstrom, P. et al. 2004. Pre-PCR processing: strategies to generate PCR-compatible samples. *Mol Biotechnol* 26(2), pp. 133-146. doi: 10.1385/MB:26:2:133